

**For Reference**

---

**NOT TO BE TAKEN FROM THIS ROOM**



Ex libris  
UNIVERSITATIS  
ALBERTAENSIS













T H E   U N I V E R S I T Y   O F   A L B E R T A

RELEASE FORM

NAME OF AUTHOR	Brian Thomas Greaves
TITLE OF THESIS	Satellite Measured Changes In Thermal Fields Of An Arctic Island
DEGREE FOR WHICH THESIS WAS PRESENTED	Master of Science
YEAR THIS DEGREE GRANTED	1981

Permission is hereby granted to THE UNIVERSITY OF ALBERTA LIBRARY to reproduce single copies of this thesis and to lend or sell such copies for private, scholarly or scientific research purposes only.

The author reserves other publication rights, and neither the thesis nor extensive extracts from it may be printed or otherwise reproduced without the author's written permission.





THE UNIVERSITY OF ALBERTA

SATELLITE MEASURED CHANGES IN  
THERMAL FIELDS OF AN ARCTIC ISLAND

by



BRIAN THOMAS GREAVES

A THESIS

SUBMITTED TO THE FACULTY OF GRADUATE STUDIES AND RESEARCH  
IN PARTIAL FULFILMENT OF THE REQUIREMENTS FOR THE DEGREE  
OF MASTER OF SCIENCE

IN

METEOROLOGY

DEPARTMENT OF GEOGRAPHY

EDMONTON, ALBERTA

SPRING, 1981





THE UNIVERSITY OF ALBERTA

FACULTY OF GRADUATE STUDIES AND RESEARCH

The undersigned certify that they have read, and recommend to the Faculty of Graduate Studies and Research, for acceptance, a thesis entitled "Satellite Measured Changes In Thermal Fields Of An Arctic Island" submitted by Brian Thomas Greaves in partial fulfilment of the requirements for the degree of Master of Science in Meteorology.



## ABSTRACT

Infrared satellite information from two days in the summer of 1977 was examined for evidence of coastal circulation patterns on Banks Island in the northwestern Canadian Arctic. The satellite data were calibrated to degrees Celsius and plotted in the form of contoured isotherms. Information was available from several consecutive orbits of the NOAA-5 polar orbiting satellite, providing coverage of the study area over an eight to ten hour period each day. The synoptic situation over Banks Island on both days was believed to have been conducive to coastal sea breeze formation along the western shorelines of the island. Evidence for coastal sea breeze circulations was found in the behaviour of thermal gradients along the western coastline, and in the formation and motion of cloud along the coastline. It is believed that the method presented can provide more detailed information on limited-scale thermal patterns than can conventional satellite imagery using gray-scaled techniques, particularly in the study of thermal gradients along coastlines.





## ACKNOWLEDGMENTS

I would like to express my gratitude to Dr. E. R. Reinelt who acted as my departmental supervisor and guided me through the preparation of this thesis. His suggestions and encouragement were always kindly proffered and thankfully received.

Appreciation is also extended to Dr. K. D. Hage and Dr. G. Rostoker who, with Dr. Reinelt, served on my examining committee.

I would also like to thank Barry Green, whose original thesis was the starting point of this study, as well as the other meteorology students I have worked with, who offered many helpful suggestions during the course of this work. Special thanks is extended to Denis Oracheski who made numerous useful comments on the satellite meteorology used in this study and was always ready to offer his time and experience when either was required.

Thanks is also extended to the members of the Photographic Services Division of the Department of Geography at the University of Alberta who helped in the preparation of the figures in this thesis.

Finally, I would like to especially thank my Mother, Mrs. Beryl Greaves, who typed this thesis. Her time and patience were truly appreciated.

I was aided in the completion of this thesis by a Postgraduate Fellowship from the Natural Sciences and Engineering Research Council of Canada. This thesis was completed, in part, while on educational leave from the Atmospheric Environment Service of Canada.





## TABLE OF CONTENTS

	Page
ABSTRACT.....	iv
ACKNOWLEDGEMENTS.....	v
TABLE OF CONTENTS.....	vi
LIST OF TABLES.....	viii
LIST OF FIGURES.....	ix
CHAPTER	
I        CLIMATOLOGY OF AN ARCTIC ISLAND.....	1
1.1    Introduction.....	1
1.2    Thermally Driven Circulations of an Arctic Island.....	3
1.3    Synoptic Circulation Over Banks Island In Mid July of 1977.....	10
II       INFRARED SATELLITE DATA.....	25
2.1    Introduction.....	25
2.2    Satellite Scanning.....	25
2.3    Satellite Resolution.....	27
2.4    Internal Calibration of Infrared Satellite Data.....	35
2.5    External Calibration of Infrared Satellite Data.....	37
III      TEMPERATURE FIELD PLOTTING OF INFRARED SATELLITE DATA..	44
3.1    Introduction.....	44
3.2    Temperature Field Plotting With SURFACE II.....	45
3.3    Identification of Regions of Interest.....	47
IV       DAILY DEVELOPMENT OF THE TEMPERATURE FIELD PATTERN OVER BANKS ISLAND.....	52



CHAPTER		Page
4.1	Introduction.....	52
4.2	Satellite Measured Temperature Fields of an Arctic Island.....	52
4.3	Temperature Fields of Banks Island on Two Days in July of 1977.....	67
4.3.1	Explanation of Figures.....	67
4.3.2	Case 1 July 15 of 1977.....	69
4.3.3	Case 2 July 16 of 1977.....	102
V	SUMMARY AND CONCLUSIONS.....	125
	REFERENCES.....	137
APPENDIX		
A	CALCULATING LOCATIONS OF LATITUDE-LONGITUDE INTERSECTIONS ON SATELLITE IMAGERY.....	145
B	INTERNAL CALIBRATION CURVE FITTING.....	150
C	COMPUTER PROGRAMS.....	153
C.1	Program TAPERD-1.....	154
C.2	Program SCAN-2.....	162
C.3	Subroutine ITERA.....	177
C.4	Subroutine SMOO.....	178
C.5	Subroutine CALI.....	179
C.6	Program RERUN.....	181
C.7	Sample Input and Output Information.....	183
C.7.1	Input for Program TAPERD-1.....	183
C.7.2	Output from Program TAPERD-1.....	183
C.7.3	Input for Program SCAN-2.....	186
C.7.4	Output from Program SCAN-2.....	186





## LIST OF TABLES

TABLE	Page
1.1 Wind, temperature and cloud abstracts for Sachs Harbour (YSY) on July 14, 15 and 16 of 1977.	16
1.2 Wind and temperature profiles for Sachs Harbour (YSY) on July 15, 16 and 17 of 1977.	20



## LIST OF FIGURES

FIGURE		Page
1.1	Geography of the northwestern Canadian Arctic.	7
1.2	Topography of Banks Island.	9
1.3	Mean sea level pressure analysis of the northwestern Canadian Arctic at 1800Z on July 14, 1977.	12
1.4	500-mb constant pressure analysis of the northwestern Canadian Arctic at 0000Z on July 15, 1977.	12
1.5	Mean sea level pressure analysis of the northwestern Canadian Arctic at 1800Z on July 15, 1977.	13
1.6	500-mb constant pressure analysis of the northwestern Canadian Arctic at 0000Z on July 16, 1977.	13
1.7	Mean sea level pressure analysis of the northwestern Canadian Arctic at 1800Z on July 16, 1977.	14
1.8	500-mb constant pressure analysis of the northwestern Canadian Arctic at 0000Z on July 17, 1977.	14
1.9	Wind profiles from Sachs Harbour on July 14, 15 and 16 of 1977.	21
2.1	Geometry of the NOAA-5 scanning radiometer.	27
2.2	One scan of satellite information from Orbit 4347 of NOAA-5 on July 15, 1977.	30
2.3	Unaveraged temperature-field plot of the Banks Island region of Orbit 4347 of NOAA-5 at 2120Z on July 15, 1977.	31
2.4	Averaged temperature-field plot of the Banks Island region of Orbit 4347 of NOAA-5 at 2120Z on July 15, 1977.	32
2.5	Reflectance-field plot of the Banks Island region of Orbit 4347 of NOAA-5 at 2120Z on July 15, 1977.	33
2.6	Infrared calibration curve for the Banks Island region of Orbit 4347 of NOAA-5 at 2120Z on July 15, 1977.	36



FIGURE

Page

2.7	Averaged and smoothed temperature-field plot of the Beaufort Sea region of Orbit 4347 of NOAA-5 at 2120Z on July 15, 1977.	39
2.8	External calibration curve for NOAA-5 orbits on July 14, 15 and 16 of 1977.	41
4.1	Averaged and smoothed temperature-field plot of the Banks Island region of Orbit 4345 of NOAA-5 at 1731Z on July 15, 1977.	70
4.2	Averaged and smoothed temperature-field plot of the Banks Island region of Orbit 4346 of NOAA-5 at 1936Z on July 15, 1977.	71
4.3	Averaged and smoothed temperature-field plot of the Banks Island region of Orbit 4347 of NOAA-5 at 2120Z on July 15, 1977.	72
4.4a	Infrared image of Beaufort Sea region of Orbit 4347 of NOAA-5 at 2120Z on July 15, 1977.	73
4.4b	Visible image of 4.4a.	73
4.5	Averaged and smoothed temperature-field plot of the Banks Island region of Orbit 4348 of NOAA-5 at 2314Z on July 15, 1977.	74
4.6a	Infrared image of Beaufort Sea region of Orbit 4348 of NOAA-5 at 2315Z on July 15, 1977.	75
4.6b	Visible image of 4.6a.	75
4.7	Averaged and smoothed temperature-field plot of the Banks Island region of Orbit 4349 of NOAA-5 at 0108Z on July 16, 1977.	76
4.8a	Infrared image of Beaufort Sea region of Orbit 4349 of NOAA-5 at 0110Z on July 16, 1977.	77
4.8b	Visible image of 4.8a.	77
4.9	Averaged and smoothed temperature-field plot of the Banks Island region of Orbit 4350 of NOAA-5 at 0303Z on July 16, 1977.	78





FIGURE	Page
4.10a Infrared image of Beaufort Sea region of Orbit 4350 of NOAA-5 at 0305Z on July 16, 1977.	79
4.10b Visible image of 4.10a.	79
4.11 Averaged and smoothed temperature-field plot of the Banks Island region of Orbit 4358 of NOAA-5 at 1843Z on July 16, 1977.	104
4.12 Averaged and smoothed temperature-field plot of the Banks Island region of Orbit 4359 of NOAA-5 at 2037Z on July 16, 1977.	105
4.13a Infrared image of Beaufort Sea region of Orbit 4359 of NOAA-5 at 2035Z on July 16, 1977.	106
4.13b Visible image of 4.13a.	106
4.14 Averaged and smoothed temperature-field plot of the Banks Island region of Orbit 4360 of NOAA-5 at 2231Z on July 16, 1977.	107
4.15a Infrared image of Beaufort Sea region of Orbit 4360 of NOAA-5 at 2230Z on July 16, 1977.	108
4.15b Visible image of 4.15a.	108
4.16 Averaged and smoothed temperature-field plot of the Banks Island region of Orbit 4361 of NOAA-5 at 0025Z on July 17, 1977.	109
4.17a Infrared image of Beaufort Sea region of Orbit 4361 of NOAA-5 at 0025Z on July 17, 1977.	110
4.17b Visible image of 4.17a.	110
4.18 Averaged and smoothed temperature-field plot of the Banks Island region of Orbit 4362 of NOAA-5 at 0219Z on July 17, 1977.	111
4.19a Infrared image of Beaufort Sea region of Orbit 4362 of NOAA-5 at 0220Z on July 17, 1977.	112
4.19b Visible image of 4.19a.	112
A.1 Geometry of a near-polar orbiting satellite.	146



FIGURE		Page
A.2	Geometry of a satellite scanning radiometer.	149
B.1	Calibration points and infrared calibration curve for the Banks Island region of Orbit 4346 of NOAA-5 at 1930Z on July 15, 1977.	152



# CHAPTER I

## CLIMATOLOGY OF AN ARCTIC ISLAND

### 1.1 Introduction

The exploration of the Arctic spans a thousand years of Canadian history. From Ninth Century Vikings searching the Davis Strait for new lands to colonize, to Europeans seeking the North West Passage to the Orient, to more recent forays by mining and oil interests, the boundaries of the north have been steadily pushed back. But the same barren landscape and forbidding climate that led to the failure of many Arctic expeditions have also slowed colonization of this region. At the turn of the century, most Arctic settlements were still only trading posts, and even these were few and scattered. As a result, most historical information on Arctic weather conditions is available only in the journals of Arctic explorers. Though meteorological information has been collected from a small number of northern sites since the early 1900's, most Arctic meteorological stations were not established until after the Second World War. Even today, fewer than thirty stations in the Canadian Arctic report hourly weather throughout the day. However, with the establishment of drilling platforms in the Beaufort Sea and with the ever increasing search for resources available in the far north, the need for a better understanding of the weather patterns of the Arctic has continually grown, a need which the few meteorological stations in this region cannot hope to fulfill.





This deficiency may be partly alleviated by the use of meteorological satellites.

It has been found that satellites can provide useful meteorological information in remote regions where conventional reporting stations do not exist. Since the early 1960's, when the first meteorological satellites were launched, the utility of this type of information has steadily increased and become more refined. Early studies concentrated primarily on the use of satellite photographs in identifying various types of cloud and their associated circulation patterns (Anderson and Veltishchev, 1973; World Meteorological Organization, 1977). While the first Earth-orbiting satellites were able to produce only imagery in the visible part of the spectrum, recent advances have resulted in satellites equipped to collect other information, as well. Satellite sensors detecting infrared radiation have been used to measure ocean surface temperatures (Rao, et al, 1971; Salter, 1977; Breaker, et al, 1978) and to identify cold upwellings in lakes and oceans which tend to be rich in nutrients and abound with marine life (Sidran and Hebard, 1972; Strong, et al, 1974). Infrared and visible images are now used together to aid in producing ice charts for maritime interests (McClain, 1975), to determine the onset of snow and ice melting (McGinnis, 1972) and to detect thunderstorms in forest-fire control (Jayaweera and Ahlnas, 1974). Still other sensors measure radiation in narrow spectral intervals to produce vertical temperature soundings of the atmosphere (Fritz, 1977). However, such information can be received only by specially equipped



stations, and the areal coverage of each station is limited. The University of Alberta at Edmonton is fortunate in being situated far enough north that it can provide satellite coverage of the Canadian Arctic.

This investigation uses infrared satellite data received at the University of Alberta Satellite Laboratory to study the daily development of the thermal regime of an Arctic island. The method used allows for faster and more accurate representation of the temperature field of a given area than is usually available by conventional means. Green (1977) studied secondary circulation patterns in the Western Canadian Arctic. This study attempts to extend this research and to identify certain features of thermally-driven circulations in this region.

## 1.2 Thermally Driven Circulations of an Arctic Island

The Arctic Islands are unique in their pattern of yearly temperature extremes. During several months of the winter the sun does not rise above the horizon nor the temperature above  $0^{\circ}\text{C}$ , and the islands and the waters surrounding them are predominantly covered in ice and snow. For several months of the summer the sun does not set, and most of the ice and snow cover melts from the islands under the continual insolation. Surface temperatures may rise to  $20^{\circ}\text{C}$  or more. Yet much of the adjoining sea remains covered with ice and even in areas which are ice-free during the summer, the continual sunshine is less effective in raising surface temperatures because of turbulent mixing in the surface layers and the large heat capacity of water. Hence, the water temperatures of ice-free



regions of the Arctic never rise far above freezing, except perhaps in shallower waters close to shorelines.

The summer contrast between warm land surfaces and near freezing water surfaces produces many localized weather features. Formation of fog or low stratus may occur if warm, moist air is advected over the cold water surface. Advection of cold air over the warmer land will lead to convection and possible cloud formation. For example, Malkus and Stern (1953a) suggest that the effect of small heated islands on a synoptic-scale flow is equivalent to that of mountain barriers, producing lee-wave cumulus formation downstream. For large islands, this effect may result in cloud formation near the coastline or further inland, depending on the moisture content of the air. However, the most widespread effect of the strong land to water temperature contrast is in the development, under suitable conditions, of the thermally driven coastal circulation known as the sea breeze.

The sea breeze phenomenon is observed along coastlines throughout the world and has been extensively studied and documented. The general development of a coastal sea breeze is described by Willet (1944), Estoque (1961) and Hsu (1970). In the absence of a gradient wind, the sea breeze begins near the shoreline in the mid-morning. At first, the breeze is light and only a few hundred meters in depth, but strengthens and deepens as the morning progresses. The onshore part of the circulation in the lower levels is accompanied by a weaker but more extensive offshore return flow above. The sea breeze reaches its maximum strength at the coastline in the mid-afternoon, when the surface air temperature reaches a maximum and





hence the land-sea temperature contrast is largest. Thereafter, the breeze slowly diminishes in strength, first along the coastline, and later further inland. By nightfall the breeze dies away completely and may be replaced by a lighter land breeze. However, if the water is cold enough, the nighttime land breeze will not develop.

Peak horizontal velocities attained by sea breezes at maximum development are about 5 to 15 meters per second (10 to 30 knots). The region of maximum velocity, known as the sea breeze front, follows the landward penetration of the sea breeze during the afternoon. The sea breeze front is characterized by low level convergence, vertical motions of up to 50 centimeters per second, and cloud formation (Simpson, 1964; Newmann and Mahrer, 1974). Seaward of the frontal zone is a region of subsidence which extends out over the water surface. Thus, the sea breeze circulation can be identified by a band of cloud in the vicinity of the sea breeze front which moves inland during the day, and clearer conditions towards the coastline (Bugaev, 1973; Anderson and Veltishchev, 1973).

The maximum landward penetration of the sea breeze itself occurs in the late afternoon. In mid latitudes, the sea breeze may be observed 30 to 50 kilometers inland, while in tropical regions, the breeze may extend 100 kilometers or more from the coastline. The onshore component of the sea breeze is gradually deflected during the afternoon by the action of the Coriolis force. In the Northern Hemisphere, this results in a veering of the sea breeze by the late afternoon.

In the presence of a light gradient wind, the sea breeze tends



to develop later in the day and exhibits a much weaker flow. However, a light offshore gradient flow at upper levels tends to strengthen the sea breeze circulation (Estoque, 1962; Sumner, 1977). A strong gradient wind will prevent the occurrence of the sea breeze, though a sea breeze component may still be found in winds near the shoreline (Willet 1944, pg 265-266).

Though sea breeze occurrence along continental coastlines is well documented, rather less is known of sea breeze development on islands. The effect of even a light gradient wind will have a different effect on sea breeze circulation on each part of the island. Newmann and Mahrer (1974), in a theoretical study dealing with circular islands of less than 100 kilometers in radius, found a stronger sea breeze circulation than for long, straight coastlines, with pronounced central convergence and vertical motion.

If little is known of circulation patterns on islands in general, even less is known of circulations on Arctic islands. No extensive studies have been performed on Arctic sea breezes. Green (1977) suggests that since the temperature contrasts between sea and land on Arctic islands is larger than in mid latitude locations, the Arctic sea breeze may be more intense. However, this large temperature contrast also implies that the nighttime land breeze will not occur, and climatological information suggests that only the onshore component of the sea breeze cycle is observed in the Arctic (Department of Transport, 1970).

Banks Island was chosen as the principal region of interest for this study. Figure 1.1 shows the location of this island in





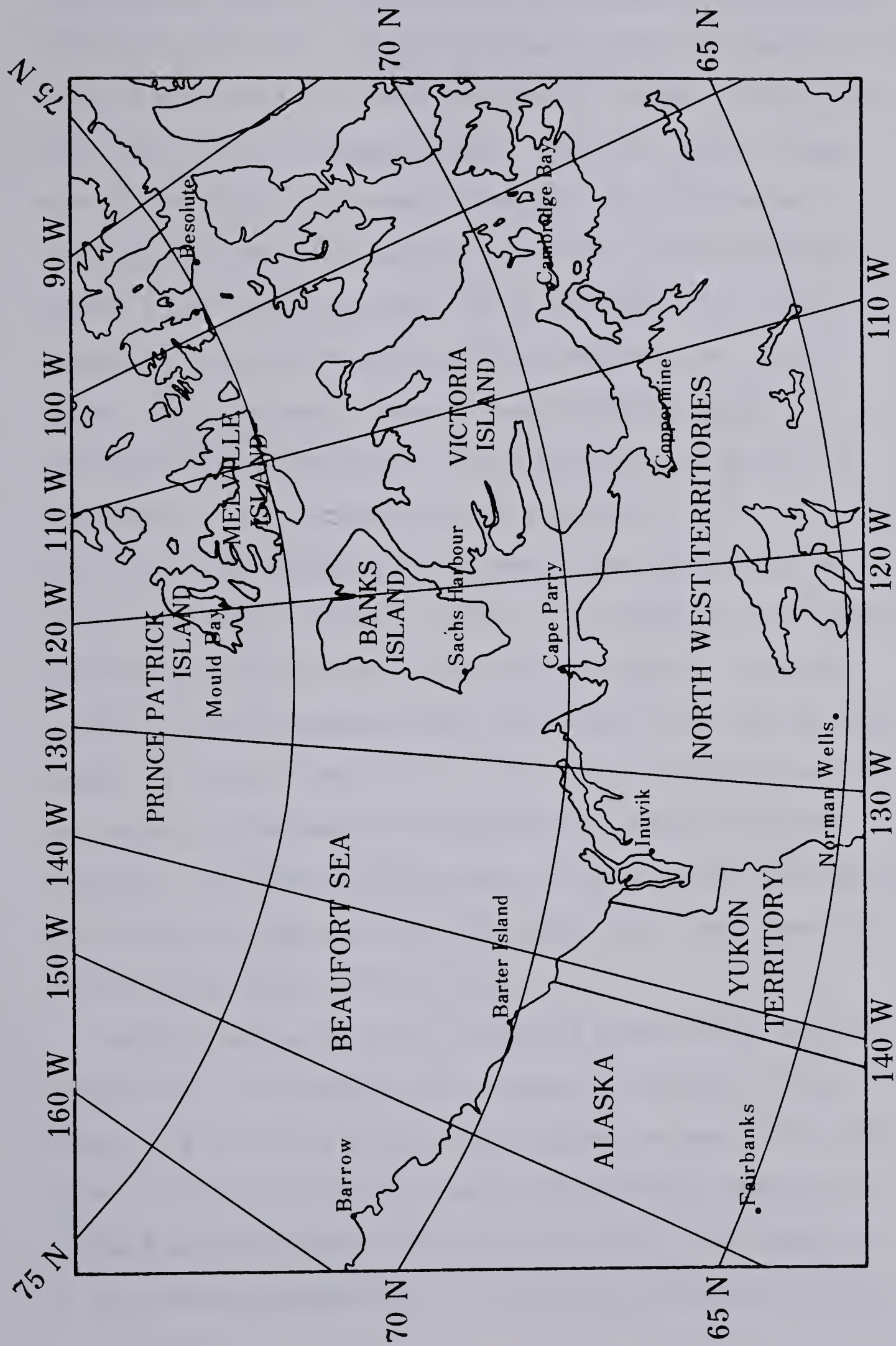


FIGURE 1.1 Geography of the northwestern Canadian Arctic. Locations of selected meteorological stations are also included.





the Western Canadian Arctic, and also locations of meteorological stations in this area. During the summer months, the region to the west and south of Banks Island is normally ice-free, while to the north, the ice cover remains intact. Figure 1.2 shows a larger view of the island with contour elevations and geographical locations included. The island is about 200 by 350 kilometers in extent; it is fairly uniformly flat in the center with higher elevations at the northern and southern ends and, to a lesser degree, along the eastern coast. Sumner (1977) suggests that in coastline regions consisting of hills and valleys, "sea breeze occurrence . . . is probably as much a function of the topography as it is of the atmosphere and related factors generating the breeze circulation" (Sumner, pg 200). The relatively flat western coastline should therefore be the primary region of interest in a study of a pure thermally-driven sea breeze circulation on Banks Island. A seaward flow of warm air from this coastline over the cold waters of the Beaufort Sea might result in fog along the shoreline. The absence of fog when the synoptic situation suggests an offshore flow might therefore be a hint that a sea breeze type of circulation exists in this area.

Banks Island is snow free during the summer months (Hare and Orvig, 1958). The geology of the western and central portions of the island is a mixture of glacial drift, gravel and sand. The higher elevation along the northern, eastern and southern coastlines is composed mainly of barren rock or glacial drift. The vegetation of the island is characteristic of an Arctic semi-desert; mosses,



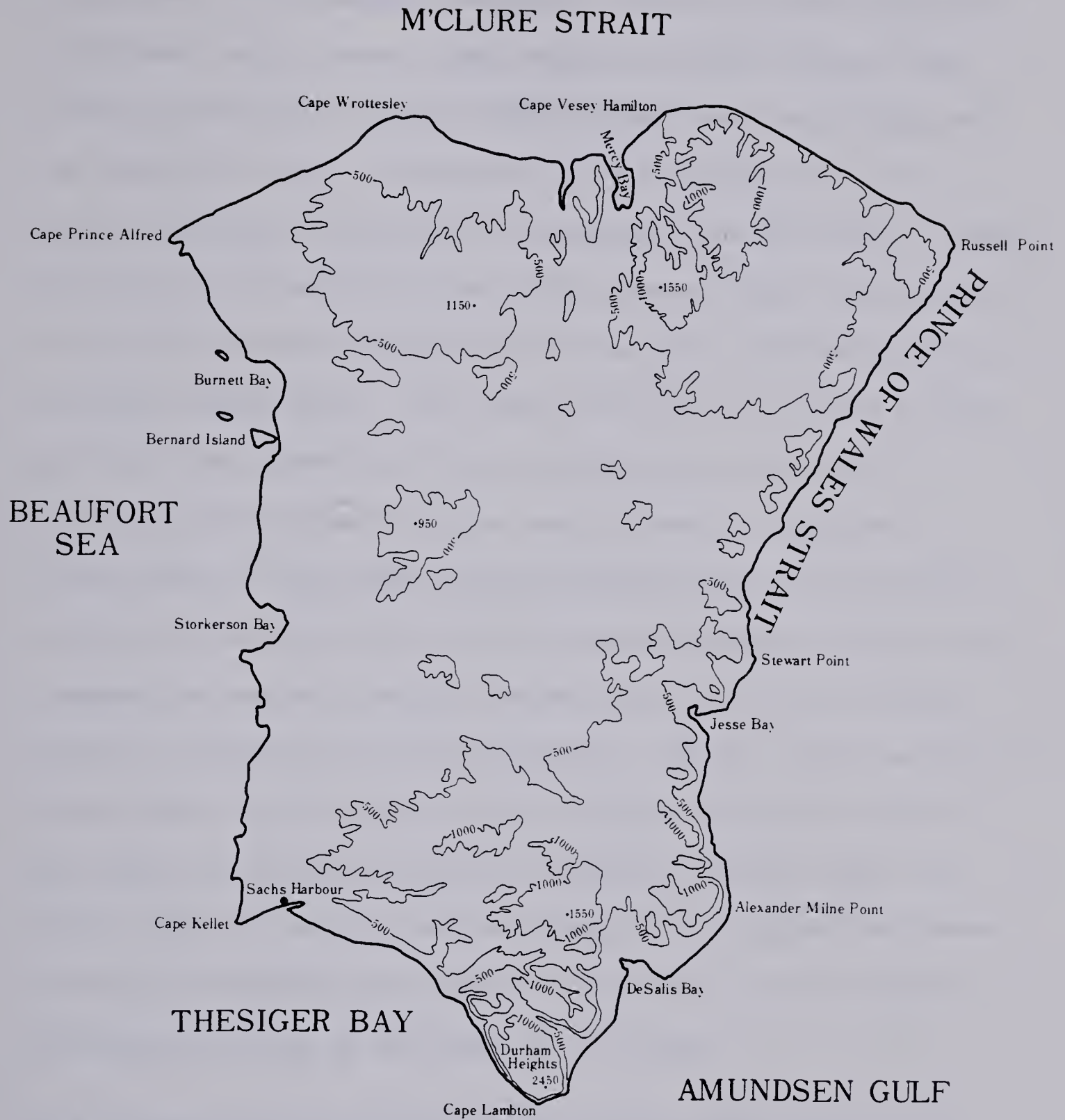


FIGURE 1.2 Topography of Banks Island. Elevations are in feet above sea level. Geographical features around the island are also identified. (After Department of Energy, 1974a and 1974b)



lichens and grasses, with some low shrub growth along the major stream beds of the western coastline. With such sparse vegetation, the island should possess a heat capacity not much greater than that of barren rock, and will therefore heat and cool quickly over the course of a day. It should be noted that there will be a fairly large daily variation of temperature over the island. Though the sun does not set during the Arctic summer "night", the elevation of the sun above the horizon is low enough that its heating effect is small (Green, 1977). Also, under the influence of even a light gradient wind, advection of cold air from the ice and water surrounding the island will also tend to lower the nighttime temperatures. Thus, Banks Island experiences much the same daily temperature variation as is found in coastal regions elsewhere: the temperature reaches a maximum several hours after local noon and falls to a minimum in the early morning. However, nighttime insolation, though small, nevertheless prevents overnight temperature falls of the magnitude experienced in more southerly locations (Hare and Orvig, 1958). Thus, the daytime character of a typical sea breeze circulation should be maintained in the Arctic, but the nighttime land breeze portion of the cycle may not occur.

### 1.3 Synoptic Circulation Over Banks Island In Mid July of 1977

The surface temperature field of Banks Island will only be visible under clear conditions. Absence of cloud above most of the island was therefore the first criterion for choosing possible days for study. The synoptic situation on selected cloud-free days was the next criterion considered. Since the western coastline of





Banks Island is the most conducive to pure breeze circulation, both conditions of no gradient flow and conditions of a light easterly flow, producing offshore winds along the west coast, were considered. Finally, surface wind reports from Sachs Harbour were consulted. Sachs Harbour is located on the southwestern coast of Banks Island (Figures 1.1 and 1.2) and is the only meteorological station on the island. If the wind reports from Sachs Harbour suggested a sea breeze circulation, it was likely that a sea breeze would also exist along the remainder of the western coastline.

A week of cloud-free days during mid July of 1977 was chosen for further examination. Surface-pressure charts and 500-mb upper-air charts produced by the Atmospheric Environment Service at Edmonton, Alberta were used to study the synoptic background. Surface-pressure charts were available for 0000Z and at three-hour intervals thereafter for each day. The surface situation at 1800Z (1000 local time at Sachs Harbour) was chosen as being representative of the circulation before the onset of the coastal sea breeze. 500-mb charts were available for 0000Z and 1200Z only; those at 0000Z (1600 local time on the preceding day at Sachs Harbour) were used to show the upper-air circulation. Figures 1.3, 1.5 and 1.7 show surface-pressure charts for July 14 to July 16 at 1800Z for the region around Banks Island. Figures 1.4, 1.6 and 1.8 show 500-mb charts for July 15 to July 17 at 0000Z for the same region. Comparison of the surface charts indicated little change over the three-day period. The surface pattern was dominated by a high pressure system over the Beaufort Sea which resulted in a 10 to 15 knot (5 to 8 m/s) northerly to northeasterly flow over Banks Island.





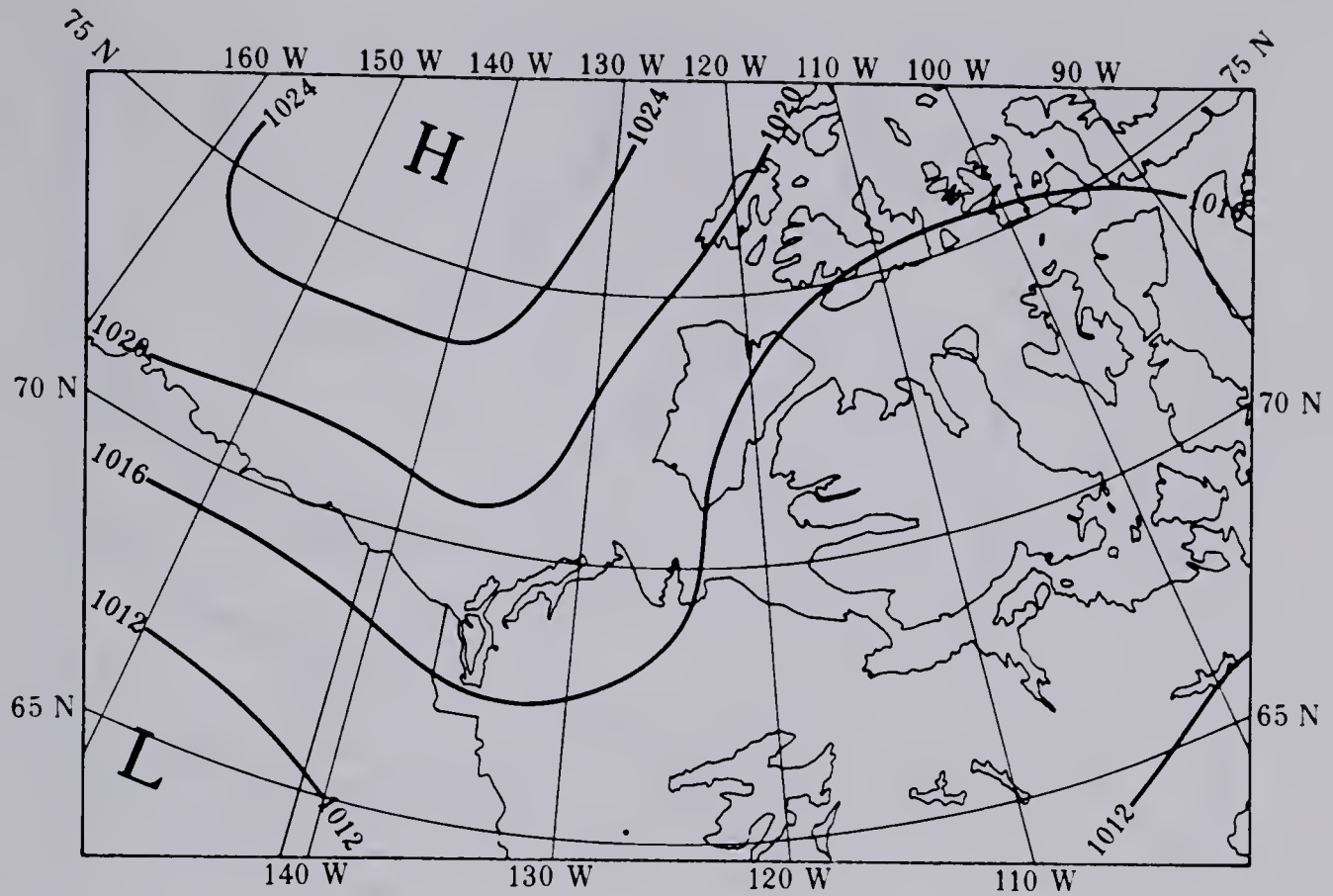


FIGURE 1.3 Mean sea level pressure analysis of the northwestern Canadian Arctic at 1800Z on July 14, 1977. Isobars are labelled in millibars.

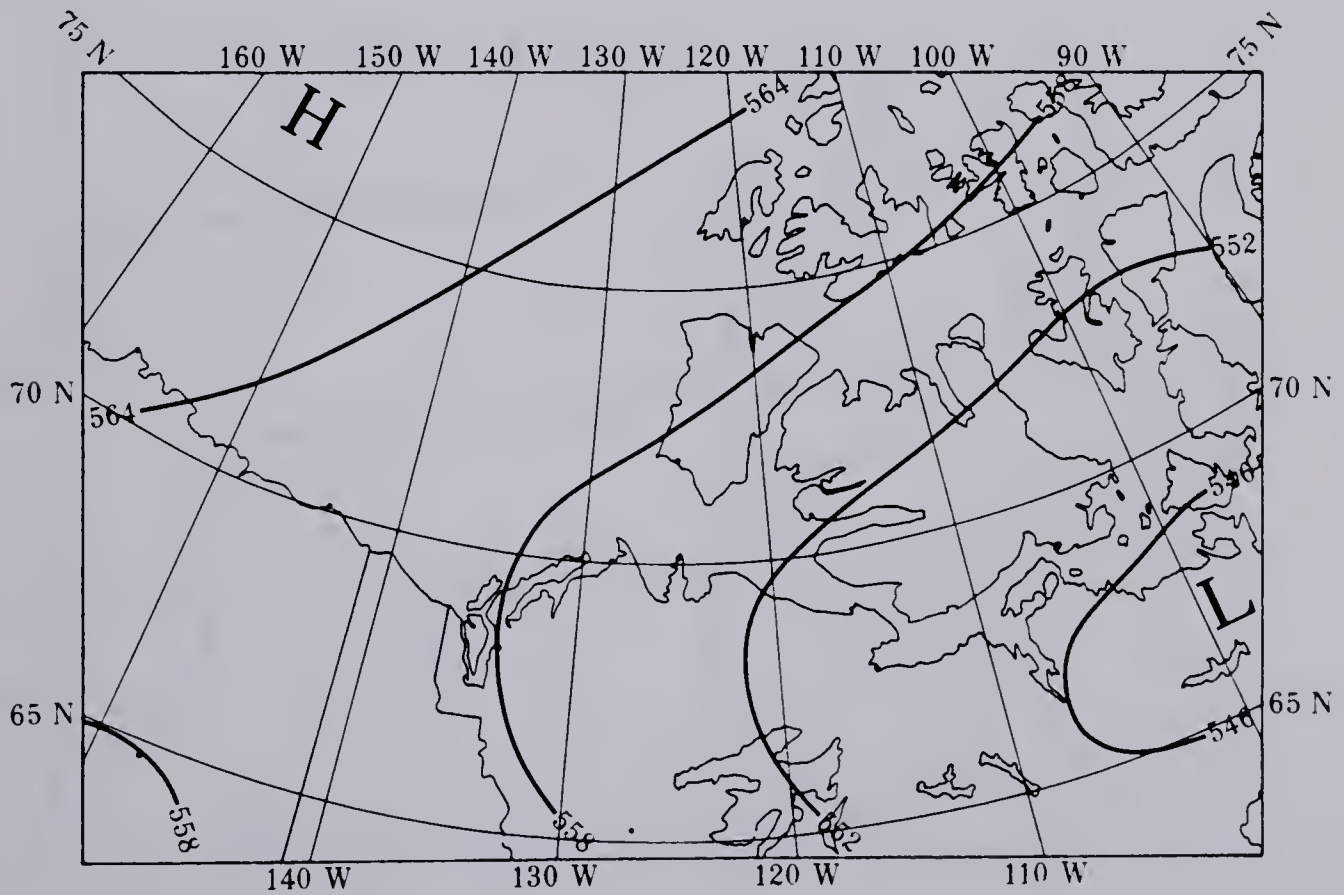


FIGURE 1.4 500-mb constant pressure analysis of the northwestern Canadian Arctic at 0000Z on July 15, 1977. Isobars are labelled in geopotential decameters.



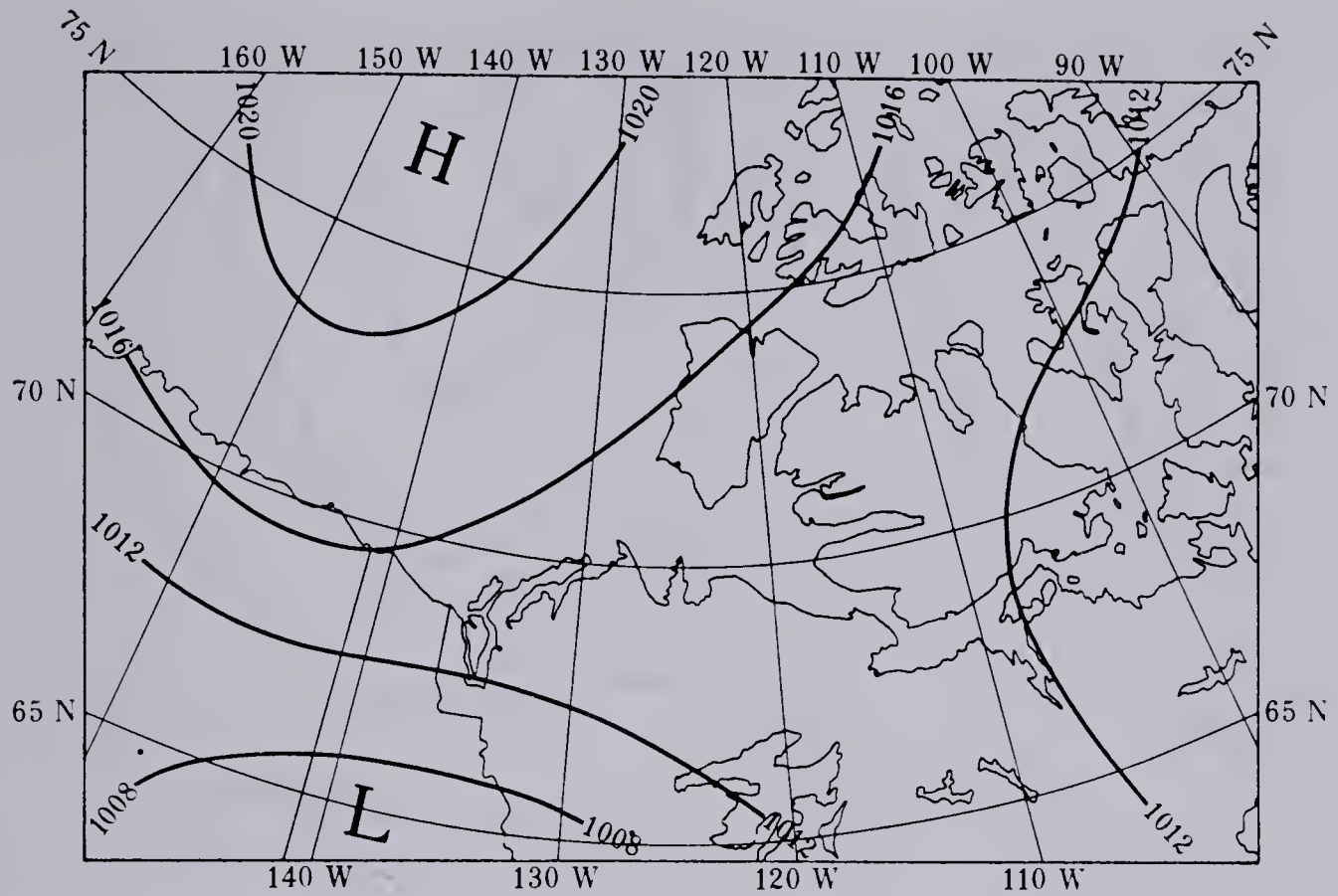


FIGURE 1.5 Mean sea level pressure analysis of the northwestern Canadian Arctic at 1800Z on July 15, 1977. Isobars are labelled in millibars.

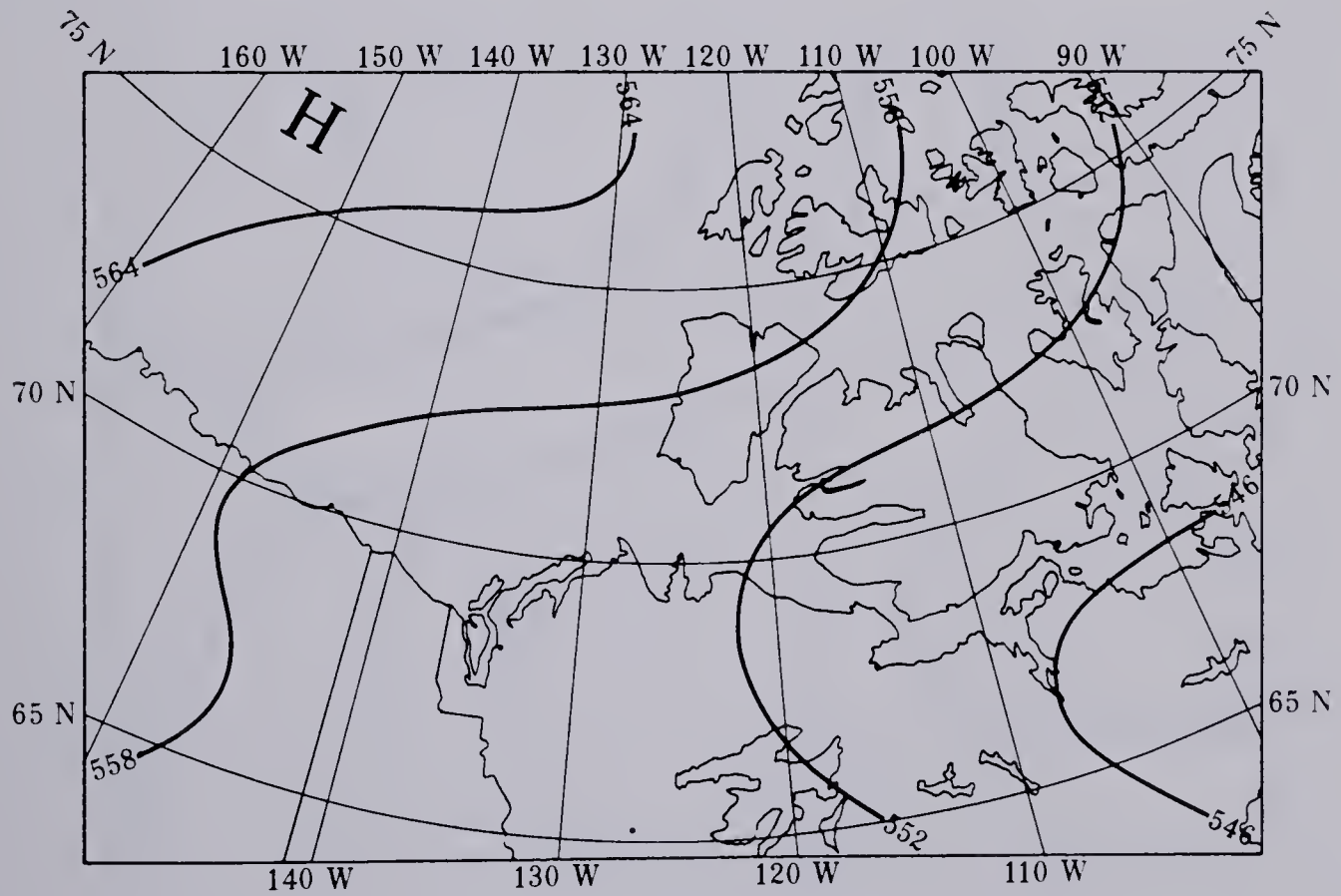


FIGURE 1.6 500-mb constant pressure analysis of the northwestern Canadian Arctic at 0000Z on July 16, 1977. Isobars are labelled in geopotential decameters.





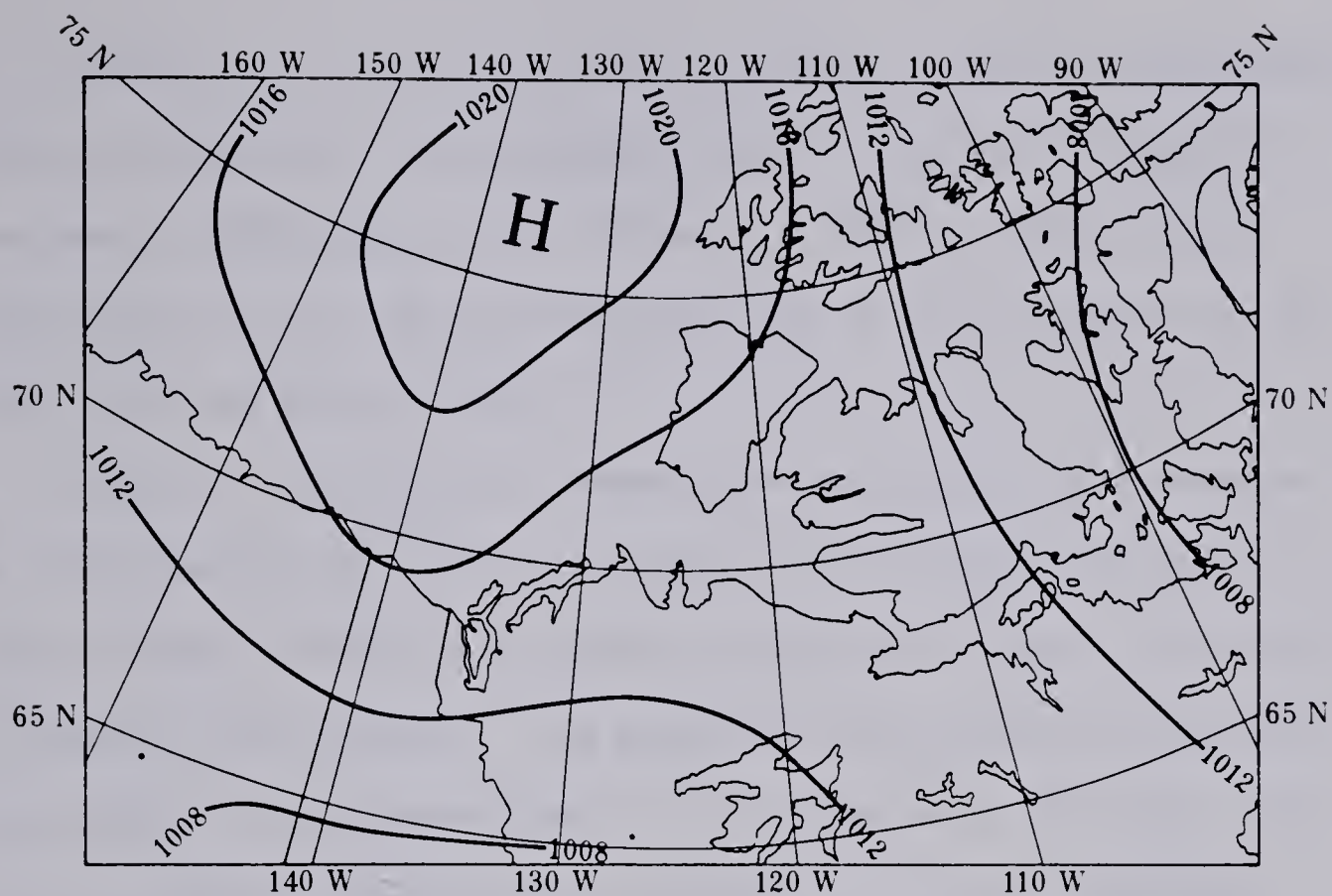


FIGURE 1.7 Mean sea level pressure analysis of the northwestern Canadian Arctic at 1800Z on July 16, 1977. Isobars are labelled in millibars.

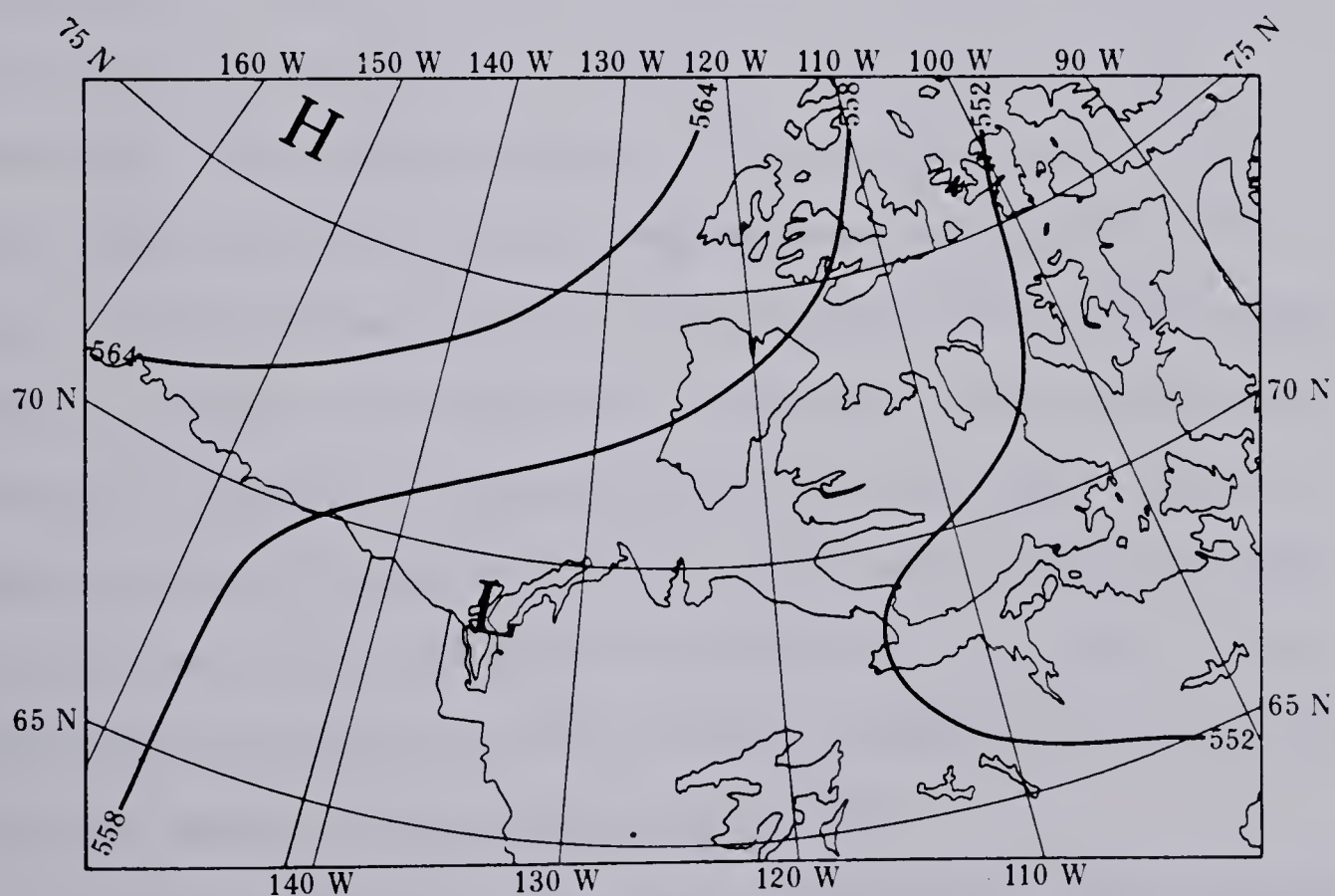


FIGURE 1.8 500-mb constant pressure analysis of the northwestern Canadian Arctic at 0000Z on July 17, 1977. Isobars are labelled in geopotential decameters.





Comparison of the 500-mb charts showed a similar northeasterly flow pattern aloft. The synoptic situation was thus conducive to sea breeze development along the western coast of Banks Island, particularly on the latter two days (July 15 and 16) when the low-level flow was more easterly.

Table 1.1 lists winds, temperatures and cloud cover observed at Sachs Harbour on July 14, 15 and 16 of 1977. On July 14, the wind at Sachs Harbour was northerly throughout the day, with speeds of about 15 knots (8m/s). The gradient flow appeared to have been too strong to allow development of a sea breeze on this day. On July 15, the wind was from the southeast in the early morning, shifting to easterly by mid-morning. The abrupt shift to a southwesterly flow around 2200Z (1600 local time) marked the appearance of the sea breeze. The breeze reached its maximum speed of 10 knots (5m/s) only one hour later, and slowly died away thereafter. The late appearance of the sea breeze on this day was likely due to the fairly strong gradient flow earlier. On July 16, the wind was easterly in the morning, but slightly weaker than on July 15. The shift to a southwesterly flow occurred much earlier on this day, at about 1900Z (1100 local time). The sea breeze reached its maximum velocity in the early afternoon (2300Z or 1500 local time), and died away thereafter. The shift in wind direction to northerly by 0100Z on July 17 showed the effect of the Coriolis force on the sea breeze on this day.

Further evidence of a sea breeze circulation on July 15 and 16 could be found by examining the hourly temperature and cloud reports.



TABLE 1.1 Wind, temperature and cloud abstracts for Sachs Harbour (YSY) on July 14, 15 and 16 of 1977. (Wind speeds in knots, Temperature in degrees Celsius, Cloud height in hundreds of feet above surface, Cloud amount in tenths of sky obscured)

HOUR (GMT)	WIND		TEMPERATURE	CLOUD	
	DIRECTION	SPEED		HEIGHT	TYPE/AMOUNT
July 14	08	360/14	2	X/F/10	
	09	360/16	2	X/F/10	
	10	360/18	1	X/F/10	
	11	360/16	1	X/F/10	
	12	10/15	1	X/F/10	
	13	-	-	-	
	14	360/15	2	X/F/6	2/ST/3
	15	-	-	-	
	16	-	-	-	
	17	360/13	7		230/CI/4+
	18	360/12	8		230/CI/4+
	19	350/15	8		230/CI/4+
	20	350/13	10		230/CI/3+
	21	350/15	10		230/CI/2
	22	340/16	10		230/CI/1
	23	350/15	12		230/CI/1
July 15	00	350/14	13	20/CI/1	230/CI/1
	01	3-0/15	13	20/CI/1	230/CI/1
	02	360/15	13	20/CI/1	230/CI/1
	03	350/15	13	20/CI/1	230/CI/1
	04	360/13	13	20/CI/1	230/CI/1
	05	30/10	12	20/CI/1	230/CI/2
	06	110/06	10	20/CI/2	230/CI/2+
	07	120/08	9	30/SC/2	230/CI/1



TABLE 1.1 (continued) Wind, temperature and cloud abstracts for  
Sachs Harbour.

HOUR (GMT)		WIND DIRECTION/SPEED	TEMPERATURE	CLOUD HEIGHT/TYPE/AMOUNT
July 15	08	120/10	9	30/SC/2 230/CI/2*
	09	130/07	8	30/SC/2 230/CI/2*
	10	120/06	8	30/SC/2 230/CI/2*
	11	110/07	7	30/SC/1 230/CI/2
	12	120/09	8	30/SC/1 230/CI/3*
	13	-	-	-
	14	90/12	8	30/SC/1 180/AS/2 230/CI/3*
	15	-	-	-
	16	70/12	10	20/SC/1 90/AS/1 230/CI/3*
	17	70/12	10	20/CU/1 230/CI/3*
	18	80/10	12	20/CU/1 230/CI/2*
	19	-	-	-
	20	-	-	-
	21	90/10	14	25/CU/3 230/CI/0
	22	190/07	14	25/CU/4 230/CI/1
	23	230/10	13	25/CU/5 230/CI/1
July 16	00	230/09	13	25/CU/5 230/CI/1
	01	-	-	-
	02	220/07	13	25/CU/3 230/CI/1
	03	220/06	12	25/CU/1 70/AC/3 230/CI/1*
	04	-	-	-
	05	250/04	12	40/SC/6 230/CI/1
	06	250/04	12	40/SC/6 230/CI/1
	07	-	-	-





TABLE 1.1 (continued) Wind, temperature and cloud abstracts for Sachs Harbour.

WIND		TEMPERATURE	CLOUD	
HOUR (GMT)	DIRECTION/SPEED		HEIGHT/TYPE/AMOUNT	
July 16	08	CALM	11	40/SC/5
	09	CALM	11	40/SC/2
	10	CALM	11	40/SC/1
	11	60/07	11	40/SC/1
	12	90/07	12	40/SC/1 210/CI/0
	13	70/09	12	40/SC/1 210/CI/0
	14	90/08	13	40/SC/1 210/CI/0
	15	130/05	13	210/CI/0
	16	70/09	13	210/CI/0
	17	90/09	15	30/CU/1 210/CI/1
	18	-	-	-
	19	230/08	15	30/CU/1 210/CI/1
	20	190/08	15	30/CU/1 210/CI/1
	21	220/07	16	30/CU/2 210/CI/1*
	22	220/07	16	30/CU/2 210/CI/1*
	23	250/10	16	30/CU/4 210/CI/1*
July 17	00	270/03	16	30/CU/3 210/CI/1*
	01	320/09	17	30/CU/1 210/CI/2*
	02	280/07	16	30/CU/1 210/CI/2
	03	170/00	17	30/CU/1 210/CI/1
	04	30/11	17	30/CU/1 210/CI/1
	05	30/14	15	30/CU/1 210/CI/1
	06	40/13	15	30/CU/1 210/CI/1
	07	-	14	30/S-/- 210/CI/2

- Denotes missing report      X Denotes surface phenomenon  
 \* Denotes amount of cloud greater than listed, but thin enough to see through

Types of Cloud    F Fog    ST Stratus    SC Stratocumulus  
                          CU Cumulus    AS Altostratus    AC Altocumulus  
                          CI Cirrus





Comparison of overnight minimum temperatures to maximum daytime temperatures showed that on July 14 the temperature rose  $11^{\circ}\text{C}$  during the day, while only  $6^{\circ}\text{C}$  increases were observed on July 15 and 16. The advection of cooler air onshore during the sea breeze days was likely to have been one cause of the smaller temperature changes.

The extent of convective activity at Sachs Harbour on July 15 and 16 also suggested the occurrence of a sea breeze on these days. Maximum convective activity is expected in the afternoon, and on all three days listed in Table 1.1, the largest amounts of cumulus cloud occurred at this time. However, while only one-tenth of cumulus cloud was observed on July 14, five-tenths and four-tenths of cumulus were reported on July 15 and 16 respectively. It is likely that the enhanced cumulus formation on the latter two days was the result of convergence between the onshore flow of the sea breeze and the prevailing offshore flow suggested by the surface charts.

Examination of upper-air wind profiles on the three days illustrated the character of the sea breeze observed at Sachs Harbour. Table 1.2 contains wind and temperature abstracts from radiosonde ascents at Sachs Harbour at 0000Z and 1200Z of July 15, 16 and 17 of 1977. As can be seen, the vertical temperature profile changed little over the three day period, while there was considerable variation in the winds, particularly in the low levels. The winds were plotted in Figures 1.9a to 1.9f to show the variation of wind speed with height.



TABLE 1.2 Wind and temperature profiles for Sachs Harbour (YSY) on July 15, 16 and 17 of 1977. (Wind speed in knots, Temperature in degrees Celsius, Pressure height in millibars, Surface pressure height approximately 1015mb)

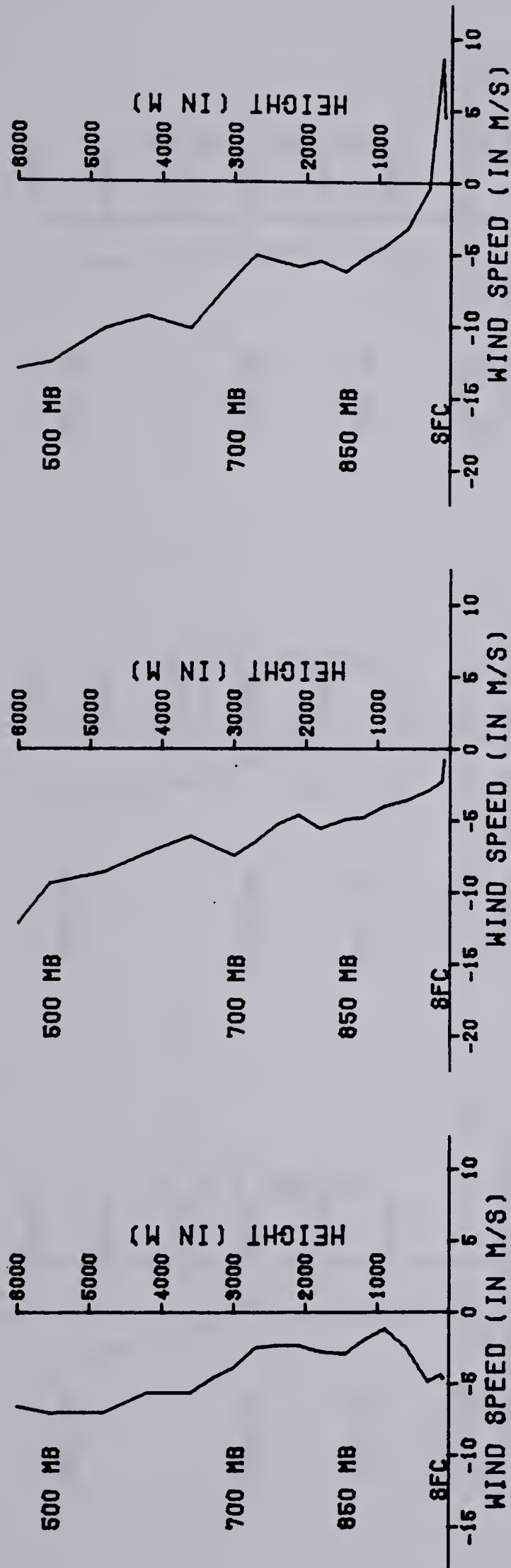
PRESSURE HEIGHT	JULY 15, 1977 WIND	0000Z	JULY 15, 1977 WIND	1200Z
	DIRECTION/SPEED	TEMPERATURE	DIRECTION/SPEED	TEMPERATURE
SURFACE	350/14	13	120/09	8
1000	340/17	11.2	80/06	8.2
850	25/06	4.2	55/10	3.4
700	20/08	-3.7	55/16	-5.3
500	65/15	-23.3	55/20	-21.7
400	80/15	-35.7	60/22	-34.5
250	70/18	-47.3	-	-

PRESSURE HEIGHT	JULY 16, 1977 WIND	0000Z	JULY 16, 1977 WIND	1200Z
	DIRECTION/SPEED	TEMPERATURE	DIRECTION/SPEED	TEMPERATURE
SURFACE	230/09	13	90/07	12
1000	240/18	13.0	90/05	10.4
850	70/14	2.0	70/08	1.6
700	80/17	-5.7	100/11	-7.1
500	60/26	-23.7	90/20	-21.5
400	65/32	-34.5	85/27	-32.9
250	60/25	-45.1	90/31	-51.5

PRESSURE HEIGHT	JULY 17, 1977 WIND	0000Z	JULY 17, 1977 WIND	1200Z
	DIRECTION/SPEED	TEMPERATURE	DIRECTION/SPEED	TEMPERATURE
SURFACE	270/03	16	50/09	11
1000	270/07	15.4	60/10	11.4
850	75/13	3.4	355/08	3.4
700	115/13	-5.5	20/04	-4.9
500	90/13	-21.5	95/12	-21.7
400	80/16	-31.5	80/18	-31.5
250	90/36	-54.7	70/32	-54.9

- Denotes missing report





a) 0000Z July 15

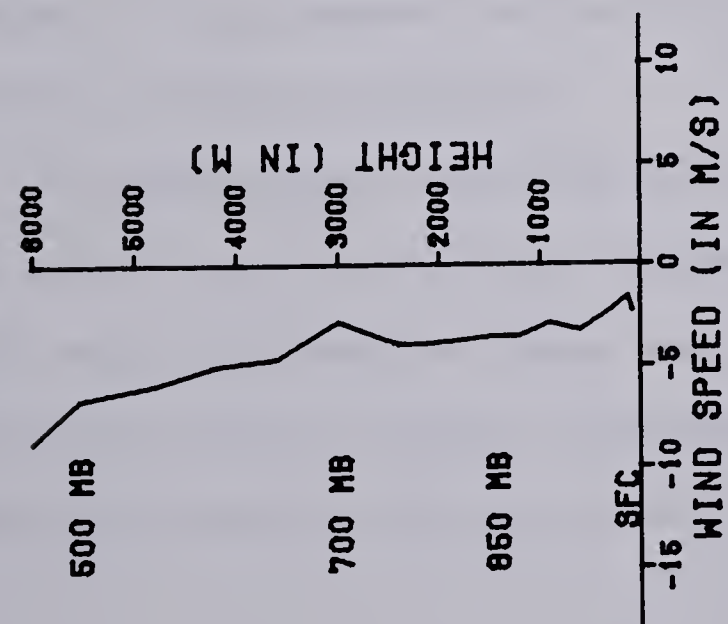
b) 1200Z July 15

c) 0000Z July 16

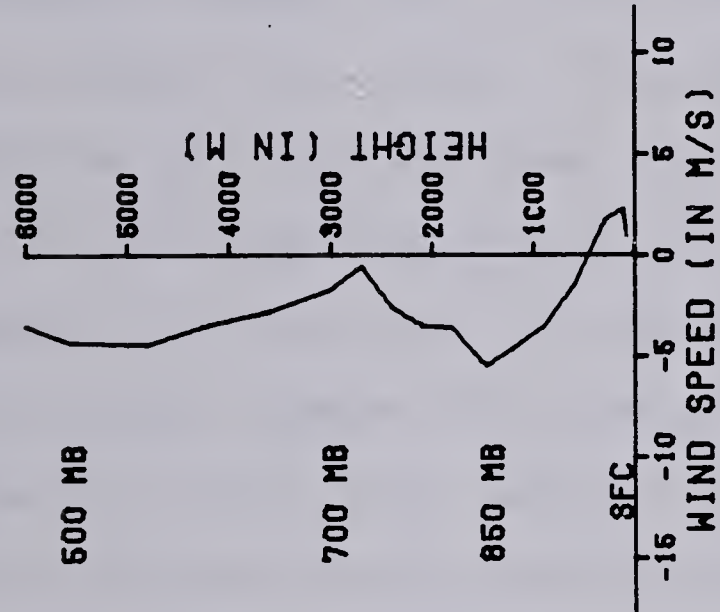
FIGURE 1.9 Wind profiles from Sachs Harbour on July 14, 15 and 16 of 1977. Wind speeds are given as a component of the onshore wind, with winds from 220° considered as directly onshore. The labels along the left side of each graph show approximate pressure height levels in millibars.



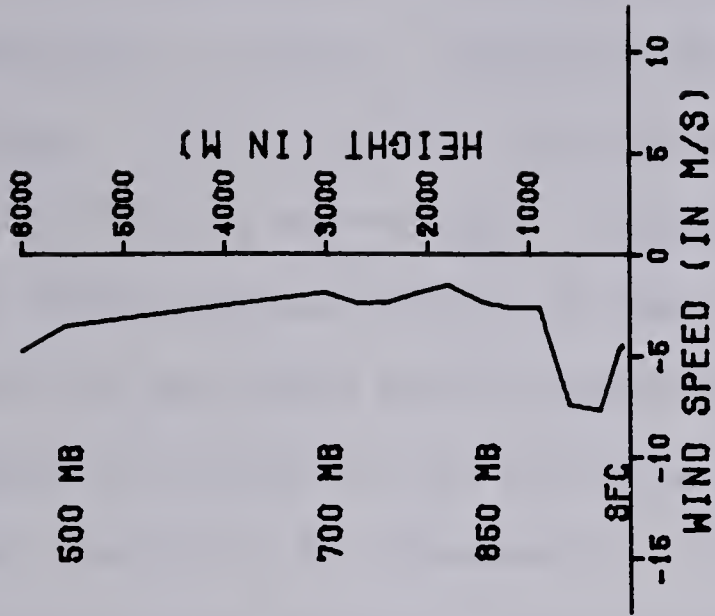




d) 1200Z July 16



e) 0000Z July 17



f) 1200Z July 17

FIGURE 1.9 (continued) Wind profiles from Sachs Harbour.



The magnitude of the wind was expressed as either an onshore (positive) or offshore (negative) component of the wind at Sachs Harbour. Winds from  $220^{\circ}$  true were considered to be directly onshore. The 1200Z plots corresponded to nighttime wind conditions, while the 0000Z plots corresponded to wind conditions near the time at which the sea breeze would be expected to have been strongest. Figure 1.9a (0000Z on July 15) shows the wind profile observed at Sachs Harbour on the afternoon of July 14. No onshore component to the wind can be seen. The nighttime wind profiles for the three day period (Figures 1.9b, 1.9d and 1.9f) likewise show no evidence of an onshore flow. However, the profiles shown in Figures 1.9c (0000Z on July 16 or 1600 local time on July 15) and 1.9e (0000Z on July 17 or 1600 local time on July 16) give evidence of an onshore flow in the lowest few hundred meters, while the upper flow remained offshore. The strongest onshore flow occurred just above the surface, with a magnitude of about 9m/s (17 knots) on July 15 and 2m/s (4 knots) on July 16. Also, the offshore flow at mid-levels (850mb or about 1500m) was stronger when the low level onshore flow was present, and extended through a deeper layer than did the low level circulation.

The meteorological evidence thus suggests the existence of a sea breeze circulation at Sachs Harbour on July 15 and July 16 of 1977, but no apparent sea breeze development on July 14. It was therefore decided to produce temperature-field plots of Banks Island from satellite imagery of July 15 and 16. These plots



show the development of the thermal patterns of Banks Island during the time period at which sea breezes occurred at Sachs Harbour, and identify features which mark this circulation.





## CHAPTER II

### INFRARED SATELLITE DATA

#### 2.1 Introduction

The satellite information used in this study was taken from the NOAA-5 satellite, a second-generation meteorological satellite. Complete descriptions of the design and operating parameters of this satellite can be found in Fortuna and Hambrick (1972) and Schwalb (1972). Only a general description of the satellite characteristics is contained herein.

The NOAA-5 satellite occupies a near polar orbit at a height of approximately 1525 kilometers above the Earth's surface, with an orbital period of approximately 2 hours, and a regression rate of approximately 30 degrees longitude west per orbit. These parameters are such that the satellite is Sun-synchronous; that is, the satellite crosses the equator at a certain longitude at the same local times each day, once on an ascending (or northward travelling) sector of an orbit, and once approximately 12 hours later on a descending (southward) sector of an orbit. The satellite also has a precession rate of approximately one degree longitude east per day. This ensures nearly-constant satellite orientation over the course of the year.

#### 2.2 Satellite Scanning

The satellite carries two scanning radiometers which measure the intensity of radiation in the visible part of the spectrum (0.5 to 0.7 micrometers) and in the infrared window region



(10.5 to 12.5 micrometers). The radiometers contain a scanning mirror which rotates at 48 revolutions per minute about the axis of the satellite's direction of motion. Therefore, the radiometers scan the Earth in strips perpendicular to the satellite's orbital path and, when combined with the motion of the satellite itself, provide complete areal coverage of any region over which the satellite passes.

However, only the central portion of each strip or "scan" contains useful information. Since the scanning mirror rotates at a constant rate, the minimum area on the Earth which the radiometer can resolve increases as the angle of scanning steepens. This leads to drastic foreshortening of the satellite image towards the horizons. The useable portion of each scan is centered around the satellite subpoint, directly below the satellite (see Figure 2.1). Anderson and Veltishchev (1973) suggest that the "region of reliable data" lies inside a zenith angle of about  $60^{\circ}$ , implying a coverage at the equator of about  $32^{\circ}$  of longitude or about 3500 kilometers (1880 nautical miles). Since the satellite moves  $30^{\circ}$  of longitude west for each orbit, there will be some overlap of scanning on successive orbits. In polar regions, this overlap is more pronounced, and it is usual for a given area to be observed on several consecutive orbits.



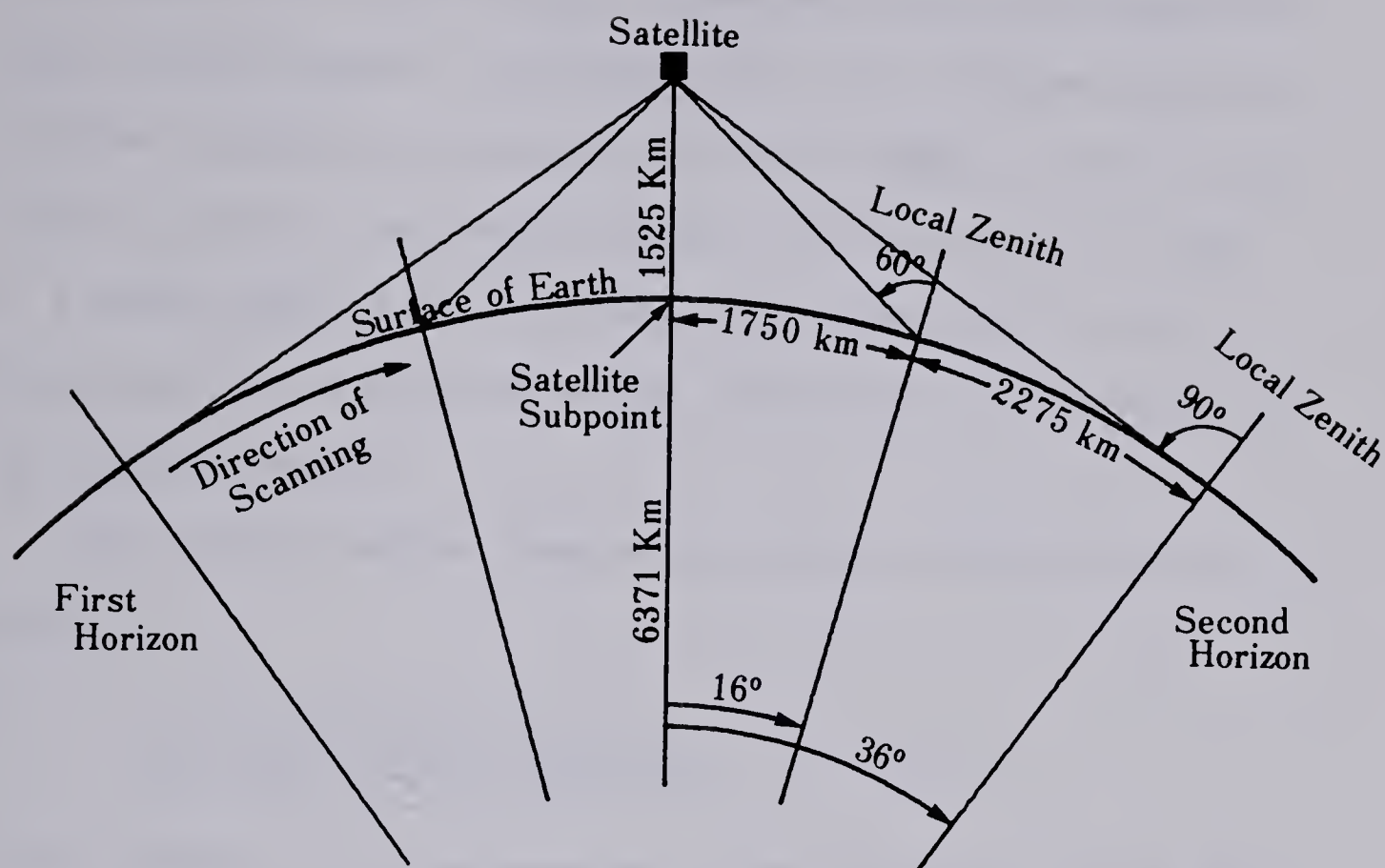


FIGURE 2.1 Geometry of the NOAA-5 scanning radiometer. The satellite is heading out of the paper. The region of reliable data lies between the  $60^\circ$  zenith angles. The resolution as measured by the radiometer's field of view decreases by a factor of 3.3 at a zenith angle of  $60^\circ$ . (After Anderson and Veltishchev, 1973)

### 2.3 Satellite Resolution

The resolution of the NOAA-5 scanning radiometer is a measure of the minimum area on the Earth's surface which the radiometer sensor can accurately resolve. The maximum resolution occurs at the satellite subpoint, and becomes progressively worse at positions further away from the subpoint as a result of enlargement of the radiometer's field of view and foreshortening caused by the curvature of the Earth. The area that the radiometer scans at a





given instant of time therefore becomes more and more rectangular away from the subpoint. The resolution of the infrared sensor of the NOAA-5 satellite is given as 4 nautical miles (7.4 km) at the subpoint, and for the visible sensor, 2 nautical miles (3.7 km). At a zenith angle of  $60^\circ$ , the resolution becomes 12.0 by 24.3 kilometers for the infrared sensor, and 6.0 by 12.1 kilometers for the visible sensor.

The distance between successive scans of satellite data is given by

$$\frac{(2\pi)(6371 \text{ km/orbit})}{(116 \text{ min/orbit})(48 \text{ scans/min})} = 7.2 \text{ km/scan}$$

at the subpoint. Due to curvature of the satellite's orbit, this distance decreases away from the subpoint, though this effect is much smaller than that of foreshortening. Since the satellite's field of view enlarges away from the subpoint, the areas the infrared sensor detects overlap between successive scans, and this overlap increases away from the subpoint. There is also a 3 kilometer "gap" between successive scans in the visible data, but this effect is not apparent in satellite pictures and disappears away from the subpoint.

The satellite laboratory at the University of Alberta is equipped to receive information from the NOAA-5 scanning radiometers over the Automatic Picture Transmission (APT) broadcast link. The received analog signal is converted to a digital value between 0 and 255 at a digitizing rate of 2400 Hertz. For infrared data, the higher numbers represent lower temperatures, and it is possible



to convert these digital values to actual temperature levels. The higher numbers for visible data represent greater reflectivities, and these can be converted to approximate albedo measurements (Anderson and Veltishchev, 1973), though this was not done in this study.

Each satellite scan produces 2500 digital values, of which about 900 contain the infrared radiation data, 900 contain the visible radiation data, and the remaining 700 values contain calibration data and other information. Figure 2.2 shows a typical scan of satellite data as received at the University of Alberta Satellite Laboratory. This scan of data was taken from Orbit 4347 of the NOAA-5 satellite. The information contained in this scan corresponds to the information along the labelled blue lines in Figures 2.3 and 2.5.

The video bandwidth of the APT transmitted infrared signal is 450 Hertz. The Nyquist signalling rate, which is the fastest rate at which independent symbols can be transmitted, is given by twice this bandwidth, or 900 Hertz. Therefore, the analog-to-digital conversion produces  $\frac{2400}{900}$  or 2.7 times as many data values as the satellite sensor can actually resolve. For this reason, it was decided to average each group of three consecutive data values to arrive at each value used in this study. This operation does not reduce the final resolution of the satellite images, but does help to smooth out some of the random noise inherent in the transmitted data, and also reduces the number of data values which must be used by a factor of three. Figure 2.3 shows a temperature field plot of the Banks Island region of Orbit 4347 of NOAA-5 with no averaging of infrared data values.



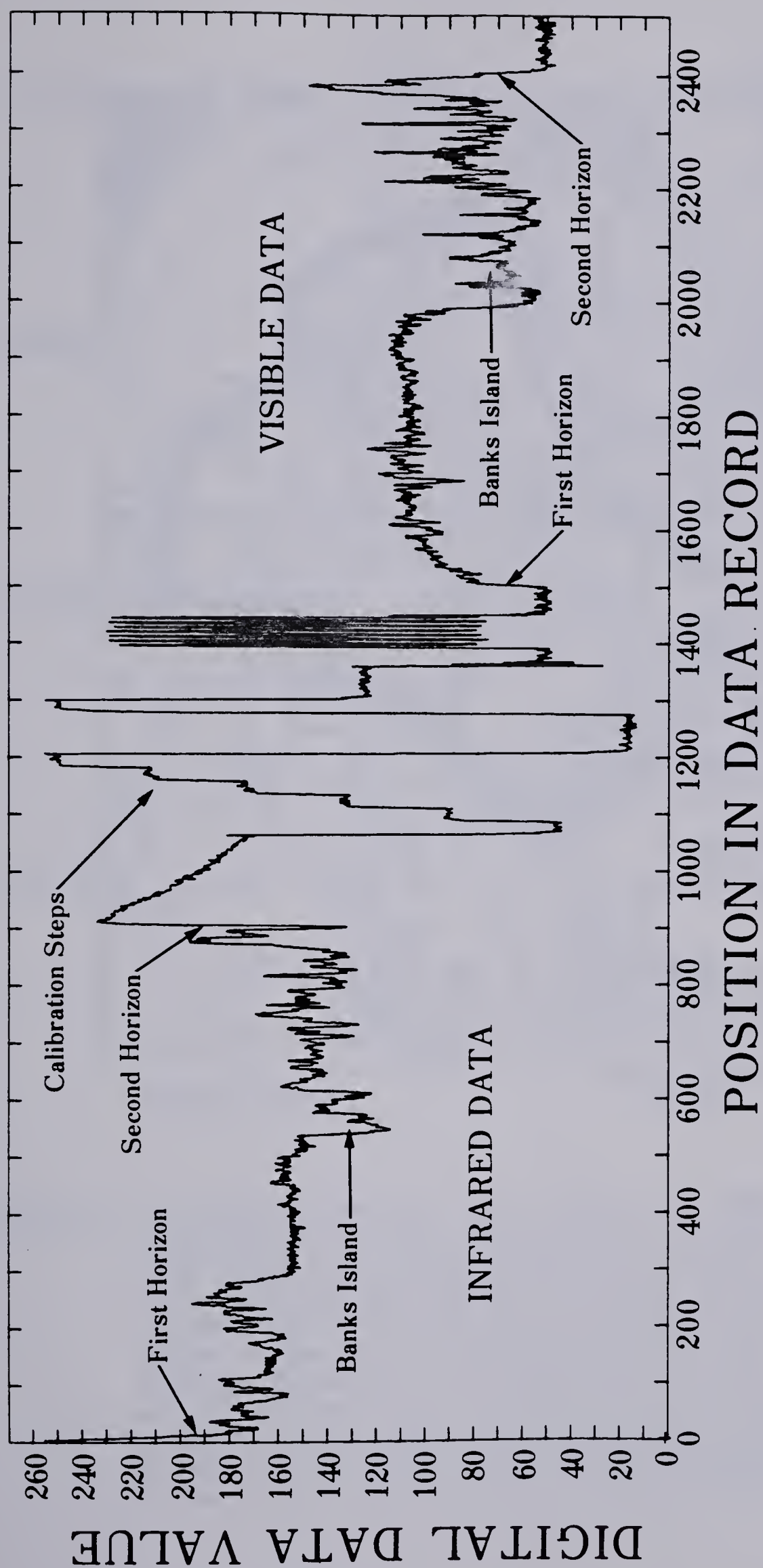


FIGURE 2.2 One scan of satellite information from Orbit 4347 of NOAA-5 on July 15, 1977.





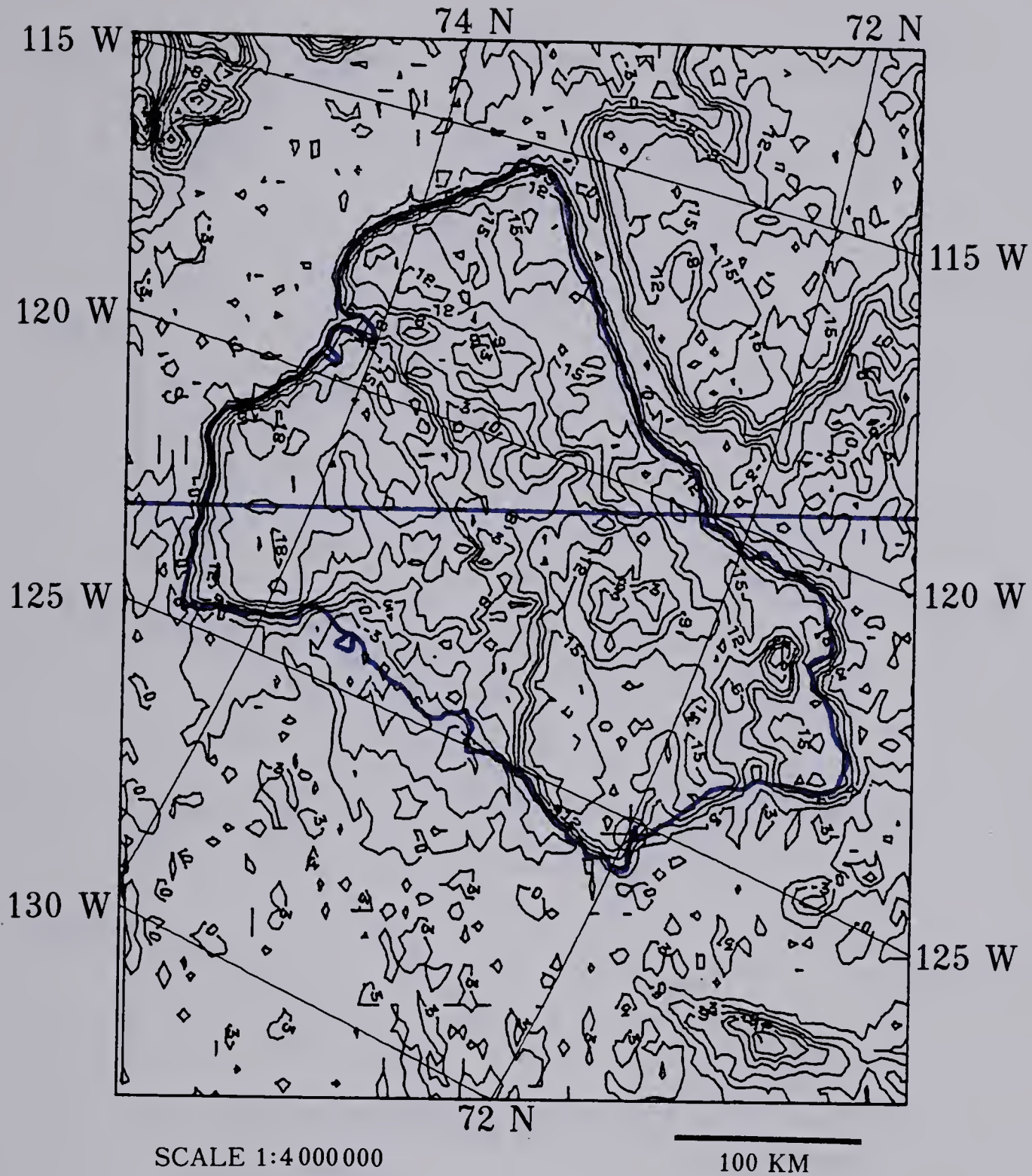


FIGURE 2.3 Unaveraged temperature-field plot of the Banks Island region of Orbit 4347 of NOAA-5 at 2120Z (1320 local time at Sachs Harbour) on July 15, 1977. Contours are labelled in degrees Celsius. Infrared information along the blue line at the center of the plot is from the same scan line shown in Figure 2.2. The blue outline on this and all following plots identifies the coastline of Banks Island. The cross hair symbol on this and all following plots identifies the location of the meteorological station at Sachs Harbour.



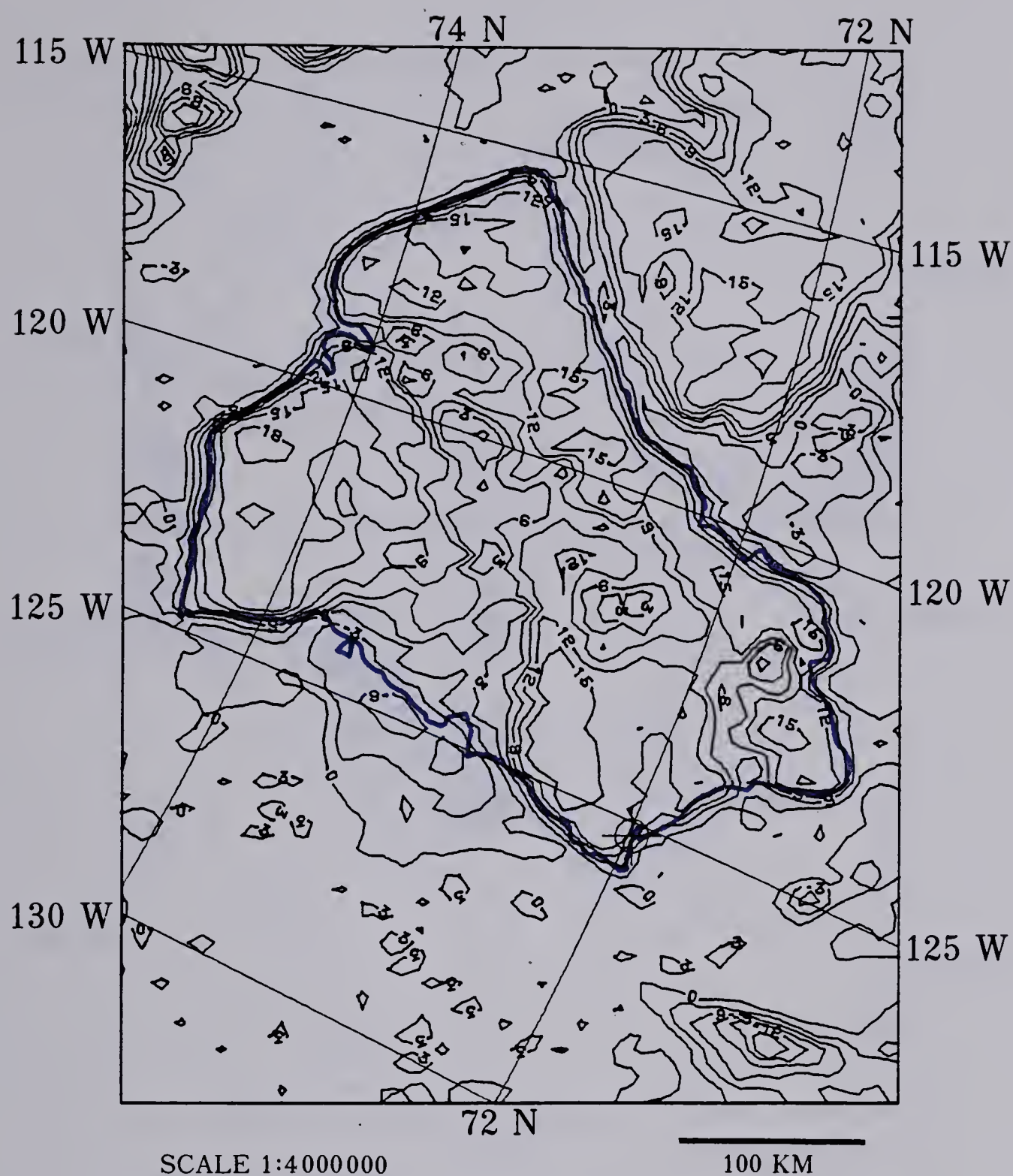


FIGURE 2.4 Averaged temperature-field plot of the Banks Island region of Orbit 4347 of NOAA-5 at 2120Z (1320 local time at Sachs Harbour) on July 15, 1977. Contours are labelled in degrees Celsius.





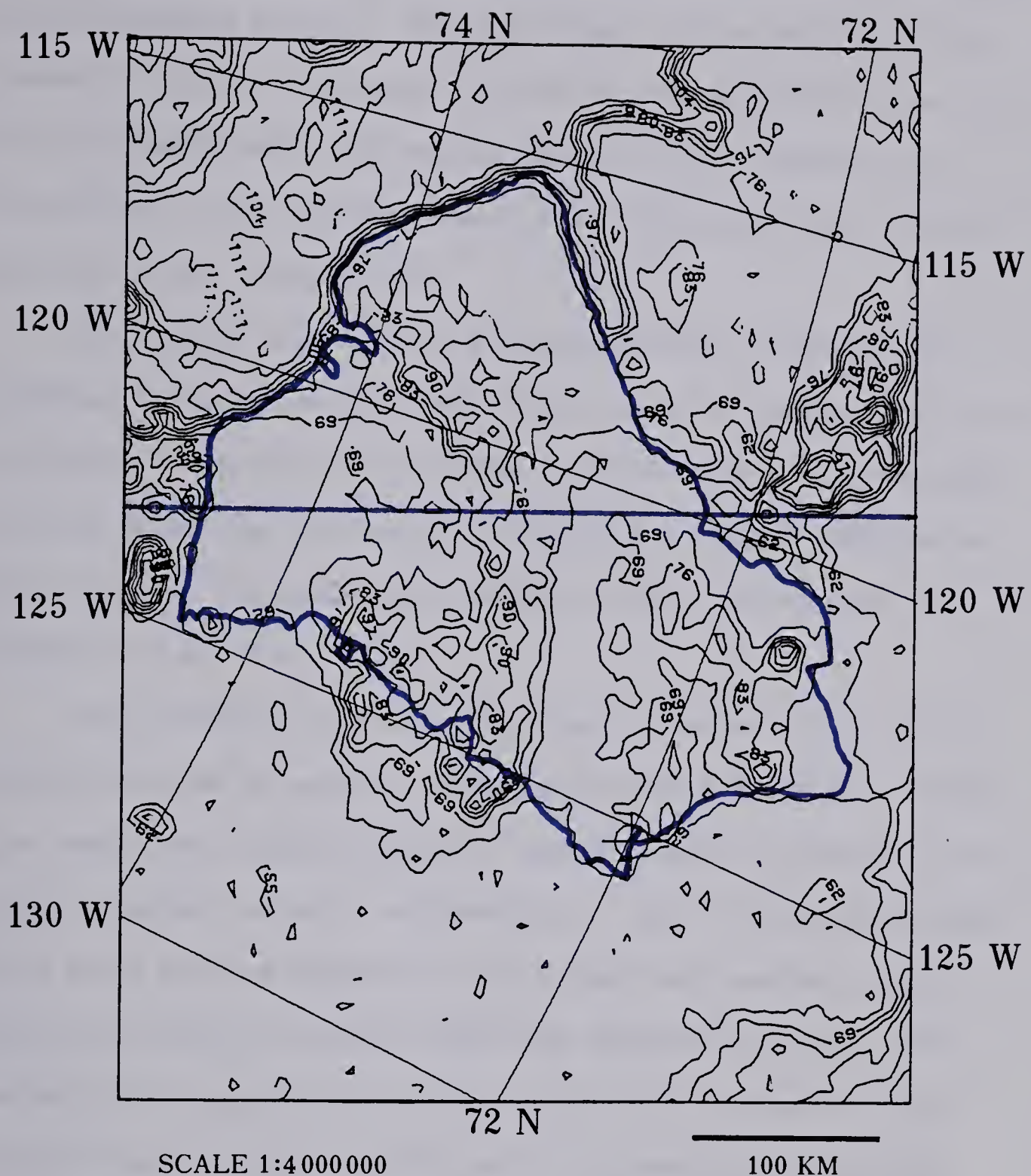


FIGURE 2.5 Reflectance-field plot of the Banks Island region of Orbit 4347 of NOAA-5 at 2120Z (1320 local time at Sachs Harbour) on July 15, 1977. Contours are labelled in digital reflectance values with higher values representing higher reflectivities. Visible information along the blue line at the center of the plot is from the same scan line shown in Figure 2.2.





Figure 2.4 shows the same Banks Island region with the three-point averaging applied. While the large scale patterns of the thermal fields are unchanged between Figures 2.3 and 2.4, much of the very small scale information has been lost. However, the resolution of the infrared sensor does not justify the retention of such finely detailed data.

The visible signal, with a video bandwidth of 900 Hertz, produces 1.3 times as many data values than the sensor resolution justifies. Therefore, when visible data were used, no averaging of data values was carried out. Figure 2.5 shows a reflectance field plot of the same region of Orbit 4347 which appears in Figures 2.3 and 2.4.

The difference in utility between the infrared and visible information can be seen by comparing Figures 2.4 and 2.5. While the coastline of Banks Island is clearly marked in Figure 2.4 by closely packed contours, representing a rapid temperature change from water and ice surfaces to the warmer land surface (except along the western coastline which was obscured by cloud), the corresponding coastline in Figure 2.5 is less obvious at the southern end of Banks Island, due to the small difference in reflectivities between land and open water. However, due to the large difference in reflectivities between land or open water and ice, the limit of ice covered water north of Banks Island is clearly delineated in Figure 2.5, while the small temperature difference between the near freezing open water of the Beaufort Sea and the frozen surface of M'Clure Strait makes the ice-water



boundary more difficult to discern in Figure 2.4, though the ice-land contrast is still well defined.

#### 2.4 Internal Calibration of Infrared Satellite Data

Before launch, the NOAA-5 scanning radiometers were calibrated to a black body. The calibration data consists of curves relating equivalent black-body temperatures to different levels of satellite signal strength for various radiometer temperatures. These calibration levels appear in each satellite scan following the infrared data, as shown in Figure 2.2. If the temperature at which the scanning radiometer operates is known, and it is assumed that all areas being scanned are black bodies, then it is possible to use the calibration data from each satellite scan to convert the digital infrared signals into equivalent temperature levels.

The computer program TAPERD-1 (APPENDIX C.1) was used to extract calibration data from the information received during each satellite orbit. System noise, as evidenced in Figure 2.2 by variations of signal strength at each calibration step level, suggests that some smoothing of the calibration data is necessary. For this reason, nine scans of data were used to provide calibration data for a given area of interest; three scans from the beginning of the area of interest, three from the middle, and three from near the end. Ten data values were extracted from each of the six calibration steps of each scan used. The resulting 90 data values for each of the levels were then averaged to arrive at six calibration data levels corresponding to six equivalent temperatures derived from the satellite calibration data for a given radiometer operating at



a given temperature. A curve-fitting method was then applied to these points to generate a calibration curve for data in the area of interest (see APPENDIX B and computer program CALI in Appendix C.5). By using such a curve, it is possible to convert the digital values received from the scanning radiometer to equivalent temperatures. Schwalb (1972) estimates the accuracy of calibrated radiometer measurements as 2 to 3°C for a 20°C target area and 8 to 10°C for a -50°C target area due to variations caused by system noise. For regions at about 0°C, the accuracy is likely to be about 3 to 4°C.

Figure 2.6 shows a typical calibration curve extracted from

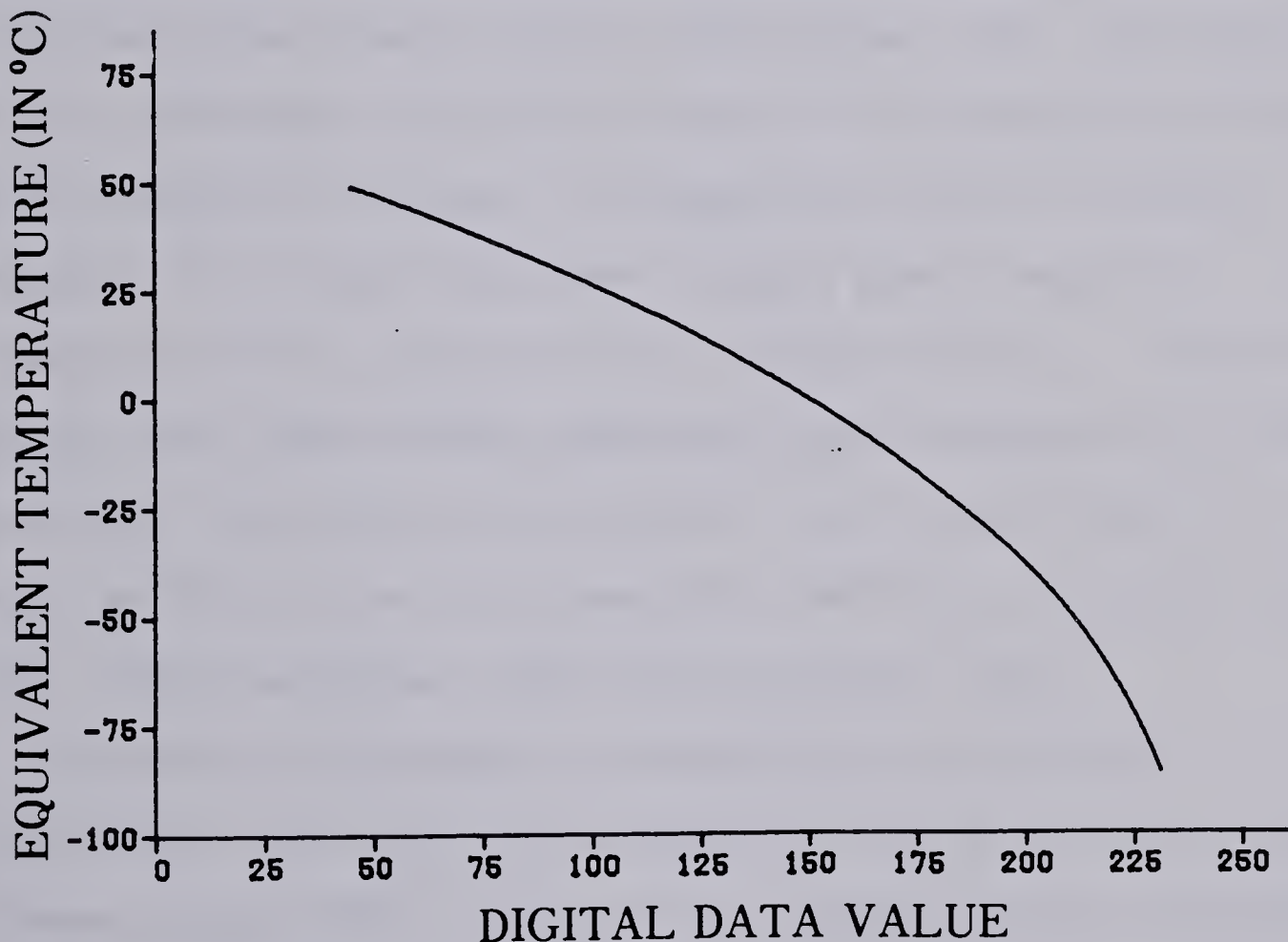


FIGURE 2.6 Infrared calibration curve for the Banks Island region of Orbit 4347 of NOAA-5 at 2120Z on July 15, 1977.





NOAA-5 satellite information. This curve was used to calibrate the infrared signals for the thermal fields of Figures 2.3, 2.4, 2.7, and 4.3.

## 2.5 External Calibration of Infrared Satellite Data

Even after internal calibration has been applied to the infrared data, the resultant equivalent temperatures may not match the actual temperatures of the areas scanned. The temperature as measured by the infrared sensor is generally lower than actual because of atmospheric attenuation, caused by scattering and absorption of the infrared radiation by atmospheric particulates, especially water vapour and carbon dioxide (Laird, 1976; Schaper, 1976). The magnitude of this attenuation varies with the state of the atmosphere and also with the angle of scanning. At distances away from the satellite subpoint, the radiation will pass through a greater amount of atmosphere and will generally be more strongly attenuated. Near the horizon, this effect becomes pronounced, and is referred to as "limb darkening." Even close to the subpoint, the attenuation may be more than  $2^{\circ}\text{C}$  for clear, dry atmospheric conditions (Curtis and Rao, 1969; Marlatt and Harlan, 1971; Maul and Sidran, 1973).

The effect of atmospheric attenuation may be corrected theoretically, but only if the atmospheric state is accurately known (Breaker, et al, 1978). However, if one assumes that the atmospheric state does not change appreciably over a horizontal distance of several hundred kilometers, a rather simpler correction may be applied. An average data value for a cloud-free sea surface area of approximately one half of one degree of latitude square may be



extracted from the satellite data. This data value can be converted to an equivalent temperature using the calibration procedure of Section 2.4. The difference between this temperature and the known sea surface temperature of the area used is the correction which must be applied to all data points to balance the effect of atmospheric attenuation.

Unfortunately, this zeroing procedure requires the knowledge of the actual sea surface temperature of an area close to the study area. Ship reports may be used, but there are difficulties in resolving satellite data, which measure "skin" surface temperatures over finite areas, to ship reports, which measure subsurface sea temperatures at a point. These two values do not always agree (Saur, 1963; Rao, et al, 1972; Saunders, 1967; Sommerscales, 1971). Errors in either the position or measured temperature reported by a ship will be nearly impossible to check unless several ship reports are available for comparison. Also, the infrequency of reporting by ships means that accurate surface temperatures from cloud-free areas may not always be available for the time of a given satellite orbit. For these reasons, ship reports were not used in this study.

Instead, weekly ice charts produced by the Atmospheric Environment Service of Canada were consulted, and areas containing approximately five to six tenths of ice were chosen as calibration areas. These areas, containing a mixture of melting ice in sea water interspersed, perhaps, with thin layers of "fresh" melt water, were assumed to be at 0°C. Figure 2.7 shows an area of the Beaufort Sea to the west of Banks Island from Orbit 4347 of NOAA-5.





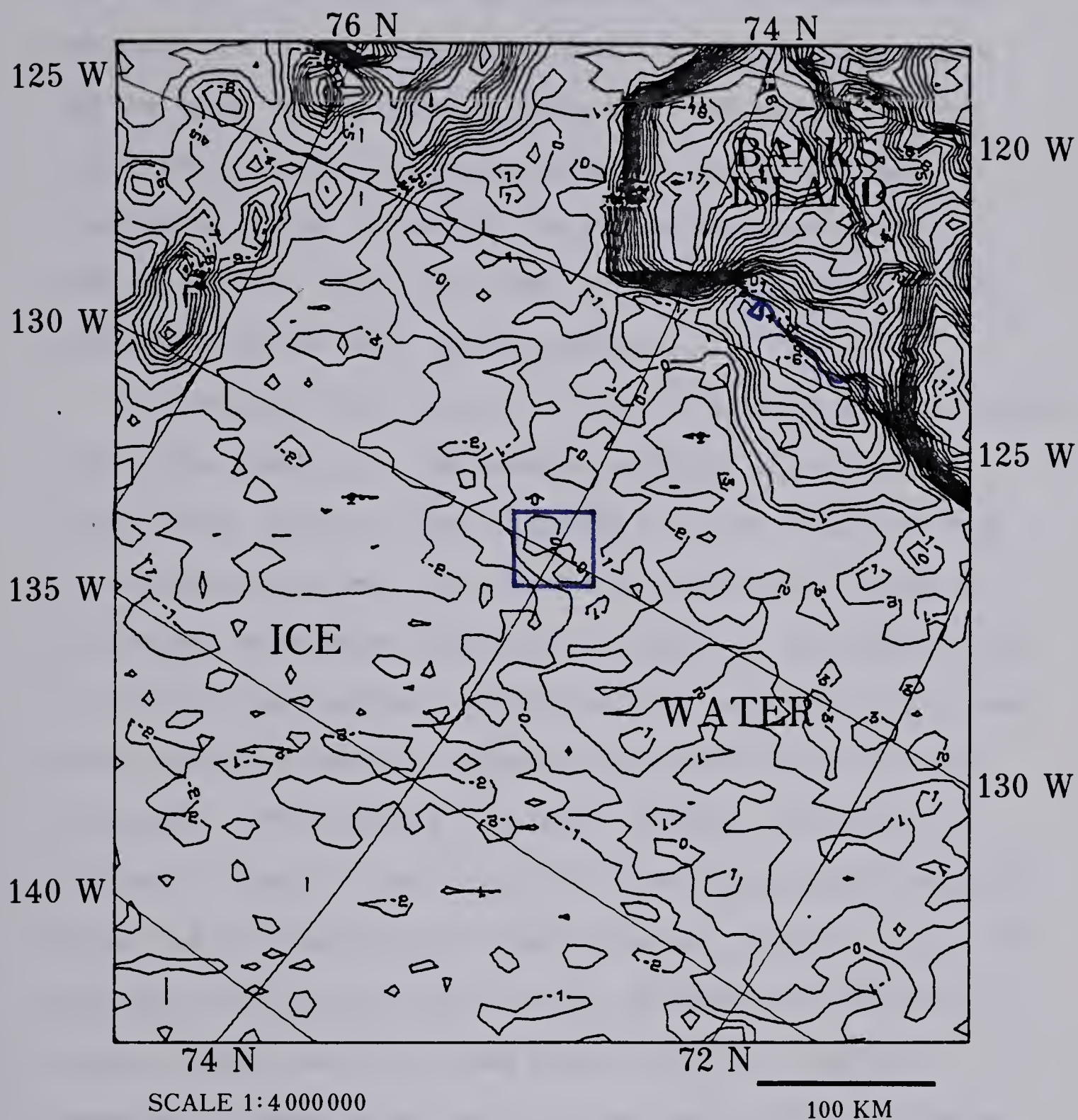


FIGURE 2.7 Averaged and smoothed temperature-field plot of the Beaufort Sea region of Orbit 4347 of NOAA-5 at 2120Z (1320 local time at Sachs Harbour) on July 15, 1977. Contours are labelled in degrees Celsius. The area within the blue box at the center of the plot identifies the area used to produce the external temperature calibration value for this orbit. (See Figure 2.8)





The central area within the blue box represents the area of ice and water used in the external calibration of the infrared data for the Banks Island region of Orbit 4347. It should be noted that since this same approximate area was used to calibrate consecutive orbits, as long as the surface temperature of this area did not vary appreciably, the relative temperatures between consecutive orbits would be very accurate.

Sea surface temperatures were used for this external calibration since there tends to be less spatial variation of sea surface temperatures, as can be seen in Figure 2.7. The large area used for calibration is required to allow for averaging of enough raw data values to **overcome the** effects of noise in the infrared data. (If the area measured has a uniform surface temperature, the data values extracted should be normally distributed about the mean temperature. The standard deviation, skewness and kurtosis of each set of data were therefore calculated to check this assumption before the calibration correction was used.) Figure 2.8 shows the mean data values used in the external calibration of consecutive orbits of NOAA-5 on July 14 and July 15 of 1977. The curve generated by these values, which relates the measured data value of the same area of the Beaufort Sea to the distance this area was from the satellite subpoint, is also shown. The increase in data value as the distance from the subpoint increases is representative of the limb-darkening effect. Since the synoptic situation did not vary appreciably between July 14 and July 16, and there was likewise little change in the temperature profiles



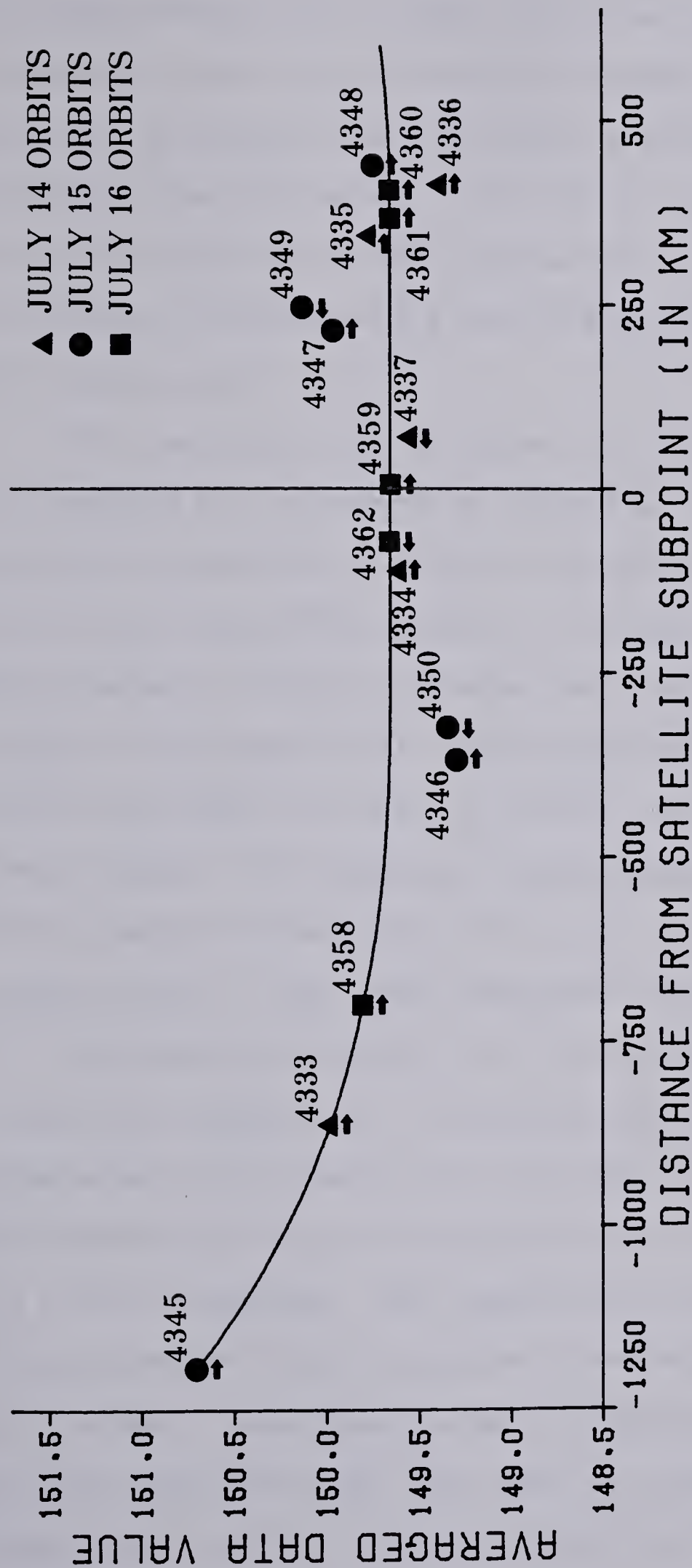


FIGURE 2.8 External calibration curve for NOAA-5 orbits on July 14, 15 and 16 of 1977. The averaged data value was obtained from an area of the Beaufort Sea centered at  $74^{\circ}\text{N}$  and  $130^{\circ}\text{W}$ . The arrows indicate the position of the center of Banks Island in relation to the calibration area for each orbit. The center of Banks Island was within about 300 kilometers of the calibration area on the first two orbits of each day, and within 200 kilometers on all other orbits. The distance from the satellite subpoint of an area located at the  $60^{\circ}$  zenith angle was 1750 kilometers (see Figure 2.1).



for Sachs Harbour shown in Table 1.2, it was assumed that the atmospheric state was also relatively constant, and that the external calibration curve would hence be valid for NOAA-5 orbits over this three-day period. This curve was therefore used for external calibration of NOAA-5 orbits on July 16, during which time this area of the Beaufort Sea was cloud obscured and not available for calibrations.

The data values shown in Figure 2.8 correspond to corrections of less than  $1^{\circ}\text{C}$ , as compared to corrections of  $2^{\circ}\text{C}$  or more mentioned earlier by other authors. Larger corrections would also be expected if the thin cirrus cloud reported in the hourly observations from Sachs Harbour in Table 1.2 extended over the entire Beaufort Sea region. This suggests that a temperature estimate of  $0^{\circ}\text{C}$  for an area of sea water and ice may be too low, that is, on the cold side. However, this discrepancy may also suggest a lesser effect from atmospheric attenuation in the Arctic than in more temperate regions because of much drier atmospheric conditions.

Atmospheric attenuation is not the only cause of errors in temperature measurements. The measured temperatures will be lower than actual if the area is not a black body (Mattson, 1969), though this problem will also be taken into account by external calibration to a known temperature. More important, the relative temperatures between areas will only be accurate if the emissivities of the areas are the same. Barren desert areas will generate lower measured infrared temperatures than ocean areas at the same actual temperatures because of the lower emissivity of barren desert, while





vegetated areas will generate temperatures that are nearly the same as ocean surfaces (Moller and Rashke, 1969). Differences in ocean surface roughness will also cause variations in measured infrared signals in cases where the actual thermal variation is small (Strong and DeRyke, 1973).

No corrections were made in this study to account for variations in source emissivities. The external calibration assumed that all areas used had the same surface emissivity as the zeroing area in the Beaufort Sea. It was felt that the variations in surface emissivity over the ocean surface or over the almost uniform surface of Banks Island would be small, and that the effect of the difference of emissivity between land and water areas would be within the  $3^{\circ}\text{C}$  accuracy of the radiometer-measured temperatures. For the purpose of comparing data from the same general area but from different orbits, it was assumed that the time variations of emissivity were negligible. During spring and fall, changes in snow-cover may have a strong and sudden effect on changes in surface emissivity (McGinnis, 1972). However, since Banks Island has no snow cover during the summer, and since new snowfall was not expected during July, nor observed at Sachs Harbour, this effect was not believed to be a problem.



## CHAPTER III

### TEMPERATURE FIELD PLOTTING OF INFRARED SATELLITE DATA

#### 3.1 Introduction

Calibrated infrared information from certain portions of consecutive scans of the NOAA-5 satellite may be used to produce a grid or matrix of temperature values covering a given area of interest. Some method must then be found to display these data to provide optimum utility of the information contained therein.

Studies using infrared satellite imagery have the drawback that the gray-scaling found in most of these images does not utilize the full satellite resolution, since the human eye has difficulty in distinguishing small differences in shades of gray. Such investigations often use some method of image enhancement to overcome this difficulty. The enhancement process applies the gray-scaling over a more limited temperature range of interest rather than over the entire range of possible temperatures. The result is a picture resolution in this temperature range which approaches the resolution of the satellite sensor, but loss of information beyond this range (Barnes, et al, 1972; Reinelt, et al, 1975; Wendler, 1977).

Computer manipulation of digital satellite data allows for full use of the satellite resolution with no comparable loss of information. A simple contouring method which assigns symbols to discrete data value intervals may be used to generate "zebra striped" plots. This pattern may then be analyzed by hand, producing a



contour map of the area of interest (Green, 1977). However, this method is time consuming, especially if the temperature field studied is complex. Contouring may be accomplished more easily if an appropriate computer facility is available. This study used a contouring package available at the University of Alberta to produce contour maps directly from calibrated satellite temperature data. This plotting package is known as SURFACE II (Sampson, 1978).

### 3.2 Temperature Field Plotting With SURFACE II

The SURFACE II Graphics System was developed by the Kansas Geological Survey as "a computer software system for creation of displays of spatially distributed data" (Sampson, pg 1). Generally, input into the SURFACE II package is in the form of either a matrix of equally spaced data points or a series of irregularly spaced points. Each data point requires two coordinates specifying its grid location, and one parameter defining its field value, for example, the calibrated temperature at that grid location. The data points therefore describe a three dimensional field that is used to produce a contour map for a given area of interest.

The satellite image of the Earth's surface will not match the usual surface maps available in geographic studies. Due to the curvature of both the Earth's surface and the satellite's orbit, locations as seen by the satellite will be unequally spaced as compared to locations on surface maps, depending on the distance from the location to the satellite subpoint. It is possible to identify the latitude and longitude coordinates of each data point





within a region of interest, and to convert this location to a grid position on a surface map. The SURFACE II routines can then use these points to estimate a new grid of equally spaced points which is required to produce a contour map of a given area. However, this estimating process requires extensive computations. Also, if the region of interest is only a few hundreds of kilometers large and near to the satellite subpoint, distortion of the satellite field of view will be small and the grid locations will be nearly linearly distributed with respect to a surface map of the same area. It is therefore possible to contour the matrix of calibrated temperatures directly with only minimal distortion. The average distances on the Earth between the rows and columns of the temperature matrix ( that is, the average distance between successive scans and the average separation of data value locations within each scan) can be calculated for each satellite orbit and region of interest, and used to scale the axes of the SURFACE II contour map to "fit" a given surface map. It was found in this study that variations between the satellite-scanned images of Banks Island and a Lambert Conformal Conic Projection of the same area were less than 5% over the width of the output, with the largest errors occurring at the picture edges.

The contouring of the temperature field is accomplished within the SURFACE II package. The program generates a set of commands used by a plotting device to draw a contour map. The positions of contours are determined by the values of the temperatures at each grid point, and these contour positions are then joined from



grid edge to grid edge by curved line segments. The number and value of contours produced is controlled in the running of the SURFACE II routines. The contour plots shown in Chapters 2 and 4 of this study were produced using the SURFACE II plotting package.

### 3.3 Identification of Regions of Interest

Visual identification of a given area of interest on a satellite image or temperature contour plot is not always possible due to poor contrast which prevents the distinguishing of surface features, or to cloud cover which obscures the surface below. Latitude and longitude lines and geographical or political boundaries are often placed on satellite imagery to alleviate this problem. Gridded overlays have been used in some studies (Ormsby, 1975; World Meteorological Organization, 1977). These overlays are calculated and drawn for certain satellite orbits and used for gridding all orbits with similar characteristics. However, many overlays are required to provide accurate identification of all possible satellite orbits, and each set of overlays must be recalculated and plotted anew if the satellite parameters change or when a new satellite is launched.

More accurate representations may be produced by calculating the positions of latitude and longitude lines for each separate satellite orbit. The positions of given latitude-longitude intersections may be deduced from known satellite orbital parameters, and transferred directly to satellite images in the form of a fiducial mark (Bonner, 1969; Madden and Parsons, 1973; Reinelt, et al,



1975). However, many points are required to identify features accurately, especially geographic features such as coastlines or islands. Since the points are placed directly upon the satellite images, they may also obscure useful information, particularly along coastlines. Even so, this method is superior to the overlay method in providing accurate delineation of areas of interest.

A variation of the point by point gridding procedure described in Reinelt, et al (1975) was used to produce the latitude and longitude lines and outlines for the contour plots of this study. The formulae used in calculating the positions of given latitude-longitude intersections is contained in Appendix A, and the computer programs, SCAN-2 and ITERA, used to generate these locations are contained in Appendices C.2 and C.3. The SURFACE II plotting package contains a routine for joining data points with straight lines. For each identifying line desired on the final contour plot, the program SCAN-2 generates a series of points within the matrix field used. The SURFACE II routine then produces a set of plotting commands joining these points. If the calculated points are close enough together, the lines will effectively be plotted as curves, and if the location of the end points of each line are outside the matrix field used, the lines will extend to the border of the final contour plot. Locations that one desires identified may also be generated using the same procedure. These points may also be plotted using SURFACE II routines. (For example, Sachs Harbour is located on all contour plots contained herein by a





cross-hair symbol.)

The temperature field contour plots which appear in Chapters 2 and 4 of this study were overlaid with identifying lines and marks using the SURFACE II plotting package and a CALCOMP plotting device. The only external addition to any of these plots were the labels identifying latitudes, longitudes and points of interest. As well, all of the satellite images appearing in Chapter 4 of this study were gridded by placing latitude-longitude marks directly on the APT satellite pictures received at the University of Alberta Satellite Laboratory.

In the course of this work, it was found that the generation of latitude and longitude lines and outlines was not as accurate as might be desired. These inaccuracies were due to assumptions made in calculating the identifying features, as well as to possible errors in satellite orbital information used in the calculations.

The first assumptions dealt with the geometry of the calculations. For simplicity, it was assumed that the satellite orbit was circular and that the Earth was spherical. Neither of these assumptions is strictly true. The NOAA-5 satellite has an elliptical orbit. However this variation from circularity is less than 1%, producing errors of less than 0.1 km near the subpoint. The Earth has the shape of an oblate spheroid, with radii of approximately 6378 km at the equator and 6357 km at the poles. As was the case for the satellite's orbit, the actual variation of Earth radius with latitude causes only minor errors of less than 1 km near the satellite subpoint. However, measurement of latitude as geocentric



(from the Earth's center) rather than as geodetic (from the Earth's focii) causes errors of about 0.1 degrees of latitude or about 12 km near the subpoint at 70°N (Oracheski, 1979). This measurement error was believed to be the major cause of gridding inaccuracy.

Comparable errors may also occur because of variation in the satellite orientation. For the purposes of the calculations, the pitch, yaw and roll of the satellite were assumed to be negligible. In practice, these orientation parameters are only controlled to within 0.5 of a degree (Schwalb, 1972). At a height of 1525 km, variation of one parameter may result in an error of

$$\pm 0.5^{\circ} \cdot (1525 \text{ km}) \frac{2\pi}{360^{\circ}} = \pm 13.3 \text{ km}$$

at the satellite subpoint.

Smaller errors are possible due to timing inaccuracy. The satellite position, and hence the position of all generated locations, is determined from the difference between the time the satellite crosses the equator and the time at which the satellite crosses the region of interest. These times are accurate only to the nearest second. Since the satellite requires 116 minutes to scan about one circumference of the Earth, a variation of

$$\pm 0.5 \text{ s} \cdot \frac{(2\pi)(6371 \text{ km})}{(116 \text{ min})(60 \text{ s/min})} = \pm 2.9 \text{ km}$$

is possible at the satellite subpoint. Larger errors will exist if the timing is not accurate to even the nearest second. As well, inaccurate information concerning the satellite orbital parameters required in the location calculations could also produce large errors, but it was expected that such inaccuracies would be either



negligible or immediately obvious.

The method of checking the accuracy of the identifying features was to compare the produced outline of Banks Island with the contoured temperature field. If the outline matched the region of tightly packed contours representing the sharp temperature gradient usually present along the shoreline of Banks Island in the summer, the fit was judged to be good. Comparison between consecutive orbits provided further help in finding the "best" outline position: one which would match the contoured temperature field along all coastlines. It was found that at the scale of 1 in 4 million which was used in all the contour maps of this study, the discernible error was approximately  $\pm 3$  kilometers, while the actual plotting errors were 10 kilometers or more. This required that the identifying features of each orbit be shifted to fit the contoured temperature field (see Appendix C.2). Unfortunately, the need for such a correction suggests that the location of a specific point after "shifting" cannot be wholly accurate, and hence that comparisons between the contoured temperature fields of different orbits can be only general. However, the relatively low resolution (about 10 kilometers near the subpoint) of the infrared information used implies that exact locations are not really required. Also, the consistency of the magnitude of shifting required for consecutive orbits suggests that a single correction may be applied for each day studied.





## CHAPTER IV

### DAILY DEVELOPMENT OF THE TEMPERATURE FIELD PATTERN OVER BANKS ISLAND

#### 4.1 Introduction

The methods of calibrating and plotting infrared satellite information described in Chapters 2 and 3 of this study were used to produce temperature-field plots of the surface of Banks Island. Reference was made in Section 2.2 to the overlap in scanning which occurs on consecutive orbits of polar orbiting satellites, particularly in northern latitudes. It was found that the NOAA-5 satellite passed over or near to Banks Island on five to six consecutive orbits each day in the summer of 1977. Temperature plots produced from these orbits could therefore be used to show changes which occurred in the thermal pattern of Banks Island over the course of a given day.

In Section 1.3, two days in July of 1977 were found to exhibit evidence of a sea breeze circulation at Sachs Harbour. It was also suggested that conditions were conducive to sea breeze development along the western coastline of Banks Island. In this Chapter, temperature-field plots for the two days were examined for evidence of sea breeze type circulations.

#### 4.2 Satellite Measured Temperature Fields of an Arctic Island

Under clear atmospheric conditions, infrared satellite imagery represents equivalent surface temperatures of the regions over which the satellite passes. These surface temperatures must not



be confused with surface air temperatures reported by meteorological stations. Satellite deduced temperatures show the approximate land or sea surface temperature, not that of the overlying air. Therefore, some discussion of land surface temperature is necessary to understand the effects a sea breeze circulation may have had on the temperature field of Banks Island on the chosen days in July of 1977.

Surface temperature is determined by a balance of heat fluxes at the Earth's surface. On clear summer days, the largest incoming flux is solar radiation which acts throughout the day during the Arctic summer, though because of the diurnal variation of solar elevation, the effect of solar heating is strongest around local noon. Infrared radiation from the atmosphere and clouds also acts as a heat source, but since this radiation depends on the temperature of the upper air, and the temperature profiles in Table 1.2 suggest this temperature did not change over the three day period of this study, this effect was assumed to be approximately constant.

Energy fluxes which tend to lower surface temperatures include radiation, conduction, and the transport of latent and sensible heat. The surface of Banks Island radiates infrared energy at a rate dependent upon its surface temperature and emissivity. However, since the surface of Banks Island has a fairly uniform composition, the surface emissivity should be nearly constant, and hence differences in the rate of infrared heat loss over the island should depend only on temperature. Conduction of heat into



the ground also acts as a surface cooling mechanism. However, because of the barren nature of Banks Island, the conductivity of the surface is small, so this effect is likely negligible. Surface cooling caused by evaporation of moisture is a major factor in the heat balance over wet ground. However, since Banks Island has a semi-desert climate, and the cases chosen for study were days with little cloud cover and hence little chance of new precipitation, the latent heat flux may not be large, except in lowlying drainage regions. Wallace and Hobbs (1977) suggest that in dry climates the flux of sensible heat is the major mechanism by which heat is passed to the lower layers of the atmosphere. This process depends on the temperature contrast between the surface and the overlying air, and continues as long as the land temperature is higher than that of the air. However, because of convection and mixing in the lowest levels of the atmosphere, the air temperature at screen level will rise rapidly. Thus, the screen temperature will reach its maximum with little lag, and shortly after the ground temperature maximum. Under these conditions, the surface temperature maximum may be higher than that measured at screen level, an effect that Fritz (1963) observed when comparing satellite measured surface temperatures to observed surface air temperatures.

The surface temperature of a region will change during the day in response to variations in the incoming or outgoing energy fluxes. Cook (1955), in a study of surface temperatures at Resolute in the Canadian Arctic (see Figure 1.1), found that the





surface temperature seemed to depend on changes in solar heating more than any other factor. Variations in the surface temperature of Banks Island on the three cloud-free days chosen for this study were therefore likely to obey the following general cycle: surface temperatures would increase throughout the morning, with the maximum temperature occurring near midday, when the effect of solar insolation would be strongest. Thereafter, decreasing solar radiation coupled with cooling from surface radiation and sensible heat transfer to the atmosphere would result in falling surface temperatures in the afternoon.

A sea breeze circulation or, indeed, any onshore advection, would change this generalized energy balance by increasing the sensible heat flux, since the advection of cooler air would increase the land-air temperature contrast. Thus, the sea breeze would tend to enhance surface cooling near the shoreline. This effect may be visible on a satellite-derived temperature field as a weakening of the coastal isotherm gradient (that is, a spreading of the coastal isotherms) throughout the afternoon. However, the early afternoon, when the sea breeze circulation is strongest and its cooling most pronounced, is already a time of general surface cooling. Unless the sea breeze has a very strong effect, this enhanced cooling may be difficult to separate from radiational cooling or purely local changes. Examination of the hourly temperatures at Sachs Harbour on July 15 and 16 of 1977 (Table 1.1) showed that when the sea breeze began, the air temperature did not



exhibit a sharp decline. If the advection of colder air was not apparent from the hourly temperatures at this coastal station, it is questionable whether surface cooling caused by the sea breeze was appreciable. Given the poor temperature resolution of the satellite data used in this study and the problems in positioning mentioned in Section 3.3, any detailed discussion of coastal temperature patterns was not possible. Therefore, it is highly unlikely that changes in coastal surface temperature patterns alone could be used to identify the existence of a sea breeze circulation.

Nevertheless, comparisons of the coastal gradients from different parts of Banks Island could give some indication of the island's circulation patterns. Under the influence of a synoptic-scale flow, the windward coasts would be subjected to a continuous cold onshore flow. Therefore, onshore cooling would be enhanced, and these coastal regions would tend to cool more quickly in the afternoon than would other areas. As well, at the time of maximum solar heating, continual cooling near the shoreline would result in the land-sea temperature contrast being confined to a narrower region. On the leeward coastline, however, the synoptic flow would be offshore, and so no enhancement of onshore cooling would be expected, nor would any cooling effects be expected in regions where the synoptic flow was parallel to the coastline. Thus, the isotherm gradient along windward coasts may be somewhat more intense than along other coastlines near local noon, but considerably weaker in the later afternoon. However, comparable isotherm gradients



along windward and leeward shores might suggest the presence of an onshore sea breeze along the leeward coast.

Only regions which were cloud-free over several consecutive orbits could be used for determining surface temperature patterns, since any cloud, even if only thin or scattered, could produce erroneous apparent changes in the observed surface temperature. The same criterion applied to measurements of coastal gradients as well, particularly in those cases where cloud was observed close to the coastline, producing apparent sudden temperature changes which may not have been representative of actual surface gradients. Measurements of surface temperatures from consecutive orbits were used in this study to illustrate the daily variation in the surface temperature of Banks Island. Measurements of coastal gradients from locations where the synoptic flow was believed to have been onshore, offshore, and parallel to the coast, were used to identify the results of different advection patterns. However, it must be stressed that these comparisons could be only approximate, since the problems in resolution and location of data precluded accurate measurements along the coastlines.

Though the cooling effect of a sea breeze on coastal surface temperatures may not be easily observed, the effect of surface heating on the overlying air can be pronounced. Only a few hours of solar heating are necessary to produce large land-air temperature differences in the Arctic (Hare and Orvig, 1958). Thereafter, the transfer of sensible heat to the cooler air will result in vertical





motion and cloud formation, though strong vertical motion and moist air is required for the formation of clouds of any thickness or areal extent. The strongest vertical motions at the Earth's surface occur when the land-air temperature contrast is largest. However, the full effect of vertical motion near the ground will not reach the middle troposphere until sometime later. The land-air temperature difference under clear summer conditions usually reaches a maximum when solar heating is at a maximum near local noon (Cook, 1955; Lewis and Callaghan, 1976). Depending on the moisture content of the air, only scattered cumulus may be observed before local noon, and maximum cloud development may not occur until the late afternoon.

Large land-air temperature contrasts often exist throughout most of the day along the coastlines of Arctic islands in the summer. Under clear summer skies, the surface temperature of Banks Island may be considerably higher than that of the surrounding water or ice. Figures 2.3 and 2.4 show the temperature contrasts which can occur. The two figures are temperature-field plots of the Banks Island region at 2121Z (1321 local time at Sachs Harbour) on July 15 of 1977. They differ only in the averaging procedure used to produce Figure 2.4, as was described in Section 2.3. While surface temperatures in excess of  $15^{\circ}\text{C}$  are observed over the interior of the island, the sea surface temperatures to the south and west and the ice surface temperatures to the north are between 0 and  $3^{\circ}\text{C}$ . The change in surface temperature occurs in a narrow band along the coastline. In some locations, this temperature change is



as much as  $15^{\circ}\text{C}$  over a distance of only 15 km. Similar isotherm gradients are also visible to the east and northeast of Banks Island, along the coastlines of Victoria Island and Melville Island respectively. Air advected from the cold surrounding surfaces over the coastlines of these islands will thus experience considerable heating, and the lift imparted by this heating may result in cloud formation. Such onshore advection may be the result of a sea breeze circulation.

The effect of a sea breeze circulation on cloud formation near a coastline was discussed in Section 1.2. The coastal cloud band associated with the sea breeze front in temperate and tropical locations has been observed on satellite imagery (Bugaev, 1973; Anderson and Veltishchev, 1973). However, the air in the Arctic Islands is considerably drier than in more temperate regions because of lower temperatures and the limited water vapour transport from the cold water or barren land surfaces (Burns, 1973b). The formation of cloud in an Arctic sea breeze front is therefore likely to be less evident than in regions closer to the equator.

The identification of cloud in conventional gray-scaled satellite imagery is well documented in Anderson and Veltishchev (1973). Temperature-field plots may be used in exactly the same manner to identify areas where cloud exists. Under clear summer conditions, the temperature field of Banks Island is likely to be nearly uniform over the interior, with strong thermal gradients along all coastlines. The occurrence of cloud at temperatures



lower than the surface temperature is therefore marked by deviations from this uniform temperature. For example, in Figures 2.3 and 2.4, a large region of cloud covers the center of Banks Island and extends beyond the west coast. However, areas of the island to the north and south are cloud-free, or very nearly so, since the observed temperatures are uniformly high. Extensive areas of overcast cloud are marked by lower temperatures in a well developed pattern, while regions of more scattered cloud cover are recognized by less well-defined isotherm patterns. For example, in Figures 2.3 and 2.4 the cloud over the interior of Banks Island is probably more scattered than that over the western coastline.

Identification of cloud types is usually done using both visual and infrared imagery. However, information can be obtained on the height of clouds using infrared information alone. In conditions where the surface is obscured by cloud, the satellite measured temperature will not be that of the surface, but rather a composite of surface and cloud top temperatures. If the cloud is thick and widespread, the only radiation sensed by the satellite will emanate from the cloud top. If a representative atmospheric sounding is available, the measured cloud top temperature may be translated into an approximate cloud top height (Rao and Winston, 1963; Rasool, 1964). However, if the cloud is thin, radiation from lower levels will penetrate the cloud and be measured by the satellite, resulting in higher apparent cloud top temperatures. This may lead to underestimates of cloud height. Alternately, very







thin cirrus cloud may not be visible on conventional satellite imagery, but nevertheless will radiate weakly at low temperatures, resulting in overestimates of cloud heights. However, if the cirrus cloud covers the entire area of study in a uniform layer, the external calibration procedure described in Section 2.5 will automatically adjust for this problem.

Changes in cloud amount can also produce misleading changes in the apparent cloud height. Scattered cloud will seem to be at a lower height than overcast cloud since more surface radiation would be measured through scattered cloud. Also, if the cloud is scattered, temperature variations of the underlying surface will also result in changes in the observed cloud temperatures. For example, scattered cloud over Banks Island in the summer would appear much warmer than the same cloud over the Beaufort Sea, since the land surface temperature is so much higher than that of the water and ice over the Beaufort Sea.

The problems of identifying regions of scattered cloud cover were particularly evident in this study. Since the resolution of the NOAA-5 satellite was only 7 km at the subpoint, only cloud formations larger than this would be accurately measured. Therefore, individual cumulus clouds which might have formed in the vicinity of a sea breeze front on the west coast of Banks Island were unlikely to be clearly visible, though areas where such cloud formed could appear as regions of slightly lower temperature on a temperature plot. However, the accuracy of very small-scale



temperature detail in the information presented in this study was also questionable because of the positioning problems discussed in Section 3.3. For these reasons, some smoothing was done on all temperature plots presented in this study. The smoothing procedure used a simple weighted average of each data point and the four points closest to it. The smoothing program, SMOO, is listed in Appendix C.5. The weighting parameter was chosen so as to remove closed contours appreciably smaller than the resolution of the satellite. The same weighting parameter was used for each temperature plot. As was the case in the averaging process discussed in Section 2.3, the smoothing did not change large-scale features of the temperature field, except along the coastline, where the gradients were spread out. However, since the smoothing procedure, and also the averaging process discussed earlier, used values which - depending on the satellite orbit - were not a constant distance apart, the effect on the information from each orbit would be slightly different, though since all the orbits in this study were near to the satellite subpoint, this problem was not expected to have been significant. Figure 4.3, shown in the following Section, shows the smoothed temperature-field plot for orbit 4347 of NOAA-5 on July 15 of 1977, and corresponds to Figures 2.3 and 2.4 presented earlier.

Though the satellite-measured temperatures may not be representative of actual cloud top temperatures, the lowest measured temperatures do identify regions with either the thickest cloud, or cloud with the highest tops. By measuring the distance



such regions move between consecutive satellite orbits, some estimate can be made of the winds at the level at which the cloud occurs. Studies have shown that satellite-determined motions are usually comparable to winds determined by other techniques (Hubert, 1979; Hasler, et al, 1976, 1977). However, only clouds which maintain their identity over a period of several satellite orbits can be successfully tracked, since radical changes in either the intensity or shape of a given cloud will make its identification on separate orbits difficult. For this study, this restriction meant that clouds to be tracked had to persist for at least two hours. Upper-level clouds are often suitable for tracking since they tend to be found in large-scale regions of vertical motion, and may persist for several hours (Hubert, 1979). In this study, the motions of several cirrus cloud formations over Banks Island were compared to upper-level winds reported at Sachs Harbour. Winds at lower levels are sometimes more difficult to determine from cloud motions observed on satellite imagery. Cumulus-type clouds are often used to measure low-level cloud movement. However, small cumulus clouds may form and dissipate over periods of time considerably shorter than the two hour period between consecutive orbits of satellite imagery used in this study. Also, because of the low resolution of the NOAA satellite, such small clouds would not normally be visible as separate entities. Hubert (1979) suggests that even though individual cumulus clouds have short lifetimes, organized patterns of such cloud may persist for several hours.







Thus, large regions of low-level cloud may be used to estimate low-level flows.

Low-level cloud tracking may also be affected by surface conditions. For example, surface heating can result in local formation of cloud and constantly changing cloud patterns. Orographic effects can also result in formation or dissipation of cloud. However, if a cloud formation has sufficient areal and vertical extent so that it will not dissipate rapidly, its motion may still be followed despite local enhancement or weakening, while changes in the observed cloud temperatures caused by such changes in intensity may provide evidence of local effects.

Thus, successful tracking depends upon cloud formations which are intense enough to persist in a reasonably unchanged state for several hours. The tracking procedure used in this study was to measure the distance travelled by the center of a region of low temperatures appearing on consecutive temperature plots, rather than tracking only the position of lowest temperatures. It was felt that the lowest measured temperatures might be affected by system noise, or change their location with respect to the remainder of the cloud pattern because of localized, small scale changes in vertical motions. However, if a region of low temperatures of similar appearance could be identified on successive satellite orbits, the approximate center of such a region was tracked.

Even if a cloud formation remained totally unchanged over a period of several hours, accurate wind speed measurements are still



not assured. The problems of accurately locating positions on the temperature-field plots, discussed in Section 3.3, also apply to locating cloud positions, and so may produce errors in apparent cloud motions. As well, the location of a cloud formation with respect to the Earth's surface is also affected by perspective. A cloud directly below the satellite, and so directly above the satellite subpoint, would appear at the correct location. But away from the subpoint, because the cloud top is a finite distance above the Earth's surface, the location of the cloud will appear to be further from the subpoint than it actually is. At a zenith angle of  $60^\circ$ , this can produce an error of 17.3 km in the location of a cloud with a top at 10 km (34,000 feet) above the Earth's surface. Also, because the satellite has a different orientation to a given region on each successive orbit, this perspective error is continually changing. However, the location of Banks Island on most of the satellite orbits in this study was considerably closer to the satellite subpoint than the 1750 km separation suggested by a  $60^\circ$  zenith angle (see Figure 2.8). Indeed, Banks Island was within about 700 km of the satellite subpoint on all orbits except 4345 on July 15. At such distances, the perspective errors would be less than 7 km between consecutive orbits. Given the inexactness of the other measurements used to determine cloud motions in this study, this was therefore not thought to be a major problem.

The motions determined by clouds tracked in this study were compared to upper-level winds reported at Sachs Harbour, listed



in Table 1.2. However, numerous problems exist in such comparisons. As was mentioned earlier, cloud top heights can only be estimated from satellite-measured temperatures if the cloud is thick and unbroken, and if a representative temperature profile of the region is available. The heights of thin or scattered clouds are impossible to determine from satellite temperatures alone, though by using conventional visible and infrared satellite imagery, it may be possible to determine the type of cloud, and hence deduce a rough estimate of cloud height. However, depending on the cloud type, the height of the tops may not be useful in estimating wind speeds. Hasler, et al (1976, 1977) have found that though cirrus clouds seem to move at speeds comparable to the average winds at their height, the motions of low-level clouds correlate better with the winds at their bases than those at their tops. Thus, if the tracked low-level clouds were not in the vicinity of Sachs Harbour, where the hourly weather reports could be used to determine the height of the cloud bases, only general comparisons with the reported winds could be made.

For the purposes of this study, it was assumed that the upper-air wind and temperature profiles for Sachs Harbour were representative of all of Banks Island. Any variations in the upper winds or temperatures over the island would therefore result in cloud motions at variance with these values. Also, though the Sachs Harbour reports were for a single location at a single time, the winds estimated from cloud motions were measures of the actual path of a





cloud formation over a two hour period. Thus, it must be stressed that no attempt was made in this study to find exact correlations between the reported winds and the cloud motions; only order-of-magnitude comparisons were carried out.

Though small regions of weak cloud formation may not be tracked with the same confidence as large, intense cloud patterns, the location of regions of minimum temperatures on satellite images can still provide useful information. As mentioned earlier, low cloud temperatures suggest either dense cloud or cloud with high tops. When considering cloud formation, both these features are associated with regions of strong lift. Regions of lowest temperature therefore imply regions with the strongest vertical motions. If cloud tracking cannot be used to identify circulation patterns, changes in the location of minimum temperatures may still provide useful information about local circulations.

#### 4.3 Temperature Fields of Banks Island on Two Days in July of 1977

##### 4.3.1 Explanation of Figures

The two days chosen for study were July 15 and July 16 of 1977. In the following sections, information from satellite orbits on these days is presented and discussed.

The temperature-field plots were produced using the procedures described in Chapters 2 and 3. The scale of all plots is 1:4 000 000. The plots are contoured in  $3^{\circ}\text{C}$  intervals and overlaid with labelled latitude and longitude lines. Banks Island is identified on each



plot by a blue outline, and Sachs Harbour by a cross-hair symbol. The change in orientation of the scanning satellite with respect to the Earth's surface on successive orbits is the reason for the change in orientation of Banks Island on each temperature plot. The approximate time at which satellite scanning of the Banks Island region began is given for each plot produced. Since information from only about 70 scans of each orbit was used, less than two minutes was required to scan the whole of Banks Island.

Conventional satellite imagery also accompanies some of the temperature plots. Unfortunately, visible imagery from the Banks Island region was not available for some morning orbits in July of 1977. Conventional imagery for these orbits was therefore not included. The same enhancement curve was used for all the infrared imagery, with the lighter shades representing colder measured temperatures. For the visible imagery, the enhancement was varied to achieve slightly better resolution between land and water surfaces on orbits from later in each day, when the solar illumination was weaker. The lighter shades on all visible imagery represent higher reflectivities.

The same area of Banks Island and the Beaufort Sea was presented for each available orbit of conventional satellite information. Since these images covered larger regions than did the corresponding temperature plots, the time given for each image was rounded to the nearest 5 minutes. The fiducial marks on each image identify particular latitude-longitude intersections. The



two rectangular marks on the right of each image were positioned at  $70^{\circ}\text{N}$  and  $120^{\circ}\text{W}$ , and  $75^{\circ}\text{N}$  and  $120^{\circ}\text{W}$ . The small parallel line marks on the left of each image were located at  $70^{\circ}\text{N}$  and  $140^{\circ}\text{W}$ , and  $75^{\circ}\text{N}$  and  $140^{\circ}\text{W}$ . No scaling was done on the conventional satellite imagery, though the approximate scale is about 1:10 000 000.

#### 4.3.2 Case 1 July 15 of 1977

On July 15 of 1977 satellite information from the Banks Island region was available on six consecutive orbits of NOAA-5, numbered 4345 through 4350. Temperature-field plots of Banks Island for each orbit are shown in Figures 4.1, 4.2, 4.3, 4.5, 4.7, and 4.9 respectively. The first orbit, 4345 (Figure 4.1) shows the temperature field at 1731Z (0931 local time at Sachs Harbour) on July 15. Intervals of approximately two hours separate each successive orbit, with the last orbit, 4350 (Figure 4.9) occurring at 0303Z on July 16 (1903 local time on July 15). Conventional satellite imagery was available for orbits 4347 through 4350. Infrared and visible images for these orbits are shown in Figures 4.4, 4.6, 4.8, and 4.10.

The six temperature plots shown cover the period during which a sea breeze circulation occurred at Sachs Harbour on July 15. Figure 4.1 shows the temperature field of Banks Island before the sea breeze was first observed. At this time the land surface was still in the process of warming. Temperatures in excess of  $12^{\circ}\text{C}$  can be seen in the southeast portion of the island, while in the north, surface temperatures had already risen past  $15^{\circ}\text{C}$  in some areas.







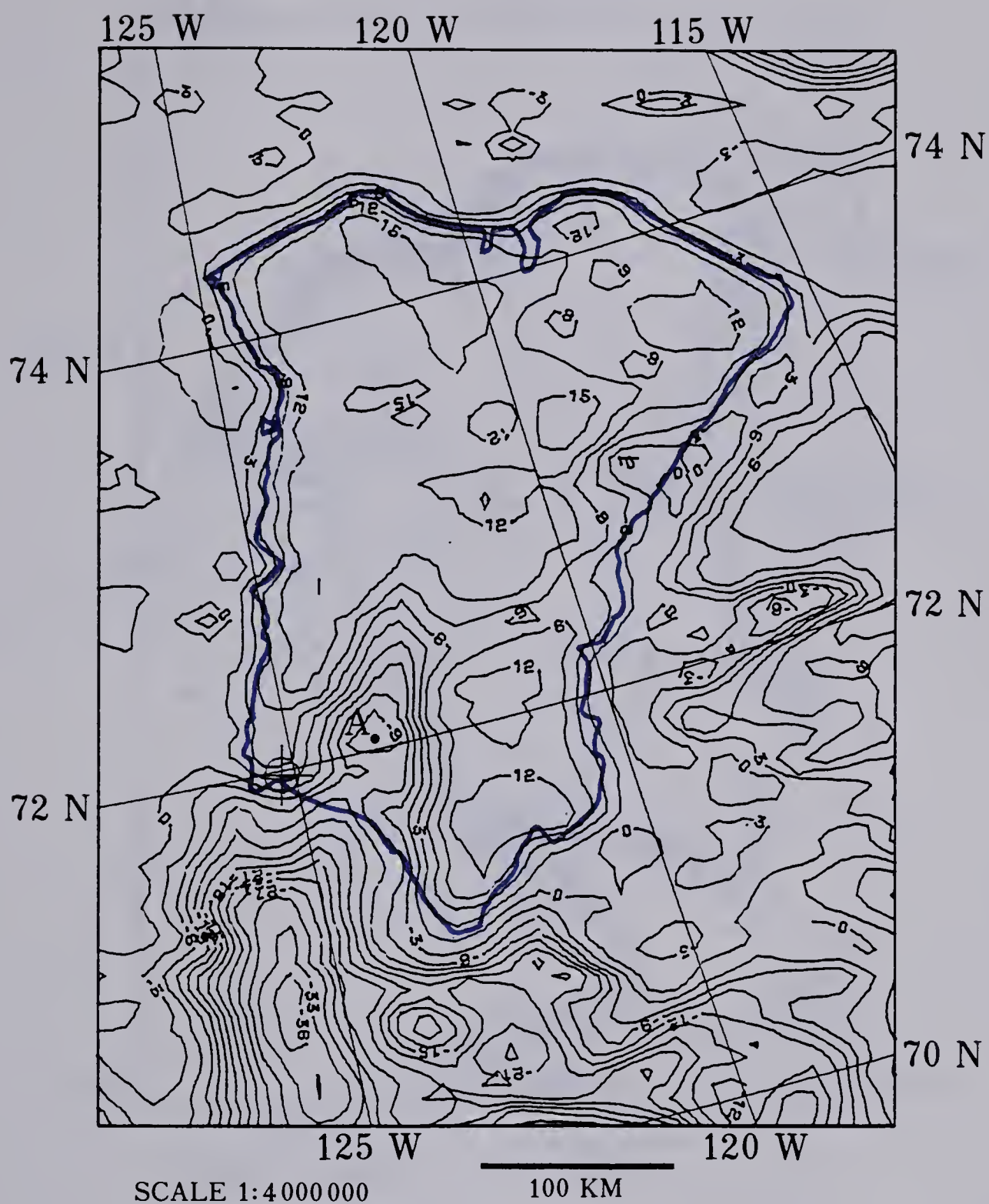


FIGURE 4.1 Averaged and smoothed temperature-field plot of the Banks Island region of Orbit 4345 of NOAA-5 at 1731Z (0931 local time at Sachs Harbour) on July 15, 1977. Contours are labelled in degrees Celsius.



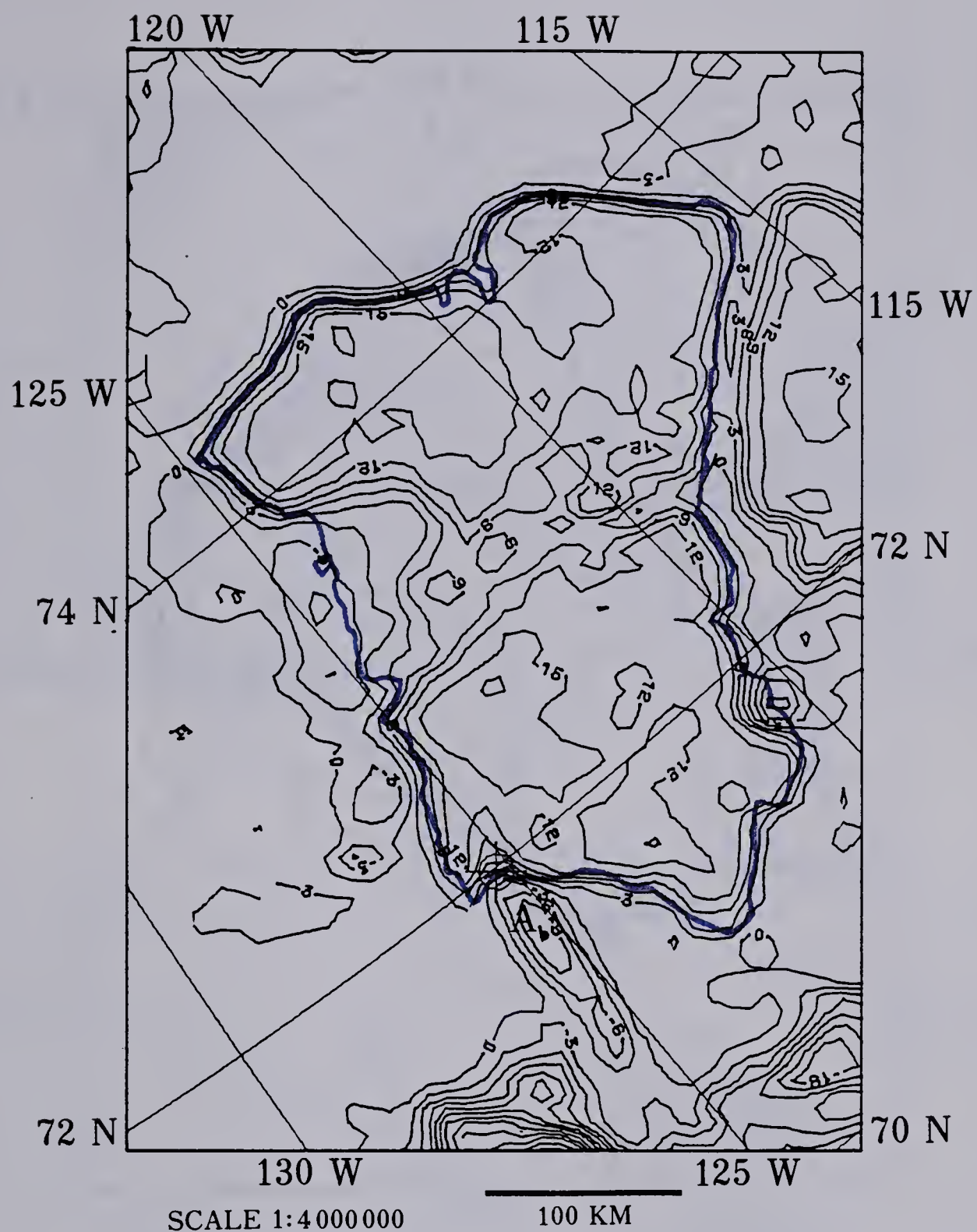


FIGURE 4.2 Averaged and smoothed temperature-field plot of the Banks Island region of Orbit 4346 of NOAA-5 at 1926Z (1126 local time at Sachs Harbour) on July 15, 1977. Contours are labelled in degrees Celsius.





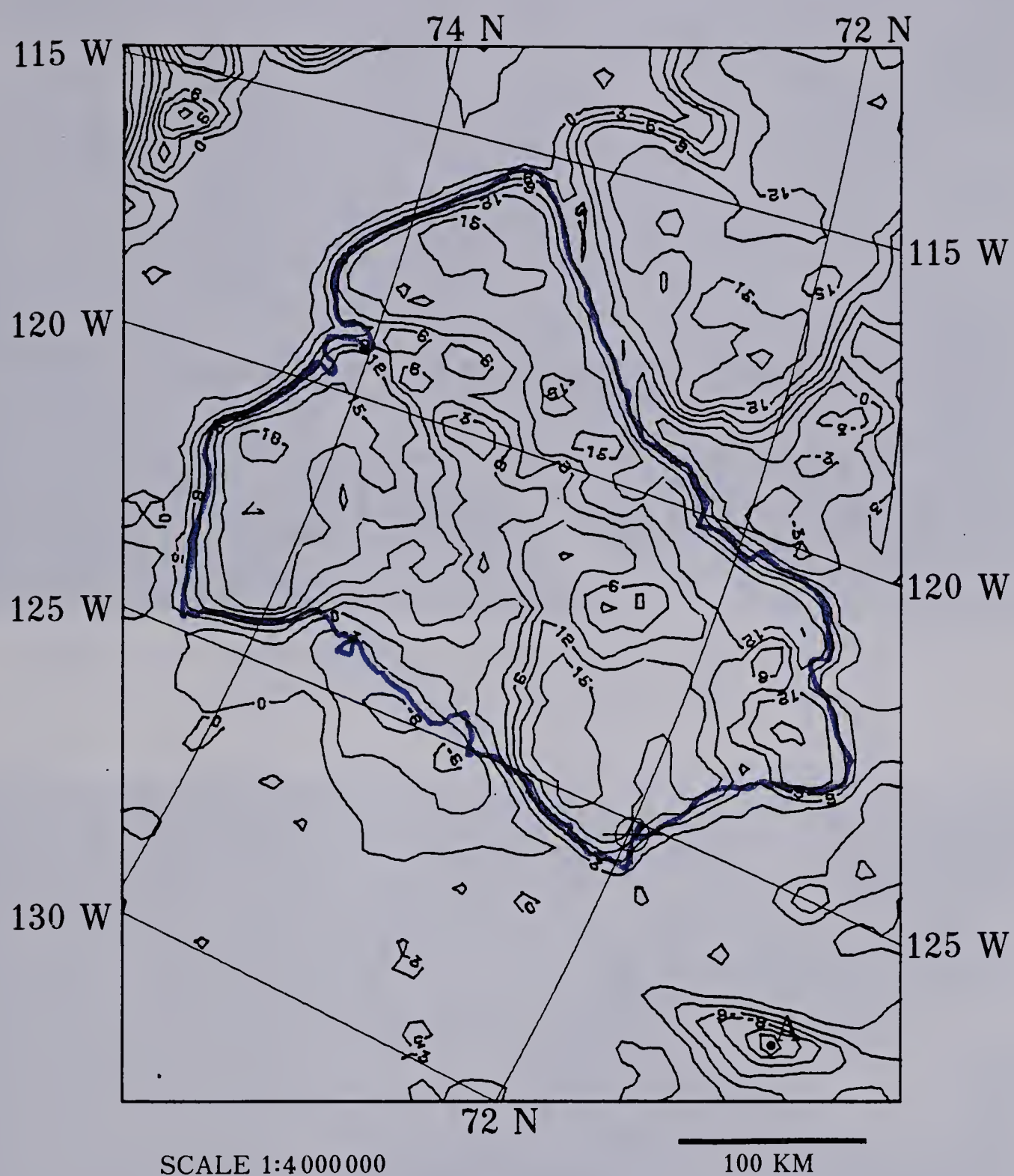


FIGURE 4.3 Averaged and smoothed temperature-field plot of the Banks Island region of Orbit 4347 of NOAA-5 at 2120Z (1320 local time at Sachs Harbour) on July 15, 1977. Contours are labelled in degrees Celsius.







FIGURE 4.4a Infrared image of Beaufort Sea region of Orbit 4347 of NOAA-5 at 2120 Z on July 15, 1977.

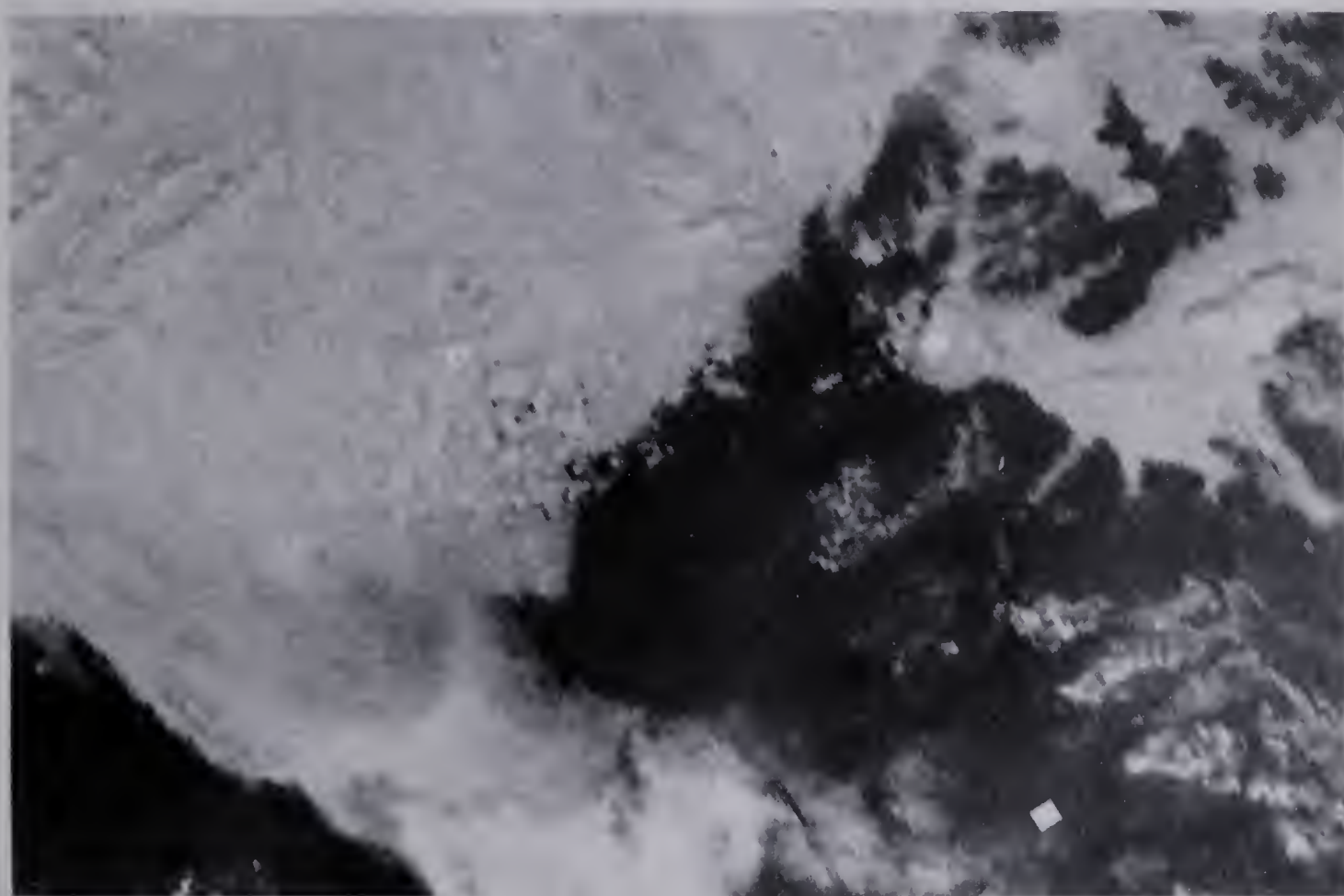


FIGURE 4.4b Visible image (as above).



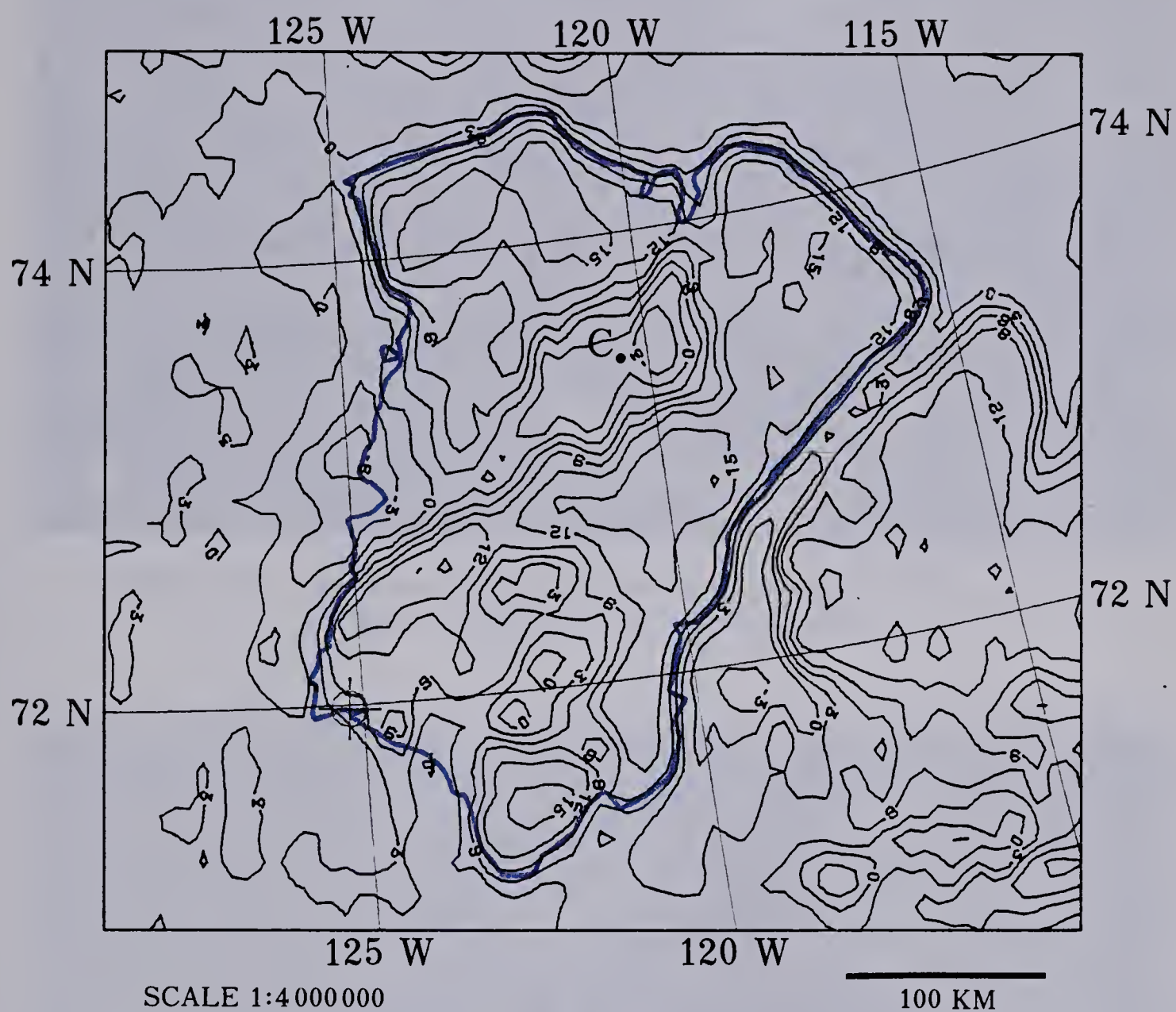


FIGURE 4.5 Averaged and smoothed temperature-field plot of the Banks Island region of Orbit 4348 of NOAA-5 at 2314Z (1514 local time at Sachs Harbour) on July 15, 1977. Contours are labelled in degrees Celsius.





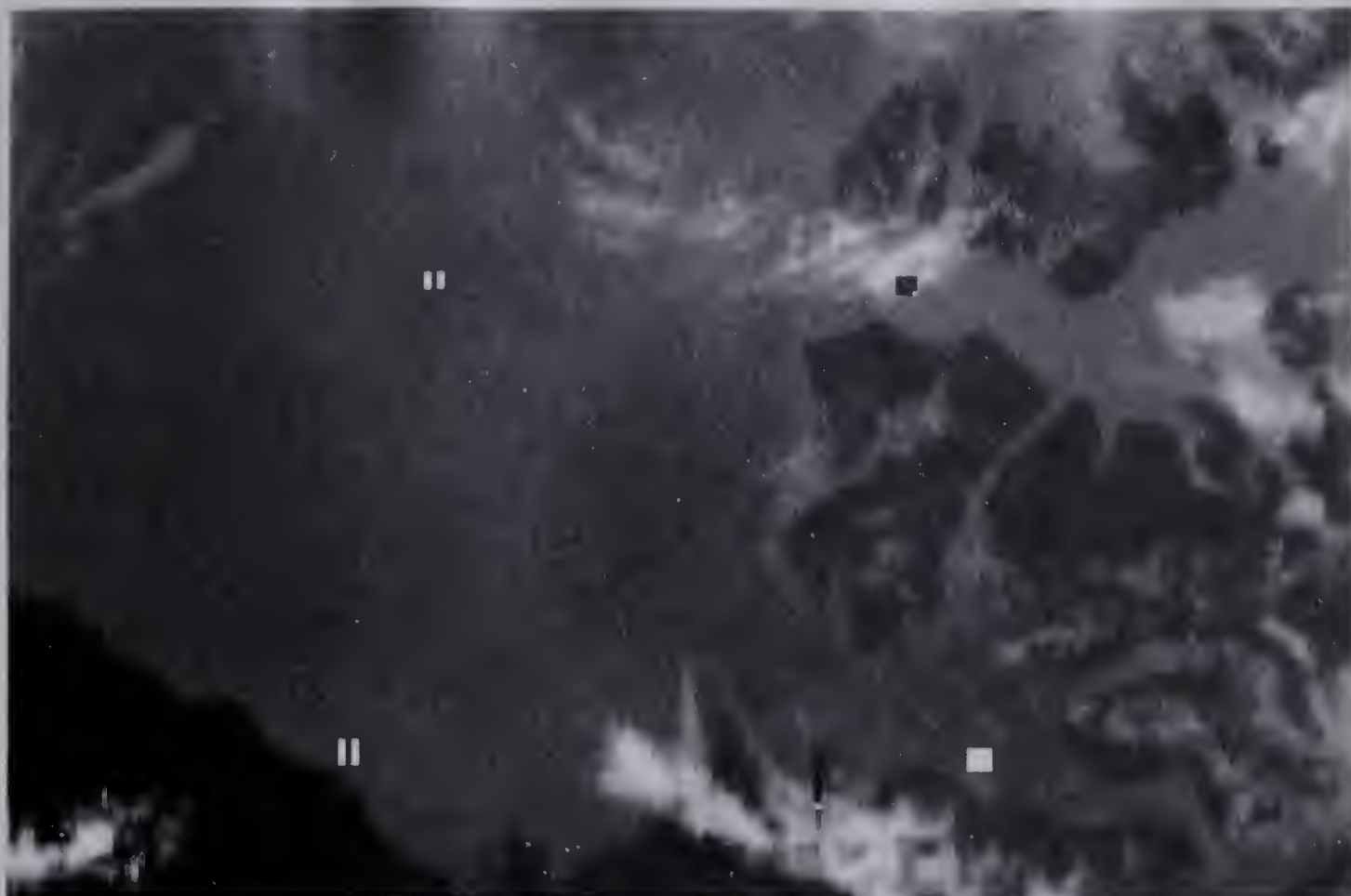


FIGURE 4.6a Infrared image of Beaufort Sea region of Orbit 4348 of NOAA-5 at 2315 Z on July 15, 1977.

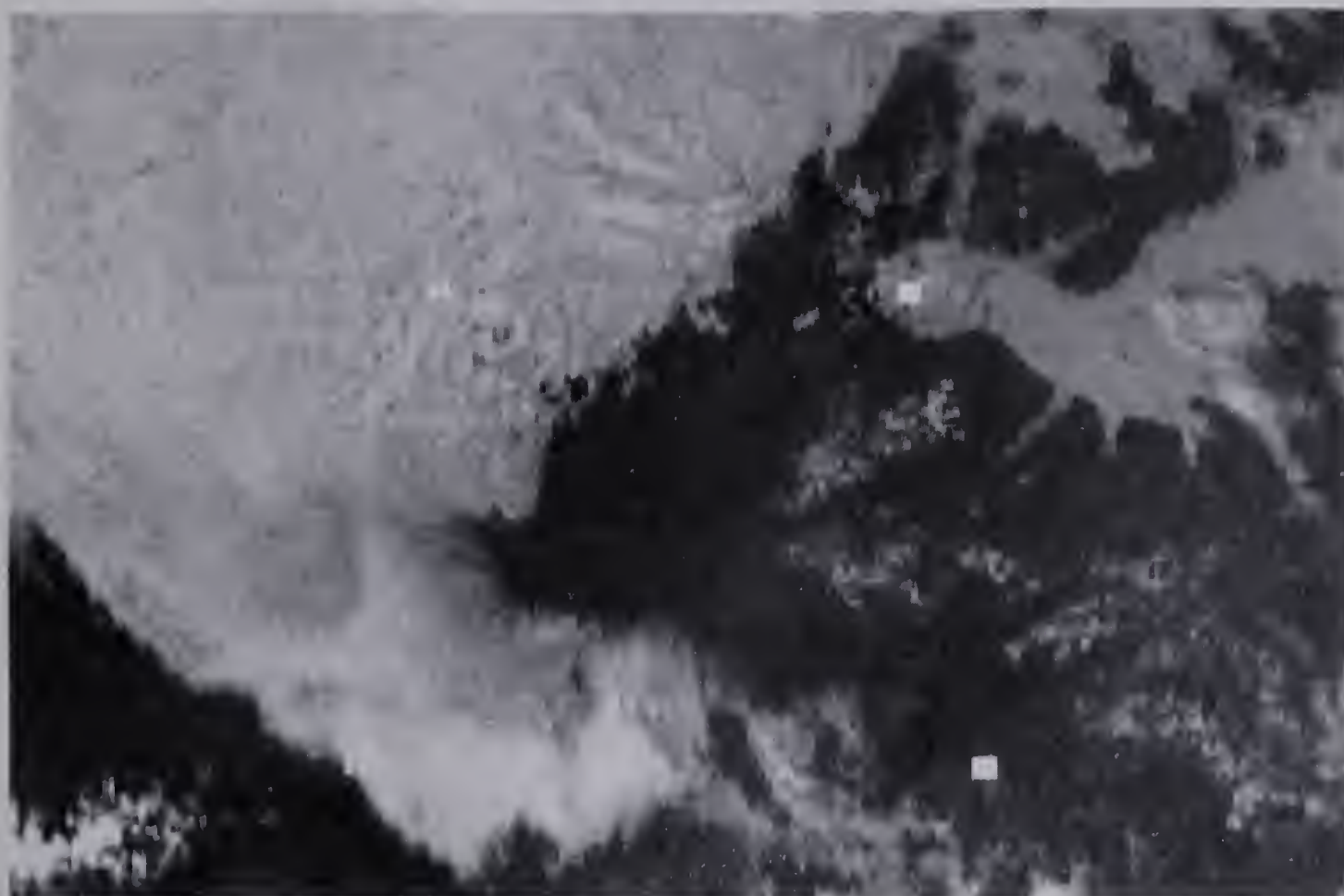


FIGURE 4.6b Visible image (as above).





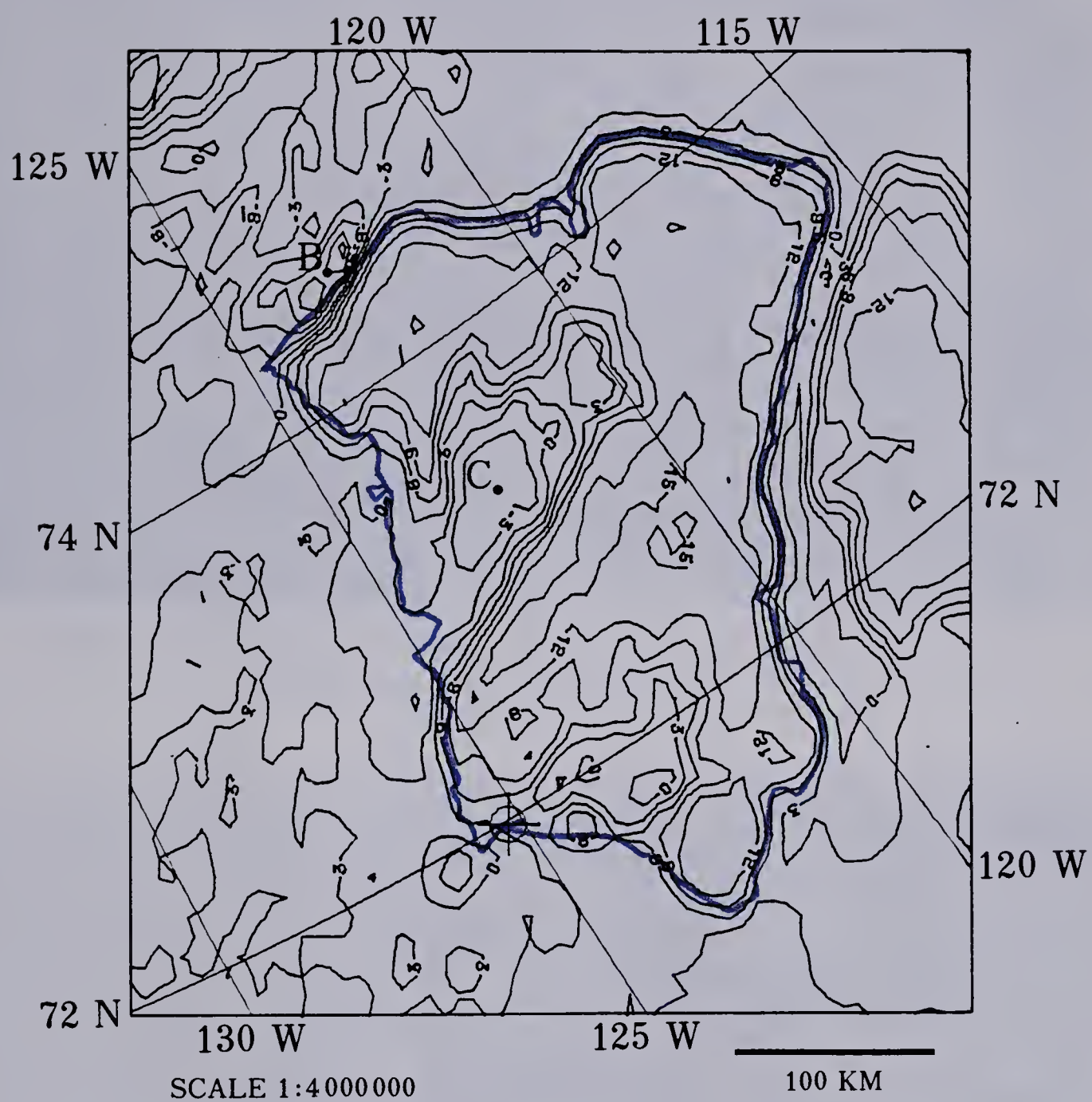


FIGURE 4.7 Averaged and smoothed temperature-field plot of the Banks Island region of Orbit 4349 of NOAA-5 at 0108Z on July 16, 1977 (1708 local time on July 15 at Sachs Harbour). Contours are labelled in degrees Celsius.





FIGURE 4.8a Infrared image of Beaufort Sea region of Orbit 4349 of NOAA-5 at 0110 Z on July 16, 1977.

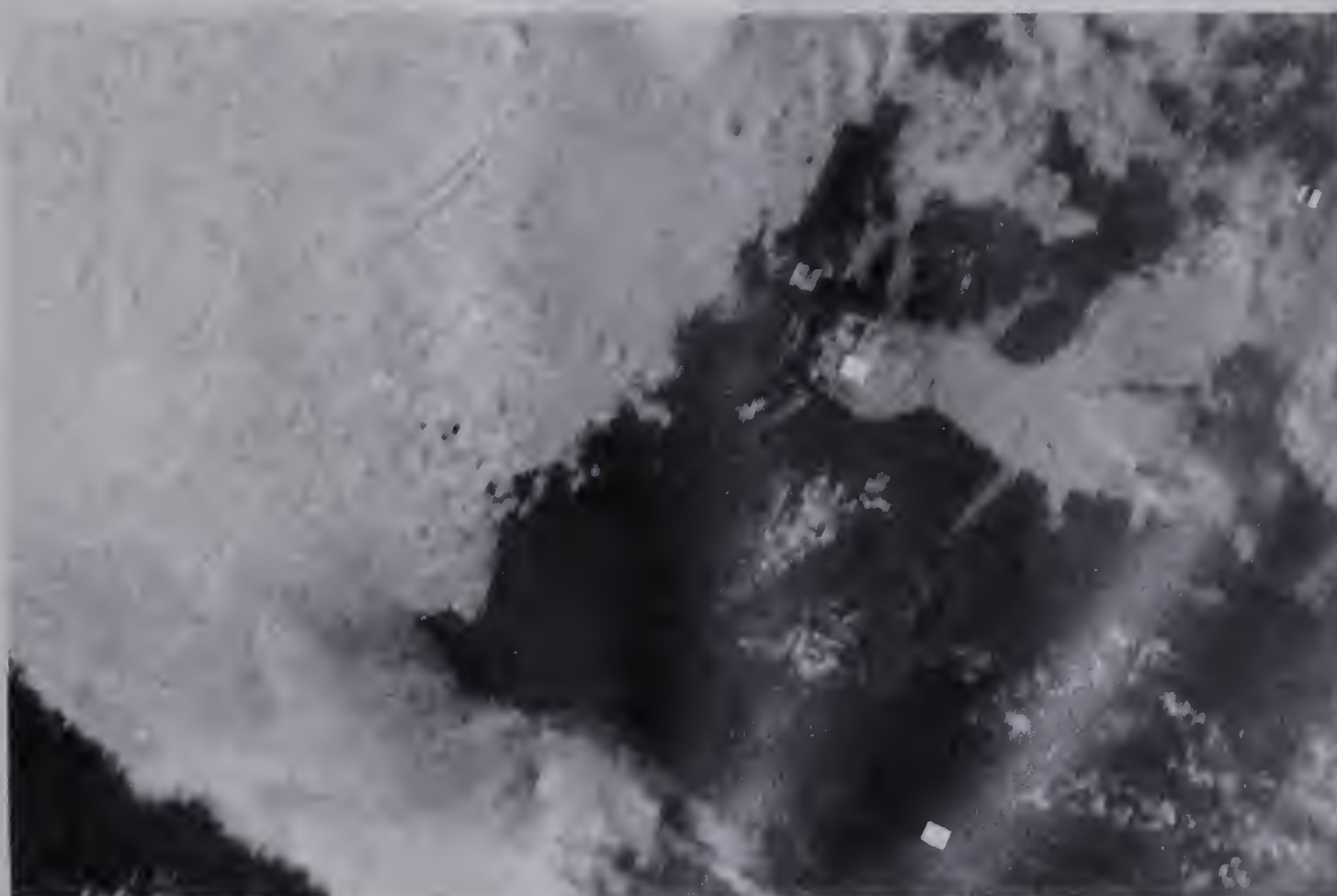


FIGURE 4.8b Visible image (as above).





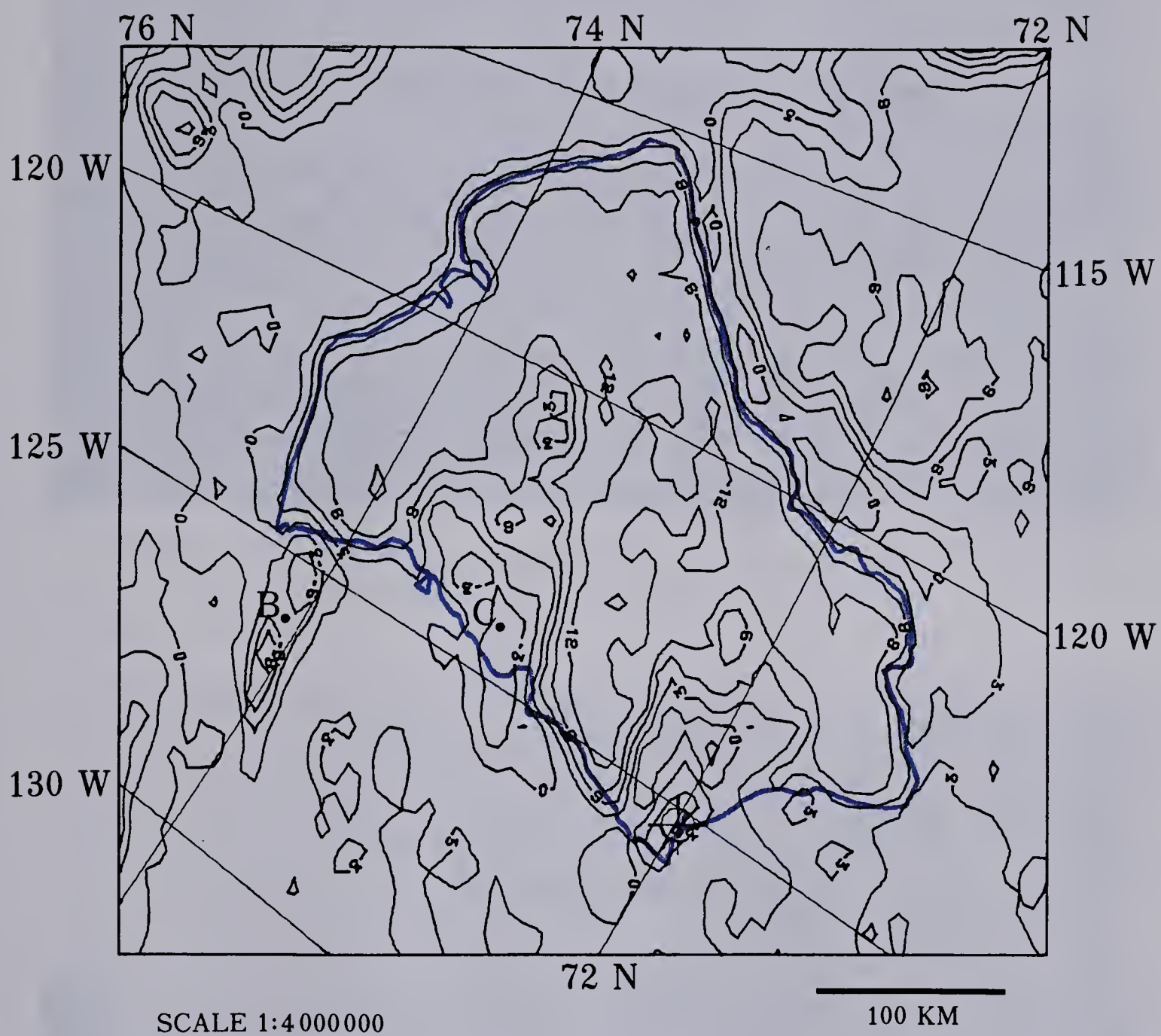


FIGURE 4.9 Averaged and smoothed temperature-field plot of the Banks Island region of Orbit 4350 of NOAA-5 at 0303Z on July 16, 1977 (1903 local time on July 15 at Sachs Harbour). Contours are labelled in degrees Celsius.







FIGURE 4.10a Infrared image of Beaufort Sea region of Orbit 4350 of NOAA-5 at 0305 Z on July 16, 1977.

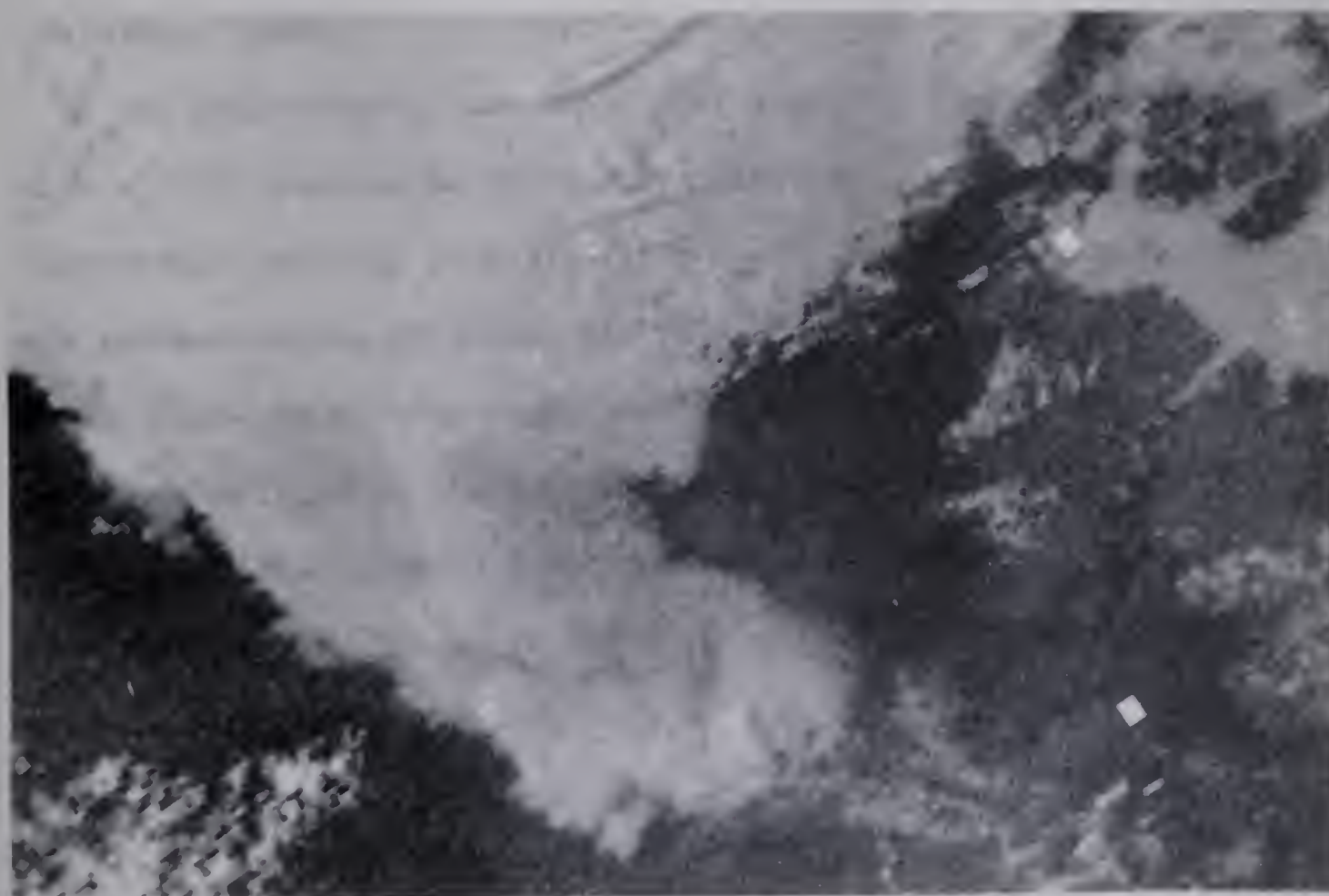


FIGURE 4.10b Visible image (as above).



However, the confused temperature pattern in the northeastern portion of the island, with closed isotherms of higher and lower temperatures in close proximity, and the absence of a well-defined isotherm gradient along the eastern coastline, both suggest the presence of thin or scattered cloud in this area.

The subzero temperatures observed in the southwestern portion of the island and off the southwestern coastline are also indicative of either thicker or higher cloud. The cloud off the coastline has central temperatures below  $-36^{\circ}\text{C}$ , which suggests a cirrus-type cloud. The upper-air profiles in Table 1.2 correlate temperatures of  $-36^{\circ}\text{C}$  with cloud tops above the 400-mb level, or about 25,000 feet, though since even thick cirrus cloud is semi-transparent to surface radiation, this height is probably only a minimum value (Valovcin, 1968).

The temperatures over the island itself are considerably higher, with a  $-9^{\circ}\text{C}$  isotherm as the lowest observed. The upper-air temperature profiles in Table 1.2 suggest that these temperatures are representative of either mid-level cloud with tops at about 12,000 feet, or thinner high-level cloud. This cloud formation can, however, be found on the two following satellite orbits, 4346 and 4347, shown in Figures 4.2 and 4.3 respectively. Conventional satellite imagery for orbit 4347, shown in Figure 4.4, suggests that this cloud was, indeed, thin cirrus, since the cloud is clearly seen on the infrared image, but not on the visible image.





Also, the hourly weather reports from Sachs Harbour in Table 1.1 show scattered mid cloud only at 1400Z and 1600Z, but a more extensive layer of thin cirrus based at 23 000 feet, which did not leave the region until sometime after 1800Z. This cloud formation was therefore likely thin cirrus.

The apparent decrease in central temperatures of this cloud as it moved away from the coastline of Banks Island in Figures 4.2 and 4.3 may have been caused by changes in the underlying surface temperature. The measured temperature of thin cirrus is affected by surface radiation (Valovcin, 1968). Since the sea surface temperature on this day was much lower than the surface temperatures observed on Banks Island, less surface radiation would have been measured as the cloud moved over the sea, and this may have resulted in lower observed temperatures.

The center of this cloud formation is marked with an A on Figures 4.1, 4.2 and 4.3. Between Orbits 4345 (Figure 4.1) and 4346 (Figure 4.2) the cloud moved about 70 km. This represents an average motion of 38 km per hour (20 knots) from  $50^{\circ}$  (NE) between 1731Z and 1926Z. The cloud moved 100 km between 1926Z (Figure 4.2) and 2120Z (Figure 4.3), an average motion of 53 km per hour (28 knots) from  $45^{\circ}$  (NE). The 400-mb winds contained in the upper air profiles of Table 1.2 correspond to winds at approximately 24 000 feet, which should be comparable to the height at which this cloud occurred. At 1200Z on July 15 the 400-mb wind at Sachs Harbour was from  $60^{\circ}$  (ENE) at 22 knots, and at 0000Z on July 16, from  $65^{\circ}$  (ENE) at 32 knots.





The average speed and direction of motion of this formation thus seems comparable to the reported upper winds.

Further upper-air wind information could be derived from the movement of cloud to the north of Banks Island. A formation of cloud could be seen over western Melville Island on the conventional infrared satellite imagery of Orbit 4347 (Figure 4.4a). However, this formation was almost invisible on the visible imagery (Figure 4.4b). The brightness of the cloud on the infrared image suggested a low-temperature high-altitude cloud. This cloud was therefore identified as cirrus. The movement of this cloud formation could also be seen on the temperature plots of the last two orbits (Figures 4.7 and 4.9). However, following the motion of this formation accurately was difficult, since the cloud was dissipating as it moved across M'Clure Strait. The isotherm pattern of Figure 4.7 (Orbit 4349) showed numerous closed isotherms, while the isotherm pattern of Figure 4.9 (Orbit 4350) from only two hours later showed but two, indicating a decrease in cloud intensity. However, a rough estimate of the cloud motion on the basis of the movement of the approximate center of the formation (marked with a B on Figures 4.7 and 4.9) suggested a wind speed of about 55 km per hour (30 knots) from 60° (ENE) between 0108Z and 0303Z of July 16. These values were also comparable to those measured at Sachs Harbour at 0000Z on July 16.

The extent of synoptic-scale cloud over Banks Island on July 15 appeared to be limited to the two cirrus formations over the northern



and southern portions of the island. All other cloud over Banks Island on this day was believed to have developed by local processes. The initial temperature-field pattern of Banks Island (Figure 4.1) showed only small regions where the temperature was more than  $3^{\circ}\text{C}$  lower than the surrounding land, implying very thin or scattered cloud cover. There was also no evidence of extensive cloud cover to the north or east of the northern half of the island, with the exception of one small region over Prince of Wales Strait where the lowest closed isotherm was  $0^{\circ}\text{C}$ , and two even smaller patches about 50 km north of the island. However, by the time of the next orbit, shown in Figure 4.2, the entire central portion of the island was covered in cloud, and the temperature differences between the cloud and nearby cloud-free land were in excess of  $10^{\circ}\text{C}$ . There was also a large area of cloud extending off the western coastline. The increase in both the areal extent and density of cloud over the two hour period between Figures 4.1 and 4.2 suggested development by local processes. The primary cause of this development was believed to have been surface heating.

The change in surface temperature during July 15 was examined in the northwestern portion of Banks Island. This region was the only portion of the island which appeared cloud free throughout the entire day. The northeastern part of the island was cloud free during the later afternoon, but showed some evidence of scattered cloud over the first two orbits (Figures 4.1 and 4.2) by the non-uniform surface pattern and isolated temperature minima in this



region. Likewise, in the southeast, there was also apparent clearing during the last few hours of satellite coverage. The cirrus formation which was over southwestern Banks Island on the first orbit of July 15 (Figure 4.1) had passed the coastline by the next (Figure 4.2). Thereafter, this region appeared cloud free until the late afternoon. Surface temperatures could therefore also be measured in these regions on July 15. Only in the center of the island, which remained cloud covered for the majority of the day, were surface temperatures not available. The surface temperature of northwestern Banks Island was measured over the period of six consecutive satellite orbits on July 15. At 0931 local time (Figure 4.1), the surface temperature in this part of the island was above  $12^{\circ}\text{C}$ , with maximum temperatures in excess of  $15^{\circ}\text{C}$ . By 1126 local time (Figure 4.2) the highest observed temperatures had risen to above  $18^{\circ}\text{C}$ . At 1320 local time (Figure 4.3), the highest surface temperature was still over  $18^{\circ}\text{C}$ , but the region of temperatures greater than  $15^{\circ}\text{C}$  was considerably smaller than that two hours earlier. This suggests that the maximum surface temperature for this region occurred at sometime between 1126 and 1320 local time, but nearer to 1126. This time of maximum surface temperature is therefore in agreement with the near-noon maxima expected as a result of solar heating, as was discussed earlier in this Chapter. Thereafter, surface temperatures would be expected to fall, and, indeed, by 1514 local time (Figure 4.5), temperatures above  $18^{\circ}\text{C}$  were no longer observed in the northwest portion of Banks Island.







The surface temperatures continued to fall over the following orbits. The highest observed surface temperature in this region at 1903 local time (Figure 4.9) was below  $15^{\circ}\text{C}$ .

A similar temperature development was observed over the southwestern portion of Banks Island on July 15. The thin cirrus cloud observed at 0931 local time (Figure 4.1) and scattered middle cloud reported near Sachs Harbour earlier (Table 1.1) may have resulted in slightly lower surface temperatures in this region, though temperatures in excess of  $18^{\circ}\text{C}$  were observed by 1126 local time (Figure 4.2) and temperatures above  $15^{\circ}\text{C}$  continued through 1320 local time (Figure 4.3). Throughout the later afternoon, however, scattered cloud cover in this region prevented further surface temperature measurements.

The highest surface temperatures observed on Banks Island on July 15 were above  $18^{\circ}\text{C}$ . However, the maximum surface temperatures on this day were likely somewhat higher than this, because the satellite measurements were not available near local noon, when the maxima would be expected. The highest surface temperatures were observed in clear regions. In regions where cloud was present for part of the day, surface temperatures were likely lower because of lessened solar insolation, depending on the amount of cloud cover. However, all regions of Banks Island experienced surface temperatures above  $12^{\circ}\text{C}$  during July 15, and probably only a few areas failed to reach  $15^{\circ}\text{C}$ . The temperature contrast between the warm island surface and the near freezing temperatures of the surrounding ice and water surfaces was thus considerable on this day.



The expected closely-packed isotherms near the coastline of Banks Island were observed on all satellite plots on July 15 when the coastline was not obscured by cloud. Unfortunately, the temperature gradient along most of the western coastline could not be measured because of persistent cloud cover over this region. However, the northern coastline was clear throughout the day, except for the cirrus formation mentioned earlier which passed over the extreme northwestern coast late in the afternoon. Only the occasional patch of cloud was observed along the eastern coastline. Measurements of thermal gradients were therefore made at various locations along both the northern and eastern coasts.

The surface-pressure chart for 1800Z on July 15 (Figure 1.5) suggested that the synoptic-scale flow over Banks Island on this day was northeasterly. This implied that the northern coastline from Cape Wroottesly to Mercy Bay (see Figure 1.2) and from Cape Vesey Hamilton to Russell Point would experience an onshore flow. Between Cape Vesey Hamilton and Mercy Bay, and from Cape Wroottesly to Cape Prince Alfred, less of an onshore flow would be expected. An onshore flow likely also occurred along the eastern coastline south of Stewart Point, while along the Prince of Wales Strait, the flow was probably almost parallel to the coastline.

The observed changes in the coastal isotherm gradients seemed to support this advection pattern. Along the northern coastline, the gradient was most intense at 1126 local time (Figure 4.2). However, the gradient weakened considerably later in the afternoon. By 1903 local time (Figure 4.9), the spacing between the coastal isotherms





was two to three times wider than near local noon. The greatest amount of spreading occurred in the regions between Russell Point and Cape Vesey Hamilton, and from Mercy Bay to Cape Wrottesly, where the onshore flow was expected to be strongest. In contrast, comparatively little change in the isotherm gradient occurred between Cape Vesey Hamilton and Mercy Bay, and west of Cape Wrottesly. (The weak gradient near Cape Prince Alfred in Figure 4.9 was likely caused by the thin cirrus cloud in the area at that time.)

The isotherm gradients along the eastern coastline were also strongest near the maximum surface temperature time (Figures 4.2 and 4.3). Again, very little isotherm spreading occurred during the afternoon along the Prince of Wales Strait. However, south of Stewart Point, the distance between the isotherms on Figure 4.9 was as much as twice as wide as that observed on Figure 4.3, though this change was not as pronounced as that observed along the northern coastline. Thus, the regions where onshore advection of cooler air was expected showed evidence of this advection by enhanced lowering of coastal surface temperatures, while those regions where less onshore advection was expected showed substantially less change in coastal temperature gradients.

The formation of cloud over Banks Island on July 15 also provided evidence of the coastal circulation pattern. On the initial temperature field plot shown in Figure 4.1, little cloud was observed over Banks Island. However, the temperature fields and satellite imagery from later in the day showed considerable cloud over the





central and southern portions of the island, and off the western coastline. Since little cloud was observed upstream, it was decided that this cloud was formed from local processes. The fact that the cloud was observed in the same general regions on each satellite orbit also suggested that the local formation processes remained in effect through the entire afternoon.

Three regions of Banks Island were studied with respect to cloud formation on July 15: the north-central part of the island, the western coastline, and the southern regions near Sachs Harbour. The first region to be studied was the north-central portion of the island. No local cloud formation was evident over the northwestern portion of the island on any of the six temperature plots of July 15. Cloud was also not observed in the northeastern part of the island, except for a few scattered patches during the first few hours of satellite coverage. Strong cloud development was observed only in the region directly south of Mercy Bay and over the central portion of the island. Comparison with the contour map of Banks Island shown in Figure 1.2 suggested that this cloud formed primarily over low-lying terrain. The explanation for this may have been the dryness of the Arctic air.

The synoptic flow over the northern portion of Banks Island on July 15 was from the northeast. Ice charts for the Beaufort Sea region on this day indicated ice cover extending westward from Cape Wroottesly along M'Clure Strait, and also along the northern portion of Prince of Wales Strait. The visible satellite imagery



in Figures 4.4b, 4.6b, 4.8b, and 4.10b also indicated ice cover was still present in these regions. Thus, air reaching the northern coastline of Banks Island on July 15 would have passed over ice-covered waters, and would therefore have had little chance of picking up additional moisture before reaching the coast. The absence of cloud along the northern coast implied that even with lift imparted by surface heating and orographic effects, this air may have been too dry for cloud to form.

However, though the flux of water vapour from an ice surface is small, evaporation from the surface of Banks Island itself may have provided sufficient water vapour for cloud formation on this day. Though the surface of the island is mostly barren, what little moisture there is tends to accumulate in low-lying drainage areas and swamps, where summer thawing produces surface wetness (Burns, 1973b). Thus the regions of cloud formation on this day could have occurred in those regions where additional surface moisture was likely to have been available.

As has been mentioned, little cloud was observed over the northern portion of Banks Island in the initial temperature-field plot of this day (Figure 4.1). The lowest cloud temperatures at this time were observed along the eastern coastline over Prince of Wales Strait. Over the interior of the island, the low temperatures were confined to a few small patches below  $9^{\circ}\text{C}$ , suggesting either very scattered cloud conditions or very low cloud tops. By 1126 local time (Figure 4.2) the amount of cloud observed



was considerably larger, with a band of temperatures lower than  $9^{\circ}\text{C}$  stretching across the center of the island, and several locations where temperatures were less than  $6^{\circ}\text{C}$ . These lower temperatures implied an increase in the lifting mechanism over the central portion of the island. However, the relatively warm temperatures (above  $6^{\circ}\text{C}$  over most of the formation) still suggested only low or scattered cloud conditions.

The problems of identifying and tracking small or scattered cloud formations are well illustrated by Figures 4.1 and 4.2. The cloud pattern over Banks Island in Figure 4.2 shows little similarity to that from only two hours before in Figure 4.1. The change in observed temperatures also makes identification of the same cloud formation at each time nearly impossible.

The first afternoon orbit at 1320 local time (Figure 4.3) again showed several changes from that of two hours earlier. No evidence of cloud was seen along the eastern coastline on this or any later afternoon orbits. The main regions of cloud cover throughout the afternoon of July 15 were in the lowland regions south of Mercy Bay and across the central portion of the island. However, though extensive cloud cover was observed over these regions in Figure 4.3, as well as in the corresponding conventional imagery of Figures 4.4a and 4.4b, the same information did not suggest that very intensive cloud formation had yet occurred. The temperature plot of Figure 4.3 showed large areas of temperatures lower than  $6^{\circ}\text{C}$  and one region about 70 km south of Mercy Bay where temperatures were below  $3^{\circ}\text{C}$ , yet







the temperature pattern was still confused and there were no intense isotherm gradients along the cloud edges, such as might be expected around a well-developed cloud system.

However, by 1514 local time (Figure 4.5) the areas of cloud cover had become better defined. As in Figure 4.3, the lowest temperatures at this later time were south of Mercy Bay; the lowest readings were now below  $-3^{\circ}\text{C}$ , and sharper gradients were visible around the central region, suggesting more overcast conditions. The conventional satellite imagery in Figures 4.6 also indicated more cloud in this region than was seen on Figures 4.4. The upper-air temperature profiles of Table 1.2 correlate temperatures of  $-3^{\circ}\text{C}$  to between the 850 and 700-mb levels. Thus, the satellite measured temperatures at this time indicated cloud topped at about 8,000 feet.

The closely packed isotherms marking the edge of this cloud formation were also evident at 1708 local time (Figure 4.7). Once again, the closed isotherms in the region south of Mercy Bay indicated the continued presence of cloud. However, the lowest temperatures at this time were found further to the west than in Figure 4.5. This apparent shifting of the location of the highest cloud tops could have been the result of new formation further west, and corresponding strong subsidence in the region south of Mercy Bay, but was more likely caused by advection. The approximate center of the region of temperatures below  $0^{\circ}\text{C}$  was marked with a C on Figures 4.5 and 4.7. The westward motion of this cooler region corresponded to a cloud motion of about 28 km per hour



(15 knots) from  $75^{\circ}$  (ENE). This motion was in agreement with the mid and low-level winds reported at Sachs Harbour for 0000Z on July 16, shown in Table 1.2.

The temperature pattern observed at 1903 local time (Figure 4.9) also supported the advection of this cloud formation rather than reformation of cloud further west. Closed  $3^{\circ}\text{C}$  isotherms were again observed in the region south of Mercy Bay on Figure 4.9, but the area of temperatures below  $3^{\circ}\text{C}$  was smaller than in Figure 4.7, and the isotherm gradient at the cloud edge was also weaker. However, there was no evidence of a sharp rise of temperature in this region such as was observed between Figures 4.5 and 4.7. If subsidence was the cause of the increasing temperatures south of Mercy Bay, less erratic changes in the cloud intensity would be more probable. Advection of the cloud formation out of the area may explain this temperature change more reasonably.

The region of temperatures below  $0^{\circ}\text{C}$  in Figure 4.9 (also marked C) was again further west than that in Figure 4.7. The motion of the center of this region was measured as about 20 km per hour (10 knots) from  $75^{\circ}$  (ENE) over the period between Figures 4.7 and 4.9. Thus, the direction of motion of this cloud again agreed with the winds reported from Sachs Harbour. The apparent decrease in speed of the cloud will be discussed later.

It was believed that the formation mechanism for cloud over the north-central portion of Banks Island on July 15 was surface heating. The general pattern of cloud formation shown in Figures



4.1 through 4.9 supported this belief. Initially, only scattered patches of cloud were observed over this region of the island, but as the surface temperature rose, the amount and intensity of cloud increased. The maximum surface temperatures were believed to have occurred sometime near local noon, but the maximum cloud formation was not observed until several hours later, likely sometime between the times of Figures 4.5 and 4.7, or near 1600 to 1700 local time. Thereafter, though the cloud already formed did not dissipate rapidly, no lower temperatures associated with high cloud tops or thicker cloud appeared. The major region of cloud formation on this day appeared to have been in the region south of Mercy Bay. The motion of the eastern edge of this cloud also suggested formation by surface heating. The strongest vertical motions at the Earth's surface would be expected near the time of maximum ground-air temperature difference, or near local noon. Thereafter, the vertical motions would weaken progressively as the surface temperature dropped. Thus, during the afternoon, air parcels would tend to be advected further by the synoptic-scale flow before cloud would form. This mechanism could explain the steady westward shift of the eastern edge of the cloud south of Mercy Bay on the afternoon temperature plots of July 15.

The next region of cloud formation considered was the western coastline of Banks Island north of Cape Kellet. The initial temperature plot at 0931 local time (Figure 4.1) showed a well-defined coastal isotherm gradient and little evidence of cloud. Yet, less than two hours later (Figure 4.2) cloud covered the entire western







shoreline. Similar cloud patterns in this region were also observed in Figures 4.3 and 4.5. Comparison of these thermal plots with the conventional satellite imagery for the same times (Figures 4.4 and 4.6) indicated that the seaward extent of this cloud could be delineated by the  $0^{\circ}\text{C}$  isotherm. The small difference in temperature between this cloud formation and the sea surface temperatures, the offshore synoptic flow expected over this coast, and the cloud's location close to the coastline suggested that this cloud was a type of low stratus formed by the advection of warm air from Banks Island over the colder coastal waters. Such cloud formation is often observed along Arctic coastlines in the summer when the synoptic flow is offshore (Kruger, 1960; Burns, 1973b).

The lowest observed cloud-top temperatures off the western coastline were below  $-6^{\circ}\text{C}$ . However, the upper-air profiles from Sachs Harbour could not be used to estimate the heights of these cloud tops. Though reasonable estimates of cloud heights could be obtained over Banks Island by assuming the upper-air temperature profile over the land was approximately constant, such an assumption would not be valid over the sea surface, where the surface temperatures were vastly different. At offshore locations, though temperatures in the upper levels would likely be comparable to temperatures over the island, the low-level temperature profile would be very different. Rao (1970) suggests that an estimated height based on the type of cloud may be derived by comparing the cloud top temperature to the surface temperature. The sea-surface



temperature along the western coastline in Figure 4.1 was between 0 and  $3^{\circ}\text{C}$ , while the cloud formations in Figures 4.2, 4.3 and 4.5 had average temperatures of about  $-3^{\circ}\text{C}$ . Thus, the surface land difference in temperature was likely only about 3 to  $6^{\circ}\text{C}$ , again suggesting cloud formation at a very low level.

The temperature-field plots in Figures 4.2, 4.3, and 4.5 and the conventional imagery of Figures 4.4 and 4.6 showed little change in the intensity or areal extent of this coastal cloud between 1230 and 1515 local time. However, the temperature plot at 1708 local time (Figure 4.7) and the conventional imagery for the same time (Figures 4.8) indicated cloud coverage which was vastly reduced in both area and intensity. This rapid dissipation was not likely to have been the result of radiational effects, since the afternoon is usually a time of radiational cooling. The formation of an advection cloud of this type is often dependent on the wind speed. The sudden appearance of this cloud between the times of Figures 4.1 and 4.2 may have been caused by an increase in the surface wind speed at that time. The reported surface winds at Sachs Harbour (Table 1.1) showed considerable variation in speed during the morning, and it is possible that similar variations also occurred along the western coastline. However, once this cloud was formed, a decrease in wind speed would not necessarily cause rapid cloud dissipation.

The most common cause for dissipation of an advection cloud is a change in wind direction. However, the surface and upper-air



charts presented in Section 1.3 did not indicate any sudden changes in wind direction during this time period. Therefore, a change in direction, if it occurred, was a local change only. Closer examination of the temperature plots also indicated that the region of lowest temperatures enclosed by the  $-3^{\circ}\text{C}$  isotherm was in the vicinity of Burnett Bay in Figure 4.2, but moved steadily southwards over the next two orbits. Also, though thin coastal cloud was still evident south of Bernard Island in Figure 4.7, none was visible north of this location. This implied that whatever the mechanism for cloud dissipation was, it was strongest along the coastline north of Burnett Bay.

In Section 1.3, it was found that on July 15, 1977, a sea breeze circulation was observed at Sachs Harbour. If conditions at Sachs Harbour were representative of conditions along the western part of Banks Island on this day, then the sea breeze circulation would have begun along the western coastline at about 2200Z or 1400 local time, and would have reached its maximum landward and seaward extent several hours later. Thus, the dissipation of cloud along the western coastline between 1515 and 1710 local time may well have been caused by the development of a sea breeze circulation in this area, and the resultant change in local wind direction. Also, the synoptic-scale flow over Banks Island on this day was northeasterly. Therefore, the region north of Burnett Bay would have experienced a larger offshore component of the wind than those areas further south. This stronger offshore







flow may have resulted in a stronger enhancement of the offshore part of the sea breeze circulation in this region, producing an earlier appearance of the onshore sea breeze flow, and a stronger breeze itself. This may have been the reason for the early clearing of cloud along the northern portion of the west coast, while the regions further south were cloud obscured for several hours longer.

Further evidence of a sea breeze circulation along the western coastline was provided by the movement of cloud formed over the central portion of Banks Island, discussed earlier. This cloud formation was advected over the western coast during the afternoon of July 15. The direction of motion of the center of this formation between the times of Figures 4.5 and 4.9 was in agreement with the mid and low-level winds reported at Sachs Harbour. The speed of motion measured between Figures 4.5 and 4.7 was also in agreement with the reported wind speeds. However, the speed decreased by about 5 knots as the cloud approached the western coastline. The orientation of the formation also changed as it moved towards the shore of Banks Island. In Figure 4.5, the region of below  $0^{\circ}\text{C}$  temperatures was lying almost east-to-west. However, in Figure 4.9, the orientation of this same region changed to almost north-to-south. This rotation implied a slower motion of the southern portion of this cloud system, which reached the western coastline first. Indeed, the isotherm pattern in Figure 4.9 suggested that the cloud which remained onshore at this time was oriented almost parallel to the coast.



This cloud motion could be explained by the presence of a sea breeze circulation along the western coastline. If the bases of this cloud were low enough, the offshore motion of the formation would have been slowed by the onshore sea breeze itself. Though the sea breeze could prevent actual offshore advection only in the lowest few hundred meters, even the movement of mid-level cloud could have been hampered by the existence of a sea breeze circulation. The onshore convergence zone of the sea breeze would tend to enhance cloud formation inland, while the offshore subsidence zone would tend to dissipate any cloud moving away from the coast. This effect, as well as the inland motion of the convergence zone during the afternoon, could have resulted in an apparent slowing of any cloud passing through the coastal zone, and produced a realignment of this cloud formation parallel to the coastal convergence zone.

The final region of cloud formation studied on July 15 was over the southern portion of Banks Island. The Durham Heights, at the extreme southern tip of the island, were cloud-free on this day. However, the reasons for this lack of cloud may have been slightly different for this area than for the higher elevations along the northern coast. The ice charts for the Beaufort sea region and the visible satellite imagery in Figures 4.4b through 4.10b suggested that the Amundsen Gulf and the southern portion of the Prince of Wales Strait were ice free on July 15, except for isolated regions of shore-fast ice or ice floes. The northeasterly synoptic flow



over the Banks Island region on this day therefore had an open water trajectory before reaching the southeastern portion of the island. Thus, it is possible that the moisture content of the air was higher than that further north, which may explain why cloud formation over the southern part of the island was not confined to low lying areas only, though the barren Durham Heights still remained cloud-free throughout the day.

Cloud formation over the southern portion of Banks Island on July 15 was very similar to that further north. The temperature plots at 0931 and 1126 local times (Figures 4.1 and 4.2 respectively) showed little evidence of cloud. By 1320 local time (Figures 4.3 and 4.4) scattered cloud was visible over the south-central part of the island. The area and intensity of cloud cover increased during the afternoon until at 1514 local time (Figures 4.5 and 4.6) thin or scattered cloud was evident over the south-central and southwestern portions of the island, and cloud remained over these areas through the remainder of the satellite orbits on this day. The lack of cloud formation along the eastern coastline was likely caused by a lack of moisture in the air, requiring that considerable lift, and possibly even additional surface moisture, was necessary before formation occurred. However, cloud formation occurred much closer to the shoreline along the southern part of the island than over the northern coasts. This also suggested that the air advected over the southern island was moister than that further north.

As was the case in the north-central part of Banks Island,







the general pattern of cloud formation in the south-central portion of the island suggested that lift from surface heating was the major cause for this cloud. The lowest cloud temperatures in this region were observed in the late afternoon, and no strong cloud formation was observed after about 1700 local time. Also, the isotherms marking the eastern edge of cloud cover in the south moved westward during the afternoon, indicating progressively weaker lift over the region, likely caused by decreasing surface temperatures.

The cloud formation observed over the southern half of Banks Island on this day was neither as widespread nor as intense as that observed further north. Therefore, it was more difficult to trace the advection of cloud formed in this region. Nevertheless, the locations of the regions of lowest temperature still provided evidence for a sea breeze circulation along the west coast of Banks Island south of Cape Kellet. At 1514 local time (Figure 4.5) the lowest observed temperatures, and hence the most intense cloud formations, were located about 100 km west of Sachs Harbour, with central values below  $0^{\circ}\text{C}$ . At 1708 local time (Figure 4.7) the lowest temperatures were again associated with two areas below  $0^{\circ}\text{C}$  located some 40 km inland from the southwestern coast. On the final satellite orbit at 1903 local time (Figure 4.9) the region of below  $0^{\circ}\text{C}$  temperatures was located northeast of Sachs Harbour, between about 20 and 70 km inland. If these regions of minimum temperature were the result of advection of cloud formed over the



south-central part of Banks Island, then the initial motion between Figures 4.5 and 4.7 would agree in direction with the mid and low-level winds reported at Sachs Harbour, though the speed would be about 5 knots too slow. However, the motion of the cloud over the final two hours of satellite coverage was northwesterly, almost perpendicular to the reported Sachs Harbour winds. On the other hand, if these regions of cloud were not the result of advection, then the thicker cloud observed near the coastline in Figures 4.7 and 4.9 must have been formed by some other process, since the synoptic flow in this area was offshore and the general cooling of surface temperatures at that time would make new formation by surface heating unlikely.

As has been mentioned, a sea breeze was observed at Sachs Harbour on July 15 beginning just before 1400 local time, or about one hour before the time of Figure 4.5. If the conditions at Sachs Harbour were representative of conditions along the entire southwest coastline of Banks Island, then a southerly to southwesterly onshore flow would have been present in this region after about 1400 local time. Thus, if the cloud formed in the south-central portion of Banks Island in Figure 4.5 was advected by the synoptic flow, the onshore sea breeze could have produced a slower offshore cloud motion than that suggested by the reported upper winds, while the combination of the southerly sea breeze and the northeasterly synoptic flow could have resulted in the northwesterly motion of cloud near the shoreline between the times of Figures 4.7



and 4.9. If this cloud was not, however, advected from inland, then the new cloud formation along the coast could have been the result of lift in a sea breeze frontal zone. Indeed, it is possible that a combination of the two effects occurred on this day. Cloud formed over the central part of the island in the afternoon may have been advected towards the southwestern coast and enhanced in a sea breeze convergence zone, thus producing the cloud patterns and apparent cloud motions observed along this coastline on July 15.

Further evidence of a sea breeze circulation along the southwestern coastline was seen in the coastal temperature patterns of Figures 4.5 to 4.9. The rise in temperatures along the southern portion of the coastline between Figures 4.5 and 4.7, and a similar temperature rise near Sachs Harbour between Figures 4.7 and 4.9 both indicated clearing of cloud along the coastline, one of the marks of a sea breeze circulation. This coastal clearing was also visible on the infrared satellite imagery of Figures 4.8a and 4.10a, and is supported, at least in the Sachs Harbour area, by the decrease in cumulus cloud in the station reports in Table 1.1 after about 1600 local time on July 15 (0000Z on July 16). This cloud free coastal zone with an offshore synoptic flow, and cloud still evident just inland from the coastline, is the usual configuration expected in a sea breeze situation.

#### 4.3.3 Case 2 July 16 of 1977

On July 16 of 1977 satellite information from the Banks Island







region was available on five consecutive orbits of NOAA-5, numbered 4358 through 4362. Temperature plots of Banks Island for each orbit are shown in Figures 4.11, 4.12, 4.14, 4.16, and 4.18 respectively. The first orbit, 4358 (Figure 4.11) shows the temperature field at 1843Z (1043 local time at Sachs Harbour) on July 16. As in Case 1, intervals of approximately two hours separate each orbit, with the last, 4362, occurring at 0219Z on July 17 (1819 local time on July 16). Conventional satellite imagery was available for orbits 4359 through 4362; the respective infrared and visible images are shown in Figures 4.13, 4.15, 4.17 and 4.19.

The first consideration in this case was to verify the consistency of the temperature plots for this day. Reference was made in Section 2.5 to the use of data from July 14 and 15 orbits to externally calibrate the temperature values of July 16 orbits. This procedure was necessary because of the presence of cloud in the region of the Beaufort Sea which was to be used in the external calibration. Therefore, it is possible that the temperatures plotted may be in error. It was felt that the most conservative surface temperatures would be those in the Beaufort Sea and that, if temperatures in this region were comparable to those on the temperature plots of July 15, then the plotted values on the latter day would likely be accurate. In the plots of July 15 (Figures 4.1 through 4.9), the observed sea surface temperatures off the west coast of Banks Island were between 0 and 3°C, with a region about 100 km off the coast showing temperatures above 3°C in the late afternoon.



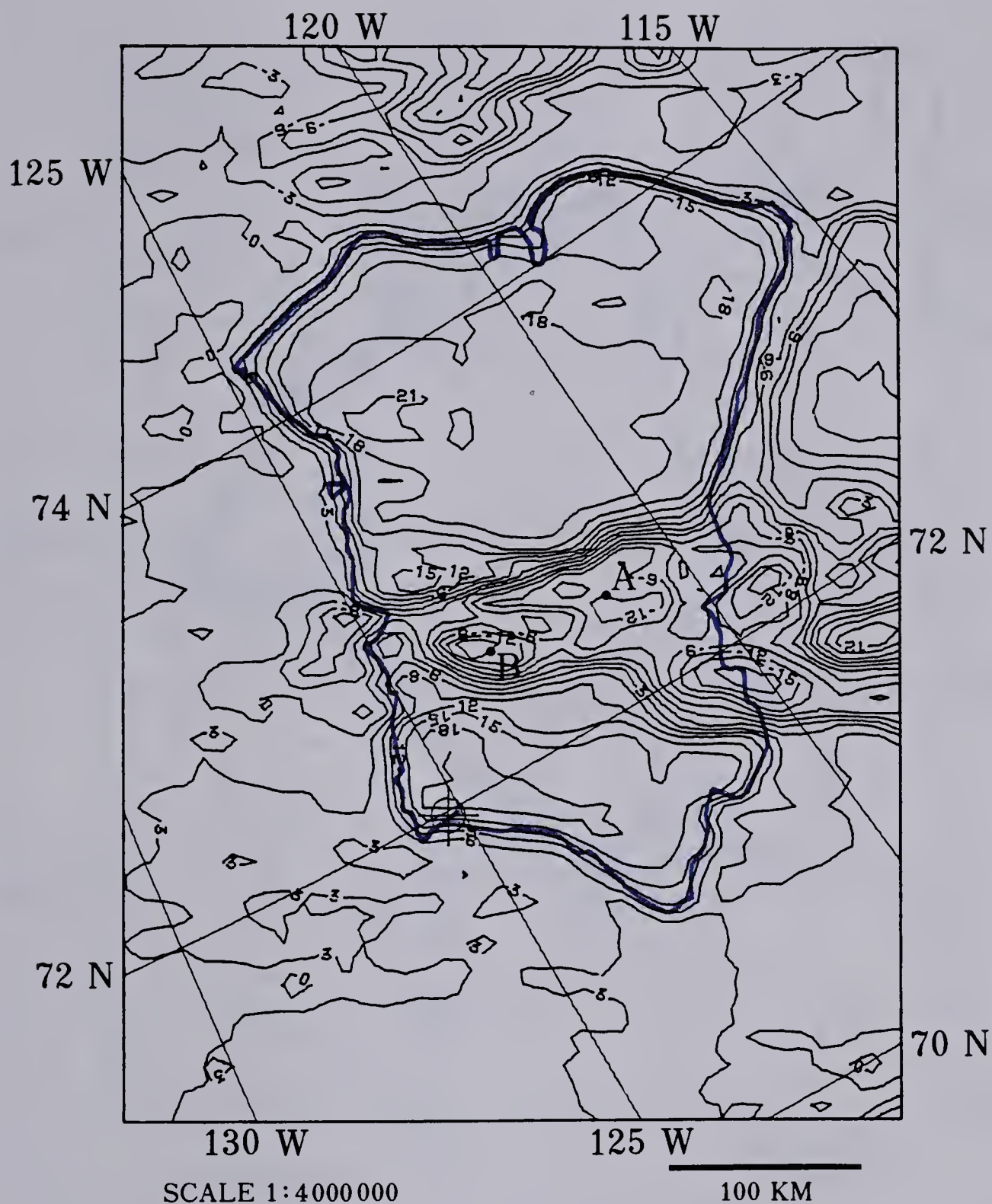


FIGURE 4.11 Averaged and smoothed temperature-field plot of the Banks Island region of Orbit 4358 of NOAA-5 at 1843Z (1043 local time at Sachs Harbour) on July 16, 1977. Contours are labelled in degrees Celsius.





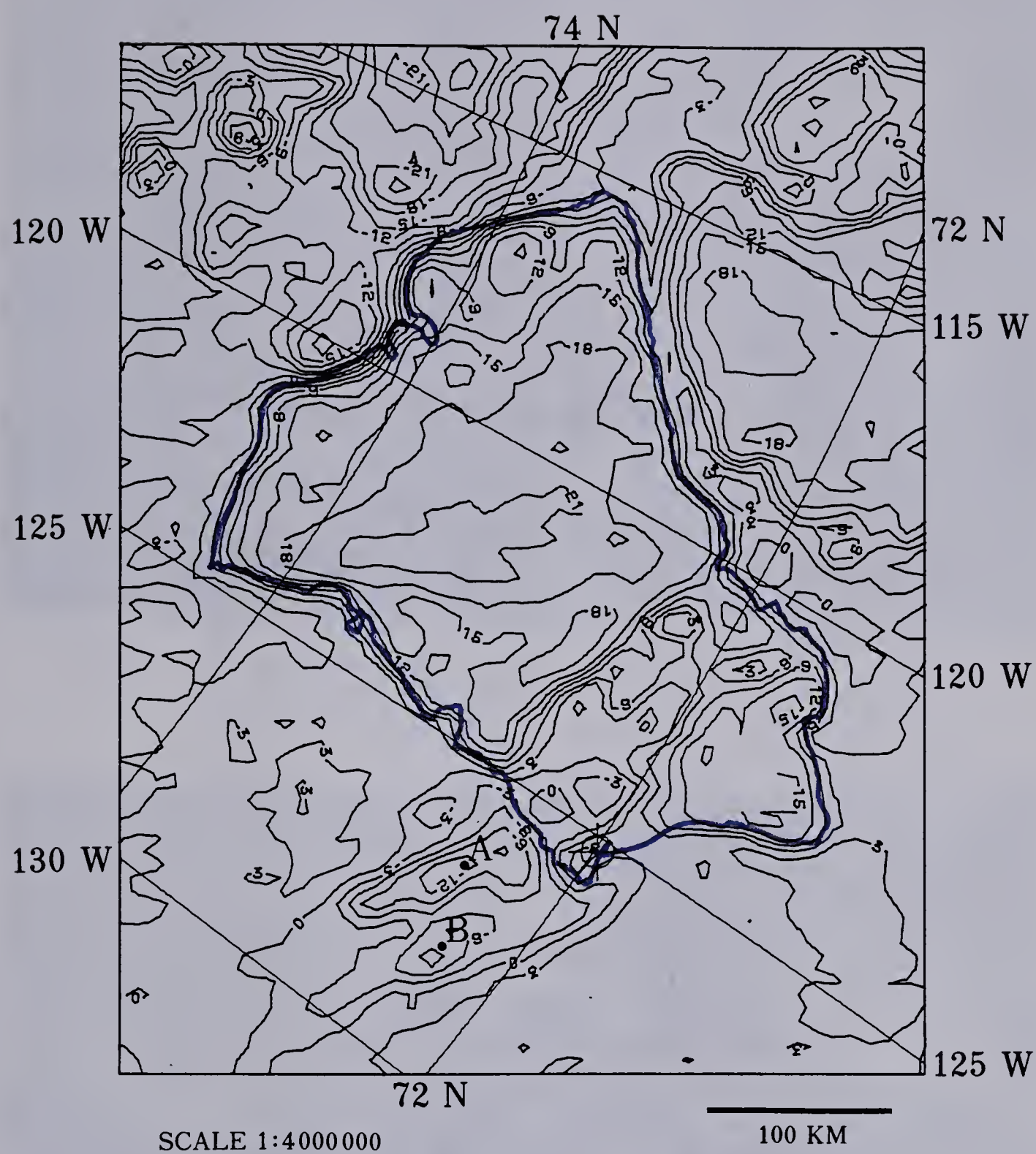








FIGURE 4.13a Infrared image of Beaufort Sea region of Orbit 4359 of NOAA-5 at 2035 Z on July 16, 1977.

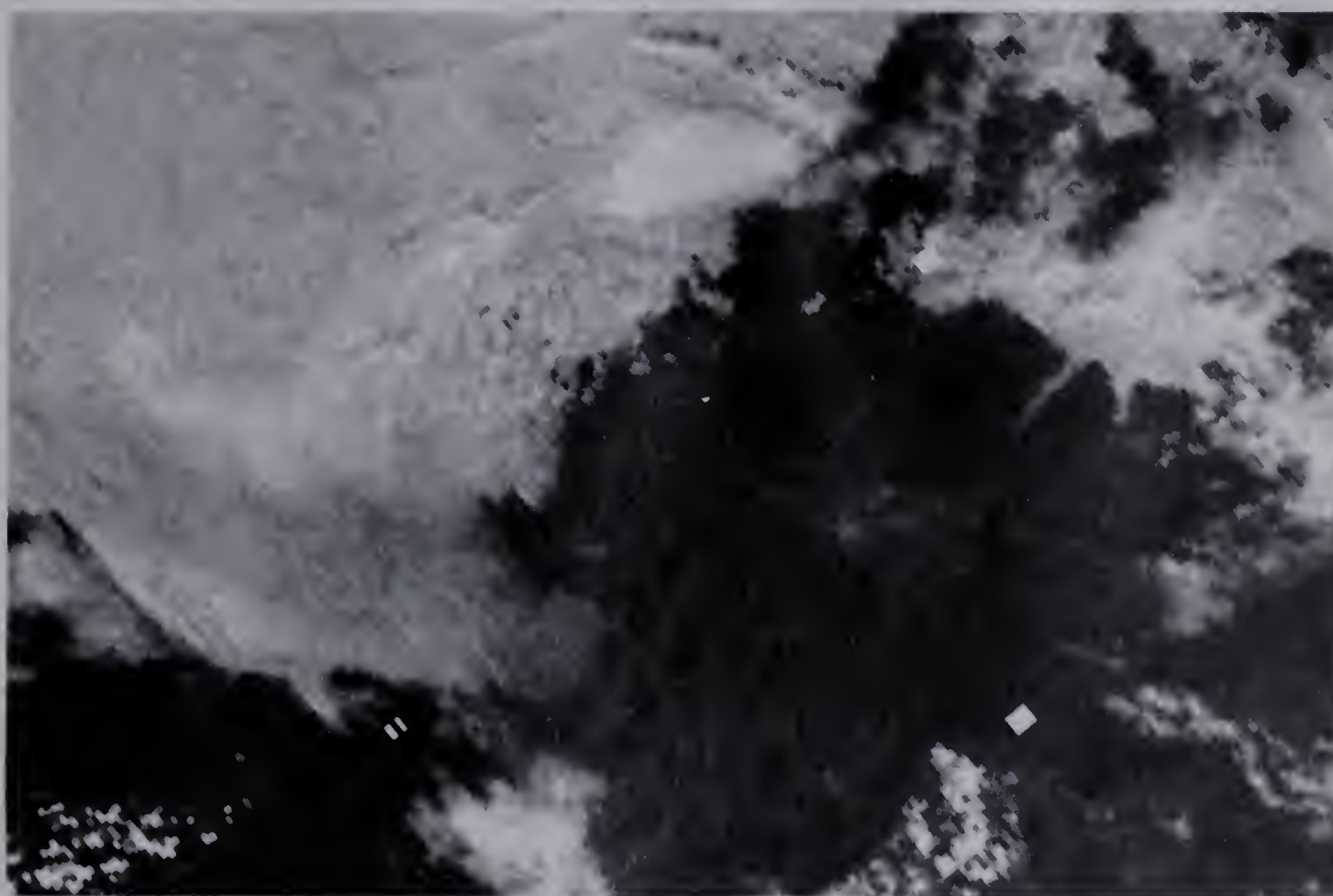


FIGURE 4.13b Visible image (as above).



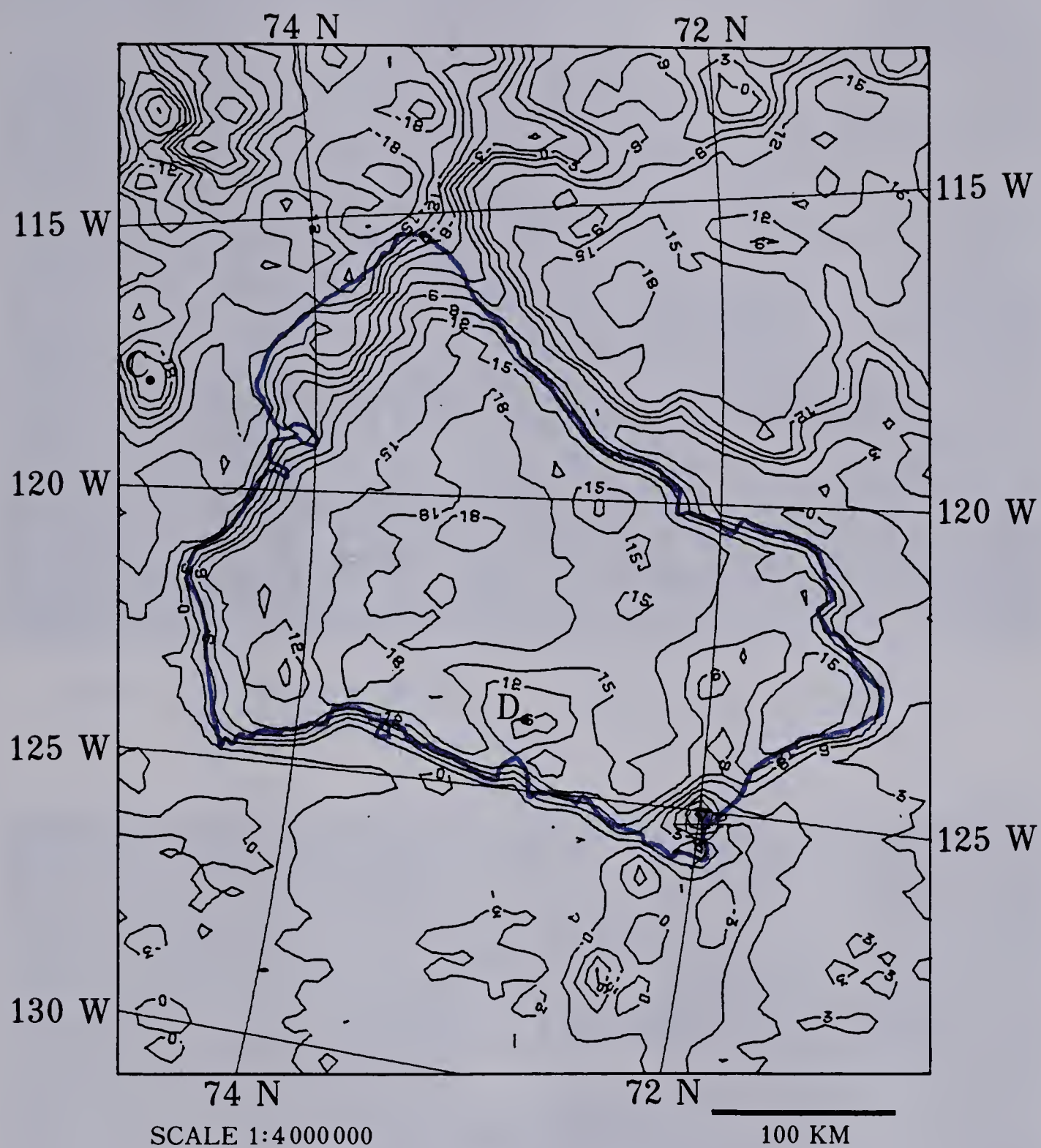


FIGURE 4.14 Averaged and smoothed temperature-field plot of the Banks Island region of Orbit 4360 of NOAA-5 at 2231Z (1431 local time at Sachs Harbour) on July 16, 1977. Contours are labelled in degrees Celsius.





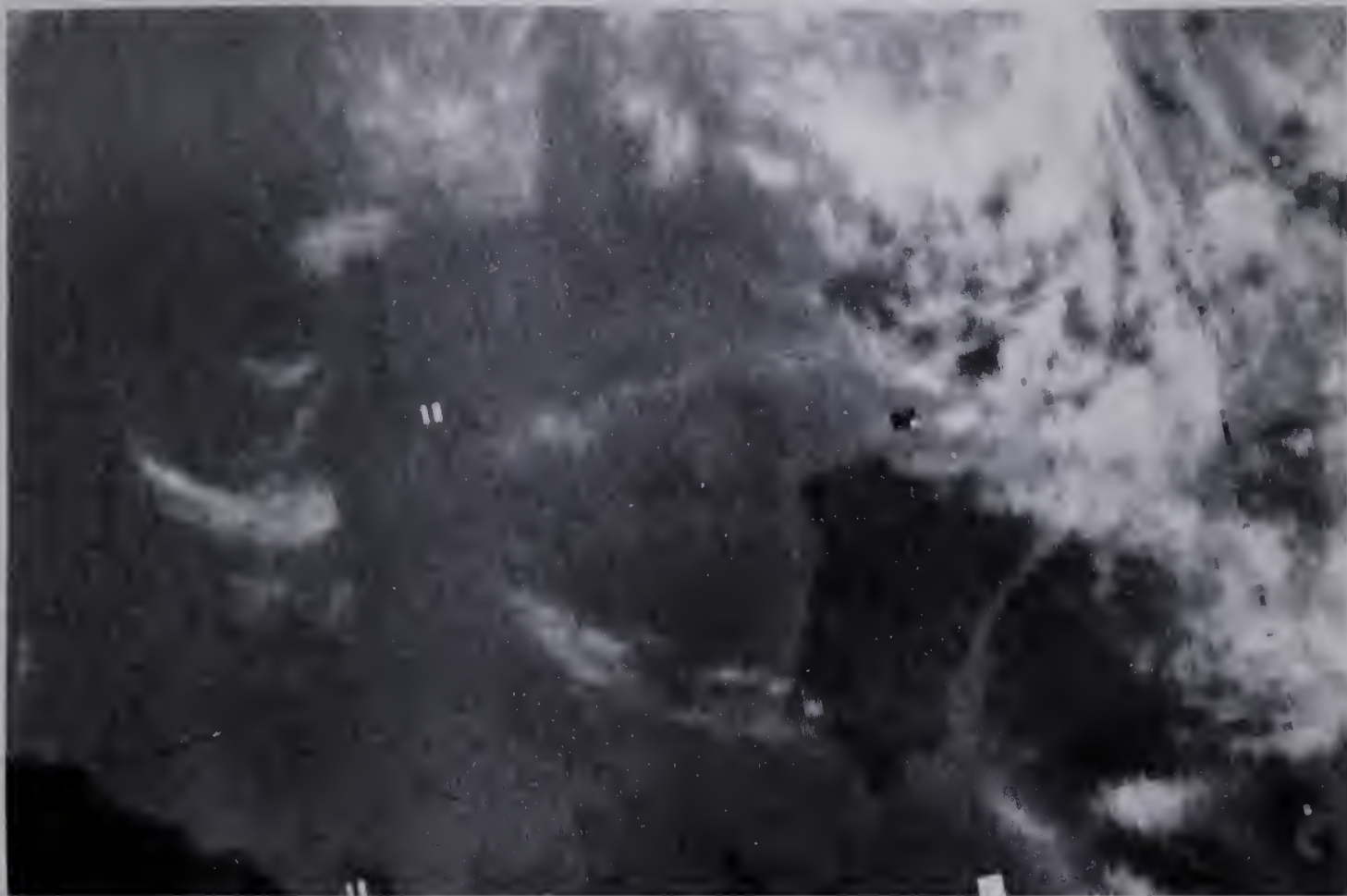


FIGURE 4.15a Infrared image of Beaufort Sea region of Orbit 4360 of NOAA-5 at 2230 Z on July 16, 1977.

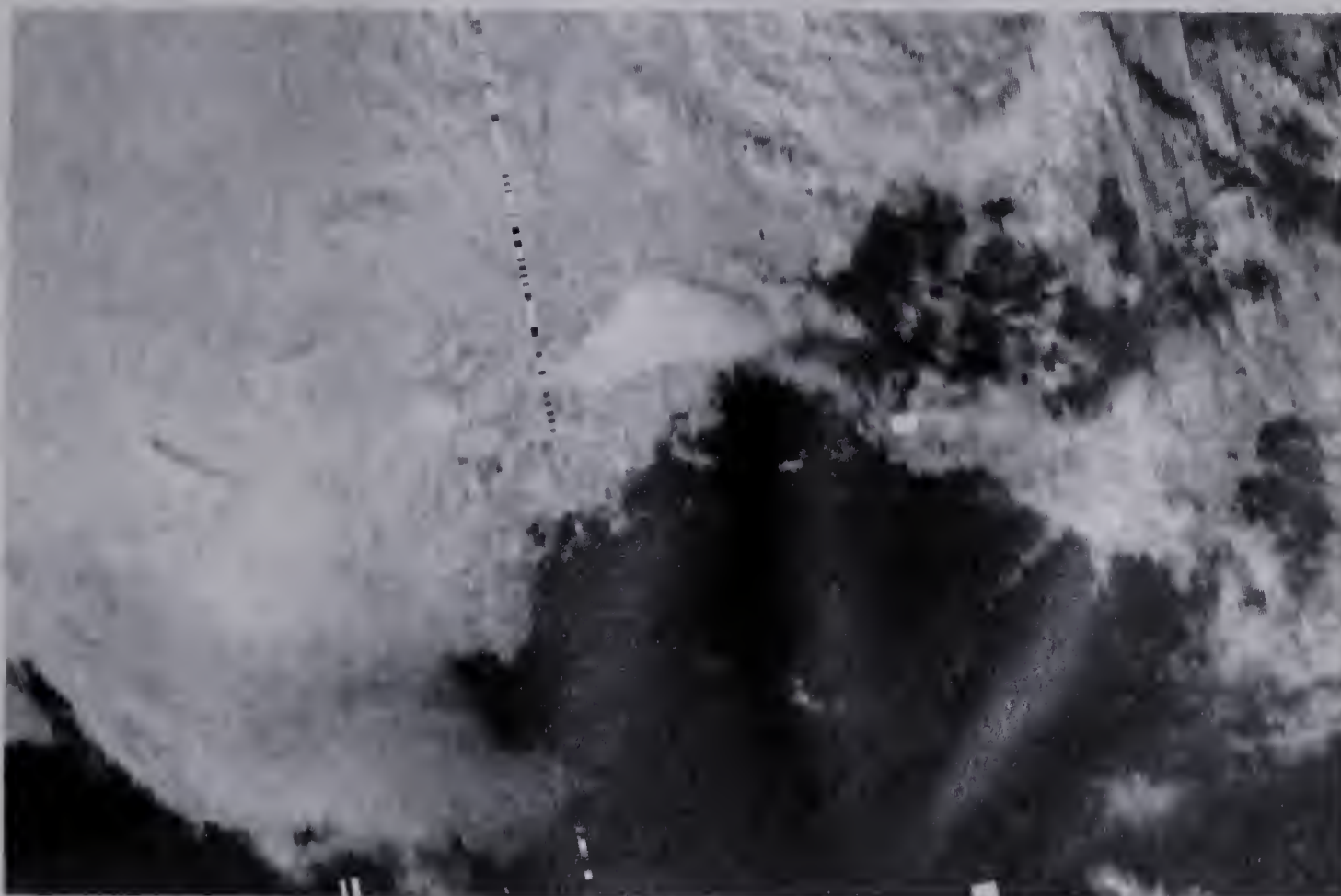


FIGURE 4.15b Visible image (as above).





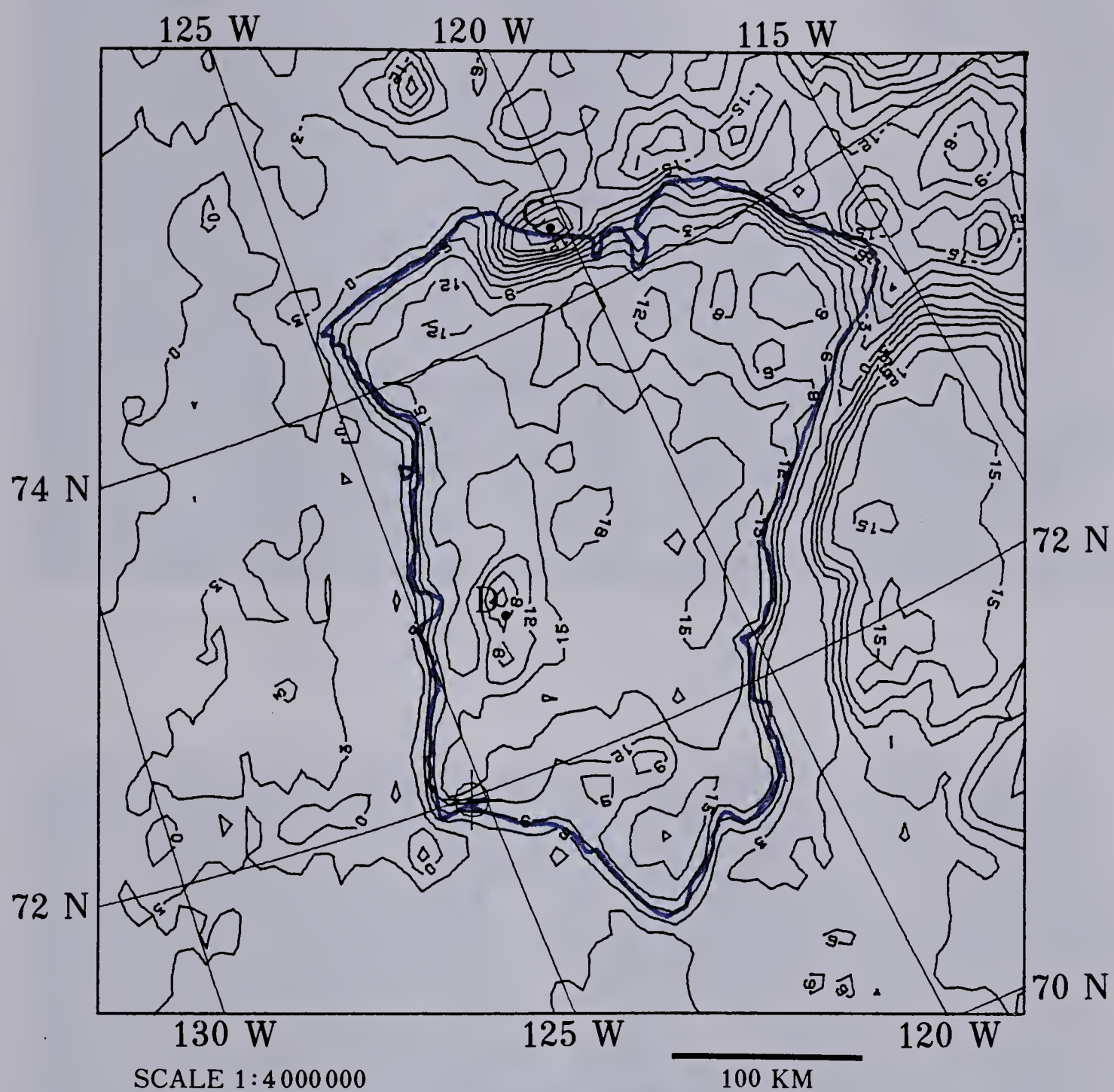


FIGURE 4.16 Averaged and smoothed temperature-field plot of the Banks Island region of Orbit 4361 of NOAA-5 at 0025Z on July 17, 1977 (1625 local time on July 16 at Sachs Harbour). Contours are labelled in degrees Celsius.



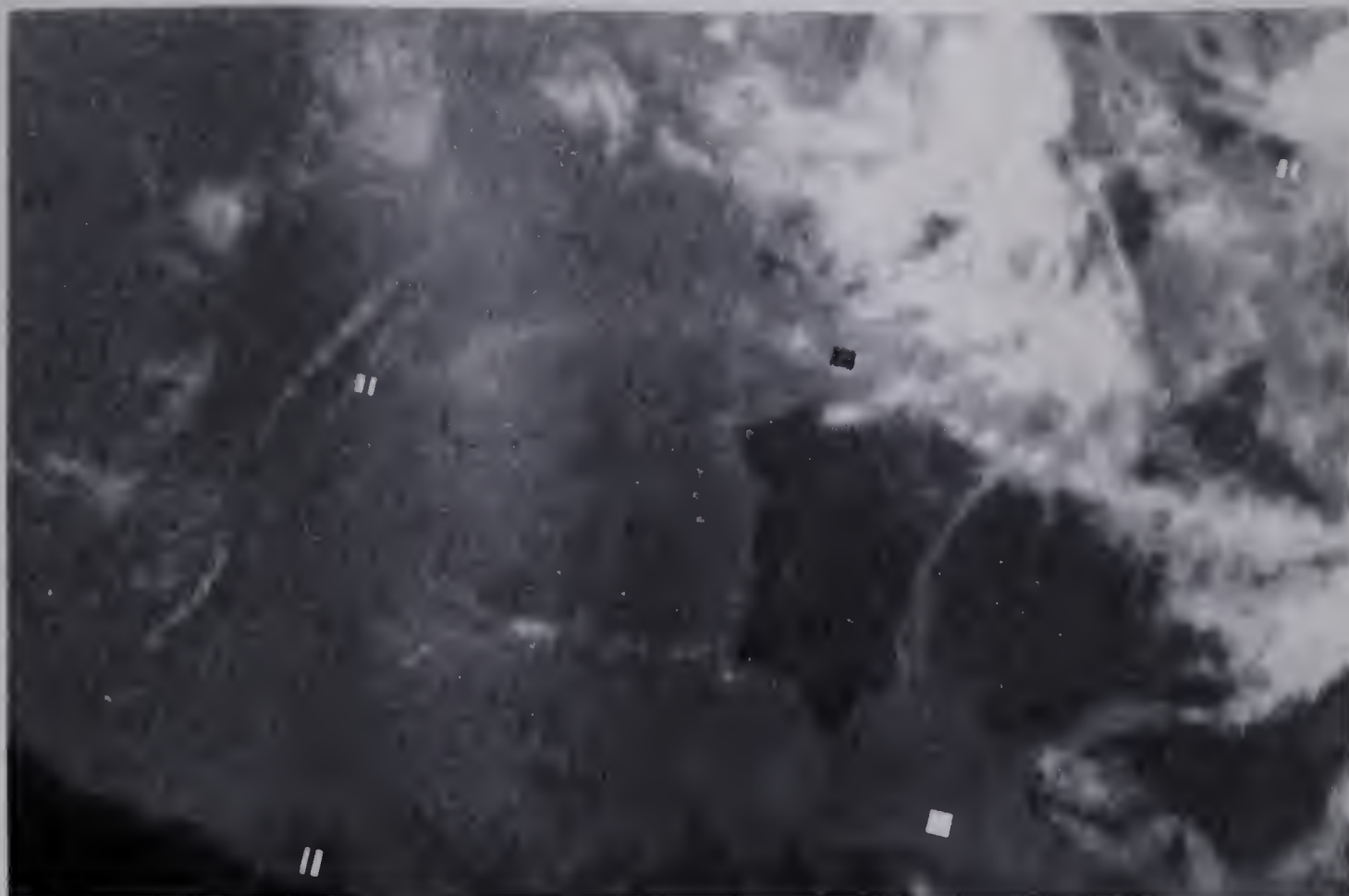


FIGURE 4.17a Infrared image of Beaufort Sea region of Orbit 4361 of NOAA-5 at 0025 Z on July 17, 1977.

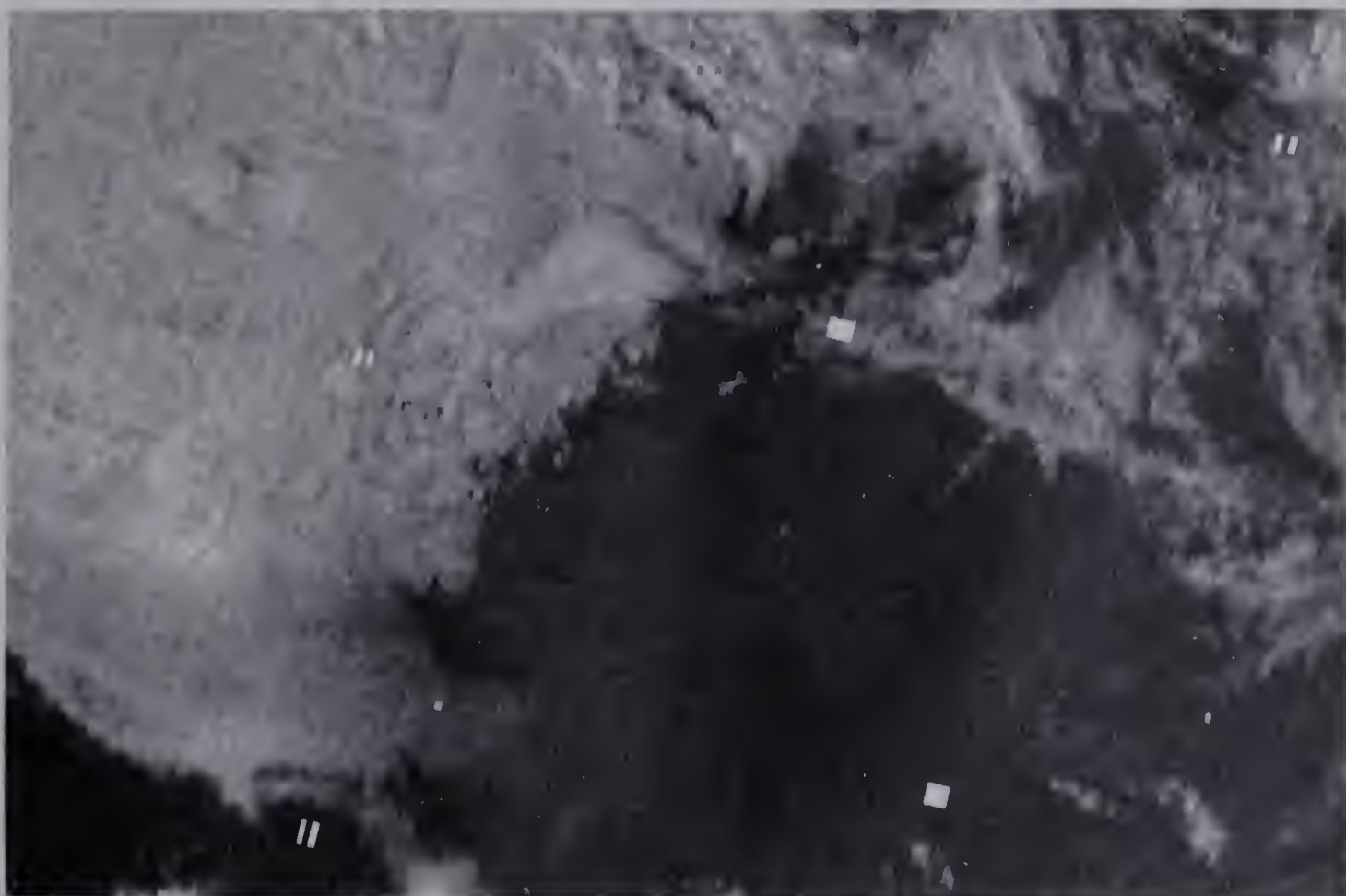


FIGURE 4.17b Visible image (as above).





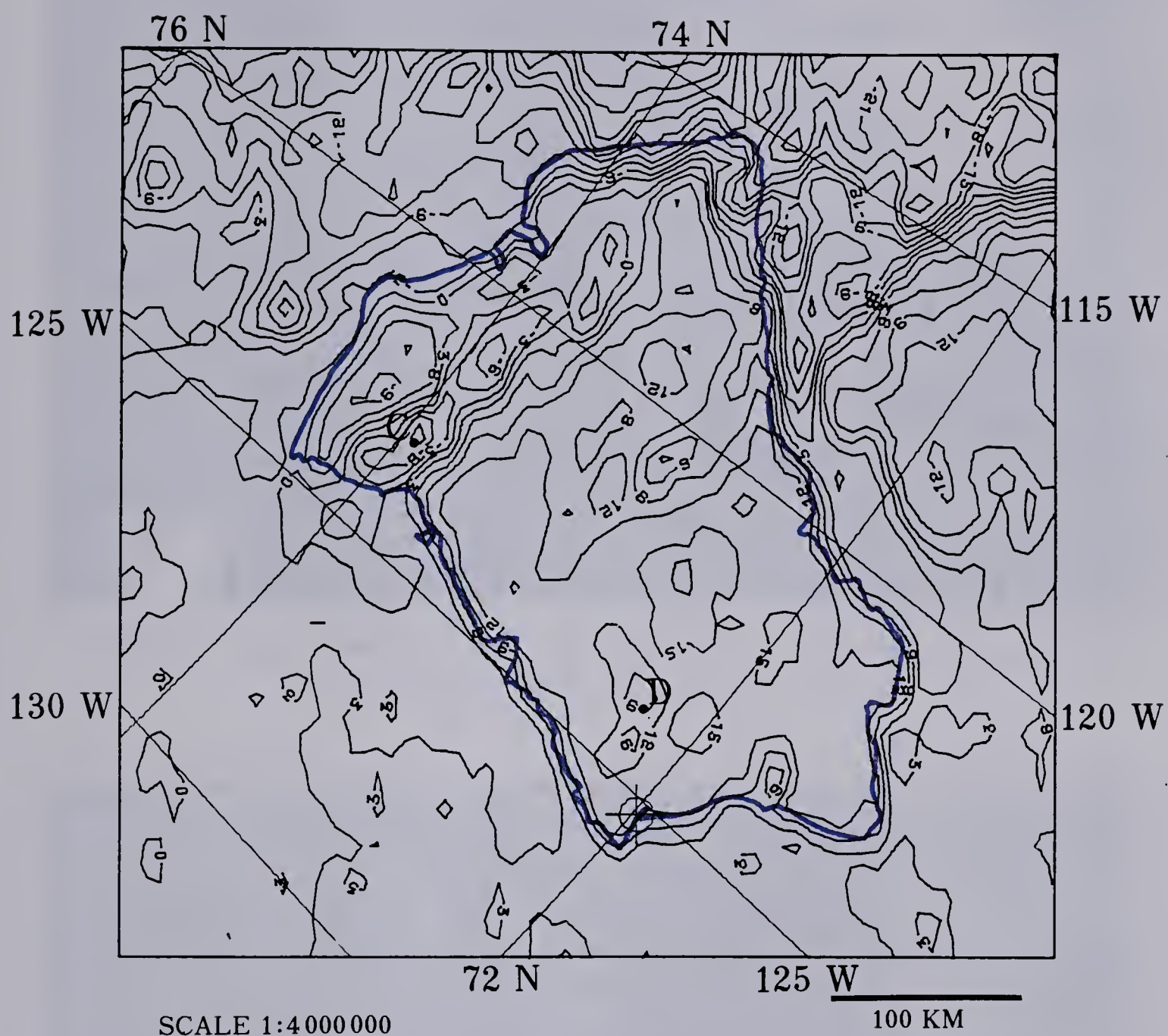








FIGURE 4.19a Infrared image of Beaufort Sea region of Orbit 4362 of NOAA-5 at 0220 Z on July 17, 1977.

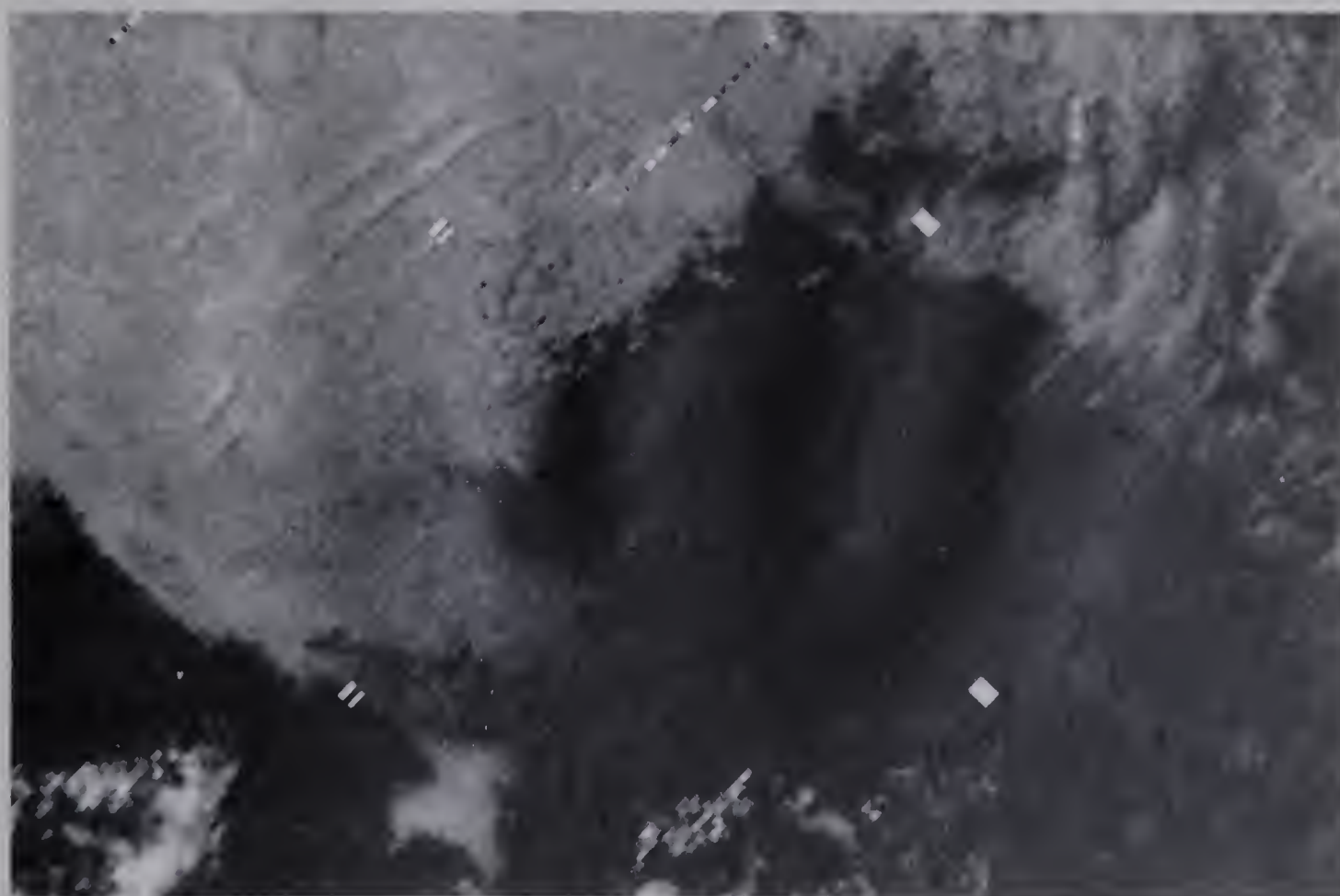


FIGURE 4.19b Visible image (as above).



In the plots of July 16 (Figures 4.11 through 4.18), the observed surface temperatures off the west coast were also in the 0 to 3°C range. However, the region of temperatures higher than 3°C was somewhat larger than on the plots of the previous day. This may indicate that this region was gradually warming under the influence of continual insolation. However, it is also possible that this may have indicated a slight error in the values used in the external calibration, though the observed sea surface temperatures indicated that any errors were well within the 3°C accuracy of the satellite measured temperatures themselves.

Based on the wind observations at Sachs Harbour in Table 1.1, the five temperature plots on this day all occurred at times during which an onshore flow was present at Sachs Harbour. Figure 4.11 shows the temperature field of Banks Island at 1043 local time, when the sea breeze circulation was likely just beginning. (The exact starting time of the sea breeze on this day was uncertain because of a missing surface report for 1800Z in Table 1.1.) Large regions with surface temperatures in excess of 18°C were already visible in both the northern and southern portions of the island, with the highest temperatures located just east of Burnett Bay with values above 21°C. The temperature patterns over the northern and extreme southern portions of the island at this time were very uniform, suggesting clear sky conditions. The central part of the island, however, was obscured by a wide band of cloud which extended beyond the eastern and western coastlines.





This cloud exhibited a complex temperature pattern, which included numerous regions with values below  $-12^{\circ}\text{C}$ . This non-uniform pattern indicated variations in the density or height of cloud in this formation.

This extensive region of cloud was also present on the temperature plots at 1237 local time (Figure 4.12) and 1431 local time (Figure 4.14) as well as on the associated conventional satellite imagery shown in Figures 4.13 and 4.15. The relatively low central temperatures in this formation suggested either a mid-level cloud or a thin high-level cloud. However, this formation was only vaguely discernible on the visible imagery of Figures 4.13b and 4.15b. As well, the hourly reports from Sachs Harbour, over which a portion of this cloud passed (in Figure 4.12), gave no indication of the presence of mid-level cloud, but did indicate increased amounts of thin cirrus near this area, sometime after 1200 local time (2000Z on July 16 in Table 1.1). Thus, it is likely that this cloud formation was thin cirrus.

The movement of this formation was difficult to track accurately. The lower central temperatures and less intense cloud-edge gradients in Figures 4.12 and 4.14 suggested that this cloud was dissipating as it moved away from Banks Island. Indeed, the remnants of this cloud can only just be seen over the Beaufort Sea on the conventional satellite imagery in Figures 4.17 and 4.19. This rapid dissipation led to the disappearance of most of the well-defined temperature minima observed within the





cloud structure in Figure 4.11. However, the center of two of these regions were identified (A and B on Figures 4.11 and 4.12), and since their orientation to each other as well as to the rest of the cloud formation seemed to indicate that they were from the same approximate region at each time, they could be used to track the motion of this formation. The movement of these centers between the times of Figures 4.11 and 4.12 was measured as about 93 km per hour (50 knots) from  $85^{\circ}$  (E) for the northern region (A), while the southern region (B) moved at about 80 km per hour (43 knots) from  $80^{\circ}$  (E). Continued rapid motion of this cloud was also evident on the conventional satellite imagery between Figures 4.13 and 4.15, as this formation moved well out over the Beaufort Sea. The Sachs Harbour wind profile closest to this time period was from 0000Z on July 17, or about 1600 local time on July 16 (see Table 1.2). Weak flows were reported at the low and mid-levels, with windspeeds over 35 knots reported only at the 250-mb level. This seemed to imply that this cloud may have been considerably higher than the 21,000 foot estimate given on the hourly reports at Sachs Harbour for that time (Table 1.1). However, though the wind direction at 250-mb agreed with the observed cloud motion, the reported wind speed was approximately 10 knots too low. Cirrus formations at high levels in the northern hemisphere are often found to the south of jet axes. Thus, the higher apparent wind speeds indicated by the cloud motion, and the faster movement of the more northerly region, may have been evidence for the presence



of a weak jet axis across the central portion of Banks Island at that time. Since Sachs Harbour was along the southern edge of this cirrus formation, the stronger wind speeds associated with the jet axis would not have been measured there. In any case, the rapid motion resulted in this cloud moving away from Banks Island by about 2300Z (1500 local time).

The only other synoptic-scale cloud observed near Banks Island on this day was an extensive area of cloud to the north. This cloud is visible on Figure 4.11 (1043 local time) as a region of low temperatures over M'Clure Strait. However, this formation had reached the northern coastline by 1237 local time (Figure 4.12), and moved slowly southwards during the remainder of the day. This cloud formation can also be seen on the infrared imagery in Figures 4.13a, 4.15a, 4.17a, and 4.19a over the region north and east of Banks Island. However, the underlying islands could still be seen on the accompanying visible imagery. Therefore, this formation was also identified as thin cirrus. The motion of an isolated finger of this formation (labelled C) was tracked over the last three temperature plots on this day (Figures 4.14, 4.16 and 4.18). The cloud motion suggested wind speeds of about 42 km per hour (28 knots) from  $45^{\circ}$  (NE) over the initial two hours, and 53 km per hour (28 knots) from  $55^{\circ}$  (NE) over the final period. The increase in speed and apparent veering motion of this cloud as it moved southwards over the northern part of Banks Island may have also been an indication of a region of stronger upper-level



winds over the center of the island.

Aside from the two cirrus formations, much of the remainder of Banks Island was cloud free on July 16. The lack of appreciable cloud over the center of the island as compared to that on July 15 may have been the result of drier air over the region on this day. Also, no stratus cloud was observed along the western coastline on this day, though the surface analysis for 1800Z on July 16, shown in Figure 1.7, suggested an offshore flow. However, the surface winds at Sachs Harbour were slightly weaker on July 16 than on July 15, and the offshore advection along the west coast may well have been too light for the production of stratus. Indeed, if the surface winds reported at Sachs Harbour were representative of the entire western portion of the island, the absence of coastal stratus may have been the result of an onshore sea breeze, since the sea breeze began at Sachs Harbour at about the time of the first temperature plot on this day.

Because of the small amounts of cloud cover over Banks Island on July 16, the development of the surface temperature field was easily observed. As was discussed earlier, at 1043 local time (Figure 4.11) the highest surface temperatures were above  $21^{\circ}\text{C}$  just east of Burnett Bay. Temperatures over  $21^{\circ}\text{C}$  were also observed east of Burnett Bay at 1237 local time (Figure 4.12), but the area was considerably larger than that of two hours before. However, by 1431 local time (Figure 4.14), surface temperatures over this region had fallen below  $21^{\circ}\text{C}$  and the area of temperatures above







18°C was smaller than that in Figure 4.12. Thereafter, the observed surface temperatures continued to fall until, at 1819 local time (Figure 4.18), only three small regions in the central portion of the island showed surface temperatures above 15°C. The changes in the temperature pattern on this day suggested a maximum surface temperature was attained sometime between Figures 4.11 and 4.12, but closer to the time of Figure 4.12, or near to local noon. The higher observed surface temperatures on this day as compared to those on July 15 were reflected by the hourly air temperatures at Sachs Harbour, shown in Table 1.1. The temperatures at Sachs Harbour on July 16 were 3°C higher than that on July 15.

The isotherm gradient along the northern coastline could not be measured on this day because of afternoon cloud cover. The eastern coastline was also obscured by cloud on the first two orbits, but coastal gradients could be seen in the afternoon. Measurements showed very little change in the isotherm gradients along this coast during the afternoon of July 16. However, the largest amount of spreading seemed to have occurred in the region south of Jesse Bay, though this effect was not nearly so apparent as that observed along this same coastline on July 15. Since the synoptic scale flow on July 16 was much the same as that on July 15, the lesser amount of spreading may have been the result of a weaker surface flow on July 16.

Isotherm gradients along the western coastline of Banks Island south of Burnett Bay were also examined. Though some



spreading of the coastal isotherms was observed during the afternoon along this shore, the amount of spreading was not large. However, along the southwestern coastline, south of Cape Kellet, a considerable change in the isotherm gradient was observed. The isotherms in this region in the late afternoon (Figure 4.18) were almost twice as far apart as near local noon (Figure 4.12). Indeed, the weakening of the gradient along this coastline was more apparent than that along the eastern coastline, even in the region south of Jesse Bay where the low level flow was likely onshore. This indication of onshore cooling along the southwestern shore when the surface analysis suggested an offshore flow pointed to the existence of an onshore sea breeze flow in this region. Conversely, the relatively small change in the isotherm gradient observed along the western coastline north of Cape Kellet suggested that if a sea breeze occurred in this region, it may have had a weaker onshore flow than that along the southwestern shore.

The formation of cloud along the western and southwestern coastlines of Banks Island on July 16 also presented evidence of sea breezes in these regions. The cirrus observed over the central portion of the island in Figure 4.11 (1043 local time) had moved away from the western coastline by Figure 4.14 (1431 local time). The rapid advection of this cloud, and the absence of any other cloud formations near enough to be advected over this area by the upper winds, suggested that any cloud observed along these coastlines on July 16 was likely formed by local processes.



Aside from the cirrus discussed earlier, the temperature pattern along the western shoreline gave no indication of the presence of cloud during the afternoon of July 16. The coastal isotherm gradient south of Burnett Bay was concentrated in a narrow, well-defined band from about 1237 local time (Figure 4.12) onwards. Likewise, the uniformly high inland temperatures near Bernard Island gave no indication of the presence of onshore cloud in that region. However, the inland temperature pattern observed to the east of Storkerson Bay suggested afternoon formation of cloud. At 1237 local time (Figure 4.12) temperatures below  $15^{\circ}\text{C}$  were observed to the north and east of Storkerson Bay, but the conventional satellite imagery for the same time (Figure 4.13) suggested that if there was any cloud present at that time, it was either thin or scattered. However, at 1431 local time (Figure 4.16) temperatures below  $6^{\circ}\text{C}$  were observed. The conventional imagery in Figures 4.15 and 4.17 also showed evidence of a more intense cloud formation at these later times, particularly on the visible imagery, where the high reflectivity of the cloud tops produced bright patches onshore. At 1819 local time (Figure 4.18), the lowest observed temperatures were again in the  $9^{\circ}\text{C}$  range, and the cloud was also less well defined in the conventional imagery of Figures 4.19. Thus, this cloud appeared to have developed near the western coastline on the afternoon of July 16, with the most intense development occurring about the time of Figure 4.16 (1625 local time).





The cloud formation was aligned in a band parallel to the coastline at 1625 local time. This north-to-south orientation was also apparent at 1819 local time (Figure 4.18). Though this pattern was not so obvious at 1431 local time in Figure 4.14, the north-south extent of the cloud still exceeded its extent inland. This alignment suggested that the formation mechanism for the cloud along the coastline was not confined to a single location, but extended along a considerable length of the western shore.

The movement of this region of cloud was also measured. The area enclosed by the  $12^{\circ}\text{C}$  isotherm was considered representative of this formation. The approximate center, marked with a D on Figures 4.14, 4.16. and 4.18, was located east of Storkerson Bay at 1431 local time, but moved well to the south of Storkerson Bay by 1819 local time. The fastest motion of about 26 km per hour ( $14$  knots) from  $20^{\circ}$ (NNE) occurred over the last two hours. At the same time, an inland motion of about 15 km occurred between the position observed at 1431 local time, and that observed later in the day. This inland motion was also accompanied by an apparent clearing of cloud along the coastline, indicated by the rise in observed surface temperatures just inland of the coastal isotherm gradient between 1431 and 1625 local times (Figures 4.14 and 4.16).

The cloud along the western coastline thus exhibited the characteristics of cloud in a sea breeze circulation. The most intense development took place during the mid afternoon, when the sea breeze would be expected to have had its furthest inland penetration. The



formation was aligned in a band parallel to the coastline, and moved inland during the afternoon when the expected synoptic flow was offshore. The inland motion and coastal clearing later in the afternoon corresponds to the expected inland motion of a sea breeze front -- where the strongest cloud development usually occurs -- and the development of a coastal subsidence zone. Finally, the southward cloud motion, especially after 1625 local time, may have been the result of advection by the synoptic-scale flow, with the onshore sea breeze component producing a southerly rather than a southwesterly motion. As well, veering of the sea breeze during the afternoon because of the Coriolis force may have also been a factor in the southerly cloud motion. A veering of the sea breeze on this day was also observed in the winds at Sachs Harbour (see Table 1.1).

The maximum inland extent of the approximate center of the cloud formation along the western coastline was between 40 and 50 km. The rather low inland temperatures also suggested that there may well have been thin or scattered cloud over the interior of the island, some 50 km or more beyond the coast. If this cloud did indeed correspond to the position of a sea breeze front, this inland penetration is certainly comparable to the inland extent of sea breezes in more southerly locations (see Section 1.2). Indeed, since the sea breeze itself penetrates further inland than does the frontal zone, these observations would seem to suggest a stronger circulation than is observed at mid-latitudes. This





may be the result of greater land-to-ocean temperature contrasts in the Arctic as compared to those in mid-latitudes. However, because of the dryness of Arctic air, the development of extensive cloud is unlikely, even with an intense sea breeze circulation. This may explain why sea breeze cloud formation is not often observed on satellite imagery from the Arctic.

The formation of cloud along the southwestern coastline on July 16 was not so well defined as that along the western shore. Only small, isolated areas of thin or scattered cloud could be identified in this region. This cloud was first observed at 1431 local time (Figure 4.14) over the region to the east of Sachs Harbour. The lowest temperatures were below  $9^{\circ}\text{C}$ . Similar temperatures were observed to the southeast of Sachs Harbour at 1625 local time (Figure 4.16) and at 1819 local time (Figure 4.18). This cloud was very difficult to find on the conventional satellite imagery. In both Figures 4.14 and 4.16 the centers of the cloud were inland of the southwestern coastline. However, the cloud was located further to the south and east in the latter figure. Though the southerly motion could be explained by a component of the synoptic-scale flow, the easterly movement suggested an onshore component to the wind. Since a sea breeze circulation was observed along the northern part of this coastline at Sachs Harbour on this day, it was likely that this onshore motion was the result of a more general sea breeze circulation. On Figure 4.18, however, the cloud was much closer to the coastline than on either



of the two previous orbits, and the inland extent of the cloud was much reduced. The hourly wind reports from Sachs Harbour (Table 1.1) showed that on July 16, an onshore flow was not observed after 0200Z (1800 local time). Therefore, if the sea breeze at Sachs Harbour was representative of conditions along the southwestern coastline, the intensity of the sea breeze circulation was likely already slackening by the time of Figure 4.18. This lesser circulation coupled with the offshore synoptic flow could explain the reduced extent of cloud at this later time.



## CHAPTER V

### SUMMARY AND CONCLUSIONS

The temperature plots in Chapter 4 show that detailed temperature information is available from infrared satellite imagery, even from the relatively low resolution scanning radiometers aboard the NOAA-5 satellite. Such thermal plots can be used to supplement conventional meteorological information, as well as to provide additional data in regions where conventional observations are not available. In remote regions such as the Canadian Arctic, where surface stations lie hundreds of kilometers apart, satellite imagery is often the sole tool of the forecaster. Information from polar-orbiting satellites is particularly useful in this respect in the Canadian Arctic, because of the overlap in orbits discussed in Chapters 2 and 4. The temperature plots in Chapter 4 illustrate that satellite coverage of some Arctic regions is available over an eight to ten hour period daily. Thus, not only can surface temperature fields and cloud formations be studied, but changes in thermal patterns and motions of cloud systems can also be examined.

The method of contouring temperature plots from infrared satellite data has several advantages over conventional gray-scaling techniques. The most notable advantages are in the retention of small-scale information without the need for enhancement, and the ability to smooth or manipulate the data before output. As well, the contouring routines also allow for output of the final contour





plot on any scale required to fit available surface maps, and for identification of areas of interest by overlaid latitude and longitude lines or geographical outlines. The major disadvantages of temperature-field plotting are the necessity for a computer large enough to handle a contouring-plotting package, and the cost involved in computing and drawing the plots themselves. In this respect, the use of low-resolution scanning radiometer information has some advantage over the high-resolution data available from the latest polar-orbiting satellites such as NOAA-6 or TIROS-N. Doubling the resolution available from satellite imagery effectively quadruples the number of data values over a given region of interest, thus greatly increasing the computations and expense involved in producing a temperature plot. The increase in accuracy of the thermal field as a result of the increased satellite resolution may not justify this increased cost, and the more detailed information produced may still require averaging and smoothing to produce plots simple enough to be useable.

One of the most useful aspects of the computer plotting routines used in this study was in the procedure for identifying surface locations. The calculation of latitude and longitude lines and geographic outlines for each satellite orbit greatly increases the accuracy of locating cloud positions or surface features when compared to conventional overlays. The use of contour plots rather than gray-scaled imagery also ensures that identifying marks will not permanently obscure surface data, as, for example, is done by the fiducial marks on the conventional satellite images in Chapter 4.



However, it was suggested in Chapter 4 that it may be desirable to improve the identification process still further by including an adjustment to calculate latitudes as geodetic rather than geocentric. It is believed that this change would increase the accuracy of placement of surface features to within the resolution of the current NOAA satellites.

The direct calibration of the infrared satellite data to degrees Celsius may also have some advantages over traditional gray-scaling. Comparisons in the temperatures of different areas or determinations of temperature changes can be made very easily from contoured plots, while the use of gray-scaled information requires conversion tables. As well, the temperatures on contour plots can be more accurate without the necessity of enhancement. The calibrations used in this study were recalculated for each satellite orbit, and the temperatures were further calibrated to a surface region of known temperature. This procedure adjusted, to some extent, for atmospheric attenuation of the infrared radiation, though significant changes in the atmospheric state over the region of interest would not be taken into account. Also, the assumed temperature of the water surface used in the external calibration of each orbit may not have been accurate. However, if the atmospheric state did not vary much over the course of the day, and the temperature of the water surface also remained constant, the relative temperatures between orbits would be accurate even if the absolute values for each orbit were not. Since the change in temperature is often more important in meteorology than the actual temperature value at a given time, this calibration procedure should





be useful in meteorological applications.

The case studies presented in Chapter 4 illustrate two approaches which can be applied to infrared satellite imagery. The first approach is to use the observed surface temperatures in cloud-free areas to determine changes in surface thermal fields. In particular, changes in the isotherm gradients along coastlines may provide information about coastal advection patterns. The second approach, used when cloud is present, is to track the centers of organized cloud formations, providing information on upper-level winds. Also, changes in the temperature fields of cloud-covered areas may identify the formation or dissipation of cloud in those regions, and may point to local mechanisms which cause these changes.

The observed temperature fields of Banks Island on the two days studied in Chapter 4, July 15 and 16 of 1977, showed considerable differences between the surface temperatures of land and water or ice surfaces. On both days, temperatures over the water and ice surfaces ranged between about 0 and 3°C. These offshore surface temperatures did not change appreciably during the two days, though this may have been the result of calibrating the infrared temperatures to a water surface more than a lack of actual change. However, much larger temperature changes were observed over the surface of Banks Island itself. Average temperatures less than 15°C were observed on early morning and late afternoon satellite orbits for each day. The changes in the surface temperature patterns suggested that the maxima on each day were attained near local noon, with values above 18°C on July 15 and above 21°C on July 16. Thus, the temperature contrast between



the surface of Banks Island and that of the surrounding water and ice was likely greater than  $15^{\circ}\text{C}$  for an appreciable part of each day.

The change in temperature from water or ice to the surface of Banks Island was restricted to a narrow zone close to the coastline, with the greatest temperature change occurring over a distance of only 20 to 30 km. Changes in the intensity of these coastal isotherm gradients were observed on both July 15 and 16. In general, the isotherms were most closely "packed" at local noon, with spreading of the isotherms occurring throughout the afternoon. However, comparatively more spreading was observed along shorelines where the synoptic-scale flow was directly onshore as compared to shorelines where the flow was either parallel or at a shallow angle to the coast. The reason for this difference was believed to have been a result of enhanced cooling along coastal sections having strong onshore flows.

The synoptic circulation over Banks Island on July 15 and 16 of 1977 was described in Chapter 1. On both days, the flow pattern suggested light northerly to northeasterly low-level winds over Banks Island. Thus, the northern and eastern coastlines of the island were likely subject to a cool onshore flow throughout each day. This was evidenced by the weakening of isotherm gradients along the windward coastlines of the island during the afternoon.

However, spreading of coastal isotherms was also observed along the western and southwestern coastlines of Banks Island during the afternoon of July 16, even though the synoptic flow along these coasts was offshore, so that no enhanced cooling was expected. Even



so, enhanced cooling seemed to have occurred and was, in fact, even more pronounced along the leeward southwestern coastline than along the southeastern coastline, where the flow was directly onshore. This evidence of enhanced cooling along lee coasts was believed to be an indication that an onshore sea breeze advection occurred at these locations.

The dynamics of the sea breeze circulation were discussed in Chapter 1. The formation of a sea breeze requires a strong land-to-water temperature contrast and a light synoptic-scale flow. As has been shown, both these conditions existed on the two days studied in Chapter 4. The hourly weather observations from Sachs Harbour, shown in Chapter 1, suggested an onshore sea breeze flow occurred during the afternoons of July 15 and 16 of 1977. If Sachs Harbour was representative of conditions along the western coastline of Banks Island on these two days, then sea breeze circulations likely occurred over an appreciable portion of this coast. Thus the enhanced coastal cooling observed along the western and southwestern coasts of Banks Island during the afternoon of July 16 were likely a result of an onshore sea breeze flow, even though the synoptic situation suggested an offshore wind.

The magnitude and direction of upper-level winds on each of the two days studied were estimated by tracking the motion of cloud systems between successive satellite orbits. Though accurate comparisons of these derived winds with those which actually existed were not possible, the general motion of these clouds, especially those at higher levels, were in agreement with the winds measured at





Sachs Harbour. The major problems in these comparisons were the inability to determine accurate cloud heights from the satellite-measured temperatures because of thin or scattered cloud conditions, and the difficulties in matching wind observations fixed in both space and time with those estimated from motions over a two hour period in regions remote from Sachs Harbour itself. Nevertheless, while this study did not attempt to verify wind fields by the use of satellite data, since this would have required far more information than was available, the two cases did illustrate that the motion of cloud formations could be used to approximate upper-level winds in locations where conventional measurements do not exist.

Tracking the motion of cloud systems was possible only when the formation was well developed, and thus could maintain its identity over the two-hour period between successive satellite orbits. Thin or scattered cloud, or cloud which appeared or dissipated during the period separating orbits, could not be accurately tracked. However, the formation and dissipation of cloud over Banks Island also provided evidence of local processes on the two days studied. On both days, cloud was observed over the eastern portion of Banks Island, in regions where no cloud was seen upstream in the synoptic-scale flow on earlier orbits. This cloud was therefore likely formed by local processes. Since the lowest cloud temperatures, and hence the strongest cloud formation, occurred during the early afternoon, and little cloud was seen before this time and little new formation occurred thereafter, the formation mechanism was believed to be surface heating. Also, it is likely that cloud formation



along the eastern coast was enhanced by orographic lift brought about by the onshore synoptic-scale flow. However, even the combined effects of surface heating and orographic lift failed to produce appreciable amounts of cloud close to the eastern coastline. Indeed, the most intense cloud formation observed over the northern half of Banks Island on July 15 occurred over low-lying terrain, suggesting that additional surface moisture may have been necessary for cloud to form in this region. Additional moisture may also have been supplied by flow over open water; cloud formation along the southeastern shore of Banks Island on July 15, where the onshore flow was off open water, occurred closer to the coastline than that over the northeastern shore, where the onshore flow was off an ice-covered surface. The more extensive cloud formation over those areas where additional surface moisture may have been available, and the lack of appreciable formation elsewhere, pointed to a general dryness of the air in the lower levels on each of the two days studied.

The formation and motion of cloud along the western coastline of Banks Island on July 15 and 16 provided evidence for the existence of coastal sea breezes on each of the two days studied. On July 15, a large area of cloud was observed over the western coastline of Banks Island on the morning and early afternoon orbits, but none was seen during the late afternoon. The offshore synoptic-scale flow over this coastline and the relatively small difference in temperature between the cloud tops and the sea surface below suggested a low-level stratus formed by advection of warm air





over the cool sea surface. The rapid dissipation of this cloud was thought to have been caused by a change in wind direction from offshore to onshore, brought about by the development of a sea breeze circulation. This suggestion was supported by the hourly wind reports from Sachs Harbour, which indicated the onset of a sea breeze flow just before the time at which the cloud along the west coast began to dissipate. No coastal stratus was observed on the temperature plots of July 16. However, the wind reports from this day show an earlier onset of the sea breeze, which may explain the absence of stratus along the west coast on July 16.

The motion of cloud over the interior of Banks Island also gave some indication of coastal sea breezes. On July 15, an area of cloud which formed over the northern part of the island was advected in the synoptic-scale flow towards the western coastline, and slowed and rotated to lie parallel to the coastline as it approached the shore. These changes suggested an onshore flow, or at least a weaker offshore flow, near the western coastline, or enhancement of the cloud by upward vertical motions inland of the coastline, both indicative of a sea breeze circulation. Along the southwestern coastline, evidence of clearing of cloud along the shoreline during the afternoon while onshore cloud was still apparent also suggested the presence of a sea breeze flow.

On July 16, an area of cloud along the western coastline exhibited an inland motion during the afternoon. The motion of this cloud and its alignment in a band parallel to the coast both suggested the type of formation expected in a sea breeze front. The observed



clearing of cloud along the coastline itself late in the afternoon also supported the explanation of this cloud as sea breeze related. The inland penetration of the cloud band was about 50 km, a value comparable to reported limits of the inland extent of sea breezes in more temperate locales. Thus, it is possible that the circulation of an Arctic sea breeze can be stronger than coastal sea breezes found at mid latitudes.

The behaviour of cloud formed along the southwestern coastline of Banks Island on July 16 also suggested an onshore flow where the synoptic-scale flow was believed to be offshore. Though cloud formation along this coastline was not as extensive as that along the western coastline, the temperature plots did suggest either a motion of the cloud in a northwesterly direction, or continued formation of cloud in the late afternoon, when the effects of surface heating would likely be weakening. However, both effects could be explained by an onshore sea breeze flow, either in advecting the cloud against the synoptic-scale flow, or in providing onshore convergence and vertical motions sufficient to produce new development throughout the afternoon.

Thus, the two days studied in Chapter 4 illustrated three effects of a sea breeze on coastal features visible on temperature plots. Enhanced cooling from the onshore sea breeze flow was observed in the spreading of coastal isotherms during the afternoon. Secondly, slowing and realignment of cloud advected towards the coastline by the synoptic-scale flow suggested both the onshore flow of the sea breeze, as well as the enhancing effects of vertical



motion in the sea breeze convergence zone. Lastly, the formation and motion of cloud as a result of the sea breeze and sea breeze front themselves were also apparent, though the amount of cloud formation observed was much less extensive than that seen in the sea breeze fronts of mid latitudes.

However, two case studies are certainly not sufficient evidence for any general remarks on the behaviour of a coastal sea breeze on the temperature fields of Arctic islands. Though the use of contoured temperature plots to present infrared satellite information shows some promise, primarily in identifying coastal gradients and temperature changes, more study is required before any firm conclusions can be drawn on the effects of advection patterns on coastal surface temperatures. The lack of density in conventional reporting stations in the Arctic also makes verification of localized flow patterns nearly impossible. It may be useful at some time to study temperature-field plots along more southerly coastlines where more surface information is available, and hence where more exact measurements can be made. However, the use of more southerly study locations will also limit the useable data because of less overlap on consecutive satellite orbits. This overlap and the resultant extended coverage period over Arctic locations is one of the major reasons why satellite information is so useful in northern sites. Temperature-field plotting provides another method of displaying infrared satellite data, in a way which can supply more accurate and finer detailed information than is usually available from more conventional techniques. If accurate generalizations on the effects





of local flow patterns on thermal features is known, the techniques of temperature plotting can be applied to Arctic locations, providing useful information in what is undeniably a data sparse wilderness.



## REFERENCES

- Advisory Commision on the Development of Government in the North West Territories, 1966: Atlas of the Northwest Territories, Canada, Volume 2, Ottawa.
- Anderson, R. K. and N. F. Veltishchev (Editors), 1973: The Use of Satellite Pictures in Weather Analysis and Forecasting. W M O Technical Note Number 124, Geneva, 275pp.
- Barnes, James C., David T. Chang and James H. Willand, 1972: Image Enhancement Techniques for Improving Sea-Ice Depiction in Satellite Infrared Data. Journal of Geophysical Research, 77(3), 453-462.
- Barrett, E. C. and I. D. Watson, 1977: Problems in Analysing and Interpreting Data from Meteorological Satellites. Enviromental Remote Sensing 2: Practices and Problems, Edited by Eric C. Barrett and Leonard F. Curtis, London, 276-303.
- Barry, R. G. and C. I. Jackson, 1969: Summer Weather Conditions at Tanquary Fiord, N.W.T. Arctic and Alpine Research, 1(3), 169-180.
- Bartholic, J. F. and R. A. Sutherland, 1976: Cold Climate Mapping Using Satellite High Resolution Thermal Imagery. Seventh Conference on Aerospace and Aeronautical Meteorology and Symposium on Remote Sensing from Satellites Nov 16-19, 1976, American Meteorological Society, 137-140.
- Bess, T. Dale and G. Louis Smith, 1976: Estimation of Regional Heat Flux from Scanning Radiometer Measurements. Seventh Conference on Aerospace and Aeronautical Meteorology and Symposium on Remote Sensing from Satellites Nov 16-19, 1976, American Meteorological Society, 291-297.
- Bonner, William D., 1969: Gridding Scheme for APT Satellite Pictures. Journal of Geophysical Research, 74(18), 4581-4587.
- Boreal Institute for Northern Studies: Canadian Arctic Renewable Resource Mapping Project, Map Supplement to Volume 2.
- Breaker, Laurence, Jack Klein and Michael Pitts, 1978: Quantitative Measurements of Sea Surface Temperature at Several Locations Using the NOAA-3 Very High Resolution Radiometer. NOAA Technical Memorandum NESS 98, Washington, D. C., 28pp.
- Buettner, Konrad J. K. and Clifford D. Kern, 1965: The Determination of Infrared Emissivities of Terrestrial Surfaces. Journal of





Geophysical Research, 70(6), 1329-1337.

- Bugaev, V. A., 1973: Dynamic Climatology in the Light of Satellite Information. Bulletin of the American Meteorological Society, 54(5), 394-418.
- Burns, B. M., 1973a: The Climate of the Mackenzie Valley - Beaufort Sea, Volume 1. Environment Canada, Toronto, 227pp.
- Burns, B. M., 1973b: The Climate of the Mackenzie Valley - Beaufort Sea, Volume 2. Environment Canada, Toronto, 239pp.
- Carlson, A. Bruce, 1968: Communication Systems - An Introduction to Signals and Noise in Electrical Communication. McGraw-Hill, New York, 470pp.
- Christie, R. L., J. G. Fyles, R. Thorsteinsson and E. T. Tozer, 1959: Geology Banks, Victoria and Stefansson Islands District of Franklin. Geological Survey of Canada, Map 1135A.
- Cook, Frank A., 1955: Near Surface Soil Temperature Measurements at Resolute Bay, Northwest Territories. Arctic, 8(4), 237-249.
- Cross, Robert Kenneth, 1979: Application of Satellite Infra-red Data in the Derivation of Sea Surface Temperatures in the Canadian Arctic. Unpublished M.Sc. Thesis, University of Alberta, Edmonton, 126pp.
- Curtis, William R. and P. Krishna Rao, 1969: Gulf Stream Thermal Gradients from Satellite, Ship and Aircraft Observations. Journal of Geophysical Research, 74(28), 6984-6990.
- Department of Energy, Mines and Resources, Canada, Surveys and Mapping Branch, 1974a: ICAO 1:1 000 000 World Aeronautical Chart, a N.T.S. Nos. 87 and 97. Ottawa.
- Department of Energy, Mines and Resources, Canada, Surveys and Mapping Branch, 1974b: ICAO 1:1 000 000 World Aeronautical Chart, a N.T.S. Nos. 88 and 98. Ottawa.
- Department of Transport, Canada, Meteorological Branch, 1970: Climate of the Canadian Arctic. Ottawa, 71pp.
- Dirmhirn, Inge and Frank D. Eaton, 1977: Radiative Surface Characteristics and Their Effect on Remote Sensing. Radiation in the Atmosphere, Edited by H. J. Bolla, Science Press, Princeton, 438-444.
- Environment Canada, Atmospheric Environment, 1976: Climatological Station Data Catalogue, The North Y.T. and N.W.T. Downsview.



- Estoque, M. A., 1961: A Theoretical Investigation of the Sea Breeze. Quarterly Journal of the Royal Meteorological Society, 87(372), 136-146.
- Estoque, M. A., 1962: The Sea Breeze as a Function of the Prevailing Synoptic Situation. Journal of the Atmospheric Sciences, 19(3), 244-250.
- Fleagle, Robert G. and Joost A. Businger, 1963: An Introduction to Atmospheric Physics. Academic Press, New York, 346pp.
- Fortuna, Joseph J. and Larry N. Hambrick, 1974: The Operation of the NOAA Polar Satellite System. NOAA Technical Memorandum NESS 60, Washington, D. C., 127pp.
- Fritz, Sigmund, 1963: The Diurnal Variation of Ground Temperature as Measured from TIROS II. Journal of Applied Meteorology, 2(5), 645-648.
- Fritz, Sigmund, 1964: Pictures from Meteorological Satellites and Their Interpretation. Space Science Reviews, Volume 3, D. Reidel, Dordrecht - Holland, 541-580.
- Fritz, Sigmund, 1977: Temperature Retrievals from Satellite Radiance Measurements - An Empirical Method. Journal of Applied Meteorology, 16(2), 172-176.
- Garnier, B. J., 1972: The Remote Sensing of Surface Radiative Temperatures Over Barbados. Climatological Research Series No. 7, McGill University, Montreal, 52pp.
- Green, Barry Cameron, 1977: An Investigation of Thermal Fields and Secondary Circulations in the Canadian Western Arctic. Unpublished M.Sc. Thesis, University of Alberta, Edmonton, 166pp.
- Hare, F. Kenneth and Svenn Orvig, 1958: The Arctic Circulation. Arctic Meteorology Research Group, Publication in Meteorology No. 12, Montreal, 211pp.
- Hare, F. Kenneth and Morley K. Thomas, 1974: Climate Canada. Wiley, Toronto, 256pp.
- Hartl, P. H., 1976: Digital Picture Processing. Remote Sensing for Environmental Sciences, Edited by Erwin Schanda, Springer-Verlag Heidelberg, 304-350.
- Hasler, A. F., W. Shenk and W. Skillman, 1976: Wind Estimates from Cloud Motions: Phase I of an in situ Aircraft Verification Experiment. Journal of Applied Meteorology, 15(1), 10-15.
- Hasler, A. F., W. E. Shenk and W. C. Skillman, 1977: Wind Estimates





from Cloud Motions: Results from Phases I, II and III of an in situ Aircraft Verification Experiment. Journal of Applied Meteorology, 16(8), 812-815.

Hsu, Shih-Ang, 1967: Mesoscale Surface Temperature Characteristics of the Texas Coast Sea Breeze. Report No. 6, Atmospheric Science Group, University of Texas College of Engineering, Austin, 74pp.

Hsu, Shih-Ang, 1970: Coastal Air-Circulation System: Observations and Empirical Model. Monthly Weather Review, 98(7), 487-509.

Hubert, Lester F., 1979: Wind Derivation from Geostationary Satellites. Quantitative Meteorological Data from Satellites, Edited by Jay S. Winston, W M O Technical Note Number 166, Geneva, 33-59.

Jayaweera, K. O. L. F. and Kristina Ahlnas, 1974: Detection of Thunderstorms from Satellite Imagery for Forest Fire Control. Journal of Forestry, 72(12), 767-770.

Kays, Marvin D., 1978: Satellite Ground Truth Measurements. Conference on Atmospheric Environment of Aerospace Systems and Applied Meteorology Nov 14-16, 1978, American Meteorological Society, 122-125.

Kruger, H. B., 1960: Notes on Meteorology of the Canadian Arctic. CIR-3396 TEC-334, Meteorological Branch, Department of Transport, Canada.

Kung, Ernest C., Reid A. Bryson and Donald H. Lenschow, 1964: Study of a Continental Surface Albedo on the Basis of Flight Measurements and Structure of the Earth's Surface Cover Over North America. Monthly Weather Review, 92(12), 543-564.

Laird, A. G., 1976: Passive Infrared Sensing of the Environment. Remote Sensing of the Terrestrial Environment: Proceedings of the Twenty-Eighth Symposium of the Colston Research Society April 5-9, 1976, Butterworths, London, 26-37.

Lee, S. S., T. N. Veziroglu, S. Sengupta and N. L. Weinberg, 1974: Remote Sensing Applied to Thermal Pollution. Remote Sensing Applied to Energy-Related Problems: A Symposium Course Dec 2-4, 1974, University of Miami, Coral Gables - Florida, S5.33-S5.70.

Lewis, M. C. and T. V. Callaghan, 1976: Tundra. Vegetation and the Atmosphere, Volume 2 Case Studies, Edited by J. L. Monteith, Academic Press, London, 399-433.

Lubitz, E. D. and J. M. Powell, 1974: Some Computer Techniques for Presentation of Thermal Infrared Line Scan Data. Northern Forest Research Centre Information Report NOR-X-79, Department of the Environment, Canadian Forestry Service, 21pp.





- Madden, R. and C. Parsons, 1973: A Technique for Real-Time, Quantitative Display of APT Scanning Radiometer Data. *Journal of Applied Meteorology*, 12(2), 381-385.
- Malkus, Joanne Starr and Melvin E. Stern, 1953a: The Flow of a Stable Atmosphere Over a Heated Island, Part I. *Journal of Meteorology*, 10(1), 30-41.
- Malkus, Joanne Starr and Melvin E. Stern, 1953b: The Flow of a Stable Atmosphere Over a Heated Island, Part II. *Journal of Meteorology*, 10(2), 105-120.
- Manning, T. H., 1956: Narrative of a Second Defence Research Board Expedition to Banks Island, With Notes on the Country and Its History. *Arctic*, 9(1&2), 3-77.
- Marlatt, William E. and James C. Harlan, 1971: A Study of the Attenuation by Atmospheric Particulates of Thermal Infrared Radiation. Proceedings of the Seventh International Symposium on Remote Sensing of Environment May 17-21, 1971, Volume 3, University of Michigan, Ann Arbor, 1791-1806.
- Marvill, Stephen and K. O. L. F. Jayaweera, 1975: Investigations of Strong Valley Winds in Alaska Using Satellite Infrared Imagery. *Monthly Weather Review*, 103(12), 1129-1136.
- Mattsson, J. O., 1969: Infrared Thermography- A New Technique in Microclimatic Investigations. *Weather*, 24(3), 106-112.
- Maul, George A. and Miriam Sidran, 1973: Atmospheric Effects on Ocean Surface Temperature Sensing from the NOAA Satellite Scanning Radiometer. *Journal of Geophysical Research*, 78(12), 1909-1916.
- McClain, E. Paul, 1975: Potential Value of Earth Satellite Measurements to Oceanographic Research in the Southern Ocean. NOAA Technical Memorandum NESS 61, Washington, D. C., 18pp.
- McClain, E. Paul, 1979: Satellite Derived Earth Surface Temperatures. Quantitative Meteorological Data from Satellites, Edited by Jay S. Winston, W M O Technical Note Number 166, Geneva, 60-86.
- McGinnis, David F., 1972: Satellite Detection of Melting Snow and Ice by Simultaneous Visible and Near IR Measurements. Proceedings of the Eighth International Symposium on Remote Sensing of Environment Oct 2-6, 1972, Volume 1, Environmental Research Institute of Michigan, Ann Arbor, 231-240.
- Moller, F. and E. Raschke, 1969: Problems of Meteorological Observations from Satellites. *Space Science Reviews* Volume 9, D. Reidel, Dordrecht - Holland, 90-148.



- Mowat, Farley (Editor), 1961: Ordeal by Ice. McClelland and Stewart, Toronto, 364pp.
- Mowat, Farley (Editor), 1976: The Polar Passion. McClelland and Stewart, Toronto, 365pp.
- Neumann, J. and Y. Mahrer, 1974: A Theoretical Study of the Sea and Land Breezes of Circular Islands. Journal of the Atmospheric Sciences, 31(8), 2027-2039.
- National Oceanic and Atmospheric Administration (NOAA), 1976: NOAA APT Information Note 76-5. United States Department of Commerce.
- Orcheski, Dennis, 1979: Personal Communication based on operating procedures for the University of Alberta Satellite Laboratory.
- Ormsby, James P., 1975: Image Stretching on a Curved Surface to Improve Satellite Gridding. Journal of Applied Meteorology, 14(8), 1594-1599.
- Petterssen, Sverre, 1956: Weather Analysis and Forecasting, Second Edition Volume I, Motion and Motion Systems. McGraw-Hill, New York, 428pp.
- Phillips, G. M. and P. J. Taylor, 1973: Theory and Applications of Numerical Analysis. Academic Press, London, 380pp.
- Physick, William, 1976: A Numerical Model of the Sea-Breeze Phenomenon Over a Lake or Gulf. Journal of the Atmospheric Sciences, 33(11), 2107-2135.
- Physick, W. L. and R. A. D. Byron-Scott, 1977: Observations of the Sea Breeze in the Vicinity of a Gulf. Weather, 32(10), 373-381.
- Rao, P. Krishna, 1970: Estimating Cloud Amount and Height from Satellite Infrared Radiation Data. ESSA Technical Report NES-54, Washington, D. C., 11pp.
- Rao, P. Krishna, 1975: Picture of the Month - "Invisible" Cirrus Clouds in NOAA-2 VHR Imagery. Monthly Weather Review, 103(1), 72-77.
- Rao, P. Krishna and E. Paul McClain, 1974: Images from the NOAA-3 Very High Resolution Radiometer Over the North Sea and Adjoining Countries. Weather, 29(12), 436-442.
- Rao, P. Krishna, W. L. Smith and R. Koffler, 1972: Global Sea Surface Temperature Distribution Determined from an Environmental Satellite. Monthly Weather Review, 100(1), 10-14.
- Rao, P. Krishna, Alan E. Strong and Russell Koffler, 1971: Sea





Surface Temperature Mapping Off the Eastern United States Using NASA's ITOS Satellite. Proceedings of the Seventh International Symposium on Remote Sensing of Environment May 17-21, 1971, Volume 1, University of Michigan, Ann Arbor, 683-691.

Rao, P. Krishna and Jay S. Winston, 1963: An Investigation of Some Synoptic Capabilities of Atmospheric "Window" Measurements from Satellite TIROS II. *Journal of Applied Meteorology*, 2(1), 12-23.

Rasool, S. I., 1964: Cloud Heights and Nighttime Cloud Cover from TIROS Radiation Data. *Journal of the Atmospheric Sciences*, 21(2), 152-156.

Reinelt, E. R., P. Hof, D. Oracheski and J. Broszkowski, 1975: Research Studies of Numerical Enhancement of APT Scanning Radiometer Data for Application to Arctic Weather and Ice Prediction. Final Report, DDS(AES) Contract OSV4-0183, University of Alberta at Edmonton, 204pp.

Salter, P. R., 1977: Some Results of the Interpretation of High Resolution Imagery Data from NOAA Spacecraft. *Weather*, 32(6), 208-216.

Sampson, Robert J., 1978: Surface II Graphics System. Kansas Geological Survey, 240pp.

Saunders, Peter M., 1967: The Temperature at the Ocean-Air Interface. *Journal of the Atmospheric Sciences*, 24(3), 269-273.

Saur, J. F. T., 1963: The Study of the Quality of Sea Water Temperatures Reported in Logs of Ship's Weather Observations. *Journal of Applied Meteorology*, 2(3), 417-425.

Schaper, P. W., 1976: Infrared Sensing Methods. Remote Sensing for Environmental Sciences, Edited by Erwin Schanda, Springer-Verlag, Heidelberg, 84-109.

Schwalb, A., 1972: Modified Version of the Improved TIROS Operational Satellite (ITOS D-G). NOAA Technical Memorandum NESS 35, Washington, D. C., 48pp.

Sidran, Miriam and Frank Hebard, 1972: Charting the Loop Current by Satellite. Proceedings of the Eighth International Symposium on Remote Sensing of Environment Oct 2-6, 1972, Volume 2, Environmental Research Institute of Michigan, Ann Arbor, 1121-1126.

Simpson, J. E., 1964: Sea Breeze Fronts in Hampshire. *Weather*, 19(7), 208-220.



- Somerscales, E. F. C., 1971: A Technique for the Comparison of Contact and Non-Contact Measurements of Water Surface Temperature. Proceedings of the Seventh International Symposium on Remote Sensing of Environment May 17-21, 1971, Volume 2, University of Michigan, Ann Arbor, 1089-1093.
- Strong, A. E. and R. J. DeRycke, 1973: Ocean Current Monitoring Employing a New Satellite Sensing Technique. *Science*, 182(4111), 482-484.
- Strong, Alan E., Harry G. Stumpf, Julia L. Hart and John A. Pritchard, 1974: Extensive Summer Upwelling on Lake Michigan During 1973 Observed by NOAA-2 and ERTS-1 Satellites. Proceedings of the Ninth International Symposium on Remote Sensing of Environment April 15-19, 1974, Volume 2, Environmental Research Institute of Michigan, Ann Arbor, 923-932.
- Sumner, G. N., 1977: Sea Breeze Occurrence in Hilly Terrain. *Weather*, 32(6), 200-208.
- Valovcin, Francis R., 1968: Infrared Measurements of Jet-Stream Cirrus. *Journal of Applied Meteorology*, 7(5), 817-826.
- Wallace, John M. and Peter V. Hobbs, 1977: Atmospheric Science An Introductory Survey. Academic Press, New York, 467pp.
- Walsh, John E., 1974: Sea Breeze Theory and Applications. *Journal of the Atmospheric Sciences*, 31(8), 2012-2026.
- Wendler, G., 1977: Special Products of Satellite Imagery. Radiation in the Atmosphere, Edited by H. J. Bolla, Science Press, Princeton, 357-358.
- Wendland, Wayne M. and Reid A. Bryson, 1969: Surface Temperature Patterns of Hudson Bay from Aerial Infrared Surveys. Remote Sensing in Ecology, Edited by Philip L. Johnson, University of Georgia Press, Athens, 185-193.
- Willett, Hurd C., 1944: Descriptive Meteorology. Academic Press, New York, 305pp.
- Winston, Jay S., 1965: Comments on "Cloud Heights and Nighttime Cloud Cover from TIROS Radiation Data". *Journal of the Atmospheric Sciences*, 22(3), 333-338.
- World Meteorological Organization, 1977: The Use of Satellite Imagery in Tropical Cyclone Analysis. W M O Technical Note Number 153, Geneva, 384pp.





## APPENDIX A

### CALCULATING LOCATIONS OF LATITUDE-LONGITUDE INTERSECTIONS ON SATELLITE IMAGERY

The positions of given latitude-longitude intersections were used in this study to generate latitude and longitude lines and outlines of geographic features. The method for calculating the location of these intersections was adapted from the point by point gridding procedure described by Reinelt, et al (1975, pg 135-141). The equations used assumed that the Earth was spherical and the satellite orbit circular, that the satellite scanned in lines perpendicular to its direction of motion, and that the pitch, yaw and roll of the satellite were negligible (see Section 3.3).

The equations in this study differ from those given by Reinelt, et al only in the form of the angle of inclination used; in this study the satellite inclination was measured from a meridian rather than from the equator (in Figure A.1, the angle  $i'$  was used rather than  $i$ ). Therefore, only a general description of the derivations and the final form of each equation are included herein. Reference should be made to Reinelt, et al for intermediate steps in the derivations.

Figure A.1 shows the geometry of the polar orbiting satellite. It is assumed that the satellite starts at the equator, at  $\phi_0, \theta_0$  where  $\phi_0$  is the latitude in radians (zero, in this case) and  $\theta_0$  is the longitude, also in radians. (All longitudes are measured from  $0^\circ$  Greenwich, with longitudes to the east of  $0^\circ$  being positive.)





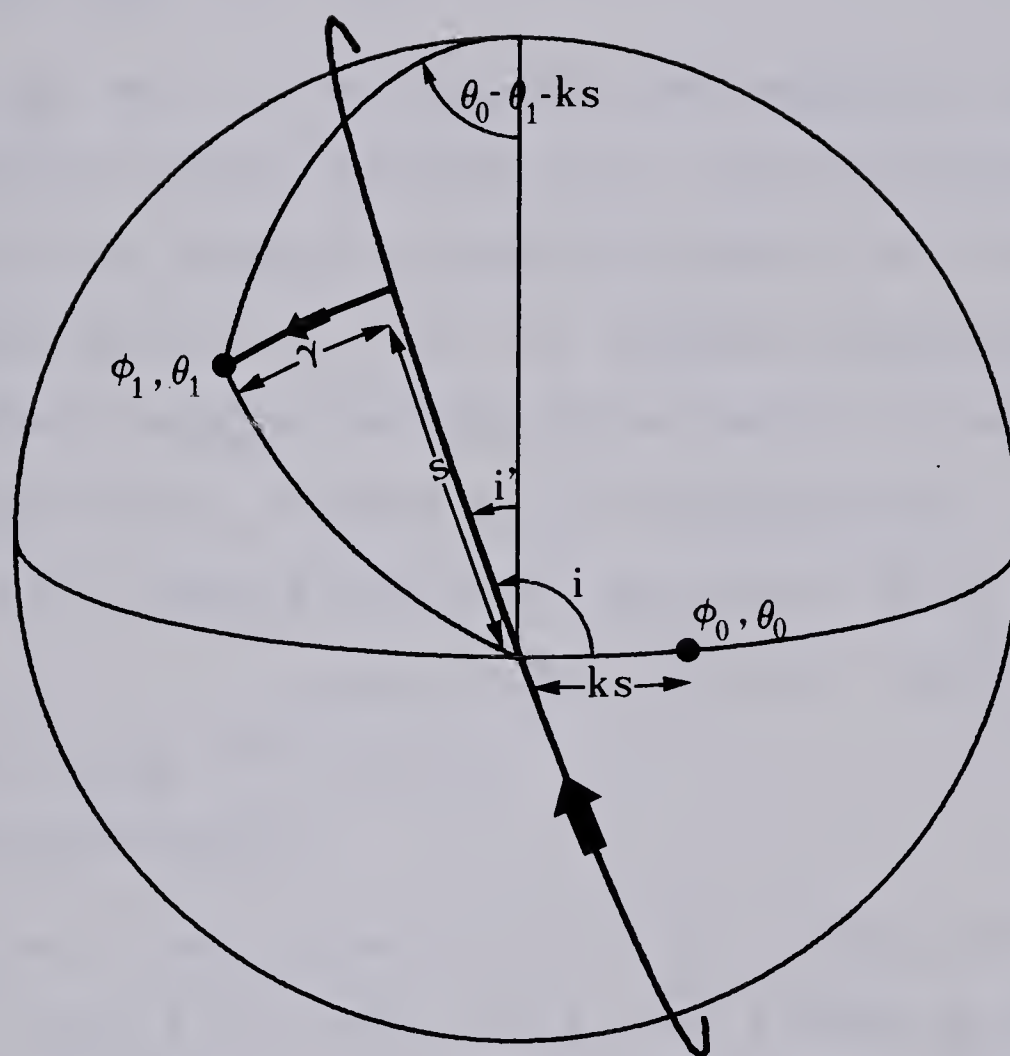


FIGURE A.1 Geometry of a near-polar orbiting satellite. The track of the satellite on a "non-rotating" Earth is shown by the large arrow. The direction of scanning of the satellite radiometer is shown by the smaller arrow. (After Reinelt, et al, 1975)



The satellite moves along an orbital arc of length  $s$  before the onboard radiometer scans the line which crosses a given latitude ( $\phi_1$ ) and longitude ( $\theta_1$ ). During the same time, the Earth rotates through a distance given by

$$\frac{s}{2\pi} \cdot \frac{2\pi L}{360} = ks \quad (1)$$

where  $k = \frac{L}{360}$  and  $L$  is the longitudinal displacement per orbit of the satellite in degrees (see Figure A.1). The total longitudinal displacement which ensues as the satellite scans an arc of length  $s$  is therefore given by  $\theta_0 - \theta_1 - ks$ . Spherical trigonometry is used to derive an equation relating the arc length  $s$  to the latitude and longitude values. The final form of the equation is

$$\begin{aligned} F(s) = \sin s \cos(\theta_0 - \theta_1 - ks) \cos \phi_1 - \cos s \cos i' \sin \phi_1 \\ - \cos s \sin(\theta_0 - \theta_1 - ks) \sin i' \cos \phi_1 = 0 \end{aligned} \quad (2)$$

(cf. Reinelt, et al, (41), pg 137)

Taking derivatives yields

$$\begin{aligned} F'(s) = \cos s \cos(\theta_0 - \theta_1 - ks) \cos \phi_1 + k \sin s \sin(\theta_0 - \theta_1 - ks) \\ \cos \phi_1 + \sin s \cos i' \sin \phi_1 + \sin s \sin(\theta_0 - \theta_1 - ks) \\ \sin i' \cos \phi_1 + k \cos s \cos(\theta_0 - \theta_1 - ks) \sin i' \cos \phi_1 \end{aligned} \quad (3)$$

Successive approximations from the iteration

$$s_{i+1} = s_i - \frac{F(s_i)}{F'(s_i)} \quad (4)$$

generate a series which converges to the root of Equation (2)

(Reinelt, et al, pg 138). The initial guess for the iteration,

$s_0$ , is determined by rewriting Equation (2) as

$$\frac{\sin s_0}{\cos s_0} = \tan s_0 = \frac{\sin(\theta_0 - \theta_1 - ks_0) \sin i' \cos \phi_1 + \cos i' \sin \phi_1}{\cos(\theta_0 - \theta_1 - ks_0) \cos \phi_1} \quad (5)$$





and setting  $s_0 = \phi_1$  on the right hand side of the equation. The number of the scan line passing through the point  $\phi_1, \theta_1$  is given by

$$s = \frac{(P)(RPM)}{2\pi} \quad (6)$$

where P is the orbital period of the satellite in minutes and RPM is the rotation rate of the scanning radiometer in revolutions per minute.

The position along the scan line of  $\phi_1, \theta_1$  is determined from the arc length  $\gamma$ . Again, using spherical trigonometry, one obtains the equation

$$\sin \gamma = \sin(\theta_0 - \theta_1 - ks) \cos i' \cos \phi_1 - \sin i' \sin \phi_1 \quad (7)$$

The arc length  $\gamma$  measured on the Earth's surface corresponds to a rotation of the scanning radiometer,  $\eta$ , given by

$$\tan \eta = \frac{R \sin \gamma}{H + R(1 - \cos \gamma)} \quad (8)$$

where R is the radius of the Earth and H is the height of the satellite above the Earth's surface (see Figure A.2). The position of the point  $\phi_1, \theta_1$  in the scan line is thus given by

$$\eta = \frac{(DIGF)(60)}{(2\pi)(RPM)} \quad (9)$$

where DIGF is the digitizing frequency of the satellite in data values per second and RPM is the rate of rotation of the satellite in revolutions per minute.

At the North Pole where  $s = \phi_1 = \frac{\pi}{2}$  Equation (7) reduces to

$$\sin \gamma = -\sin i' \quad (10)$$

and Equation (8) becomes

$$\tan \eta = \frac{-R \sin i'}{H + R(1 - \cos i')} \quad (11)$$



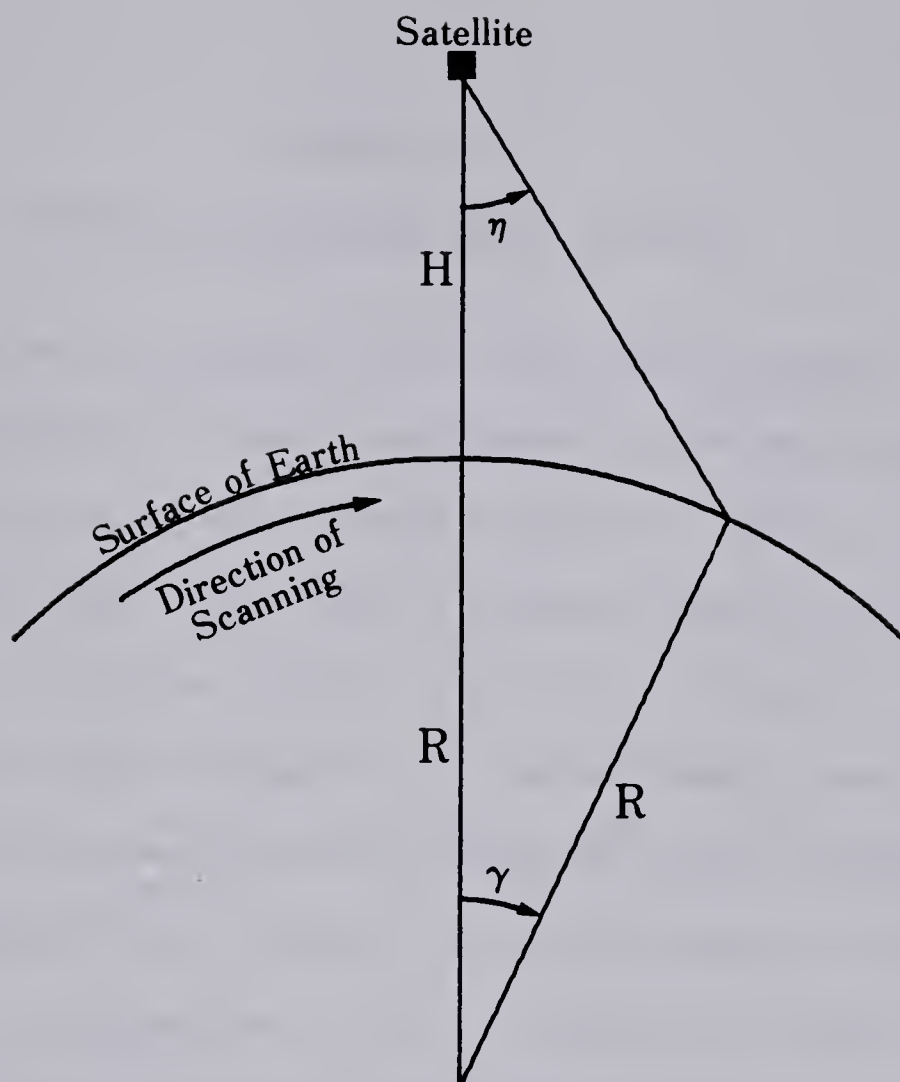


FIGURE A.2 Geometry of a satellite scanning radiometer.  
The satellite is heading out of the paper.  
(After Reinelt, et al, 1975)

Equations (1) through (9) are contained in the subroutine ITERA listed in Appendix C.3. Equations (10) and (11) are contained in the program SCAN-2 listed in Appendix C.2. The equations were used in calculating scan and position locations of all latitude and longitude lines and outlines shown in the temperature plots of Chapters 2 and 4.



## APPENDIX B

### INTERNAL CALIBRATION CURVE FITTING

The internal calibration used in this study converts the digital satellite information to equivalent black-body temperatures. This procedure makes use of the on-board calibration system of the NOAA series of satellites. Each scan of infrared satellite information from the NOAA satellites contains a six-level calibration measurement similar to that shown in Figure 2.2. Before launch, each scanning radiometer on the satellites was calibrated to known temperatures at every calibration level, and also at various radiometer temperatures. The calibration information for both the NOAA-4 and NOAA-5 satellites was obtained from the National Oceanic and Atmospheric Administration of the United States Department of Commerce.

The calibration information for the NOAA-4 and NOAA-5 satellites was used in the computer program TAPERD-1 (Appendix C.1). For each satellite orbit, TAPERD-1 extracted an average digital value for each calibration level from the scanning radiometer information, and calculated an appropriate equivalent temperature from the calibration data for the satellite. These values were then used to deduce equivalent temperatures for other digital information. However, the variation of the digital calibration values to the equivalent temperatures was not linear (see Figure 2.6), and thus a simple interpolation technique could not be applied to the calibration. Instead, a method of polynomial fitting was necessary.

It was believed that the calibration curves were smooth enough





for a very simple curve fitting technique to be used in the calibration process. The method of divided differences first developed by Isaac Newton and described in Phillips and Taylor (1973, pg 59-62) was chosen. If four calibration levels were used<sup>1</sup>, with the digital values denoted by  $x_1, x_2, x_3$  and  $x_4$  and the equivalent temperatures by  $y_1, y_2, y_3$  and  $y_4$ , then the equivalent temperature of the digital value  $X$  would be given by

$$Y = y_1 + (X-x_1)C_{12} + (X-x_1)(X-x_2)C_{123} + (X-x_1)(X-x_2)(X-x_3)C_{1234} + R$$

where  $R$  was the error in the approximation and the calibration constants  $C_{12}$ ,  $C_{123}$  and  $C_{1234}$  were calculated by successive differences according to the following scheme.

$$\begin{array}{l} x_1 \quad y_1 \\ x_2 \quad y_2 \\ x_3 \quad y_3 \\ x_4 \quad y_4 \end{array} \quad \begin{array}{l} C_{12} = \frac{y_2 - y_1}{x_2 - x_1} \\ C_{23} = \frac{y_3 - y_2}{x_3 - x_2} \\ C_{34} = \frac{y_4 - y_3}{x_4 - x_3} \end{array} \quad \begin{array}{l} C_{123} = \frac{C_{23} - C_{12}}{x_3 - x_1} \\ C_{234} = \frac{C_{34} - C_{23}}{x_4 - x_2} \end{array} \quad C_{1234} = \frac{C_{234} - C_{123}}{x_4 - x_1}$$

If the calibration constants approached zero in the higher orders, it could be assumed that the error in the approximation was negligible.

The calibration calculations using the divided difference method appear in subroutine CALI in Appendix C.5. Figure B.1 shows the calibration points and corresponding calibration curve used in the internal calibration of Orbit 4346 of NOAA-5 on July 15 of 1977. The calibration levels and calculated calibration constants used to produce this curve are also shown in the sample output from programs

---

1. The use of more than four calibration points would require calculation of higher order calibration constants and further terms in the polynomial equation.



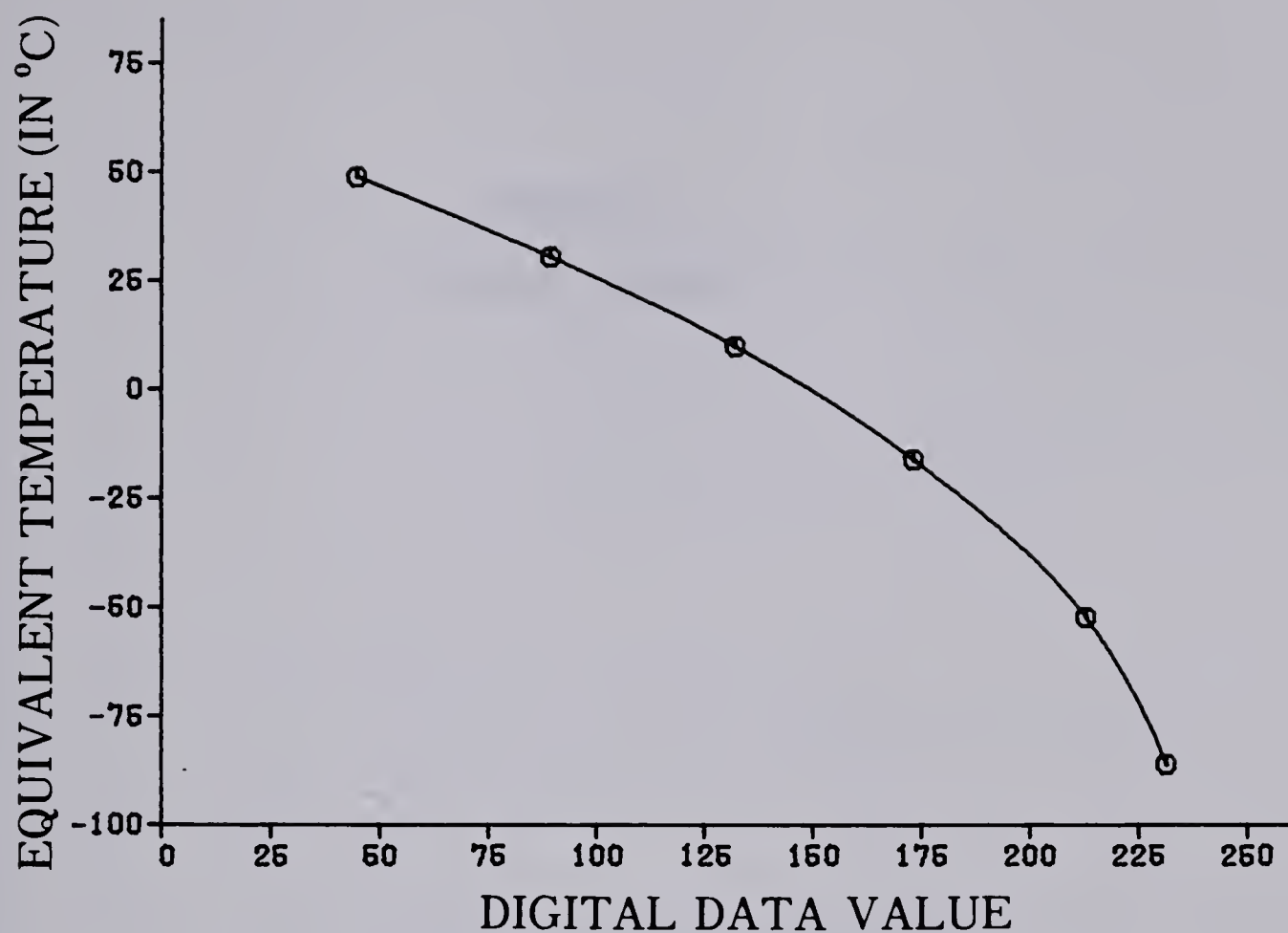


FIGURE B.1 Calibration points and infrared calibration curve for the Banks Island region of Orbit 4346 of NOAA-5 at 1930Z on July 15, 1977.

TAPERD-1 and SCAN-2 in Appendices C.7.2 and C.7.4.





APPENDIX C  
COMPUTER PROGRAMS



C.1 Program TAPERD-1

```

1      C          PROGRAM TAPERD-1
2      C
3      C          PROGRAM FOR IDENTIFYING SATELLITE SCAN INFORMATION AND CONVERTING
4      C          MAG TAPE INFORMATION TO COMPUTER USEABLE FORM
5      C
6      C          INPUT FROM  UNIT 1 : RAW TAPE DATA IN ONE BYTE INTEGER FORM
7      C          UNIT 5 : PROGRAM PARAMETERS
8      C
9      C          OUTPUT TO   UNIT 3 : (RAW TAPE DATA IN ONE BYTE FORM)
10     C          UNIT 6 : PROGRAM PARAMETERS, TAPE DOCUMENTATION,
11     C          (TAPE DATA IN INTEGER FORM),
12     C          (CALIBRATION DATA)
13     C
14     C          TAPE PARAMETERS
15     C
16     C          SPB = NUMBER OF SCANS PER DATA BLOCK
17     C          BPS = NUMBER OF BYTES PER SCAN
18     C          LDR = LENGTH OF DATA RECORD (ONE SCAN)
19     C          (BPS BYTES PLUS TWO BYTES CONTAINING SCAN NUMBER)
20     C          LDB = LENGTH OF DATA BLOCK (SPB SCANS)
21     C          LEN = LENGTH OF ANY BLOCK
22     C          LRN = INTERNAL COUNTER FOR DATA INPUT
23     C
24     C          OUTPUT PARAMETERS
25     C
26     C          ID(J) = OUTPUT IN INTEGER FORM (UNIT 6)
27     C          LA(J) = OUTPUT IN ONE BYTE FORM (UNIT 3)
28     C          NSC(N) = TWO BYTE NUMBER OF SCAN OUTPUTTED
29     C          MINSC = FIRST SCAN OUTPUTTED
30     C          MAXSC = LAST SCAN OUTPUTTED
31     C          NSOUT = NUMBER OF SCANS OUTPUTTED
32     C          X(I)  = DATA VALUES FOR CALIBRATION LEVELS
33     C          T(I)  = CORRESPONDING TEMPERATURE VALUES FOR CALIBRATION LEVELS
34     C          AOJ   = AVERAGED DATA VALUE FOR TEMPERATURE ADJUSTMENT
35     C *****
36     C
37     C          LOGICAL*1 LFMT(1) / ' ' /
38     C          LOGICAL*1 FL(18), DTXT(52), LA(8192)
39     C          INTEGER*2 IA(4096)
40     C          EQUIVALENCE (LA(1), IA(1))
41     C          INTEGER*2 LEN, ISC(64), LL(18), OOC(52), NSC(12), ID(2512)
42     C          INTEGER*4 LRN
43     C          INTEGER BPS, SPB, NX(10), NY(150)
44     C          REAL*8 IROV(2)
45     C          REAL AV(10,10), X(10), T(10), TCSET(4), TCAL(6,5,2,2)
46     C
47     C          DATA ISC/1H , 1H! , 1H" , 1H# , 1H$ , 1H% , 1H& , 1H' , 1H( , 1H) , 1H* , 1H+ , 1H , , 1H- ,
48     C          1 1H. , 1H/ , 1H0 , 1H1 , 1H2 , 1H3 , 1H4 , 1H5 , 1H6 , 1H7 , 1H8 , 1H9 , 1H: , 1H; , 1H. , 1H= ,
49     C          2 1H> , 1H? , 1H@ , 1HA , 1HB , 1HC , 1HD , 1HE , 1HF , 1HG , 1HH , 1HI , 1HJ , 1HK , 1HL , 1HM ,
50     C          3 1HN , 1HO , 1HP , 1HQ , 1HR , 1HS , 1HT , 1HU , 1HV , 1HW , 1HX , 1HY , 1HZ ,
51     C          4 1H( , 1H/ , 1H) , 1H| , 1H_ /
52     C          DATA IROV/8H      IR , 8HVISIBLE /
53     C          DATA TCSET/-5. , 5. , 15. , 25. /
54     C          DATA TCAL/55.0,36.0,15.0,-11.5,-50.0,-86.0,56.0,37.0,16.0,
55     C          1 -10.0,-48.0,-84.0,57.0,38.0,17.0,-9.5,-48.0,-84.0,60.5,40.5,
56     C          2 19.0,-8.5,-47.0,-83.0,99999.0,43.5,21.5,-6.5,-45.0,-81.0,
57     C          3 57.5,38.5,16.5,-10.0,-49.0,-84.0,57.5,38.5,17.0,-9.5,-48.0,
58     C          4 -82.0,58.5,39.5,18.0,-9.5,-48.0,-82.0,60.5,41.5,19.5,
59     C          5 -7.5,-46.0,-80.0,99999.0,43.0,21.0,-6.5,-46.0,-80.0,
60     C          6 49.5,31.5,10.5,-15.5,-53.0,-86.0,48.5,30.5,10.0,-16.0,
61     C          7 -53.0,-86.0,49.0,31.0,10.5,-15.5,-52.0,-86.0,50.0,32.0,
62     C          8 11.0,-15.0,-52.0,-86.0,53.0,34.0,13.0,-13.5,-52.0,-86.0,
63     C          9 45.0,28.5,7.0,-18.0,-54.0,-86.0,46.0,29.0,8.0,-17.0,-56.0,
64     C          1 -86.0,47.0,29.5,8.5,-16.5,-54.0,-86.0,49.5,31.5,10.5,-15.5,

```



```

65      2 -55.0,-86.0,50.0,36.0,15.0,-11.5,-50.0,-86.0/
66      C
67      C *****
68      C
69      C      INPUT DATA IS FORMAT FREE, DIVIDED BY COMMAS
70      C
71      C      NFS = NUMBER OF FILES TO BE SKIPPED
72      C      NBS = NUMBER OF BLOCKS TO BE SKIPPED
73      C      NBR = NUMBER OF BLOCKS TO BE READ AND OUTPUTTED
74      C      KOUT= OUTPUT OPTION
75      C      KOUT=6  OUTPUTS FORMATTED BLOCKS TO UNIT 6
76      C      KOUT=3  OUTPUTS UNFORMATTED BLOCKS TO UNIT 3
77      C      (FILE OR MAG TAPE FOR USE IN SCAN-2)
78      C      WITH OPTIONAL CALIBRATION
79      C      KOUT=0  OUTPUTS CALIBRATION ONLY
80      C
81      C      INPUT DATA: FOR UNIT 3 OUTPUT ONLY
82      C
83      C      ITYPE = OUTPUT TYPE OPTION
84      C      ITYPE=1  OUTPUTS IR DATA
85      C      ITYPE=2  OUTPUTS VISIBLE DATA (NO CALIBRATION REQUIRED)
86      C      LCAL = CALIBRATION OPTION
87      C      LCAL=0  NO CALIBRATION
88      C      LCAL=1  CALIBRATION IS CARRIED OUT
89      C
90      C      INPUT DATA: FOR CALIBRATION ONLY
91      C
92      C      NSAT = SATELLITE NUMBER (CALIBRATION AVAILABLE ONLY FOR
93      C      NOAA 4 (NSAT=4) AND NOAA 5 (NSAT=5))
94      C      NRAD = RADIOMETER NUMBER (1 OR 2)
95      C      TRAD = RADIOMETER TEMPERATURE IN DEGREES C
96      C      NSCAN,NPOSN = SCAN AND POSITION LOCATION OF AREA OF KNOWN
97      C      TEMPERATURE USED TO ZERO THE CALIBRATION. THE
98      C      OUTPUTTED DATA VALUE IS AVERAGED OVER AN AREA
99      C      OF APPROXIMATELY ONE HALF A DEGREE OF
100     C      LATITUDE SQUARE.
101     C      IF NSCAN=0, THIS STEP IS NOT DONE
102     C
103     C *****
104     C
105     C      READ TAPE INPUT DATA
106     C      READ(5,LFMT) NFS,NBS,NBR,KOUT
107     C
108     C      WRITE(6,90)
109     C      90 FORMAT(1H1,10X,'INPUT PARAMETERS')
110     C      WRITE(6,95) NFS,NBS,NBR,KOUT
111     C      95 FORMAT(1H0,5X,'FILES SKIPPED =',I3,5X,'BLOCKS SKIPPED =',I3,
112     C      1 5X,'BLOCKS READ =',I4,5X,'OUTPUT OPTION =',I2)
113     C      IF(KOUT.EQ.6) GO TO 20
114     C      IF(KOUT.EQ.0) GO TO 5
115     C
116     C      READ UNIT 3 INPUT DATA
117     C      READ(5,LFMT) ITYPE,LCAL
118     C      IBGN=0
119     C      IF(ITYPE.EQ.2) IBGN=1500
120     C      WRITE(6,96) IROV(ITYPE)
121     C      96 FORMAT(1H0,5X,A8,'INFORMATION TRANSFERRED TO UNIT 3')
122     C      IF(LCAL.EQ.0) GO TO 10
123     C
124     C      READ CALIBRATION INPUT DATA
125     C      5 READ(5,LFMT) NSAT,NRAD,TRAD,NSCAN,NPOSN
126     C      GO TO 20
127     C      10 WRITE(6,97)
128     C      97 FORMAT(1H0,5X,'NO CALIBRATION FOR OUTPUT PRODUCED')
129     C
130     C      20 REWIND 1

```





```

131      C
132      C      SKIP TO FILE
133      C
134      CALL SKIP(NFS,O,1,&980)
135      C
136      C      READ AND INTERPRET FILE LABEL
137      C
138      CALL READ(FL,LEN,O,LRN,1,&900)
139      DO 40 L=1,LEN
140      ID(L)=IBYTE(FL(L))
141      IDX=ID(L)-31
142      IF(IDX .LT. 1) IDX=1
143      IF(IDX .GT. 64) IDX=1
144      LL(L)=ISC(IDX)
145      40 CONTINUE
146      WRITE(6,211) (LL(K),K=1,4),LL(2),LL(1),LL(4),LL(3),LEN,LRN
147      211 FORMAT(1H0,5X,'FILE LABEL=',4A1,5X,'ORBIT ',4A1,
148      1 5X,'LENGTH=',I3,5X,'LRN=',I5)
149      C
150      C      READ AND INTERPRET FILE DOCUMENTATION
151      C
152      50 CALL READ(DTXT,LEN,O,LRN,1,&901)
153      ID(1)=JBYTE(DTXT(1))
154      ID(2)=IBYTE(DTXT(2))
155      ID(3)=JBYTE(DTXT(3))
156      ID(4)=IBYTE(DTXT(4))
157      BPS=ID(1)+ID(2)
158      SPB=ID(3)+ID(4)
159      DO 60 L=5,LEN
160      ID(L)=IBYTE(DTXT(L))
161      IDX=ID(L)-31
162      IF(IDX .LT. 1) IDX=1
163      IF(IDX .GT. 64) IDX=1
164      DOC(L)=ISC(IDX)
165      60 CONTINUE
166      WRITE(6,212) (DOC(K),K=5,LEN),LEN,LRN
167      212 FORMAT(1H0,5X,'DOCUMENTATION:',48A1,5X,
168      1 'LENGTH=',I3,5X,'LRN=',I5)
169      WRITE(6,213) BPS,SPB
170      213 FORMAT(1H0,5X,I5,' BYTES PER SCAN',4X,I2,' SCANS PER BLOCK')
171      LDR=BPS+2
172      LDB=SPB*LDR
173      NS=LDR/2
174      C
175      C      SKIP NBS BLOCKS OF DATA
176      C
177      65 CALL SKIP(O,NBS,1,&990)
178      ISCAN=SPB*NBS
179      MINSC=ISCAN
180      NSOUT=O
181      C
182      IF(KOUT.EQ.O) GO TO 110
183      C
184      C      READ AND CONVERT NBR BLOCKS OF DATA
185      C
186      DO 100 KK=1,NBR
187      NBCNT=NBS+KK
188      C      READ ONE BLOCK OF DATA
189      CALL READ(IA,LEN,O,LRN,1,&902)
190      C      CHECK TO SEE IF BLOCK LENGTH CORRECT (BLOCKS
191      C      OF INCORRECT LENGTH ARE NOT OUTPUTTED)
192      IF(LEN .NE. LDB) GO TO 903
193      C
194      DO 70 N=1,SPB
195      IX=(N-1)*NS+1
196      NSC(N)=IA(IX)

```



```

197 C      CHECK TO SEE IF SCAN NUMBER CORRECT (MISSED SCANS ARE NOTED)
198     IF(NSC(N).EQ.ISCAN) GO TO 68
199     IF(NSC(N)-ISCAN.GT.1) GO TO 66
200     WRITE(6,215) ISCAN
201 215 FORMAT(1H0,5X,'MISSED SCAN =',I5)
202     GO TO 67
203     66 NSS=NSC(N)-1
204     WRITE(6,216) ISCAN,NSS
205 216 FORMAT(1H0,5X,'SCANS',I5,2X,'TO',I5,2X,'MISSED')
206     67 ISCAN=NSC(N)
207     68 ISCAN=ISCAN+1
208     70 CONTINUE
209     IF(KOUT.EQ.3) GO TO 80
210 C
211 C      UNIT 6 DATA OUTPUT
212 C
213 C      WRITE BLOCK DOCUMENTATION
214     WRITE(6,214) LEN,LRN,(NSC(N),N=1,SPB)
215 214 FORMAT(1H0,5X,'DATA BLOCK LENGTH=',I5,
216     1 5X,'LRN=',I5,5X,'SCANS',10I5)
217 C
218     DO 75 I=1,SPB
219     NJ=(I-1)*LDR
220     DO 72 J=1,LDR
221     ID(J)=IBYTE(LA(J+NJ))
222     72 CONTINUE
223 C      OUTPUT ONE SCAN OF DATA
224     WRITE(6,666)I,J,ID(1),ID(2)
225     WRITE(6,666) (ID(J),J=3,LDR)
226 666 FORMAT(10I10)
227     NSOUT=NSOUT+1
228     75 CONTINUE
229     GO TO 100
230 C
231 C      UNIT 3 DATA OUTPUT
232 C
233 C      NOTE FOR MAG TAPE OUTPUT:  UNIT 1 IS REWOUND
234 C      AT BEGINNING OF PROGRAM.  UNIT 3 IS NOT REWOUND.
235 C      THEREFORE, SECTIONS OF SEVERAL FILES FROM UNIT 1
236 C      CAN BE TRANSFERRED TO SUCCESSIVE FILES OF UNIT 3
237 C      BY RE-RUNNING TAPERD, USING NEW INPUT PARAMETERS FOR
238 C      EACH RUN
239 C
240     80 DO 85 I=1,SPB
241     JB=3+(I-1)*LDR+IBGN
242     JE=JB+919
243     WRITE(3) NSC(I),(LA(J),J=JB,JE)
244     NSOUT=NSOUT+1
245     85 CONTINUE
246 C
247 100 CONTINUE
248 C
249 C      PRINT OUTPUT PARAMETERS
250 C
251     MAXSC=NSC(SPB)
252     WRITE(6,217) MINSC,MAXSC,NSOUT
253 217 FORMAT(1H0,5X,'FIRST SCAN OUTPUTTED =',I5,5X,'LAST SCAN',
254     1 ' OUTPUTTED =',I5,5X,'NUMBER OF SCANS OUTPUTTED =',I5)
255 C
256     IF(KOUT.EQ.6) GO TO 1000
257 C
258     ENDFILE 3
259     IF(LCAL.EQ.0) GO TO 1000
260 C *****
261 C
262 C      REPOSITION TAPE TO BEGINNING OF BLOCKS READ AND OUTPUTTED

```





```

263      C
264      NRPA=2+NBS
265      CALL SKIP(-1,0,1,&981)
266      CALL SKIP(1,NRPA,1,&991)
267      110 WRITE(6,220) MINSC
268      220 FORMAT(1H-,5X,'CALIBRATION BEGINS AT SCAN',I5)
269      NBH=NR/2-2
270      IF(NBH.LT.0) NBH=0
271      NBCNT=0
272      NBERR=0
273      C
274      C      OUTPUT CALIBRATION FROM NINE SCANS OF DATA
275      C      (THREE FROM BEGINNING, THREE FROM MIDDLE AND
276      C      THREE FROM NEAR END OF OUTPUTTED DATA SCANS)
277      C      TEN POINTS FROM SIX LEVELS OF EACH SCAN
278      C      CALIBRATION ARE USED
279      C
280      115 NBCNT=NBCNT+1
281      IF(NBERR.GT.2) GO TO 1000
282      C      READ ONE BLOCK OF DATA
283      CALL READ(IA,LEN,0,LRN,1,&910)
284      C      CHECK TO SEE IF BLOCK LENGTH CORRECT
285      C      (BLOCKS OF INCORRECT LENGTH ARE NOT OUTPUTTED.
286      C      MORE THAN TWO BLOCKS OF INCORRECT LENGTH FOUND
287      C      IN ONE CALIBRATION RESULTS IN PROGRAM FAILURE)
288      IF(LEN.NE.LDB) GO TO 911
289      DO 130 N=1,3
290      JJJ=(NBCNT-1)*SPB+N
291      IX=(N-1)*NS+1
292      NSC(JJJ)=IA(IX)
293      WRITE(6,221) NSC(JJJ)
294      221 FORMAT(1H0,5X,'CALIBRATION SCAN',I5)
295      NJ=(N-1)*LDR+1074
296      NJP=NJ+115
297      KKK=0
298      C      OUTPUT CALIBRATION VALUES FOR SIX LEVELS
299      DO 130 NN=NJ,NJP,23
300      KKK=KKK+1
301      AV(JJJ,KKK)=0.0
302      C      OUTPUT TEN POINTS FOR EACH LEVEL
303      DO 120 NNN=1,10
304      NX(NNN)=IBYTE(LA(NN+NNN-1))
305      AV(JJJ,KKK)=AV(JJJ,KKK)+FLOAT(NX(NNN))
306      120 CONTINUE
307      AV(JJJ,KKK)=AV(JJJ,KKK)/10.
308      WRITE(6,222) KKK,(NX(I),I=1,10),AV(JJJ,KKK)
309      222 FORMAT(1H , 'CALIBRATION STEP',I3,5X,'LEVELS',10I5,5X,'MEAN',F7.1)
310      130 CONTINUE
311      IF(NBCNT.GE.3) GO TO 140
312      CALL SKIP(0,NBH,1,&992)
313      GO TO 115
314      C      DETERMINE AVERAGE DATA VALUES OF CALIBRATION LEVELS
315      140 DO 160 KK=1,KKK
316      X(KK)=0.0
317      DO 150 JJ=1,JJJ
318      X(KK)=X(KK)+AV(JJ,KK)
319      150 CONTINUE
320      X(KK)=X(KK)/JJJ
321      160 CONTINUE
322      IF(KKK.NE.6) GO TO 912
323      X(6)=X(5)+(X(6)-X(5))/2.
324      C      DETERMINE CALIBRATION TEMPERATURES FOR EACH LEVEL
325      C      (NOTE FOR NOAA 4 ONLY: THE FIRST LEVEL AT RADIOMETER
326      C      TEMPERATURE 35 DEG C IS NOT GIVEN. IF TRAD IS BETWEEN
327      C      25 AND 35 DEG C, THIS LEVEL SHOULD THEREFORE NOT BE USED)
328      170 NTEMP=0

```



```

329      IF(TRAD.GE.-5..AND.TRAD.LT.5.) NTEMP=1
330      IF(TRAD.GE.5..AND.TRAD.LT.15.) NTEMP=2
331      IF(TRAD.GE.15..AND.TRAD.LT.25.) NTEMP=3
332      IF(TRAD.GE.25..AND.TRAD.LE.35.) NTEMP=4
333      IF(NTEMP.EQ.0) GO TO 920
334      LLS=0
335      IF(NSAT.EQ.4) LLS=1
336      IF(NSAT.EQ.5) LLS=2
337      IF(LLS.EQ.0) GO TO 921
338      DO 175 II=1,6
339      T(II)=TCAL(II,NTEMP,NRAD,LLS) + (TCAL(II,NTEMP+1,NRAD,LLS)-
340      1 TCAL(II,NTEMP,NRAD,LLS))*(TRAD-TCSET(NTEMP))/10.
341      175 CONTINUE
342      C      OUTPUT CALIBRATION VALUES
343      WRITE(6,225) NSAT,NRAD,TRAD,(I,X(I),T(I),I=1,KKK)
344      225 FORMAT(1H-,//,10X,'CALIBRATION OF SATELLITE NOAA',I2,//,5X,
345      1 'RADIOMETER NUMBER',I2,2X,'AT',F6.1,' DEGREES C',//,
346      2 5X,'CALIBRATION STEP',5X,'DATA LEVEL',5X,'TEMPERATURE',
347      3 ' (IN DEG C)',//,10(12X,I2,11X,F8.2,13X,F7.2,/),//)
348      C
349      IF(NSCAN.EQ.0) GO TO 1000
350      C *****
351      C
352      C      REPOSITION TAPE TO BLOCK CONTAINING NSCAN
353      C
354      NRPB=2+(NSCAN-3)/SPB
355      IF(NRPB.LT.2) GO TO 935
356      IF(NPOSN.LT.8.OR.NPOSN.GT.913) GO TO 936
357      CALL SKIP(-1,0,1,&982)
358      CALL SKIP(1,NRPB,1,&993)
359      C
360      C      OUTPUT ZEROING ADJUSTMENT FROM SEVEN SCANS
361      C      AND FIFTEEN POSITIONS
362      C
363      NBERR=0
364      SUM1=0.0
365      LLL=1
366      180 DO 185 IP=1,4
367      IF(NBERR.GT.2) GO TO 1000
368      CALL READ(IA,LEN,0,LRN,1,&930)
369      IF(LEN.NE.LDB) GO TO 931
370      DO 185 N=1,SPB
371      IX=(N-1)*NS+1
372      NSC(LLI)=IA(IX)
373      IF(NSC(LLI).LT.NSCAN-3) GO TO 185
374      NN=2+(N-1)*LDR+NPOSN-7
375      DO 184 NNN=1,15
376      NDAT=IBYTE(LA(NN+NNN-1))
377      NY((LLI-1)*15+NNN)=NDAT
378      SUM1=SUM1+FLOAT(NDAT)
379      184 CONTINUE
380      LLL=LLL+1
381      IF(LLI.GT.7) GO TO 190
382      185 CONTINUE
383      190 LLLE=LLL-1
384      LCT=15*(LLLE)
385      LCTM=LCT-1
386      WRITE(6,230) (NY(LM),LM=1,LCT)
387      230 FORMAT(1H-,5X,'CALIBRATION ADJUSTMENT FROM DATA VALUES',//,
388      1 7(15I8,/))
389      C      CALCULATE STANDARD DEVIATION (STDEV), SKEWNESS (SSKEW),
390      C      AND KURTOSIS (SKURT) OF DATA POINTS
391      SMEAN=SUM1/FLOAT(LCT)
392      SUM2=0.0
393      SUM3=0.0
394      SUM4=0.0

```



```

395      DO 195 IY=1,LCT
396      SNYM=FLOAT(NY(IY))-SMEAN
397      SNYM2=SNYM*SNYM
398      SUM2=SUM2+SNYM2
399      SUM3=SUM3+SNYM2*SNYM
400      SUM4=SUM4+SNYM2*SNYM2
401 195 CONTINUE
402      SUM2=SUM2/FLOAT(LCT)
403      SUM3=SUM3/FLOAT(LCT)
404      SUM4=SUM4/FLOAT(LCT)
405      SVARI=SUM2
406      STDEV=SQRT(SVARI)
407      SSKEW=SUM3/(SUM2**1.5)
408      SKURT=SUM4/(SUM2*SUM2)-3.0
409      WRITE(6,231) SMEAN,SVARI,STDEV,SSKEW,SKURT
410 231 FORMAT(1H0,5X,'MEAN OF DATA VALUES =',F8.2,5X,
411      1 'VARIANCE =',F9.4,5X,'STANDARD DEVIATION =',F8.4,/,
412      2 10X,'SKEWNESS =',F9.4,5X,'KURTOSIS =',F9.4)
413      NPOSNB=NPOSN-7
414      NPOSNE=NPOSN+7
415      WRITE(6,250) NPOSNB,NPOSNE,(NSC(I),I=1,LLLE)
416 250 FORMAT(1H0,5X,'CALIBRATION ADJUSTMENT ',
417      1 'FROM POSITIONS',I5,' TO',I5,5X,'AND SCANS',7I5,/)
418 C
419      GO TO 1000
420 C *****
421 C
422 C      ERROR DEFAULT STATEMENTS
423 C
424      900 WRITE(6,1900)
425 1900 FORMAT(1H0,5X,'***ERROR IN FILE LABEL INPUT***')
426      GO TO 50
427      901 WRITE(6,1901)
428 1901 FORMAT(1H0,5X,'***ERROR IN DOCUMENTATION INPUT***')
429      GO TO 65
430      902 WRITE(6,1902) NBCNT
431 1902 FORMAT(1H0,5X,'***ERROR IN RECORD INPUT AT BLOCK',I5,'***')
432      GO TO 1000
433      903 WRITE(6,1903) NBCNT,LDB,LEN,LDR,BPS,SPB
434 1903 FORMAT(1H0,5X,'***ERROR IN LENGTH OF DATA BLOCK',I5,'***',
435      1 '//,5X,'LDB =',I7,5X,'LEN =',I6,5X,'LDR =',I6,5X,'BPS =',
436      2 I6,5X,'SPB =',I3)
437      GO TO 100
438      910 WRITE(6,1910) NBCNT
439 1910 FORMAT(1H0,5X,'***ERROR IN CALIBRATION INPUT BLOCK',I5,'***')
440      GO TO 1000
441      911 WRITE(6,1911) NBCNT,LDB,LEN,LDR,BPS,SPB
442 1911 FORMAT(1H0,5X,'***ERROR IN LENGTH OF CALIBRATION BLOCK',I5,'***',
443      1 '//,5X,'LDB =',I7,5X,'LEN =',I6,5X,'LDR =',I6,5X,'BPS =',
444      2 I6,5X,'SPB =',I3)
445      NBERR=NBERR+1
446      NBCNT=NBCNT-1
447      GO TO 115
448      912 WRITE(6,1912) KKK
449 1912 FORMAT(1H0,5X,'***ERROR IN CALIBRATION',I5,' STEPS***')
450      IF(KKK.LT.6) GO TO 170
451      GO TO 1000
452      920 WRITE(6,1920) TRAD
453 1920 FORMAT(1H0,5X,'***ERROR RADIOMETER TEMPERATURE',F6.2,
454      1 ' IS OUTSIDE -5 TO 35 DEG C CALIBRATION RANGE***')
455      GO TO 1000
456      921 WRITE(6,1921) NSAT
457 1921 FORMAT(1H0,5X,'***ERROR NO CALIBRATION DATA FOR SATELLITE',
458      1 I3,' ***')
459      GO TO 1000
460      930 WRITE(6,1930) IP

```





```

461      1930 FORMAT(1H0,5X,'***ERROR IN ZEROING INPUT BLOCK',I5,'***')
462      GO TO 1000
463      931 WRITE(6,1931) IP,LDB,LEN,LDR,BPS,SPB
464      1931 FORMAT(1H0,5X,'***ERROR IN LENGTH OF ZEROING BLOCK',I5,'***',
465      1 //,5X,'LDB =',I7,5X,'LEN =',I6,5X,'LDR =',I6,5X,'BPS =',
466      2 I6,5X,'SPB =',I3)
467      NBERR=NBERR+1
468      GO TO 180
469      935 WRITE(6,1935) NRPB
470      1935 FORMAT(1H0,5X,'***ERROR BLOCK',I5,' DOES NOT CONTAIN ',
471      1 'CALIBRATION DATA***')
472      GO TO 1000
473      936 WRITE(6,1936) NPOSN
474      1936 FORMAT(1H0,5X,'***ERROR AREA CONTAINING NPOSN (',I5,
475      1 ') IS BEYOND LIMITS OF DATA RECORD***')
476      GO TO 1000
477      980 WRITE(6,1980)
478      1980 FORMAT(1H0,5X,'***ERROR ON FILE SKIP***')
479      GO TO 1000
480      981 WRITE(6,1981)
481      1981 FORMAT(1H0,5X,'***ERROR ON FIRST FILE RETURN***')
482      GO TO 1000
483      982 WRITE(6,1982)
484      1982 FORMAT(1H0,5X,'***ERROR ON SECOND FILE RETURN***')
485      GO TO 1000
486      990 WRITE(6,1990)
487      1990 FORMAT(1H0,5X,'***ERROR ON DATA BLOCK SKIP***')
488      GO TO 1000
489      991 WRITE(6,1991)
490      1991 FORMAT(1H0,5X,'***ERROR ON FIRST CALIBRATION REPOSITION***')
491      GO TO 1000
492      992 WRITE(6,1992)
493      1992 FORMAT(1H0,5X,'***ERROR ON CALIBRATION BLOCK SKIP***')
494      GO TO 1000
495      993 WRITE(6,1993)
496      1993 FORMAT(1H0,5X,'***ERROR ON SECOND CALIBRATION REPOSITION***')
497      GO TO 1000
498      1000 STOP
499      END
500      C
501      C
502      FUNCTION IBYTE(NUM)
503      C
504      C      CONVERTS ONE BYTE NUMBER TO TWO BYTE INTEGER
505      C
506      LOGICAL*1 NUM,INT(2)
507      INTEGER*2 I/O/
508      EQUIVALENCE (I,INT)
509      INT(2)=NUM
510      IBYTE=I
511      RETURN
512      END
513      C
514      C
515      FUNCTION JBYTE(NUM)
516      C
517      C      CONVERTS ONE BYTE NUMBER TO TWO BYTE MULTIPLE OF 255
518      C
519      LOGICAL*1 NUM,INT(2)
520      INTEGER*2 I/O/
521      EQUIVALENCE (I,INT)
522      INT(1)=NUM
523      JBYTE=I
524      RETURN
525      END

```

END OF FILE



## C.2 Program SCAN-2

The input parameters in the program SCAN-2 determine the apparent surface location of satellite information. However, because of problems in the location process discussed in Section 3.3, some adjustment is required to produce a reasonably accurate match between the satellite imagery and known surface features. The parameters used for this adjustment are GRID and ZDRP, both of which are explained on the following pages. The parameter GRID is used to control the scan line location, while ZDRP is used to control the position along a given scan line. In this study, GRID and ZDRP were varied until the outline of Banks Island was approximately centered on the strong coastal isotherm gradient visible along each shoreline of the island on the temperature-field plots produced.

```

1      C      PROGRAM SCAN-2
2      C
3      C      PROGRAM TO CONVERT TAPE INFORMATION TO A GRIDDED DATA FIELD
4      C      AND TO GENERATE GRID POINT LOCATIONS OF LATITUDE AND
5      C      LONGITUDE LINES FOR USE IN CALCOMP PLOTTING ROUTINES
6      C
7      C      INPUT FROM   UNITS 1,2 AND 3 : LATITUDE - LONGITUDE COORDINATES
8      C                        OF OUTLINES TO BE COMPUTED
9      C                        UNIT 4 : RAW VALUES OF SATELLITE INFORMATION
10     C                        (PRODUCED BY PROGRAM TAPERD-1)
11     C                        UNIT 5 : PROGRAM PARAMETERS
12     C
13     C      OUTPUT TO   UNIT 6 : PROGRAM PARAMETERS, CALCULATED VALUES,
14     C                        AND ERROR STATEMENTS
15     C                        UNIT 7 : AVERAGED (SMOOTHED AND CALIBRATED) DATA
16     C                        FIELD
17     C                        (UNITS 8, 9 AND 10 ALSO USED IF NECESSARY)
18     C                        UNIT 11 : GRID COORDINATES OF LATITUDE AND
19     C                        LONGITUDE LINES
20     C                        (UNITS 12, 13 AND 14 ALSO USED IF NECESSARY)
21     C                        UNIT 15 : POSTING OF NORTH POLE AND OTHER LOCATIONS
22     C                        UNIT 16 : GRID COORDINATES OF OUTLINES
23     C                        (UNITS 17, 18 AND 19 ALSO USED IF NECESSARY)
24     C
25     C      LOGICAL*1 LFMT(1)/'*'/
26     C      LOGICAL*1 LA(920)
27     C      INTEGER RORBIT,RQ,RHR,RMIN,RSEC,LOUT2(3)
28     C      INTEGER*2 HSCAN,BSCAN,ESCAN
29     C      REAL LAINC,LOINC,SLAT(500),SLONG(500)
30     C      REAL*8 IROV,POS1,IR,VISIBL,SNAME,NOAA4,NOAA5,BLANK

```





```

31      REAL*8 QUAD,EAST,WEST,HEAD,NOR,SOU,POL,MONTH(12)
32      DATA POSI/8HPOSITION/,IR/8HINFRAREO/,VISIBL/8H VISIBLE/
33      DATA NOAA4/8H NOAA-4 /,NOAA5/8H NOAA-5 /,BLANK/8H      /
34      DATA EAST/8H EAST /,WEST/8H WEST /
35      DATA NOR/8H NORTH /,SOU/8H SOUTH /,POL/8H AT POLE/
36      DATA MONTH/8H JANUARY,8HFEBRUARY,8H MARCH,8H APRIL,
37      1 8H MAY,8H JUNE,8H JULY,8H AUGUST,8HSEPTembr,
38      2 8H OCTOBER,8HNOVEMBER,8HDECEMBER/
39      C
40      COMMON/TFIELD/TEMP(301,400)
41      COMMON/CONSTO/PIT2,PIB2,CMULF,SB,XKB,XIIB,XKJ
42      COMMON/CONSTS/RTSC,TPL,H,ZDRP,RGAMH,SINC,CINC
43      COMMON/VARI/SP,SINL,COSL,THETA
44      COMMON/VARIO/SCAN(500),POSN(500)
45      C
46      C *****
47      C
48      C      CONSTANTS AND CHECKS
49      C
50      COMMON/BLOCK/R,PI
51      PIT2=PI*2.
52      PIB2=PI/2.
53      C1=PIT2/360.0
54      C2=1.0/C1
55      DATA DIGF/2400./,SRPM/48./,C3/2.54/,MZERO/O/,ZERO/O.O/
56      CMULF=DIGF*60./ (SRPM*PIT2)
57      C
58      C      R      = RAOIUS OF EARTH IN KM
59      C      PI      = PI
60      C      PIT2    = PI*2
61      C      PIB2    = PI/2
62      C      C1      = CONVERSION FACTOR  DEGREES TO RAOIANS
63      C      C2      = CONVERSION FACTOR  RAOIANS TO DEGREES
64      C      DIGF    = DIGITIZING FREQUENCY OF SATELLITE IN OATA VALUES
65      C                  PER SECOND
66      C      SRPM    = SCAN RATE OF SATELLITE IN REVOLUTIONS PER MINUTE
67      C                  (ONE REVOLUTION EQUALS ONE SCAN)
68      C      C3      = CONVERSION FACTOR  CM TO INCHES
69      C      CMULF= CONVERSION FACTOR (RADIAN SCAN ANGLE TO DATA VALUE
70      C                  POSITION). DIGF IS FIXED AT 2400 DATA VALUES PER SECONO.
71      C      SRPM    IS FIXED AT 48 SCANS PER MINUTE. THEREFORE, SATELLITE
72      C      PRODUCES DIGF*60/SRPM OR 3000 DATA VALUES PER SCAN. FOR
73      C      EACH SCAN, SATELLITE ROTATES THROUGH TWO PI RADIAN.
74      C      THEREFORE, CMULF IS GIVEN BY 3000/(2*PI) OR 477.7
75      C      DATA VALUES PER RADIAN. THE ZERO DEGREE REFERENCE FOR
76      C      SATELLITE IS OIRECTLY ABOVE THE SUBPOINT AT DATA VALUE
77      C      ZDRP. FIRST AND SECONO HORIZONS ARE MEASURED FROM 'THE
78      C      ZERO DEGREE REFERENCE OF SATELLITE..
79      C      EACH OATA RECORD (EITHER IR OR VISIBLE DATA) CONTAINS
80      C      920 DATA VALUES (PLUS A SCAN NUMBER). MIOPOINT IS AT
81      C      DATA VALUE ZDRP. THEREFORE, ALL VALUES MEASURED
82      C      FROM ZERO DEGREE REFERENCE ARE CONVERTED TO OATA
83      C      VALUE POSITIONS BY MULTIPLYING BY CMULF AND AODING
84      C      ZORP. (COOROINATES OF FINAL OUTPUT POSITIONS ARE
85      C      AFFECTED BY KJ AS EXPLAINED BELOW)
86      C
87      C *****
88      C
89      C      INPUT OATA
90      C
91      C      INPUT OATA IS READ FROM UNITS 1,2,3,4 AND 5. ALL INPUT OATA IS
92      C      FORMAT FREE. VALUES ARE DIVIOED BY BLANKS OR COMMAS. FORTRAN G
93      C      COMPILER INSERTS MISSING DECIMAL PLACES FOR REAL DATA AND OELETES
94      C      UNNECESSARY DECIMAL PLACES  FOR INTEGER OATA INCORRECTLY ENTERED

```



```

95      C
96      C      THERE ARE ELEVEN READ STATEMENTS FOR UNIT 5
97      C
98      C      1 INPUT TYPE AND INCREMENTS
99      C
100     C      KINP = INPUT TYPE
101     C      KINP=0  NO INPUT FROM UNIT 3. USED TO CHECK POSITIONS OR
102     C      OUTPUT LAT-LON LINES ONLY
103     C      KINP=1  IR DATA FROM FILE SOURCE
104     C      KINP=2  VISIBLE DATA FROM FILE SOURCE
105     C      KINP=3  IR DATA FROM MAG TAPE SOURCE
106     C      KINP=4  VISIBLE DATA FROM MAG TAPE SOURCE
107     C      BSCAN = SCAN NUMBER TO BEGIN OUTPUT
108     C      ESCAN = SCAN NUMBER TO END OUTPUT
109     C
110     C      PARAMETER HSCAN IS READ DIRECTLY FROM UNIT 3 FOR EACH SCAN.
111     C      IT REPRESENTS THE NUMBER OF SCANS SINCE FIRST ARRIVAL OF
112     C      SATELLITE SIGNAL, FROM PROGRAM TAPERO-1. IF SCAN NUMBER CORRES-
113     C      PONDING WITH BSCAN IS NOT AVAILABLE FROM UNIT 3, PROGRAM
114     C      WILL BEGIN READING FIRST SCAN AVAILABLE. HOWEVER, VALUES FROM
115     C      MISSED SCANS USED IN SMOOTHING WILL BE UNDEFINED. IF ESCAN
116     C      IS LARGER THAN THE LAST SCAN TRANSFERRED BY PROGRAM TAPERO-1
117     C      TO UNIT 3, AN END OF FILE MARK WILL BE ENCOUNTERED. BOTH
118     C      CASES RESULT IN PROGRAM FAILURE
119     C
120     C      KB    = POSITION TO BEGIN OUTPUT
121     C      KE    = POSITION TO END OUTPUT
122     C
123     C      PARAMETER KJ (AND XKJ) GIVES THE NUMBER OF POSITIONS TO BE
124     C      AVERAGED. FOR IR SCANNING, THREE POSITIONS ARE AVERAGED TO
125     C      OBTAIN ONE GRID POINT. THIS DOES NOT RESULT IN LOSS
126     C      OF DATA SINCE THE DIGITIZING OF THE COMPUTER PRODUCES
127     C      ABOUT THREE TIMES AS MANY POINTS AS THE SATELLITE
128     C      RESOLUTION JUSTIFIES, BUT ALLOWS FOR LARGER AREAS TO BE USED.
129     C      NO AVERAGING IS DONE FOR VISIBLE DATA
130     C
131     C      LENGTH OF OUTPUT (NUMBER OF COLUMNS) IS GIVEN BY PARAMETER
132     C      MAXSC. MAXIMUM LENGTH IS 400 SCANS
133     C      WIDTH OF OUTPUT (NUMBER OF ROWS) IS GIVEN BY IPOS (AND XPOS).
134     C      MAXIMUM WIDTH IS 301 POSITIONS, WHICH CORRESPONDS TO THE TOTAL
135     C      WIDTH OF AVAILABLE IR SCANNING OR A THIRD OF TOTAL WIDTH
136     C      OF AVAILABLE VISIBLE SCANNING
137     C      SIZE OF OUTPUT IS GIVEN BY MTMAT (MAXSC*IPOS).
138     C
139     C      SF      = MAP SCALING FACTOR (1:10,000,000 INPUTTED AS 10E6)
140     C
141     C      2 ORBITAL DATA
142     C
143     C      NORBIT = NUMBER OF ORBIT
144     C      NYR    = YEAR OF ORBIT
145     C      NMO    = MONTH OF ORBIT
146     C      NOY    = DAY OF ORBIT
147     C      GRID  = NUMBER OF SCANS BETWEEN LAST EQUATOR CROSSING AND
148     C      FIRST ARRIVAL OF SATELLITE
149     C      NSAT   = SATELLITE NUMBER (04 = NOAA 4)
150     C
151     C      3 ORBITAL DATA FOR REFERENCE ORBIT
152     C
153     C      RORBIT = NUMBER OF REFERENCE ORBIT
154     C      RHR    = HOUR OF REFERENCE ORBIT (Z)
155     C      RMIN   = MINUTE OF REFERENCE ORBIT
156     C      RSEC   = SECOND OF REFERENCE ORBIT
157     C      RQ     = QUADRANT OF REFERENCE ORBIT EQUATOR CROSSING
158     C      RQ=0 (5)  0 TO 90 DEGREES LONGITUDE WEST
159     C      RQ=1 (6)  90 TO 180 DEGREES LONGITUDE WEST
160     C      RQ=2 (7)  90 TO 180 DEGREES LONGITUDE EAST

```





```

161 C      RQ=3 (8)  0 TO 90 DEGREES LONGITUDE EAST
162 C      0,1,2,3 ARE QUADRANTS FOR NORTHERN HEMISPHERE
163 C      5,6,7,8 ARE QUADRANTS FOR SOUTHERN HEMISPHERE
164 C      RLONG = 'LONGITUDE' OF REFERENCE ORBIT EQUATOR CROSSING
165 C      RQ AND RLONG ARE CODED VALUES READ DIRECTLY FROM T-BUS.
166 C      THE PROGRAM CALCULATES RLONGC FROM THESE VALUES BY ASSUMING
167 C      RIGHT ASCENSION OF THE ORBIT, THAT IS, LONGITUDE IS TAKEN
168 C      TO BE POSITIVE TO EAST AND NEGATIVE TO WEST (T-BUS CODE
169 C      ASSUMES 0 TO 180 DEGREES BOTH EAST AND WEST)
170 C
171 C  4 SATELLITE PARAMETERS
172 C
173 C      PT = ORBITAL PERIOD IN MINUTES
174 C      PL = LONGITUDINAL DISPLACEMENT PER ORBIT IN DEG LONG TO WEST
175 C      H = HEIGHT OF SATELLITE AT FIRST SCAN IN KM
176 C      ORIN = INCLINATION OF SATELLITE AT FIRST SCAN IN DEGREES
177 C      (PROGRAM USES ORIN-90.)
178 C      ZORP = ZERO DEGREE REFERENCE POSITION OF SATELLITE
179 C
180 C  5 AVERAGING PARAMETER (REQUIRED ONLY IF KINP=0)
181 C
182 C      KJ = POSITIONS TO BE AVERAGED
183 C      KJ=1 NO POSITIONS AVERAGED. USED FOR LOCATING AREAS
184 C      OR WITH VISIBLE DATA
185 C      KJ=3 THREE POSITIONS AVERAGED. USED WITH IR DATA
186 C
187 C  5 DATA INPUT PARAMETERS (NOT REQUIRED IF KINP=0)
188 C
189 C      NSKIP = NUMBER OF SCANS OF INPUT TO BE SKIPPED (FOR USE WITH MAG
190 C      TAPE INPUT ONLY. FOR FILE INPUT, PROGRAM WILL READ EACH
191 C      SCAN OF DATA, AND BEGIN OUTPUT WHEN BSCAN IS REACHED)
192 C
193 C      LSMT = SMOOTHING CHECKING PARAMETER
194 C      LSMT=0 NO SMOOTHING IS DONE
195 C      LSMT=1 SMOOTHING IS CARRIED OUT
196 C      LCAL = CALIBRATION CHECKING PARAMETER
197 C      LCAL=0 NO CALIBRATION IS DONE
198 C      LCAL=1 CALIBRATION IS CARRIED OUT
199 C
200 C  6 CHECKING PARAMETERS
201 C
202 C      LCHK1 = FIRST LATITUDE-LONGITUDE CHECKING PARAMETER
203 C      LCHK1=0 LAT-LON LINES ARE NOT COMPUTED
204 C      LCHK1=1 LAT-LON LINES ARE COMPUTED
205 C      LOUT1 = OUTLINE CHECKING PARAMETER
206 C      LOUT1=0 NO OUTLINES ARE COMPUTED
207 C      LOUT1=1,2 OR 3 ONE, TWO OR THREE OUTLINES ARE COMPUTED
208 C      (MAXIMUM OF THREE OUTLINES ALLOWED)
209 C
210 C  7 OUTLINE TYPE (NOT REQUIRED IF LOUT1=0)
211 C      NOTE : EACH OUTLINE REQUIRES A SEPARATE LOUT2 PARAMETER
212 C
213 C      LOUT2 = OUTLINE TYPE PARAMETER
214 C      LOUT2=1 INPUTTED POINTS OUTPUTTED TO UNIT 6.
215 C      CALCULATED GRID POINT LOCATIONS OUTPUTTED
216 C      TO UNIT 16 (17,18 AND 19)
217 C      LOUT2=2 NO OUTPUT OF INPUTTED POINTS.
218 C      CALCULATED GRID POINT LOCATIONS OUTPUTTED
219 C      TO UNIT 16 (17,18 AND 19). MAXIMUM AND
220 C      MINIMUM ROW AND COLUMN OF GRID LOCATIONS
221 C      CALCULATED AND OUTPUTTED
222 C      LOUT2=3 NO OUTPUT OF INPUTTED POINTS.
223 C      MAXIMUM AND MINIMUM ROW AND COLUMN OF
224 C      GRID LOCATIONS CALCULATED AND OUTPUTTED
225 C      LOUT2=4 INPUTTED POINTS OUTPUTTED TO UNIT 6.
226 C      CALCULATED GRID POINT LOCATIONS OUTPUTTED

```





```

227 C          TO UNIT 15 FOR POSTING
228 C          LOUT2=5 INPUTTED PDINTS WITHIN GRID FIELD DUTPUTTED TO UNIT 6.
229 C          CALCULATED GRID POINT LDCATIONNS DUTPUTTED
230 C          TO UNIT 6
231 C
232 C      8 LATITUDE AND LDNGITUDE INCREMENTS (NDT REQUIRED IF LCHK1=0)
233 C
234 C          LAINC = INCREMENT FOR LATITUDE LINES (IN DEGREES)
235 C          LDINC = INCREMENT FOR LDNGITUDE LINES (IN DEGREES)
236 C          LCHK2 = SECOND LATITUDE-LDNGITUDE CHECKING PARAMETER
237 C          LCHK2=0  DEFAULT VALUES FOR LATITUDE AND LDNGITUDE
238 C                   PLDTTNG USED
239 C          LCHK2=1  VALUES FOR LATITUDE AND LONGITUDE PLDTTNG
240 C                   MUST BE INPUTTED
241 C
242 C          THE DEFAULT VALUES ARE LATITUDES FRDM 0 TO 90 DEGREES NORTH,
243 C          LDNGITUDES FRDM 0 TO 360 DEGREES EAST. PDINTS ARE CALCULATED
244 C          FOR EVERY LATITUDE-LDNGITUDE INTERSECTION, BUT IF THE
245 C          DUTPUTTED AREA IS SMALL, MDST OF THESE POINTS ARE NOT USED.
246 C          THEREFDRE, JUDICIDUS CHDICE OF LATITUDE AND LDNGITUDE
247 C          PARAMETERS LEADS TO GREAT TIME SAVING
248 C
249 C      9 LATITUDE AND LONGITUDE PLOTTING VALUES
250 C          (NDT REQUIRED IF LCHK1=0 DR LCHK2=0)
251 C
252 C          LAB  = LATITUDE TO BEGIN PLDTTNG
253 C          LAE  = LATITUDE TO END PLOTTNG
254 C          LOB  = LONGITUDE TO BEGIN PLDTTNG
255 C          LDE  = LDNGITUDE TO END PLDTTNG
256 C          LHEM = LONGITUDE HEMISPHERE
257 C          LHEM=1  BOTH LONGITUDES INPUTTED AS DEGREES EAST
258 C          LHEM=2  BDTH LDNGITUDES INPUTTED AS DEGREES WEST
259 C
260 C          LATITUDES ARE EXPRESSED IN DEGREES NDRTH
261 C          LONGITUDES ARE EXPRESSED IN DEGREES EAST DR WEST
262 C          NDTE: LATITUDE (LDNGITUDE) TO BEGIN PLOTTNG MUST
263 C          BE SMALLER THAN LATITUDE (LDNGITUDE) TO END PLDTTNG
264 C
265 C          A MAXIMUM OF 500 POINTS ALLDWED FOR EACH LINE
266 C
267 C      10 SMOOTHING PARAMETERS (NDT REQUIRED IF KINP=0 OR LSMT=0)
268 C          (SEE SUBROUTINE SMDO)
269 C
270 C      11 CALIBRATION PARAMETERS (NDT REQUIRED IF KINP=0 DR LCAL=0)
271 C          (SEE SUBROUTINE CALI)
272 C
273 C
274 C          THERE IS ONE READ STATEMENT FOR UNIT 4, WHICH IS CALLED
275 C          ESCAN-BSCAN+1 TIMES. UNIT 4 IS EITHER A FILE OR A MAG TAPE UNIT.
276 C
277 C
278 C          THERE IS ONE READ STATEMENT FOR UNITS 1, 2 AND 3. EACH CARD OR
279 C          LINE OF EACH UNIT CONSISTS OF A SINGLE LATITUDE-LONGITUDE
280 C          INTERSECTION WHICH THE PROGRAM CONVERTS TO GRID POINT COORDINATES.
281 C          THE PROGRAM CONTINUES TO READ UNTIL 500 PDINTS ARE INPUTTED OR
282 C          AN END OF FILE MARK IS ENCOUNTERED. DEPENDING ON LOUT2,
283 C          GRID COORDINATES OF THE OUTLINE ARE DUTPUTTED EITHER TO
284 C          UNIT 6 OR TO UNIT 16 (17, 18 AND 19). THIS OUTLINE CAN
285 C          THEN BE USED WITH THE GRID FIELD IN CALCDMP PLDTTNG
286 C
287 C          XLATD = LATITUDE COORDINATE OF POINT (IN DEGREES)
288 C          XLATM = LATITUDE COORDINATE OF PDINT (AND MINUTES)
289 C          XLDND = LDNGITUDE COORDINATE OF POINT (IN DEGREES)
290 C          XLONM = LDNGITUDE COORDINATE OF PDINT (AND MINUTES)
291 C          LHEM  = LDNGITUDE HEMISPHERE
292 C          LHEM=1  LONGITUDE INPUTTED IN DEGREES EAST

```



```

293 C          LHEM=2  LONGITUDE INPUTTED IN DEGREES WEST
294 C
295 C *****
296 C
297 READ(5,LFMT) KINP,BSCAN,ESCAN,KB,KE,SF
298 READ(5,LFMT) NORBIT,NYR,NMO,NDY,GRID,NSAT
299 READ(5,LFMT) RORBIT,RHR,RMIN,RSEC,RQ,RLONG
300 READ(5,LFMT) PT,PL,H,ORIN,ZDRP
301 IF(KINP.EQ.0) READ(5,LFMT) KJ
302 IF(KINP.NE.0) READ(5,LFMT) NSKIP,LSMT,LCAL
303 READ(5,LFMT) LCHK1,LOUT1
304 IF(LOUT1.GT.0) READ(5,LFMT) (LOUT2(I),I=1,LOUT1)
305 IF(LCHK1.EQ.0) GO TO 6
306 READ(5,LFMT) LAINC,LOINC,LCHK2
307 IF(LCHK2.EQ.0) GO TO 5
308 READ(5,LFMT) LAB,LAE,LOB,LOE,LHEM
309 C
310 C          CONVERT LONGITUDE TO DEGREES EAST AND CONVERT
311 C          BEGINNING AND ENDING LATITUDES AND LONGITUDES
312 C          TO VALUES USED IN DO LOOPS
313 IF(LAE.LT.LAB) GO TO 900
314 2 LAB=LAB*10+10
315 LAE=LAE*10+10
316 IF(LOE.LT.LOB) GO TO 901
317 3 IF(LHEM.NE.2) GO TO 4
318 LOST=LOE
319 LOE=360-LOB
320 LOB=360-LOST
321 4 LOB=LOB*10+10
322 LOE=LOE*10+10
323 GO TO 6
324 5 LAB=10
325 LAE=910
326 LOB=10
327 LOE=3610
328 C
329 C          DETERMINE OUTPUT TYPE AND SATELLITE NAME
330 6 IF(KINP.LT.0.OR.KINP.GT.4) GO TO 910
331 IROV=POSI
332 IF(KINP.EQ.1.OR.KINP.EQ.3) IROV=IR
333 IF(KINP.EQ.2.OR.KINP.EQ.4) IROV=VISIBL
334 SNAME=BLANK
335 IF(NSAT.EQ.4) SNAME=NOAA4
336 IF(NSAT.EQ.5) SNAME=NOAA5
337 C
338 C          CALCULATE PROGRAM CONSTANTS FROM INPUT PARAMETERS
339 C
340 C          CONVERT INPUT LONGITUDE TO LONGITUDE IN DEGREES EAST
341 IF(RQ.EQ.0.OR.RQ.EQ.5) RLONGC=360.-RLONG
342 IF((RQ.EQ.1.OR.RQ.EQ.6).AND.RLONG.GE.90.) RLONGC=360.-RLONG
343 IF((RQ.EQ.1.OR.RQ.EQ.6).AND.RLONG.LT.90.) RLONGC=360.-RLONG-100.
344 IF((RQ.EQ.2.OR.RQ.EQ.7).AND.RLONG.LT.90.) RLONGC=RLONG+100.
345 IF((RQ.EQ.2.OR.RQ.EQ.7).AND.RLONG.GE.90.) RLONGC=RLONG
346 IF(RQ.EQ.3.OR.RQ.EQ.8) RLONGC=RLONG
347 C          CALCULATE LONGITUDE OF LAST EQUATOR CROSSING
348 RL=RLONGC-(NORBIT-RORBIT)*PL
349 RL=AMOD(RL,360.0)
350 IF(RL.LT.0.0) RL=RL+360.0
351 RRL=RL*C1
352 C          CONVERT TO EAST-WEST LONGITUDE FOR OUTPUT ONLY
353 QUAD=EAST
354 RLOUT=RL
355 IF(180.0-RL) 7,8,9
356 7 QUAD=WEST
357 RLOUT=360.-RL
358 GO TO 9

```





```

359      8 QUAO=BLANK
360      C      DETERMINE TIME AT FIRST OUTPUTTED SCAN OF ORBIT
361      9 RTIME=RHR*60.+RMIN+RSEC/60.
362      STIME=RTIME+(NORBIT-RORBIT)*PT+(GRID+BSCAN)/SRPM
363      SHR=AMOO(STIME,1440.0)
364      IF(SHR.LT.0.0) SHR=SHR+1440.0
365      NHR=SHR/60.
366      SMIN=SHR-NHR*60.
367      NMIN=SMIN
368      SSEC=SMIN-NMIN
369      NSEC=SSEC*60.
370      C      SET AVERAGING PARAMETER KJ
371      IF(KINP.EQ.1.OR.KINP.EQ.3) KJ=3
372      IF(KINP.EQ.2.OR.KINP.EQ.4) KJ=1
373      XKJ=FLOAT(KJ)
374      IF(KB.LE.0.OR.KE+KJ-1.GT.920.OR.KE-KB+1.LE.KJ) GO TO 920
375      XKB=FLOAT(KB)
376      C      DETERMINE GRID LENGTH, WIDTH AND SIZE OF FINAL OUTPUT
377      IPOS=(KE-KB+KJ)/KJ
378      XPOS=FLOAT(IPOS)
379      MAXSC=ESCAN-BSCAN+1
380      IF(KINP.EQ.0) GO TO 11
381      IF(MAXSC.GT.400) GO TO 921
382      IF(IPOS.GT.301) GO TO 922
383      MTMAT=MAXSC*IPOS
384      RTMAT=MTMAT/1000.
385      C      DETERMINE NUMBER OF SCANS PER RADIAN OF ORBIT,
386      C      AND CONVERT BSCAN AND ESCAN TO RADIAN ANGLES
387      11 RTSC=PT*SRPM/(PI*2)
388      SB=(BSCAN+GRID)/RTSC
389      SE=(ESCAN+GRID)/RTSC
390      C      DETERMINE LIMITS FOR POSITIONS AND SCANS OF LAT-LON LINES
391      DPOS=0.050*XPOS
392      PB1=1.0-DPOS
393      PB2=PB1-2.*DPOS
394      OSCAN=0.050*(SE-SB)
395      SB1=SB-DSCAN
396      SB2=SB1-2.*OSCAN
397      SB3=SB2-2.*OSCAN
398      SE1=SE+DSCAN
399      SE2=SE1+2.*DSCAN
400      SE3=SE2+2.*OSCAN
401      C      DETERMINE SATELLITE HEADING
402      HEAD=POL
403      IF(SB.LT.PIB2.AND.SE.LT.PIB2) HEAO=NOR
404      IF(SB.GT.PIB2.AND.SE.GT.PIB2) HEAO=SOU
405      TPL=PL/360.
406      C      DETERMINE SCAN ANGLE FOR HORIZONS AND HORIZON POSITIONS
407      RETAH=ARSIN(R/(R+H))
408      RGAMH=PIB2-RETAH
409      DHRZ=RETAH*CMULF
410      HORZ1=ZDRP-OHRZ
411      HORZ2=ZORP+OHRZ
412      C      DETERMINE DISTANCE BETWEEN POSITIONS AND SCANS
413      C      (DISTANCE BETWEEN POSITIONS CALCULATED OVER
414      C      MIDDLE TWO-THIRDS OF OUTPUT WIDTH.
415      C      DISTANCE BETWEEN SCANS CALCULATED AT
416      C      MIDDLE POINT OF OUTPUT LENGTH)
417      APOS=(KE-KB)/6.
418      ETAH1=(KB+APOS-ZORP)/CMULF
419      X1=R*R*COS(ETAH1)*COS(ETAH1) - H*(H+2.*R)*SIN(ETAH1)*SIN(ETAH1)
420      XX1=(R+H)*COS(ETAH1) - SQRT(X1)
421      BETA1=ARSIN(XX1*SIN(ETAH1)/R)
422      ETAH2=(KE-APOS-ZORP)/CMULF
423      X2=R*R*COS(ETAH2)*COS(ETAH2) - H*(H+2.*R)*SIN(ETAH2)*SIN(ETAH2)
424      XX2=(R+H)*COS(ETAH2) - SQRT(X2)

```



```

425      BETA2=ARSIN(XX2*SIN(ETAH2)/R)
426      BETA=ABS(BETA2-BETA1)
427      DISTP=R*BETA*XKJ/(APOS*4.)
428      R2=R*COS((BETA1+BETA2)/2.)
429      DISTS=R2/RTSC
430      C      DETERMINE SCALING FACTORS (IN GRID UNITS PER INCH)
431      SF=SF*1E-6
432      SCALP=SF*10.*C3/DISTP
433      SCALS=SF*10.*C3/DISTS
434      C      ADJUST OUTPUT WIDTH FOR CALCOMP PLOTTING
435      IPCNT=IPOS
436      IF(KINP.EQ.0) GO TO 12
437      IF(XPOS/SCALP.GT.32.) IPCNT=IFIX(32.*SCALP)
438      C      CONVERT SATELLITE INCLINATION TO PROGRAM FORM
439      12 RINC=(ORIN-90.)*C1
440      SINC=SIN(RINC)
441      CINC=COS(RINC)
442      C
443      C      PRINT INPUT DATA AND PRELIMINARY CALCULATIONS
444      WRITE(6,500) IROV,NORBIT,SNAME,MONTH(NMO),NDY,NYR,NHR,NMIN,NSEC,
445      1 HEAO,GRI0,RL0UT,QUAO,RORBIT,RLONGC,RHR,RMIN,RSEC,
446      2 PT,PL,H,R,ORIN,SRPM
447      WRITE(6,501) BSCAN,ESCAN,KB,KE,ZDRP,HORZ1,HORZ2,
448      1 DISTS,SCALS,OISTP,SCALP,SF
449      500 FORMAT(1H1,4X,A8,1X,'INFORMATION FROM ORBIT',I6,2X,'OF SATELLITE',
450      1 A8,5X,'ON ',A8,1X,I2,2X,I4,5X,'FROM TIME',I3,1H:,I2,1H:,I2,2H Z,
451      2 //,5X,'SATELLITE HEAOING IS',A8,5X,F7.1,' SCANS PASSED SINCE',
452      3 ' SATELLITE LAST CROSSED EQUATOR AT LONGITUDE',F7.2,' DEGREES',
453      4 A8,///,5X,'REFERENCE ORBIT',I6,5X,'CROSSED EQUATOR AT LONGITUOE',
454      5 F7.2,' DEGREES EAST',5X,'AT TIME',I3,1H:,I2,1H:,I2,2H Z,///,5X,
455      6 'ORBITAL PERIOD =',F10.5,' MIN',5X,'LONGITUONAL INCREMENT =',
456      7 F6.2,' DEGREES TO WEST',///,5X,'HEIGHT OF SATELLITE AT EQUATOR =',
457      8 F6.0,' KM',5X,'RAOIUS OF EARTH =',F6.0,' KM',///,5X,
458      9 'ORBITAL INCLINATION =',F7.2,' OEG',5X,'SCANNING RATE =',
459      1 F4.0,' SCANS PER MINUTE')
460      501 FORMAT(1H-,4X,'SCANNING BEGINS AT',I6,2X,'AND ENDS AT',I6,
461      1 10X,'OUTPUT TAKES UP',I4,' TO',I4,' OF AVAILABLE WIOTH',///,5X,
462      2 'ZERO DEGREE REFERENCE POSITION OF SATELLITE =',F7.2,///,5X,
463      3 'FIRST HORIZON POSITION =',F7.2,5X,'SECONO HORIZON POSITION =',
464      4 F7.2,///,5X,'DISTANCE BETWEEN SCANS =',F6.2,' KM',5X,'SCALING =',
465      5 1PE11.4,' GRID UNITS PER INCH IN X OIRECTION',///,
466      6 5X,'OISTANCE BETWEEN POINTS =',OPF6.2,' KM',5X,'SCALING =',
467      7 1PE11.4,' GRI0 UNITS PER INCH IN Y DIRECTION',///,
468      8 5X,'MAP SCALE = 1 :',OPF5.2,' MILLION')
469      C
470      IF(KINP.EQ.0) GO TO 76
471      C      *****
472      C
473      C      INPUT LOOP FOR DATA FIELD
474      C
475      IF(KINP.NE.3.AND.KINP.NE.4) GO TO 25
476      C      SKIP NSKIP SCANS OF DATA (FOR MAG TAPE ONLY)
477      CALL SKIP(0,NSKIP,4,&930)
478      C      READ AND INPUT SCANS BETWEEN BSCAN AND ESCAN
479      25 READ(4) HSCAN,LA
480      IF(HSCAN.LT.BSCAN) GO TO 25
481      IF(HSCAN.GT.ESCAN) GO TO 35
482      MSCAN=HSCAN-BSCAN+1
483      ICNT=0
484      C      AVERAGE KJ OATONS TO PRODUCE ONE DATA VALUE
485      C      FOR EACH GRIDPOINT
486      DO 30 JB=KB,KE,KJ
487      SUM=0.0
488      ICNT=ICNT+1
489      JE=JB+KJ-1
490      DO 28 JN=JB,JE

```



```

491      DATUM=FLOAT(IBYTE(LA(JN)))
492      SUM=SUM+DATUM
493      28 CONTINUE
494      TEMP(ICNT,MSCAN)=SUM/XKJ
495      30 CONTINUE
496      IF(ICNT.NE.IPOS) GO TO 940
497      GO TO 25
498      35 IF(MAXSC-MSCAN) 941,40,941
499      40 WRITE(6,510)
500      510 FORMAT(1H-.,/,10X,'DATA FIELD PARAMETERS')
501      C      *****
502      C
503      C      SMOOTHING OF DATA FIELO
504      C
505      IF(LSMT.EQ.O) GO TO 45
506      CALL SMOO(MAXSC,IPOS)
507      GO TO 50
508      C
509      45 WRITE(6,520)
510      520 FORMAT(1H-.,14X,'NO SMOOTHING OF OATA FIELD USED')
511      C      *****
512      C
513      C      CALIBRATION OF OATA FIELD
514      C
515      50 IF(LCAL.EQ.O) GO TO 55
516      CALL CALI(MAXSC,IPOS,&70,&55)
517      C
518      55 WRITE(6,525)
519      525 FORMAT(1H-.,14X,'NO CALIBRATION OF DATA FIELD USED')
520      C      *****
521      C
522      C      OUTPUT LOOP FOR DATA FIELO (OUTPUT OF DATA GRID TO
523      C      UNIT 7 (8,9 AND 10) IN 30 INCH LONG STRIPS)
524      C
525      70 IUNIT=7
526      DO 75 IB=1,IPOS,IPCNT
527      IE=MINO(IPOS,IB-1+IPCNT)
528      TMIN=500.O
529      TMAX=-500.O
530      DO 72 II=IB,IE
531      WRITE(IUNIT,1000) (TEMP(II,J),J=1,MAXSC)
532      1000 FORMAT(1H.,2(20OF6.1))
533      C      FINO MAXIMUM AND MINIMUM OF OATA FIELO
534      DO 72 JJ=1,MAXSC
535      IF(TEMP(II,JJ).LT.TMIN) TMIN=TEMP(II,JJ)
536      IF(TEMP(II,JJ).GT.TMAX) TMAX=TEMP(II,JJ)
537      72 CONTINUE
538      WRITE(6,600) IUNIT,MAXSC,IB,IE,RTMAT,TMIN,TMAX
539      600 FORMAT(1H-.,14X,'DATA FIELO OUTPUTTED TO UNIT',I3,/,/,
540      1 5X,'GRID DIMENSIONS : COLUMNS 1 TO',I5,5X,
541      2 'ROWS',I4,' TO',I5,/,/,5X,'GRID SIZE =',F6.2,'K ELEMENTS',/,/,
542      3 5X,'MINIMUM OF OATA FIELO =',F6.1,5X,
543      4 'MAXIMUM OF OATA FIELO =',F6.1)
544      IUNIT=IUNIT+1
545      IF(IUNIT.GT.10) GO TO 950
546      75 CONTINUE
547      C
548      76 IF(LCHK1.EQ.O) GO TO 201
549      C      *****
550      C
551      C      OETERMINE INCREMENTS FOR FINOING LATITUOE AND LONGITUOE CURVES
552      C      (INCREMENTS MUST BE AT LEAST 1)
553      C
554      LALAT=LAINC*10
555      IF(LALAT.LT.1) LALAT=1
556      LOLAT=LAINC*2

```





```

557         IF (LOLAT.LT.1) LOLAT=1
558         LOLON=LOINC*10
559         IF (LOLON.LT.1) LOLON=1
560         LALON=LOINC*1
561         IF (LALON.LT.1) LALON=1
562         WRITE(6,530) LAINC,LOINC
563 530 FORMAT(1H- ,/,10X,'LATITUDE-LONGITUDE PARAMETERS',///,
564 1 5X,'LATITUDE LINES GENERATED EVERY',F5.1,' DEGREES',
565 2 5X,'500 POINTS ALLOWED FOR EACH LINE',//,5X,
566 3 'LONGITUDE LINES GENERATED EVERY',F5.1,' DEGREES',5X,
567 4 '500 POINTS ALLOWED FOR EACH LINE')
568 C *****
569 C
570 C OUTPUT LOOP FOR LATITUDE AND LONGITUDE LINES (OUTPUT OF LINES
571 C TO UNIT 11 (12,13 AND 14) IN 30 INCH LONG STRIPS)
572 C
573         JUNIT=11
574         DO 200 IIB=1,IPOS,IPCNT
575         IF (JUNIT.GT.14) GO TO 951
576         IIE=MINO(IPOS,IIB-1+IPCNT)
577         XIIB=FLOAT(IIB)
578         IIPOS=IIE-IIB+1
579         PE1=FLOAT(IIPOS)+DPOS
580         PE2=PE1+2.*DPOS
581         WRITE(6,531) JUNIT
582 531 FORMAT(1H- ,14X,'LATITUDE-LONGITUDE LINES OUTPUTTED TO UNIT',I3)
583         KCHK=0
584 C *****
585 C
586 C DETERMINE POINTS FOR LATITUDE LINES
587 C
588         WRITE(6,540)
589 540 FORMAT(1H0,7X,'LATITUDE LINES',/)
590         MLL=1
591 C MLL=1 DENOTES LATITUDE LINES IN OUTPUT
592 C
593 C INCREMENT LATITUDE LINES TO BE FOUND
594         DO 100 LAT=LAB,LAEL,LALAT
595         ALAT=(LAT-10)/10.
596         LLAT=IFIX(ALAT)
597         LOLATA=LOLAT
598 C ONLY ONE-FIFTH NUMBER OF POINTS USED IN
599 C LATITUDE LINES NORTH OF 80 DEGREES
600         IF (ALAT.GT.80.) LOLATA=5*LOLAT
601         IF (ALAT.EQ.90.) GO TO 115
602         IF (ALAT.GT.90.) GO TO 960
603         SP=C1*ALAT
604         COSL=COS(SP)
605         SINL=SIN(SP)
606         MCHK=0
607         MM=0
608 C
609 C INCREMENT LONGITUDE INTERSECTIONS TO DETERMINE
610 C EACH LATITUDE LINE
611         DO 80 LONG=LOB,LOE,LOLATA
612         BLONG=(LONG-10)/10.
613         THETA=RRL-BLONG*C1
614         CALL ITERA(ALAT,BLONG,MM,MCHK,SB1,SB2,SE1,SE2,PB1,PE1)
615         IF (MCHK.EQ.1.OR.MM.LE.1) GO TO 80
616 C OUTPUT LATITUDE LINE SEGMENT
617         WRITE(6,541) ALAT,MM
618 541 FORMAT(1H ,5X,'LATITUDE =',F5.1,' DEGREES NORTH',6X,
619 1 'POINTS IN LATITUDE LINE =',I4)
620         WRITE(JUNIT,550) MM,MZERO,MLL,LLAT
621 550 FORMAT(4I4)
622         WRITE(JUNIT,551)(SCAN(I),POSN(I),I=1,MM)

```



```

623      551 FORMAT(2F7.2)
624      KCHK=KCHK+1
625      MCHK=0
626      MM=0
627      80 CONTINUE
628      IF(MCHK.EQ.0.AND.MM.LE.1) GO TO 100
629      C      OUTPUT LATITUDE LINE SEGMENT (FIVE SEGMENTS ARE
630      C      POSSIBLE FOR EACH LATITUDE LINE)
631      WRITE(6,541) ALAT,MM
632      WRITE(JUNIT,550) MM,MZERO,MLL,LLAT
633      WRITE(JUNIT,551)(SCAN(I),POSN(I),I=1,MM)
634      KCHK=KCHK+1
635      100 CONTINUE
636      GO TO 150
637      C      *****
638      C
639      C      POST THE NORTH POLE (IF WITHIN GRID LIMITS)
640      C
641      115 IF(PIB2.LT.SB.OR.PIB2.GT.SE) GO TO 150
642      SCAN90=(PIB2-SB)*RTSC+1.
643      X1=-R*SINC
644      X2=H+R*(1.-CINC)
645      ETAH90=ATAN2(X1,X2)
646      POSN90=(ETAH90*CMULF+ZDRP-XKB)/XKJ-XIIB+2.
647      IF(POSN90.LT.1..OR.POSN90.GT.FLOAT(IIPOS)) GO TO 150
648      WRITE(6,560) JUNIT
649      560 FORMAT(1H0,7X,'NORTH POLE POSTED IN UNIT',I4,' OUTPUT AREA')
650      WRITE(15,552) SCAN90,POSN90,ZERO
651      552 FORMAT(3F7.2)
652      C      *****
653      C
654      C      DETERMINE POINTS FOR LONGITUDE LINES
655      C
656      150 WRITE(6,570)
657      570 FORMAT(1H0,7X,'LONGITUDE LINES',/)
658      MLL=2
659      C      MLL=2 DENOTES LONGITUDE LINES IN OUTPUT
660      C
661      C      INCREMENT LONGITUDE LINES TO BE FOUND
662      DO 190 LONG=LOB,LOE,LOLON
663      ALONG=(LONG-10)/10.
664      LLONG=IFIX(ALONG)
665      IF(ALONG.GT.360.) GO TO 961
666      VLONG=ALONG/(2.*LOLON) - IFIX(ALONG/(2.*LOLON))
667      THETA=RRL-ALONG*C1
668      MCHK=0
669      MM=0
670      C
671      C      INCREMENT LATITUDE INTERSECTIONS TO DETERMINE
672      C      EACH LONGITUDE LINE
673      DO 170 LAT=LAB,LAEL,LALON
674      BLAT=(LAT-10)/10.
675      C      EXTEND ONLY EVERY SECOND LONGITUDE LINE
676      C      PAST 85 DEGREES NORTH TO AVOID CROWDING
677      IF(BLAT.GT.85..AND.VLONG.GT.0.1) GO TO 180
678      SP=C1*BLAT
679      COSL=COS(SP)
680      SINL=SIN(SP)
681      CALL ITERA(BLAT,ALONG,MM,MCHK,SB2,SB3,SE2,SE3,PB2,PE2)
682      170 CONTINUE
683      180 IF(MM.LE.1) GO TO 190
684      C      OUTPUT LONGITUDE LINE SEGMENT (ONLY ONE SEGMENT
685      C      POSSIBLE FOR EACH LONGITUDE LINE)
686      WRITE(6,571) ALONG,MM
687      571 FORMAT(1H ,5X,'LONGITUDE =',F6.1,' DEGREES EAST',5X,
688      1 'POINTS IN LONGITUDE LINE =',I4)

```





```

689      WRITE(JUNIT,550) MM,MZERO,MLL,LLONG
690      WRITE(JUNIT,551)(SCAN(I).POSN(I),I=1,MM)
691      KCHK=KCHK+1
692 190 CONTINUE
693 C
694      WRITE(6,580) KCHK,JUNIT,MAXSC,IIB,IIE,IIPPOS
695 580 FORMAT(1H0,7X,I4,' LATITUDE-LONGITUDE LINES OUTPUTTED TO UNIT',I3,
696 1 //,5X,' GRID DIMENSIONS :   COLUMNS 1   TO',I5,5X,
697 2 ' ROWS',I4,'   TO',I5,5X,'(1   TO',I5,')')
698      JUNIT=JUNIT+1
699 200 CONTINUE
700      GO TO 205
701 C
702 201 WRITE(6,581)
703 581 FORMAT(1H-.,/,10X,'NO LATITUDE LONGITUDE LINES GENERATED')
704 C
705 C
706 C      DETERMINE GRID COORDINATES OF INPUTTED LAT-LON POINTS
707 C
708 205 IF(LOUT1.EQ.0) GO TO 301
709      MLL=3
710 C      MLL=3 DENOTES OUTLINE IN OUTPUT.
711      WRITE(6,585)
712 585 FORMAT(1H-.,/,10X,'OUTLINE PARAMETERS',//)
713 C
714      DO 300 LUNIT=1,LOUT1
715      IF(LUNIT.GT.3) GO TO 970
716      WRITE(6,590) LUNIT
717 590 FORMAT(1H ,14X,'LAT-LON POINTS FROM UNIT',I3,/)
718      IF(LOUT2(LUNIT).LT.1.OR.LOUT2(LUNIT).GT.5) GO TO 980
719 C
720      KUNIT=16
721      DO 300 IIB=1,IPOS,IPCNT
722      IF(KUNIT.GT.19) GO TO 952
723      IIE=MINO(IPOS,IIB-1+IPCNT)
724      XIIB=FLOAT(IIB)
725      IIPPOS=IIE-IIB+1
726      PE2=FLOAT(IIPPOS)+2.*DPOS
727      II=0
728      MM=0
729      MCHK=0
730      KCHK=0
731 C      INPUT LOOP FOR LAT-LON OUTLINE INTERSECTIONS
732 210 II=II+1
733      READ(LUNIT,LFMT,END=250,ERR=971) XLATD,XLATM,XLOND,XLONM,LHEM
734      IF(II.GT.500) GO TO 981
735      SLAT(II)=XLATD+XLATM/60.0
736      SLONG(II)=XLOND+XLONM/60.0
737      IF(LHEM.EQ.2) SLONG(II)=360.0-SLONG(II)
738      SP=C1*SLAT(II)
739      COSL=COS(SP)
740      SINL=SIN(SP)
741      THETA=RRL-SLONG(II)*C1
742      CALL ITERA(SLAT(II),SLONG(II),MM,MCHK,SB2,SB3,SE2,SE3,PB2,PE2)
743      IF(MCHK.EQ.1.OR.MM.LE.1) GO TO 210
744      IF(LOUT2(LUNIT).EQ.3) GO TO 990
745 C      OUTPUT OUTLINE SEGMENT
746      KCHK=KCHK+1
747      IF(LOUT2(LUNIT)-4) 220,225,229
748 220 WRITE(6,591) MM,KUNIT
749 591 FORMAT(1H0,4X,I4,' GRID COORDINATE POINTS OF OUTLINE',
750 1 ' TRANSFERRED TO UNIT',I3)
751      WRITE(KUNIT,550) MM,MZERO,MLL
752      WRITE(KUNIT,551) (SCAN(I),POSN(I),I=1,MM)
753      GO TO 230
754 225 WRITE(6,592) MM,KUNIT

```



```

755      592 FORMAT(1HO,4X,I4,' GRID COORDINATE POINTS ',
756      1 'CONTAINED IN UNIT',I4,' OUTPUT AREA ',
757      2 'TRANSFERRED TO UNIT 15 FOR POSTING')
758      WRITE(15,552) (SCAN(I),POSN(I),ZERO,I=1,MM)
759      GO TO 230
760      229 WRITE(6,593)
761      593 FORMAT(1HO,4X,' INPUTTED POINTS',/)
762      WRITE(6,594) (SLAT(I),SLONG(I),I=1,MM)
763      594 FORMAT(1H ,8(F6.2,F7.2,3X))
764      WRITE(6,595)
765      595 FORMAT(1HO,4X,' GRID COORDINATES',/)
766      WRITE(6,596) (SCAN(I),POSN(I),I=1,MM)
767      596 FORMAT(1H ,8(F7.1,F6.1,3X))
768      230 MCHK=0
769      MM=0
770      GO TO 210
771      250 II=II-1
772      IF(MCHK.EQ.0.AND.MM.LE.1) GO TO 290
773      KCHK=KCHK+1
774      IF(LOUT2(LUNIT)-4) 255,260,270
775      255 IF(LOUT2(LUNIT).EQ.3) GO TO 280
776      WRITE(6,591) MM,KUNIT
777      WRITE(KUNIT,550) MM,MZERO,MLL
778      WRITE(KUNIT,551) (SCAN(I),POSN(I),I=1,MM)
779      IF(LOUT2(LUNIT)-2) 265,280,280
780      260 WRITE(6,592) MM,KUNIT
781      WRITE(15,552) (SCAN(I),POSN(I),ZERO,I=1,MM)
782      265 WRITE(6,593)
783      WRITE(6,594) (SLAT(I),SLONG(I),I=1,II)
784      GO TO 290
785      270 WRITE(6,593)
786      WRITE(6,594) (SLAT(I),SLONG(I),I=1,MM)
787      WRITE(6,595)
788      WRITE(6,596) (SCAN(I),POSN(I),I=1,MM)
789      GO TO 290
790      280 IF(MM.NE.II) GO TO 990
791      C      DETERMINE MAXIMUM AND MINIMUM SCAN AND POSITION VALUES
792      C      OF LAT-LON INTERSECTIONS WITHIN EXTENDED LIMITS OF GRID
793      SCANMN=1000.
794      SCANMX=-1000.
795      POSNMN=1000.
796      POSNMX=-1000.
797      DO 285 JI=1,MM
798      IF(SCAN(JI).LT.SCANMN) SCANMN=SCAN(JI)
799      IF(SCAN(JI).GT.SCANMX) SCANMX=SCAN(JI)
800      IF(POSN(JI).LT.POSNMN) POSNMN=POSN(JI)
801      IF(POSN(JI).GT.POSNMX) POSNMX=POSN(JI)
802      285 CONTINUE
803      WRITE(6,597) SCANMN,SCANMX,POSNMN,POSNMX
804      597 FORMAT(1HO,4X,'OUTLINE OCCUPIES BOX CONTAINING SCANS',
805      1 F5.0,' TO',F5.0,4X,'AND POSITIONS',F5.0,' TO',F5.0)
806      C
807      290 IF(KCHK.EQ.0) GO TO 982
808      IF(LOUT2(LUNIT).EQ.1.OR.LOUT2(LUNIT).EQ.2) WRITE(6,598) KCHK,LUNIT
809      598 FORMAT(1HO,4X,I4,' LINE SEGMENTS OF OUTLINE TRANSFERRED ',
810      1 'TO UNIT',I4)
811      IF(LOUT2(LUNIT).EQ.3.OR.LOUT2(LUNIT).EQ.5) GO TO 295
812      WRITE(6,599) MAXSC,IIB,IIE,IIPOS
813      599 FORMAT(1HO,4X,'GRID DIMENSIONS :   COLUMNS   1   TO',I5.5X,
814      1 'ROWS',I4,'   TO',I5.5X,'(1   TO',I5.5X,')')
815      295 WRITE(6,700)
816      700 FORMAT(1HO)
817      KUNIT=KUNIT+1
818      C
819      REWIND LUNIT
820      C

```



```

821      300 CONTINUE
822      GO TO 999
823  C
824      301 WRITE(6,586)
825      586 FORMAT(1H-./,10X,'NO OUTLINES GENERATED',//)
826      GO TO 999
827  C
828  C
829  C      ERROR DEFAULT STATEMENTS
830  C
831      900 WRITE(6,1900)
832      1900 FORMAT(1HO,'***** ERROR    LATITUDE TO BEGIN PLOTTING',
833      1 ' GREATER THAN LATITUDE TO END PLOTTING *****')
834      LAST=LAE
835      LAE=LAB
836      LAB=LAST
837      GO TO 2
838      901 WRITE(6,1901)
839      1901 FORMAT(1HO,'***** ERROR    LONGITUDE TO BEGIN PLOTTING',
840      1 ' GREATER THAN LONGITUDE TO END PLOTTING *****')
841      LOST=LOE
842      LOE=LOB
843      LOB=LOST
844      GO TO 3
845      910 WRITE(6,1910) KINP
846      1910 FORMAT(1HO,'***** ERROR    INPUT TYPE INCORRECTLY SPECIFIED',
847      1 3X,'KINP =',I3,' INPUTTED, 0 TO 4 ONLY ALLOWED *****')
848      GO TO 999
849      920 WRITE(6,1920)
850      1920 FORMAT(1HO,'***** ERROR    INVALID PARAMETERS FOR WIDTH OF ',
851      1 'OUTPUT FIELD *****')
852      GO TO 999
853      921 WRITE(6,1921) MAXSC
854      1921 FORMAT(1HO,'***** ERROR    OUTPUT TOO LONG',5X,I6,' SCANS IN ',
855      1 'OUTPUT.  FORMAT ALLOWS ONLY 400 SCANS *****')
856      GO TO 999
857      922 WRITE(6,1922) IPOS
858      1922 FORMAT(1HO,'***** ERROR    OUTPUT TOO WIDE',5X,I6,' POSITIONS IN ',
859      1 'OUTPUT.  FORMAT ALLOWS ONLY 301 POSITIONS *****')
860      GO TO 999
861      930 WRITE(6,1930)
862      1930 FORMAT(1HO,'***** ERROR IN SCAN SKIP *****')
863      GO TO 999
864      940 WRITE(6,1940) HSCAN
865      1940 FORMAT(1HO,'***** ERROR    INCORRECT DATA LENGTH FOR SCAN',I6,
866      1 ' *****')
867      GO TO 999
868      941 WRITE(6,1941) MSCAN
869      1941 FORMAT(1HO,'***** ERROR    INCORRECT DATA LENGTH',5X,I7,
870      1 ' SCANS IN OUTPUT *****')
871      IF(MSCAN.GT.400) GO TO 999
872      MAXSC=MSCAN
873      GO TO 40
874      950 WRITE(6,1950)
875      1950 FORMAT(1HO,'***** ERROR    TOO MANY OUTPUT UNITS CALLED ',
876      1 'FOR DATA FIELD OUTPUT *****')
877      GO TO 76
878      951 WRITE(6,1951)
879      1951 FORMAT(1HO,'***** ERROR    TOO MANY OUTPUT UNITS CALLED ',
880      1 'FOR LAT-LON LINE OUTPUT *****')
881      GO TO 201
882      952 WRITE(6,1952)
883      1952 FORMAT(1HO,'***** ERROR    TOO MANY OUTPUT UNITS CALLED ',
884      1 'FOR OUTLINE OUTPUT *****')
885      GO TO 301
886      960 WRITE(6,1960)

```





```

887      1960 FORMAT(1HO,'***** ERROR   END VALUE FOR FINAL LATITUDE LINE ',
888          1 'LARGER THAN 90 DEGREES *****')
889          GO TO 150
890      961 WRITE(6,1961)
891      1961 FORMAT(1HO,'***** ERROR   END VALUE FOR FINAL LONGITUDE LINE ',
892          1 'LARGER THAN 360 DEGREES *****')
893          GO TO 999
894      970 WRITE(6,1970)
895      1970 FORMAT(1HO,'***** ERROR   TOO MANY INPUT UNITS CALLED',
896          1 ' FOR OUTLINE PROCEEDURE *****')
897          GO TO 999
898      971 WRITE(6,1971) LUNIT
899      1971 FORMAT(1HO,'***** ERROR IN UNIT',I2,' READ *****')
900          GO TO 999
901      980 WRITE(6,1980) LOUT2(LUNIT)
902      1980 FORMAT(1HO,'***** ERROR   OUTLINE TYPE LOUT2 INCORRECTLY ',
903          1 'SPECIFIED AS',I6,' *****')
904          GO TO 999
905      981 WRITE(6,1981)
906      1981 FORMAT(1HO,'***** ERROR   MORE THAN 500 POINTS IN OUTLINE *****')
907          GO TO 250
908      982 WRITE(6,1982)
909      1982 FORMAT(1HO,'***** ERROR   FAILURE IN OUTLINE PROCEEDURE, NO ',
910          1 'POINTS FOUND WITHIN GRID LIMITS *****')
911          GO TO 999
912      990 WRITE(6,1990)
913      1990 FORMAT(1HO,'***** ERROR   OUTLINE EXCEEDS LIMITS OF ',
914          1 'DATA FIELD *****')
915          GO TO 290
916      999 STOP
917      END
918  C *****
919  C
920      FUNCTION IBYTE(NUM)
921  C
922  C      CONVERTS ONE BYTE NUMBER TO TWO BYTE INTEGER
923      LOGICAL*1 NUM,INT(2)
924      INTEGER*2 I/O/
925      EQUIVALENCE (I,INT)
926      INT(2)=NUM
927      IBYTE=I
928      RETURN
929      END
930  C *****
931  C
932      BLOCK DATA
933      COMMON/BLOCK/R,PI
934      DATA R/6368./,PI/3.1415927/
935      ENO

```

END OF FILE



### C.3 Subroutine ITERA

```

1      SUBROUTINE ITERA(RLAT,RLONG,MM,MCHK,SBA,SBAA,SEA,SEAA,XPOSB,XPOSE)
2      C
3      C      SUBROUTINE FOR DETERMINING IF LAT-LON INTERSECTION
4      C      IS WITHIN EXTENDED LIMITS OF GRID, AND FOR
5      C      DETERMINING EXACT LOCATION IF IT IS
6      C
7      COMMON/BLOCK/R,PI
8      COMMON/CONST0/PIT2,PIB2,CMULF,SB,XKB,XIIB,XKJ
9      COMMON/CONSTS/RTSC,TPL,H,ZDRP,RGAMH,SINC,CINC
10     COMMON/VARI/SP,SINL,COSL,THETA
11     COMMON/VARID/SCAN(500),POSN(500)
12     C
13     C      RLAT  = LATITUDE OF LAT-LON INTERSECTION
14     C      RLONG = LONGITUDE OF LAT-LON INTERSECTION
15     C      MM    = POINTS IN LINE SEGMENT
16     C      MCHK  = LOCATION PARAMETER
17     C      MCHK=0 POINT OUTSIDE EXTENDED LIMITS OF GRID
18     C      MCHK=1 POINT INSIDE EXTENDED LIMITS OF GRID
19     C      SBA   = EXTENDED SCAN TO BEGIN OUTPUT
20     C      SBAA  = OVEREXTENDED SCAN TO BEGIN OUTPUT
21     C      (FIRST CHECK ONLY)
22     C      SEA   = EXTENDED SCAN TO END OUTPUT
23     C      SEAA  = OVEREXTENDED SCAN TO END OUTPUT
24     C      (FIRST CHECK ONLY)
25     C      XPOSB = EXTENDED POSITION TO BEGIN OUTPUT
26     C      XPOSE = EXTENDED POSITION TO END OUTPUT
27     C      SCAN(I) = SCAN LOCATION OF ITH POINT IN LINE
28     C      POSN(I) = POSITION LOCATION OF ITH POINT IN LINE
29     C
30     X1=CINC*SINL + SIN(THETA-TPL*SP)*SINC*COSL
31     X2=COS(THETA-TPL*SP)*COSL
32     SO=ATAN2(X1,X2)
33     IF(SO.LT.0.0.AND.SP.GT.PIB2) SO=SO+PIT2
34     IF(SO.GE.SBAA.AND.SO.LE.SEAA) GO TO 10
35     SP=SO
36     MCHK=0
37     RETURN
38     C
39     10 DO 50 J=1,10
40         ST=THETA-TPL*SO
41         CST=COS(ST)
42         SST=SIN(ST)
43         CSO=COS(SO)
44         SSO=SIN(SO)
45         X1=SSO*CST*COSL - CSO*(SST*SINC*COSL+CINC*SINL)
46         X2=CSO*CST*(1.+TPL*SINC)*COSL + SSO*SST*(SINC+TPL)*COSL +
47         1 SSO*CINC*SINL
48         S1=SO-X1/X2
49         SP=S1
50         RGAM=ARSIN(SIN(THETA-TPL*S1)*CINC*COSL - SINC*SINL)
51         IF(ABS(RGAM).GT.RGAMH) GO TO 100
52         IF(ABS(SO-S1).LT.1E-6) GO TO 60
53         SO=S1
54     50 CONTINUE
55     WRITE(6,500) RLAT,RLONG
56     500 FORMAT(1H,'***** ERROR NO CONVERGENCE TO POINT AT',
57     1 ' LATITUDE',F7.1,2X,'AND LONGITUDE',F7.1,2X,'DEGREES *****')
58     GO TO 100
59     C
60     60 IF(S1.LT.SBA.OR.S1.GT.SEA) GO TO 100
61     MM=MM+1
62     IF(MM.GT.500) GO TO 900
63     SCAN(MM)=(S1-SB)*RTSC+1.
64     X1=R*SIN(RGAM)

```





```

65      X2=H+R*(1.-COS(RGAM))
66      RETA=ATAN2(X1,X2)
67      POSN(MM)=(RETA*CMULF+ZDRP-XKB)/XKJ-XIIB+2.
68      IF(POSN(MM).LT.XPOSB.OR.POSN(MM).GT.XPOSE) GO TO 90
69      MCHK=1
70      RETURN
71      C
72      900 WRITE(6,1900) RLAT,RLONG
73      1900 FORMAT(1H0,'***** ERROR   TOO MANY POINTS IN LINE. OVERFLOW ',
74      1 'AT LATITUDE',F6.1,' AND LONGITUDE',F7.1,' *****')
75      90 MM=MM-1
76      100 MCHK=0
77      RETURN
78      END
END OF FILE

```

#### C.4 Subroutine SMOO

```

1      SUBROUTINE SMOO(MAXSC,IPOS)
2      C
3      C      SMOOTHING SUBROUTINE
4      C
5      LOGICAL*1 LFMT(1)/'*/
6      REAL SMT(10),CORR(301,400)
7      C
8      COMMON/TFIELD/TEMP(301,400)
9      C
10     C      MAXSC = NUMBER OF COLUMNS IN DATA FIELD
11     C      IPOS  = NUMBER OF ROWS IN DATA FIELD
12     C      TEMP(I,J) = DATA VALUE AT EACH POINT (I,J)
13     C
14     C      INPUT DATA
15     C
16     C      NSMT  = NUMBER OF SMOOTHING OPERATIONS TO BE CARRIED
17     C              OUT ON GRID FIELD BEFORE OUTPUT
18     C      SMT(I)= SMOOTHING PARAMETER FOR EACH OPERATION
19     C
20     READ(5,LFMT) NSMT,(SMT(I),I=1,NSMT)
21     C
22     WRITE(6,520)
23     520 FORMAT(1H-,14X,'SMOOTHING PARAMETERS')
24     C
25     C      BEGIN SMOOTHING LOOP
26     C
27     DO 100 KK=1,NSMT
28     SM=SMT(KK)+1.
29     SMT4=SMT(KK)/4.
30     SMT3=SMT(KK)/3.
31     SMT2=SMT(KK)/2.
32     IPOS=IPOS-1
33     MXSC=MAXSC-1
34     C
35     C      TWO POINT SMOOTHING IS USED AT CORNERS OF GRID
36     C
37     CORR(1,1)=SMT2*(TEMP(2,1)+TEMP(1,2))
38     CORR(1,MAXSC)=SMT2*(TEMP(2,MAXSC)+TEMP(1,MAXSC))
39     CORR(IPOS,1)=SMT2*(TEMP(IPOS,1)+TEMP(IPOS,2))
40     CORR(IPOS,MAXSC)=SMT2*(TEMP(IPOS,MAXSC)+TEMP(IPOS,MAXSC))
41     C
42     C      THREE POINT SMOOTHING IS USED ON SIDES OF GRID
43     C
44     DO 30 J=2,MXSC
45     CORR(1,J)=SMT3*(TEMP(1,J-1)+TEMP(2,J)+TEMP(1,J+1))

```



```

46      CORR(IPOS,J)=SMT3*(TEMP(IPOS,J-1)+TEMP(IPOS,J)+TEMP(IPOS,J+1))
47      30 CONTINUE
48      DO 40 I=2,IPOSM
49          CORR(I,1)=SMT3*(TEMP(I+1,1)+TEMP(I,2)+TEMP(I-1,1))
50          CORR(I,MAXSC)=SMT3*(TEMP(I+1,MAXSC)+TEMP(I,MAXSCM)+TEMP(I-1,MAXSC))
51      40 CONTINUE
52      C
53      C      FOUR POINT SMOOTHING IS USED IN INTERIOR OF GRID
54      C
55          DO 50 J=2,MXSCM
56          DO 50 I=2,IPOSM
57              CORR(I,J)=SMT4*(TEMP(I+1,J)+TEMP(I,J+1)+TEMP(I-1,J)+TEMP(I,J-1))
58      50 CONTINUE
59      C
60      C      SMOOTHING CORRECTION IS APPLIED TO EACH GRID POINT
61      C
62          DO 70 J=1,MAXSC
63          DO 70 I=1,IPOS
64              TEMP(I,J)=(TEMP(I,J)+CORR(I,J))/SM
65      70 CONTINUE
66      C
67          WRITE(6,521) KK,SMT(KK)
68      521 FORMAT(1H0,4X,'SMOOTHING OPERATION NUMBER',I3,5X,
69      1 'SMOOTHING PARAMETER =',F6.2)
70      100 CONTINUE
71      RETURN
72      END
END OF FILE

```

### C.5 Subroutine CALI

```

1      SUBROUTINE CALI(MAXSC,IPOS,*,*)
2      C
3      C      CALIBRATION SUBROUTINE
4      C
5          LOGICAL*1 LFMT(1)/'*/
6          REAL X(10),T(10,10)
7      C
8          COMMON/TFIELD/TEMP(301,400)
9      C
10         MAXSC = NUMBER OF COLUMNS IN DATA FIELD
11         IPOS  = NUMBER OF ROWS IN DATA FIELD
12         RETURN1 = CALIBRATION PROGRAM SUCCEEDS
13         RETURN2 = CALIBRATION PROGRAM FAILS
14         TEMP(I,J) = DATA VALUE AT EACH POINT (I,J)
15     C
16     C      INPUT DATA
17     C
18         ATEMP = ZEROING TEMPERATURE IN DEGREES C
19         (IF ATEMP=999 NO TEMPERATURE ADJUSTMENT IS DONE)
20         ADJ   = AVERAGED DATA VALUE FOR TEMPERATURE ADJUSTMENT
21         (USED ONLY IF ATEMP IS NOT 999)
22         NCAL  = NUMBER OF CALIBRATION LEVELS USED
23         X(I),T(1,I) = DATA VALUES AND CORRESPONDING TEMPERATURE
24                     VALUES FOR EACH CALIBRATION LEVEL (IN PAIRS)
25     C
26         READ(5,LFMT) ATEMP,ADJ,NCAL,(X(I),T(1,I),I=1,NCAL)
27     C
28         WRITE(6,600) (X(I),T(1,I),I=1,NCAL)
29     600 FORMAT(1H-,14X,'CALIBRATION PARAMETERS',/,5X,
30     1 'CALIBRATION POINTS :',5X,'DATA LEVELS',5X,

```



```

31      2 'TEMPERATURES (IN DEG C)',/,10(31X,F8.2,14X,F7.2,/))
32      C
33      NCALM=NCAL-1
34      NCLC=NCALM
35      C      DETERMINE CALIBRATION CONSTANTS
36      DO 20 I=2,NCAL
37      DO 10 J=1,NCLC
38      T(I,J)=(T(I-1,J+1)-T(I-1,J))/(X(J+I-1)-X(J))
39      10 CONTINUE
40      NCLC=NCLC-1
41      IF(NCLC.EQ.0) GO TO 30
42      20 CONTINUE
43      C
44      30 WRITE(6,510) (T(IJ,1),IJ=2,NCAL)
45      510 FORMAT(1H0,4X,'CALIBRATION CONSTANTS CALCULATED :',10(2X,F9.6))
46      C
47      NCALTM=NCALM
48      C      REJECT CALIBRATION CONSTANTS SMALLER THAN 10E-6
49      DO 40 I=1,NCALM
50      IF(ABS(T(NCAL+1-I,1)).GE.1E-6) GO TO 50
51      NCALTM=NCALTM-1
52      40 CONTINUE
53      50 IF(NCALTM.LE.0) GO TO 900
54      NCALT=NCALTM+1
55      C
56      WRITE(6,520) (T(IJ,1),IJ=2,NCALT)
57      520 FORMAT(1H0,4X,'CALIBRATION CONSTANTS USED :',10(2X,F9.6))
58      C
59      IF(ATEMP.EQ.999) GO TO 70
60      C      DETERMINE ZEROING ADJUSTMENT FOR TEMPERATURE
61      TADJI=T(NCALT,1)
62      DO 60 I=1,NCALTM
63      XDIFF=ADJ-X(NCALT-I)
64      TADJI=TADJI*XDIFF+T(NCALT-I,1)
65      60 CONTINUE
66      TADJ=ATEMP-TADJI
67      GO TO 80
68      70 TADJ=0.0
69      80 WRITE(6,530) TADJ
70      530 FORMAT(1H0,4X,'ZEROING ADJUSTMENT FOR TEMPERATURE =',F6.1,
71      1 ' DEGREES CELSIUS')
72      C
73      C      CALIBRATE EACH GRID POINT
74      DO 100 JJ=1,MAXSC
75      DO 100 II=1,IPOS
76      TEMPC=T(NCALT,1)
77      DO 90 IJ=1,NCALTM
78      XDIFF=TEMP(II,JJ)-X(NCALT-IJ)
79      TEMPC=TEMPC*XDIFF+T(NCALT-IJ,1)
80      90 CONTINUE
81      TEMP(II,JJ)=TEMPC+TADJ
82      100 CONTINUE
83      RETURN 1
84      C
85      900 WRITE(6,1900)
86      1900 FORMAT(1H0,'***** ERROR CALIBRATION FAILURE *****')
87      RETURN 2
88      END

```

END OF FILE





C.6 Program RERUN

```

1      C      PROGRAM RERUN
2      C
3      C      PROGRAM TO SMOOTH AND CALIBRATE DATA FIELDS PRODUCED
4      C      BY PROGRAM SCAN-2
5      C
6      C      INPUT FROM  UNITS 1,2,3,4 : UNSMOOTHED OR UNCALIBRATED
7      C                        DATA FIELDS
8      C                        UNIT 5 : PROGRAM PARAMETERS
9      C
10     C      OUTPUT TO   UNIT 6 : PROGRAM PARAMETERS
11     C                        UNITS 7,8,9,10 : SMOOTHED OR CALIBRATED
12     C                        DATA FIELDS
13     C
14     C      LOGICAL*1 LFMT(1)/'*/
15     C      COMMON/TFIELD/TEMP(301,400)
16     C      *****
17     C
18     C      INPUT DATA IS FORMAT FREE, DIVIDED BY COMMAS
19     C
20     C      NINP = NUMBER OF FILES OF DATA TO BE INPUTTED
21     C
22     C      INPUT DATA FOR EACH FILE
23     C
24     C      MAXSC = NUMBER OF SCANS (COLUMNS) IN INPUTTED DATA FIELD
25     C      MAXPOS= NUMBER OF POSITIONS (ROWS) IN INPUTTED DATA FIELD
26     C      LBSC  = SCAN NUMBER TO BEGIN OUTPUT
27     C      LESC  = SCAN NUMBER TO END OUTPUT
28     C      LBPOS = POSITION NUMBER TO BEGIN OUTPUT
29     C      LEPOS = POSITION NUMBER TO END OUTPUT
30     C      LSMT  = SMOOTHING CHECKING PARAMETER
31     C      LSMT=0 NO SMOOTHING IS DONE
32     C      LSMT=1 SMOOTHING IS CARRIED OUT
33     C      LCAL  = CALIBRATION CHECKING PARAMETER
34     C      LCAL=0 NO CALIBRATION IS DONE
35     C      LCAL=1 CALIBRATION IS CARRIED OUT
36     C
37     C      SMOOTHING PARAMETERS: NEEDED ONLY IF LSMT=1
38     C      (SEE SUBROUTINE SMOO)
39     C
40     C      CALIBRATION PARAMETERS: NEEDED ONLY IF LCAL=1
41     C      (SEE SUBROUTINE CALI)
42     C
43     C      *****
44     C
45     C      READ(5,LFMT) NINP
46     C
47     C      DO 100 IUNIT=1,NINP
48     C      IF(IUNIT.GT.4) GO TO 950
49     C
50     C      READ(5,LFMT) MAXSC,MAXPOS,LBSC,LESC,LBPOS,LEPOS,LSMT,LCAL
51     C      IF(LBSC.LT.1.OR.LESC.GT.MAXSC) GO TO 910
52     C      10 IF(LBPOS.LT.1.OR.LEPOS.GT.MAXPOS) GO TO 911
53     C      15 MTMAT=(LESC-LBSC+1)*(LEPOS-LBPOS+1)
54     C      RTMAT=MTMAT/1000.
55     C      *****
56     C
57     C      INPUT LOOP FOR DATA FIELD
58     C
59     C      DO 20 II=1,MAXPOS
60     C      READ(IUNIT,1000,ERR=900) (TEMP(II,J),J=1,MAXSC)
61     C      1000 FORMAT(1H ,2(20OF6.1))
62     C      20 CONTINUE
63     C      *****
64     C

```



```

65      C      SMOOTHING OF DATA FIELD
66      C
67      40 IF(LSMT.EQ.O) GO TO 45 -
68          CALL SMOO(MAXSC,MAXPOS)
69          GO TO 50
70      C
71      45 WRITE(6,522)
72      522 FORMAT(1H-,14X,'NO SMOOTHING OF DATA FIELD USED')
73      C      *****
74      C
75      C      CALIBRATION OF DATA FIELD
76      C
77      50 IF(LCAL.EQ.O) GO TO 55
78          CALL CALI(MAXSC,MAXPOS,&70,&55)
79      C
80      55 WRITE(6,525)
81      525 FORMAT(1H-,14X,'NO CALIBRATION OF DATA FIELD USED')
82      C      *****
83      C
84      C      OUTPUT LOOP FOR DATA FIELD
85      C
86      70 JUNIT=IUNIT+6
87          TMIN=500.O
88          TMAX=-500.O
89          DO 80 II=LBPOS,LEPOS
90              WRITE(JUNIT,1000) (TEMP(II,J),J=LBSC,LESC)
91      C      FIND MAXIMUM AND MINIMUM OF DATA FIELD
92          DO 80 JJ=LBSC,LESC
93              IF(TEMP(II,JJ).LT.TMIN) TMIN=TEMP(II,JJ)
94              IF(TEMP(II,JJ).GT.TMAX) TMAX=TEMP(II,JJ)
95      80 CONTINUE
96          WRITE(6,600) JUNIT,LBSC,LESC,LBPOS,LEPOS,RTMAT,TMIN,TMAX
97      600 FORMAT(1H-,14X,'DATA FIELD OUTPUTTED TO UNIT',I3,///,
98          1 5X,'GRID DIMENSIONS :   COLUMNS',I4,' TO',I5,5X,-
99          2 'ROWS',I4,' TO',I5,///,5X,'GRID SIZE =',F6.2,'K ELEMENTS',///,
100         3 5X,'MINIMUM OF DATA FIELD =',F6.1,5X,
101         4 'MAXIMUM OF DATA FIELD =',F6.1,/)
102      100 CONTINUE
103          GO TO 999
104      C      *****
105      C
106      C      ERROR DEFAULT STATEMENTS
107      C
108      900 WRITE(6,1900) II,IUNIT
109      1900 FORMAT(1HO,'***** ERROR IN',I4,' ROW OF UNIT',I3,' READ *****')
110          GO TO 999
111      910 WRITE(6,1910) LBSC,LESC,MAXSC
112      1910 FORMAT(1HO,'***** ERROR   NUMBER OF COLUMNS IN OUTPUT ',
113          1 'FIELD (',I4,' TO',I5,') EXCEEDS NUMBER IN INPUT FIELD (',
114          2 I4,' TO',I5,') *****')
115          IF(LBSC.LT.1) LBSC=1
116          IF(LESC.GT.MAXSC) LESC=MAXSC
117          GO TO 10
118      911 WRITE(6,1911) LBPOS,LEPOS,MAXPOS
119      1911 FORMAT(1HO,'***** ERROR   NUMBER OF ROWS IN OUTPUT ',
120          1 'FIELD (',I4,' TO',I5,') EXCEEDS NUMBER IN INPUT FIELD (',
121          2 I4,' TO',I5,') *****')
122          IF(LBPOS.LT.1) LBPOS=1
123          IF(LEPOS.GT.MAXPOS) LEPOS=MAXPOS
124          GO TO 15
125      950 WRITE(6,1950)
126      1950 FORMAT(1HO,'***** ERROR   TOO MANY INPUT UNITS CALLED',
127          1 ' FOR DATA FIELD INPUT *****')
128          GO TO 999
129      999 STOP
130      END

```





## C.7 Sample Input and Output Information

The information contained in this appendix was used with the computer programs listed above to produce the temperature-field plot of Orbit 4346 of NOAA-5 shown in Figure 4.2.

### C.7.1 Input for Program TAPERD-1 (See Appendix C.1)

INPUT UNIT 1 was a magnetic tape containing information from NOAA-5 orbits on July 15, 1977.

INPUT UNIT 5 contained the following information.

NFS = 4	ITYPE = 1	NSAT = 5
NBS = 75	LCAL = 1	NRAD = 1
NBR = 60		TRAD = 16.5
KOUT = 3		NSCAN = 327
		NPOSN = 344

### C.7.2 Output from Program TAPERD-1

OUTPUT UNIT 3 was a magnetic tape onto which infrared or visible information from portions of NOAA-5 orbits contained on Input Unit 1 was transferred for use in program SCAN-2.

OUTPUT UNIT 6 was a hardcopy printout listed below.



FILES SKIPPED = 4    BLOCKS SKIPPED = 75    BLOCKS READ = 60    OUTPUT OPTION = 3

IR INFORMATION TRANSFERRED TO UNIT 3

FILE LABEL=3464    ORBIT 4346    LENGTH= 4    LRN= 1000

DOCUMENTATION: 77-07-15 4346 16BD 1920-1941Z

2500 BYTES PER SCAN    3 SCANS PER BLOCK

LENGTH= 52    LRN= 2000

FIRST SCAN OUTPUTTED = 225    LAST SCAN OUTPUTTED = 404    NUMBER OF SCANS OUTPUTTED = 180

CALIBRATION BEGINS AT SCAN 225

CALIBRATION SCAN 225

CALIBRATION STEP 1	LEVELS	43	45	44	44	47	45	44	43	45	46	MEAN	44-6
CALIBRATION STEP 2	LEVELS	91	90	89	90	89	91	90	91	90	90	MEAN	90-1
CALIBRATION STEP 3	LEVELS	133	133	133	132	134	134	133	132	132	132	MEAN	132-8
CALIBRATION STEP 4	LEVELS	174	175	174	174	172	174	175	174	174	173	MEAN	173-9
CALIBRATION STEP 5	LEVELS	212	213	214	213	213	212	213	214	214	213	MEAN	213-1
CALIBRATION STEP 6	LEVELS	250	251	249	250	250	251	250	250	251	251	MEAN	250-3

CALIBRATION SCAN 226

CALIBRATION STEP 1	LEVELS	46	45	44	44	44	47	48	46	44	46	MEAN	45-4
CALIBRATION STEP 2	LEVELS	90	88	89	89	90	91	91	90	90	90	MEAN	89-8
CALIBRATION STEP 3	LEVELS	129	132	133	136	134	133	132	132	133	132	MEAN	132-6
CALIBRATION STEP 4	LEVELS	174	173	173	174	175	174	174	175	174	176	MEAN	174-2
CALIBRATION STEP 5	LEVELS	212	213	212	212	212	213	214	213	214	214	MEAN	212-9
CALIBRATION STEP 6	LEVELS	249	249	250	249	250	250	250	251	251	251	MEAN	250-0

CALIBRATION SCAN 227

CALIBRATION STEP 1	LEVELS	44	45	45	46	46	44	44	45	46	48	MEAN	45-3
CALIBRATION STEP 2	LEVELS	90	92	93	91	90	90	91	91	89	90	MEAN	90-7
CALIBRATION STEP 3	LEVELS	132	131	131	132	134	134	132	134	132	132	MEAN	132-4
CALIBRATION STEP 4	LEVELS	173	173	173	174	174	172	173	174	174	175	MEAN	173-5
CALIBRATION STEP 5	LEVELS	214	214	215	214	214	213	214	215	214	214	MEAN	214-1
CALIBRATION STEP 6	LEVELS	248	249	249	250	250	250	250	251	251	252	MEAN	250-0

CALIBRATION SCAN 312

CALIBRATION STEP 1	LEVELS	45	44	44	44	46	44	43	45	45	44	MEAN	44-4
CALIBRATION STEP 2	LEVELS	89	90	90	88	88	89	88	87	88	90	MEAN	88-7
CALIBRATION STEP 3	LEVELS	133	132	133	133	132	132	132	132	133	133	MEAN	132-5
CALIBRATION STEP 4	LEVELS	173	174	174	173	173	173	172	173	173	173	MEAN	173-1
CALIBRATION STEP 5	LEVELS	213	214	214	213	212	212	212	214	214	213	MEAN	213-1
CALIBRATION STEP 6	LEVELS	248	249	248	250	250	249	249	250	250	250	MEAN	249-3

CALIBRATION SCAN 313

CALIBRATION STEP 1	LEVELS	44	45	44	44	44	44	44	45	44	44	MEAN	44-2
CALIBRATION STEP 2	LEVELS	88	88	86	88	89	88	88	88	89	89	MEAN	88-1
CALIBRATION STEP 3	LEVELS	133	131	132	132	132	132	132	131	132	132	MEAN	131-9
CALIBRATION STEP 4	LEVELS	172	173	173	172	170	170	172	173	173	174	MEAN	172-2
CALIBRATION STEP 5	LEVELS	212	213	212	212	212	212	212	214	214	213	MEAN	212-6
CALIBRATION STEP 6	LEVELS	249	250	251	250	250	251	250	250	250	251	MEAN	250-2

CALIBRATION SCAN 314

CALIBRATION STEP 1	LEVELS	46	46	45	44	45	44	44	44	45	47	MEAN	45-0
CALIBRATION STEP 2	LEVELS	89	89	88	88	89	88	89	90	88	87	MEAN	88-5
CALIBRATION STEP 3	LEVELS	133	132	131	131	133	133	132	132	133	133	MEAN	132-3
CALIBRATION STEP 4	LEVELS	173	172	173	173	173	174	173	171	171	171	MEAN	172-4
CALIBRATION STEP 5	LEVELS	211	213	214	212	212	212	212	213	214	215	MEAN	212-8
CALIBRATION STEP 6	LEVELS	247	249	249	250	250	250	250	250	253	252	MEAN	250-0



CALIBRATION SCAN 399

CALIBRATION STEP 1	LEVELS	45	46	45	46	45	46	45	46	45	45	46	MEAN	45.5
CALIBRATION STEP 2	LEVELS	90	90	89	89	90	90	90	90	90	90	90	MEAN	89.8
CALIBRATION STEP 3	LEVELS	134	132	130	133	131	130	130	130	130	131	133	MEAN	131.4
CALIBRATION STEP 4	LEVELS	174	172	171	171	171	173	174	174	174	173	172	MEAN	172.5
CALIBRATION STEP 5	LEVELS	212	213	212	212	212	213	213	213	215	214	212	MEAN	212.8
CALIBRATION STEP 6	LEVELS	252	251	251	249	249	250	249	249	249	249	250	MEAN	249.9

CALIBRATION SCAN 400

CALIBRATION STEP 1	LEVELS	45	46	44	44	44	43	42	45	47	45	45	MEAN	44.5
CALIBRATION STEP 2	LEVELS	90	90	90	90	90	91	91	92	92	92	90	MEAN	90.6
CALIBRATION STEP 3	LEVELS	134	133	132	130	129	130	133	133	132	132	131	MEAN	131.7
CALIBRATION STEP 4	LEVELS	171	172	173	173	174	173	173	174	173	174	174	MEAN	173.0
CALIBRATION STEP 5	LEVELS	212	212	213	213	212	211	212	213	212	212	212	MEAN	212.2
CALIBRATION STEP 6	LEVELS	250	250	250	251	251	251	250	250	248	250	250	MEAN	250.1

CALIBRATION SCAN 401

CALIBRATION STEP 1	LEVELS	43	44	43	42	45	46	46	47	45	45	45	MEAN	44.6
CALIBRATION STEP 2	LEVELS	90	89	87	88	89	90	90	91	90	90	90	MEAN	89.4
CALIBRATION STEP 3	LEVELS	131	130	130	131	131	132	131	130	131	131	133	MEAN	131.0
CALIBRATION STEP 4	LEVELS	172	173	174	173	174	173	174	172	173	173	173	MEAN	173.1
CALIBRATION STEP 5	LEVELS	211	214	214	213	211	212	212	211	212	212	213	MEAN	212.3
CALIBRATION STEP 6	LEVELS	248	249	249	251	250	249	249	248	250	251	251	MEAN	249.4

CALIBRATION OF SATELLITE NOAA 5

RADIOMETER NUMBER 1 AT 16.5 DEGREES C

CALIBRATION STEP DATA LEVEL TEMPERATURE (IN DEG C)

1	44.83	49.15
2	89.52	31.15
3	132.07	10.58
4	173.10	-15.42
5	212.88	-52.00
6	231.39	-86.00

CALIBRATION ADJUSTMENT FROM DATA VALUES

151	150	149	152	149	150	150	148	150	150	149	151	149	148	146
151	149	151	150	150	151	152	151	149	149	150	150	148	146	149
150	150	148	150	151	150	149	148	150	152	146	150	147	146	147
151	150	152	152	148	149	150	151	148	148	148	151	150	149	149
152	151	150	150	149	150	150	150	147	148	149	149	148	148	148
153	151	150	149	148	149	150	149	150	149	148	149	147	147	147
152	150	149	148	148	149	148	148	148	148	147	148	150	150	149

MEAN OF DATA VALUES = 149.30 VARIANCE = 2.1738 STANDARD DEVIATION = 1.4744  
SKEWNESS = -0.0346 KURTOSIS = -0.2346

CALIBRATION ADJUSTMENT FROM POSITIONS 337 TO 351 AND SCANS 324 325 326 327 328 329 330





### C.7.3 Input for Program SCAN-2 (See Appendix C.2)

INPUT UNIT 1 contained 225 latitude-longitude intersections of points along the coastline of Banks Island.

INPUT UNIT 2 contained the latitude and longitude of the meteorological station at Sachs Harbour, 71°59'N and 125°13'W.

INPUT UNIT 5 contained the following information.

KINP = 3	RORBIT = 4310	NSKIP = 50	LAINC = 2
BSCAN = 280	RHR = 21	LSMT = 1	LOINC = 5
ESCAN = 359	RMIN = 05	LCAL = 1	LCHK2 = 1
KB = 363	RSEC = 47		
KE = 482	RQ = 0	LCHK1 = 1	LAB = 60
SF = 4 000 000	RLONG = 6.55	LOUT1 = 2	LAE = 80
			LOB = 100
NORBIT = 4346	PT = 116.336424	LOUT2(1) = 2	LOE = 140
NYR = 1977	PL = 29.0839848	LOUT2(2) = 4	LHEM = 2
NMO = 07	H = 1525		
NDY = 15	ORIN = 102.054		
GRID = 1279.5	ZDRP = 456.5		
NSAT = 5			

(Subroutine SMOO information. See Appendix C.4)

NSMT = 1      SMT(1) = 0.80

(Subroutine CALI information. See Appendix C.5)

ATEMP = 0.0	X(1) = 44.83	T(1) = 49.15
ADJ = 149.30	X(2) = 89.52	T(2) = 31.15
NCAL = 6	X(3) = 132.07	T(3) = 10.58
	X(4) = 173.10	T(4) = -15.42
	X(5) = 212.88	T(5) = -52.00
	X(6) = 231.39	T(6) = -86.00

### C.7.4 Output from Program SCAN-2

OUTPUT UNIT 7 contained the smoothed and calibrated temperature field used in the SURFACE II plotting routines to generate a contoured temperature plot.

OUTPUT UNIT 11 contained the grid coordinates of latitude and longitude lines used in the SURFACE II plotting routines.

OUTPUT UNIT 15 contained the grid coordinates of Sachs Harbour used in the SURFACE II plotting routines.



OUTPUT UNIT 16 contained 225 grid coordinates of the outline of Banks Island used in the SURFACE II plotting routines.

OUTPUT UNIT 6 was a hardcopy printout listed below.





INFRARED INFORMATION FROM ORBIT 4346 OF SATELLITE NOAA-5 ON JULY 15 1977 FROM TIME 19:26:22 Z  
SATELLITE HEADING IS SOUTH 1279.5 SCANS PASSED SINCE SATELLITE LAST CROSSED EQUATOR AT LONGITUDE 26.43 DEGREES EAST

REFERENCE ORBIT 4310 CROSSED EQUATOR AT LONGITUDE 353.45 DEGREES EAST AT TIME 21: 5:47 Z

ORBITAL PERIOD = 116.33643 MIN LONGITUDINAL INCREMENT = 29.08 DEGREES TO WEST

HEIGHT OF SATELLITE AT EQUATOR = 1525. KM RADIUS OF EARTH = 6368. KM

ORBITAL INCLINATION = 102.05 DEG SCANNING RATE = 48. SCANS PER MINUTE

SCANNING BEGINS AT 280 AND ENDS AT 359 OUTPUT TAKES UP 363 TO 482 OF AVAILABLE WIDTH

ZERO DEGREE REFERENCE POSITION OF SATELLITE = 456.50

FIRST HORIZON POSITION = 8.30 SECOND HORIZON POSITION = 904.70

DISTANCE BETWEEN SCANS = 7.16 KM SCALING = 1.4182E+01 GRID UNITS PER INCH IN X DIRECTION

DISTANCE BETWEEN POINTS = 9.68 KM SCALING = 1.0494E+01 GRID UNITS PER INCH IN Y DIRECTION

MAP SCALE = 1 : 4.00 MILLION

#### DATA FIELD PARAMETERS

##### SMOOTHING PARAMETERS

SMOOTHING OPERATION NUMBER 1 SMOOTHING PARAMETER = 0.80

##### CALIBRATION PARAMETERS

CALIBRATION POINTS : DATA LEVELS TEMPERATURES (IN DEG C)

44.83	49.15
89.52	31.15
132.07	10.58
173.10	-15.42
212.88	-52.00
231.39	-86.00

CALIBRATION CONSTANTS CALCULATED : -0.402775 -0.000925 -0.000007 -0.000000 -0.000000

CALIBRATION CONSTANTS USED : -0.402775 -0.000925 -0.000007

ZEROING ADJUSTMENT FOR TEMPERATURE = -0.6 DEGREES CELSIUS

##### DATA FIELD OUTPUTTED TO UNIT 7

GRID DIMENSIONS : COLUMNS 1 TO 80 ROWS 1 TO 40

GRID SIZE = 3.20K ELEMENTS

MINIMUM OF DATA FIELD = -33.9 MAXIMUM OF DATA FIELD = 18.3



LATITUDE-LONGITUDE PARAMETERS

LATITUDE LINES GENERATED EVERY 2.0 DEGREES 500 POINTS ALLOWED FOR EACH LINE  
LONGITUDE LINES GENERATED EVERY 5.0 DEGREES 500 POINTS ALLOWED FOR EACH LINE

LATITUDE-LONGITUDE LINES OUTPUTTED TO UNIT 11

LATITUDE LINES

LATITUDE = 70.0 DEGREES NORTH POINTS IN LATITUDE LINE = 6  
LATITUDE = 72.0 DEGREES NORTH POINTS IN LATITUDE LINE = 40  
LATITUDE = 74.0 DEGREES NORTH POINTS IN LATITUDE LINE = 40  
LATITUDE = 76.0 DEGREES NORTH POINTS IN LATITUDE LINE = 7

LONGITUDE LINES

LONGITUDE = 230.0 DEGREES EAST POINTS IN LONGITUDE LINE = 6  
LONGITUDE = 235.0 DEGREES EAST POINTS IN LONGITUDE LINE = 13  
LONGITUDE = 240.0 DEGREES EAST POINTS IN LONGITUDE LINE = 12  
LONGITUDE = 245.0 DEGREES EAST POINTS IN LONGITUDE LINE = 7  
LONGITUDE = 250.0 DEGREES EAST POINTS IN LONGITUDE LINE = 2

9 LATITUDE-LONGITUDE LINES OUTPUTTED TO UNIT 11

GRID DIMENSIONS : COLUMNS 1 TO 80 ROWS 1 TO 40 (1 TO 40)

OUTLINE PARAMETERS

LAT-LON POINTS FROM UNIT 1

225 GRID COORDINATE POINTS OF OUTLINE TRANSFERRED TO UNIT 16  
OUTLINE OCCUPIES BOX CONTAINING SCANS 11. TO 64. AND POSITIONS 5. TO 37.

1 LINE SEGMENTS OF OUTLINE TRANSFERRED TO UNIT 1

GRID DIMENSIONS : COLUMNS 1 TO 80 ROWS 1 TO 40 (1 TO 40)

LAT-LON POINTS FROM UNIT 2

2 GRID COORDINATE POINTS CONTAINED IN UNIT 16 OUTPUT AREA TRANSFERRED TO UNIT 15 FOR POSTING

INPUTTED POINTS

71.98 234.78 71.98 234.78

GRID DIMENSIONS : COLUMNS 1 TO 80 ROWS 1 TO 40 (1 TO 40)







**B30300**